School of Civil and Mechanical Engineering

Department of Civil Engineering

Development and Implementation of an Advanced Analytical Approach for Flexible Pavement Analysis and Design in Western Australia

Pakdee Khobklang

This thesis is presented for the Degree of
Doctor of Philosophy
of
Curtin University

August 2015

DECLARATION

To the best of my knowledge and belief this thesis contains no material previously published by any other person except where due acknowledgement has been made.

This thesis contains no material which has been accepted for the award of any other degree or diploma in any university.

The following publications have resulted from the work carried out for this degree.

Refereed Journal Papers:

1. **Pakdee Khobklang**, Vanissorn Vimonsatit, Peerapong Jitsangiam and Hamid Nikraz (2013). “A Preliminary Study on Characterisation of Mechanical Behaviour of Hydrated Cement Treated Crushed Rock Base using the Disturbed State Concept”, the Journal of Scientific Research and Essays, Vol. 8(10), pp. 404-413.

2. **Pakdee Khobklang**, Vanissorn Vimonsatit, Peerapong Jitsangiam and Hamid Nikraz (2013). “DSC Modelling For Predicting Resilient Modulus Of Crushed Rock Base As A Road Base Material For Western Australia Roads”, the Journal of Traffic and Transportation Engineering(EI), Vol. 13(2), pp. 10-16.

Refereed Conference Papers:

1. **Khobklang, P.**, Vimonsatit, V., Jitsangiam, P., Nikraz, H.R. (2011) “DSC CONSTITUTIVE MODELLING OF HYDRATED CEMENT TREATED CRUSHED ROCK BASE AS A ROAD BASE MATERIAL FOR WESTERN AUSTRALIA ROADS”, the International Conference on Road and Airfield Pavement Technology (ICPT), 3-5 August, Bangkok, Thailand.

2. **Khobklang, Pakdee** and Vimonsatit, Vanissorn and Jitsangiam, Peerapong and Nikraz, Hamid. 2011. Constitutive Modelling of Hydrated Cement Treated Crush Rock Base with Cyclic-loading Behaviour, in Shahin, M. and Nikraz, H. (ed), International Conference on Advances in Geotechnical Engineering (ICAGE 2011), Nov 7-9 2011, pp. 351-356. Perth, W.A: Curtin University, Department of Civil Engineering.

3. **Khobklang, Pakdee** and Vimonsatit, Vanissorn and Jitsangiam, Peerapong and Nikraz, Hamid. 2012. Disturbed State Concept Modelling of the Resilient Modulus of Hydrated Cement Treated Crushed Rock Base for Western Australia, The 4th KKU International Engineering Conference 2012 (KKU-IENC 2012), May 10-12 2012, pp. 70-75. Khon Kaen, Thailand.

4. **Khobklang, Pakdee** and Vimonsatit, Vanissorn and Jitsangiam, Peerapong and Nikraz, Hamid. 2012. Characterization of Hydrated Cement Treated Crushed Rock Base as a Road Base Material in Western Australia using Disturbed State Concept, The 2nd International Conference on Transportation Geotechnics (IS-Hokkaido 2012), Sep 10-12 2012. Sapporo, Japan.

5. **Khobklang, Pakdee** and Vimonsatit, Vanissorn and Jitsangiam, Peerapong and Nikraz, Hamid. 2012. DSC Modelling for Predicting Resilient Modulus of Crushed Rock Base as a Road Base Material for Western Australia Roads, International Symposium on Heavy Duty Asphalt Pavements and Bridge Deck Pavements (ISAP 2012), May 23-25 2012. Nanjing, China.

Signature:……Pakdee Khobklang……

Date:……6th August 2015.....

Development and Implementation of an Advanced Analytical Approach for Flexible Pavement Analysis and Design in Western Australia

ABSTRACT

In Western Australia (WA), most of the roads are flexible pavements in which its structure comprises of wearing surface, base, subbase and subgrade layers. The wearing surface layer is relatively thin when compared to the other layers widely used in WA, therefore structural behaviours of such pavement needs to be investigated.

Currently, engineers in WA are still using a mechanistic-empirical (M-E) approach for analysis and design of road pavement. However, the aforementioned method is suitable for analysis and design of pavement structure having thick wearing surface layer. Consequently, the inaccurate results are given by the currently used analysis and design method because structural behaviour of those 2 types of pavement is different. In addition, M-E approach employs some empirical formulae, which are based on basic test of materials and on experience, in the procedure.

This research aims to improve an efficient analysis and design procedure for pavement having thin wearing surface layer by developing an advanced analytical approach that can represent real responses to loading of structural system; but computational effort is lower than that of current procedures. Disturbed state concept (DSC) is selected to model the behaviour of base course materials because the interaction between material particles can be included in its formulation, which is considered at a mechanistic level. Hence, the proposed analytical approach is based on a mechanistic approach, which is considered as a unified and versatile concept. It is capable to capture the responses of base course materials to both static and cyclic loading conditions which are usually neglected by M-E approach.

In this research, firstly, the responses to loading of base course materials were investigated by laboratory tests. The results in this step indicated that both CRB and HCTCRB exhibit stress-dependent behaviour, i.e., stress-strain (σ-ε) relation, resilient modulus (M_r) and deformations. Secondly, the potential use of DSC was evaluated for its potentiality in the modelling of base course materials. The results in this step revealed that the important factors such as the vertical stress (σ_1), the confining stress (σ_3), the number of load repetition (N), etc. can be taken into account by DSC models while the other models cannot. Thirdly, the stress conditions in pavement structure was determined by finite element analysis (FEA). All results obtained from this step were later employed in establishing an advanced analytical approach. Finally, an advanced analytical approach for analysis and design of flexible pavement having thin wearing surface layer is established based on the deformation concept. A 3D column-strip model was introduced and DSC models obtained previously were incorporated in FEA. The constitutive models for predicting the permanent deformation of pavement structure (δ_d), which is a major criterion in road design, are the main results from this step, also the influence of all factors in models on the permanent deformation was investigated.

The great advantage of the proposed analytical approach is that it can be directly used in predicting the permanent deformation of pavement structure. It is also not necessary to analyse the whole section of pavement structure, only the column strip under a wheel path is employed. This means less time is required in analysis and design of road pavement, because it consumes lower computational effort. Furthermore, the use of the proposed analytical approach provides the results which is more realistic in the resultant stresses and deformations than that of Mechanical-Empirical approach because important engineering properties such as the vertical stress, the confining stress, number of load repetition, the resilient modulus, etc. are accurately considered in calculation.

Keywords: *crushed rock*, *disturbed state concept*, *hydrated cement treated crushed rock*, *permanent deformation*, *resilient modulus*

ACKNOWLEDGEMENTS

In succession of my Ph.D. study, there were many people who provided me direct and/or indirect helps, suggestions, supports, etc. that I really would like to express my heartfelt thanks to all of them.

First of all, I would like to express my sincere thanks to my supervisor, Dr Vanissorn Vimonsatit, Curtin University, and Kasetsart University Chalermphrakiat Sakonnakhon Province Campus for the opportunity to study doctoral degree that they offered. Without them I would never stand at this point.

There was a group of advisory team that worked very hard during I was studying. The advisory team comprise of my supervisor and my co-supervisors, both Dr Peerapong Jitsangiam and Professor Hamid Nikraz. I wish to thank them with a deep sense of gratitude for their kindness, their patience and their whole-hearted support which carried me to succession. In addition, the cooperation that was provided by other faculty members, laboratory staff and administrative staff of Civil Engineering Department is also gratefully acknowledged.

The other group of people that I have to mention is the research students in Civil Engineering Department; they came from many countries including Australia. I had a chance to learn many things from them such as academic knowledge, culture, life, etc. Also they gave me both direct and indirect supports for my research work, I would like to express my thankfulness to them and the experiences with them will always stay in my mind.

Another group that I have never forgotten is all Thai friends in Australia, especially Thai students in Curtin University. For several years I lived in Australia, we had a chance to learn together and share our experiences. Also when I was very stressed by any reasons, they always looked after me and tried to make me feel better. I would like to express my overwhelming thankfulness to them.

I would like to thank Buddha for teaching all people, including me, to understand the truth of all living things. Also, I thank Buddhist community and Buddhist monastery for giving me a chance to keep walking and follow Buddha's footsteps. I would never be at peace while I was facing a tough time if I had never learned Buddhism.

Furthermore, there is a little angle who inspires me to be alive and keep going forward, she is my daughter, Pichayadha Khobklang. Without this innocent girl I would never have completed my study because she makes me realise that I have to do everything for her. I would also like to express my heartfelt gratitude to my father, my mother, my grand-mother and my grand-father for all supports helped and praying for my success.

Finally, I would like to express my sincere thankfulness to all of my colleagues at the Department of Civil and Environmental Engineering, Kasetsart University, Chalermphrakiat Sakonnakhon Province Campus who indirectly supported me and gave me heartwarming suggestions which helped me finish my thesis.

TABLE OF CONTENTS

Contents	Page
DECLARATION	ii
ACKNOWLEDGEMENTS	vi
TABLE OF CONTENTS	viii
LIST OF FIGURES	xii
LIST OF TABLES	xxii
ABBREVIATIONS	xxiv
NOTATION	xxv
Chapter 1 INTRODUCTION	1
1.1 Background	1
1.2 Objective and scope	3
1.3 Significance	4
1.4 Research Approach	4
1.5 Thesis outline	8
Chapter 2 BACKGROUND AND LITERATURE REVIEW	10
2.1 Background	10
2.2 Structure of road pavement	11
2.4 Analysis of pavement structure	14
2.4.1 Models for prediction of resilient modulus	20
2.4.2 Models for prediction of permanent deformation	21
2.4.3 Models for finite element analysis	22
2.5 Flexible pavement design	25
2.5.1 Empirical Approach	27
2.5.2 Mechanistic-Empirical Approach	28
2.6 Disturbed state concept (DSC)	33
2.6.1 Relative Intact (RI) State	35
2.6.2 Fully Adjusted (FA) State	35
2.6.3 Formulation of DSC equation	37
2.7 Summary	40
Chapter 3 LABORATORY WORKS	41
3.1 Introduction	41

3.2 Materials and Test Methods 41
3.2.1 Materials 41
3.2.2 Compaction tests 44
3.2.3 Preparation of specimen for static and repeated load triaxial tests 45
3.2.4 Static triaxial test 46
3.2.5 Repeated load triaxial (RLT) test 46
3.3 Test Results 49
3.3.1 Modified compaction tests 49
3.3.2 Static triaxial tests 51
3.3.3 Repeated load triaxial (RLT) tests 57
3.4 Summary 59
Chapter 4 APPLICATION OF DSC FOR MODELLING OF MATERIAL RESPONSES 60
4.1 Introduction 60
4.2 DSC model of stress-strain relation of base course materials 60
4.3 DSC model of resilient moduli-applied stresses relation of base course materials 66
4.4 DSC model of permanent deformation of base course materials 70
4.5 Summary 76
Chapter 5 ANALYSIS OF STRESSES IN PAVEMENT MATERIALS 78
5.1 Introduction 78
5.2 Finite element analysis 78
5.2.1 Modelling of multi-layer flexible pavement 78
5.2.2 Analysis of specimen in RLT test 84
5.3 Analysis of pavement structure 85
5.3.1 Classification of pavement structure having thin wearing surface layer 85
5.3.2 Investigation of stress distribution in base course layer 90
5.4 Analysis of specimen in RLT test 94

5.5 Modification of the applied stresses for RLT test of base course materials 96
5.5.1 Results from finite element analysis 96
5.5.2 New loading regime 102
5.6 Summary 109
Chapter 6 ADVANCED ANLYTICAL APPROACH FOR FLEXIBLE PAVEMENT IN WESTERN AUSTRALIA 111
6.1 Introduction 111
6.2 Deformation concept 111
6.3 Column-Strip Model 114
6.4 Results from deformation tests 117
6.4.1 Deformation of crushed rock base (CRB) 117
6.4.2 Deformation of hydrated cement treated crushed rock base (HCTCRB) 121
6.5 Results from finite element analysis of base course specimen 125
6.5.1 Analysis results of CRB specimen 125
6.5.2 Analysis results of HCTCRB specimen 127
6.5.3 Disturbance function for resilient deformation of base course materials 129
6.5.4 Equation for predicting the resilient modulus of base course materials 136
6.6 Investigation the behaviour of pavement structure having thin wearing surface using advanced analytical approach based on DSC 138
6.6.1 Investigation of structural pavement column using CRB as base course material 139
6.6.2 Investigation of structural pavement column using HCTCRB as base course material 154
6.7 Recommendation for design of flexible pavement having thin wearing surface layer 168
6.7.1 Relationship between thickness of wearing surface and permanent deformation 168

6.7.2 Relationship between elastic modulus of wearing surface and permanent deformation 169
6.7.3 Relationship between thickness of base layer and permanent deformation 169
6.7.4 Relationship between confining stress in base layer and permanent deformation 169
6.7.5 Influence of material property on permanent deformation of pavement structure 169
6.8 Summary 176
Chapter 7 CONCLUSIONS AND RECOMMENDATIONS 178
7.1 Conclusions 178
7.1.1 Materials characterisation 178
7.1.2 Modelling of material responses using DSC 179
7.1.3 Finite element analysis of 2D pavement structure and 3D RLT specimen 181
7.1.4 The advanced analytical approach for pavement structure 182
7.2 Recommendations for future research 184
REFERENCES 186
APPENDIXES 198
Appendix A Examples for parametric study of pavement structures 199
Appendix B Examples for parametric study of the results from static triaxial tests 202
Appendix C Examples of stress distribution in base layer 204
Appendix D Example of ABAQUS script 211

LIST OF FIGURES

Figure No.	Title	Page
Figure 1.1	Diagram of Research Methodology	5
Figure 2.1	A flexible pavement structure in Western Australia	12
Figure 2.2	Stress distribution under a wheel in pavement structure	12
Figure 2.3	Dry crushed rock base (CRB)	13
Figure 2.4	Hydrated cement treated crushed rock base (HCTCRB)	14
Figure 2.5	Free body diagram of beams on elastic foundations and forces system	15
Figure 2.6	Infinite beam on an elastic foundation and loaded at origin (Boresi and Schmidt 2003)	17
Figure 2.7	Illustration of shakedown concepts (Wong et al. 1997)	19
Figure 2.8	The modulus of materials; (a) resilient modulus and (b) elastic modulus	20
Figure 2.9	Illustration of the permanent deformation testing results and the use of Sweere's model	22
Figure 2.10	Pavement structure and its role in the road formation (AUSTROADS 2008)	26
Figure 2.11	Design chart for granular pavements with thin bituminous surfacing (AUSTROADS 2008)	28
Figure 2.12	Structural model of flexible pavement and its design criteria (AUSTROADS 2008)	30
Figure 2.13	Mechanistic-Empirical design procedure for flexible pavement (AUSTROADS 2008)	31
Figure 2.14	Definitions of stress. (Desai 2001)	34
Figure 2.15	Particle motions, degradation or softening, and healing (Desai 2001)	36
Figure 2.16	Illustration of the fundamental concept of the DSC (Desai 2001)	36
Figure 3.1	Physical aspects of crushed rock; (a) dry crushed rock and (b) wet crushed rock	42
Figure 3.2	Mixing machine uses for HCTCRB manufacturing	44

Figure 3.3	Physical aspects of HCTCRB	44
Figure 3.4	Compaction test illustrations; (a) some equipment and (b) compacted sample	45
Figure 3.5	(a) Test specimen on the base of the triaxial cell and (b) RLT test set-up on the universal testing machine (UTM-14P)	46
Figure 3.6	RLT test apparatus	47
Figure 3.7	The waveform of the vertical deviator stress	48
Figure 3.8	The applied stresses for finding the resilient modulus in accordance with the Austroads-AG:PT/T053	49
Figure 3.9	Results from the modified compaction tests of CRB	50
Figure 3.10	Results from the modified compaction tests of HCTCRB	50
Figure 3.11	Results from the static triaxial tests of CRB specimen	51
Figure 3.12	Results from the static triaxial tests of HCTCRB specimen	52
Figure 3.13	Trends of estimated elastic modulus of base course materials	52
Figure 3.14	Failure mechanism of CRB specimen after static triaxial test	54
Figure 3.15	Failure mechanism of HCTCRB specimen after static triaxial test	54
Figure 3.16	Mohr-Coulomb failure envelop of CRB	55
Figure 3.17	Mohr-Coulomb failure envelop of HCTCRB	55
Figure 3.18	*p*-*q* diagram of base course materials and the applied stresses in accordance with the Austroads AG:PT/T053	56
Figure 3.19	Resilient modulus test results for CRB and HCTCRB	57
Figure 3.20	Relationship between the resilient modulus and the bulk stress of base course materials (k-θ model)	58
Figure 3.21	Relationship between the permanent deformation, the applied stress and number of load repetition of base course materials	59
Figure 4.1	Fundamental concept of Mohr-Coulomb failure envelop for modelling of base course materials using DSC	61
Figure 4.2	Trends of tangential slope of Mohr-Coulomb failure envelop	61
Figure 4.3	Representation of the DSC modelling for the stress-strain relationship using fully plastic RI	63
Figure 4.4	Prediction of stress-strain curves of CRB using DSC equation	65

Figure 4.5 Prediction of stress-strain curves of HCTCRB using DSC equation 65
Figure 4.6 Relationship between the resilient moduli and the applied stresses of CRB specimen 67
Figure 4.7 Relationship between the resilient moduli and the applied stresses of HCTCRB specimen 67
Figure 4.8 Representation of fundamental DSC concept for predicting the resilient moduli of base course specimen 68
Figure 4.9 Prediction of the resilient moduli of CRB by the use of DSC equation (R^2 = 0.951) 70
Figure 4.10 Prediction of the resilient moduli of HCTCRB by the use of DSC equation (R^2 = 0.928) 70
Figure 4.11 Representation of strain in base course specimen subjected to cyclic loading 71
Figure 4.12 Trends of strain of CRB specimen 74
Figure 4.13 Trends of strain of HCTCRB specimen 74
Figure 4.14 Prediction of the permanent deformation of CRB by the use of DSC equation 76
Figure 4.15 Prediction of the permanent deformation of HCTCRB by the use of DSC equation 76
Figure 5.1 Structural section of road pavement uses as finite element model for analysis using ABAQUS 80
Figure 5.2 Example of the result from finite element analysis using ABAQUS 83
Figure 5.3 Example of the distribution of horizontal stresses (x-direction) under a wheel along the depth of pavement section 84
Figure 5.4 Configuration of finite element model of specimen in RLT test 85
Figure 5.5 Effect of strength of wearing surface layer on horizontal stresses at the bottom fibre of itself 86
Figure 5.6 Effect of strength of base layer on horizontal stresses at the bottom fibre of wearing surface layer 87
Figure 5.7 Effect of strength of subbase layer on horizontal stresses at the bottom fibre of wearing surface layer 87

Figure 5.8 Effect of strength of subgrade on horizontal stresses at the bottom fibre of wearing surface layer 88
Figure 5.9 Surface of σ_{xbws} = 0 in which E_{ws} = 3000 MPa, E_{sb} = 250 MPa, t_{sb} = 250 mm, E_{sg} = 50 MPa, and t_{sg} = 2500 mm 90
Figure 5.10 Stress distribution in the base layer of WSTV-BE200 with t_b reduced to 100 mm and $t_{ws} \leq t_{wsn}$ 91
Figure 5.11 Ratio of stress distribution in the base layer in case of WSTV-BE200 with t_b reduced to 100 mm and $t_{ws} \leq t_{wsn}$ 91
Figure 5.12 Stress distribution in the base layer of WSTV-BE200 with $t_{ws} \leq t_{wsn}$ 92
Figure 5.13 Ratio of stress distribution in the base layer of WSTV-BE200 with $t_{ws} \leq t_{wsn}$ 92
Figure 5.14 Stress distribution in the base layer of WSTV-BE200 with t_b increased to 200 mm and $t_{ws} \leq t_{wsn}$ 93
Figure 5.15 Ratio of stress distribution in the base layer of WSTV-BE200 with t_b increased to 200 mm and $t_{ws} \leq t_{wsn}$ 93
Figure 5.16 Example of the result from finite element analysis of the specimen in RLT test 94
Figure 5.17 p-q diagram of the applied stresses according to Austroads 95
Figure 5.18 Stress distribution along the depth of base layer in WSTV-BE200 with t_b reduced to 100 mm 97
Figure 5.19 Stress distribution along the depth of base layer in WSTV-BE200 97
Figure 5.20 Stress distribution along the depth of base layer in WSTV-BE200 with t_b increased to 200 mm 98
Figure 5.21 Stress distribution along the depth of base layer in WSTV-BE350 with t_b reduced to 100 mm 98
Figure 5.22 Stress distribution along the depth of base layer in WSTV-BE350 99
Figure 5.23 Stress distribution along the depth of base layer in WSTV-BE350 with t_b increased to 200 mm 99
Figure 5.24 Stress distribution along the depth of base layer in WSTV-BE800 with t_b reduced to 100 mm. 100

Figure 5.25 Stress distribution along the depth of base layer in WSTV-BE800 100
Figure 5.26 Stress distribution along the depth of base layer in WSTV-BE800 with t_b increased to 200 mm 101
Figure 5.27 p-q diagram of stress distribution in base course layer of pavement structure 102
Figure 5.28 Area for determination of the applied stress stages for resilient modulus test of base course materials 103
Figure 5.29 The area for determining the applied stresses in term of the relationship between stress ratio and confining stress 104
Figure 5.30 Relationship between m_1 and the expected resilient modulus 105
Figure 5.31 Example of the proposed upper limit of the applied stresses for resilient modulus test 106
Figure 5.32 Example of the results from 3D finite element analysis of CRB using the proposed applied stresses 108
Figure 5.33 Example of the results from 3-D finite element analysis of HCTCRB using the proposed applied stresses 109
Figure 6.1 The algorithm for finding the disturbance function (D) of base course materials 113
Figure 6.2 Column strip under a wheel of flexible pavement structure having thin asphalt concrete layer 116
Figure 6.3 Resilient deformation of CRB, σ_3 = 50 kPa 117
Figure 6.4 Resilient deformation of CRB, σ_3 = 100 kPa 118
Figure 6.5 Resilient deformation of CRB, σ_3 = 200 kPa 118
Figure 6.6 Permanent deformation of CRB, σ_3 = 50 kPa 119
Figure 6.7 Permanent deformation of CRB, σ_3 = 100 kPa 120
Figure 6.8 Permanent deformation of CRB, σ_3 = 200 kPa 120
Figure 6.9 Resilient deformation of HCTCRB, σ_3 = 50 kPa 121
Figure 6.10 Resilient deformation of HCTCRB, σ_3 = 100 kPa 122
Figure 6.11 Resilient deformation of HCTCRB, σ_3 = 200 kPa 122
Figure 6.12 Permanent deformation of HCTCRB, σ_3 = 50 kPa 123

Figure 6.13 Permanent deformation of HCTCRB, σ_3 = 100 kPa 124
Figure 6.14 Permanent deformation of HCTCRB, σ_3 = 200 kPa 124
Figure 6.15 Resilient deformation of CRB, σ_3 = 50 kPa 126
Figure 6.16 Resilient deformation of CRB, σ_3 = 100 kPa 126
Figure 6.17 Resilient deformation of CRB, σ_3 = 200 kPa 127
Figure 6.18 Resilient deformation of HCTCRB, σ_3 = 50 kPa 128
Figure 6.19 Resilient deformation of HCTCRB, σ_3 = 100 kPa 128
Figure 6.20 Resilient deformation of HCTCRB, σ_3 = 200 kPa 129
Figure 6.21 Disturbance function of CRB, σ_3 = 50 kPa 130
Figure 6.22 Disturbance function of CRB, σ_3 = 100 kPa 131
Figure 6.23 Disturbance function of CRB, σ_3 = 200 kPa 132
Figure 6.24 Disturbance function of HCTCRB, σ_3 = 50 kPa 133
Figure 6.25 Disturbance function of HCTCRB, σ_3 = 100 kPa 134
Figure 6.26 Disturbance function of HCTCRB, σ_3 = 200 kPa 135
Figure 6.27 Permanent deformation on structural column of pavement in case of WS·E(1000)·T(*j*) – B·CS(050)·T(100) with CRB 140
Figure 6.28 Permanent deformation on structural column of pavement in case of WS·E(3000)·T(*j*) – B·CS(050)·T(100) with CRB 141
Figure 6.29 Permanent deformation on structural column of pavement in case of WS·E(5000)·T(*j*) – B·CS(050)·T(100) with CRB 141
Figure 6.30 Permanent deformation on structural column of pavement in case of WS·E(1000)·T(*j*) – B·CS(050)·T(200) with CRB 142
Figure 6.31 Permanent deformation on structural column of pavement in case of WS·E(3000)·T(*j*) – B·CS(050)·T(200) with CRB 142
Figure 6.32 Permanent deformation on structural column of pavement in case of WS·E(5000)·T(*j*) – B·CS(050)·T(200) with CRB 143
Figure 6.33 Permanent deformation on structural column of pavement in case of WS·E(1000)·T(*j*) – B·CS(100)·T(100) with CRB 143
Figure 6.34 Permanent deformation on structural column of pavement in case of WS·E(3000)·T(*j*) – B·CS(100)·T(100) with CRB 144

Figure 6.35 Permanent deformation on structural column of pavement in case of WS·E(5000)·T(*j*) – B·CS(100)·T(100) with CRB 144
Figure 6.36 Permanent deformation on structural column of pavement in case of WS·E(1000)·T(*j*) – B·CS(100)·T(200) with CRB 145
Figure 6.37 Permanent deformation on structural column of pavement in case of WS·E(3000)·T(*j*) – B·CS(100)·T(200) with CRB 145
Figure 6.38 Permanent deformation on structural column of pavement in case of WS·E(5000)·T(*j*) – B·CS(100)·T(200) with CRB 146
Figure 6.39 Permanent deformation on structural column of pavement in case of WS·E(1000)·T(*j*) – B·CS(200)·T(100) with CRB 146
Figure 6.40 Permanent deformation on structural column of pavement in case of WS·E(3000)·T(*j*) – B·CS(200)·T(100) with CRB 147
Figure 6.41 Permanent deformation on structural column of pavement in case of WS·E(5000)·T(*j*) – B·CS(200)·T(100) with CRB 147
Figure 6.42 Permanent deformation on structural column of pavement in case of WS·E(1000)·T(*j*) – B·CS(200)·T(200) with CRB 148
Figure 6.43 Permanent deformation on structural column of pavement in case of WS·E(3000)·T(*j*) – B·CS(200)·T(200) with CRB 148
Figure 6.44 Permanent deformation on structural column of pavement in case of WS·E(5000)·T(*j*) – B·CS(200)·T(200) with CRB 149
Figure 6.45 Permanent deformation on structural column of pavement in case of WS·E(1000)·T(*j*) – B·CS(050)·T(100) with HCTCRB 155
Figure 6.46 Permanent deformation on structural column of pavement in case of WS·E(3000)·T(*j*) – B·CS(050)·T(100) with HCTCRB 155
Figure 6.47 Permanent deformation on structural column of pavement in case of WS·E(5000)·T(*j*) – B·CS(050)·T(100) with HCTCRB 156
Figure 6.48 Permanent deformation on structural column of pavement in case of WS·E(1000)·T(*j*) – B·CS(050)·T(200) with HCTCRB 156
Figure 6.49 Permanent deformation on structural column of pavement in case of WS·E(3000)T(*j*) – B·CS(050)·T(200) with HCTCRB 157
Figure 6.50 Permanent deformation on structural column of pavement in case of WS·E(5000)·T(*j*) – B·CS(050)·T(200) with HCTCRB 157

Figure 6.51 Permanent deformation on structural column of pavement in case of WS·E(1000)·T(*j*) – B·CS(100)·T(100) with HCTCRB 158
Figure 6.52 Permanent deformation on structural column of pavement in case of WS·E(3000)·T(*j*) – B·CS(100)·T(100) with HCTCRB 158
Figure 6.53 Permanent deformation on structural column of pavement in case of WS·E(5000)·T(*j*) – B·CS(100)·T(100) with HCTCRB 159
Figure 6.54 Permanent deformation on structural column of pavement in case of WS·E(1000)·T(*j*) – B·CS(100)·T(200) with HCTCRB 159
Figure 6.55 Permanent deformation on structural column of pavement in case of WS·E(3000)·T(*j*) – B·CS(100)·T(200) with HCTCRB 160
Figure 6.56 Permanent deformation on structural column of pavement in case of WS·E(5000)·T(*j*) – B·CS(100)·T(200) with HCTCRB 160
Figure 6.57 Permanent deformation on structural column of pavement in case of WS·E(1000)·T(*j*) – B·CS(200)·T(100) with HCTCRB 161
Figure 6.58 Permanent deformation on structural column of pavement in case of WS·E(3000)·T(*j*) – B·CS(200)·T(100) with HCTCRB 161
Figure 6.59 Permanent deformation on structural column of pavement in case of WS·E(5000)·T(*j*) – B·CS(200)·T(100) with HCTCRB 162
Figure 6.60 Permanent deformation on structural column of pavement in case of WS·E(1000)·T(*j*) – B·CS(200)·T(200) with HCTCRB 162
Figure 6.61 Permanent deformation on structural column of pavement in case of WS·E(3000)·T(*j*) – B·CS(200)·T(200) with HCTCRB 163
Figure 6.62 Permanent deformation on structural column of pavement in case of WS·E(5000)·T(*j*) – B·CS(200)·T(200) with HCTCRB 163
Figure 6.63 Value of coefficient f_0^a with CRB 170
Figure 6.64 Value of the term $f_4^a E_{ws}^2$ with CRB 171
Figure 6.65 Value of coefficient f_0^b with CRB 172
Figure 6.66 Value of coefficient f_0^a with HCTCRB 173
Figure 6.67 Value of the term $f_1^a t_{ws}$ with HCTCRB 173
Figure 6.68 Value of the term $f_3^a t_{ws}^2$ with HCTCRB 174
Figure 6.69 Value of coefficient f_0^b with HCTCRB 175
Figure 6.70 Value of the term $f_1^b t_{ws}$ with HCTCRB 175

Figure A.1 The effect of strength and thickness of wearing surface layer on horizontal stress in wearing surface layer under a wheel path 200
Figure A.2 The effect of strength of base layer and thickness of wearing surface layer on horizontal stress in wearing surface layer under a wheel path 200
Figure A.3 The effect of strength of subbase layer and thickness of wearing surface layer on horizontal stress in wearing surface under a wheel path 201
Figure A.4 The effect of strength of subgrade layer and thickness of wearing surface layer on horizontal stress in wearing surface layer under a wheel path 201
Figure B.5 Trends of the ultimate stress and the fully adjusted state stress of (a) CRB and (b) HCTCRB 203
Figure B.6 Trends of the friction angle and its differentiation corresponding to the confining stress of (a) CRB and (b) HCTCRB 203
Figure B.7 Trends of the strain at ultimate stress and the strain at rupture stress of (a) CRB and (b) HCTCRB 203
Figure C.8 Stress distribution in the base layer of WSTV-BE350 with t_b reduced to 100 mm and $t_{ws} \leq t_{wsn}$ 205
Figure C.9 Ratio of stress distribution in the base layer of WSTV-BE350 with t_b reduced to 100 mm and $t_{ws} \leq t_{wsn}$ 205
Figure C.10 Stress distribution in the base layer of WSTV-BE350 and $t_{ws} \leq t_{wsn}$ 206
Figure C.11 Ratio of stress distribution in the base layer of WSTV-BE350 and $t_{ws} \leq t_{wsn}$ 206
Figure C.12 Stress distribution in the base layer of WSTV-BE350 with t_b increased to 200 mm and $t_{ws} \leq t_{wsn}$ 207
Figure C.13 Ratio of stress distribution in the base layer of WSTV-BE350 with t_b increased to 200 mm and $t_{ws} \leq t_{wsn}$ 207
Figure C.14 Stress distribution in the base layer of WSTV-BE800 with t_b reduced to 100 mm and $t_{ws} \leq t_{wsn}$ 208

Figure C.15 Ratio of stress distribution in the base layer of WSTV-BE800 with t_b reduced to 100 mm and $t_{ws} \leq t_{wsn}$ 208
Figure C.16 Stress distribution in the base layer of WSTV-BE800 and $t_{ws} \leq t_{wsn}$ 209
Figure C.17 Ratio of stress distribution in the base layer of WSTV-BE800 and $t_{ws} \leq t_{wsn}$ 209
Figure C.18 Stress distribution in the base layer of WSTV-BE800 with t_b increased to 200 mm and $t_{ws} \leq t_{wsn}$ 210
Figure C.19 Ratio of stress distribution in the base layer of WSTV-BE800 with t_b increased to 200 mm and $t_{ws} \leq t_{wsn}$ 210

LIST OF TABLES

Table No.	Title	Page
Table 3.1	Chemical composition of Cockburn GP Cement (Cockburn Cement 2007)	43
Table 5.1	Material data for finite element analysis of pavement structure	81
Table 5.2	Cases of investigation on the effect of material properties on σ_{xbws} of pavement structure	82
Table 5.3	Coefficients of polynomial equation for predicting σ_{xbws}	89
Table 5.4	Example of the applied stresses from the area under the upper limit	107
Table 6.1	Coefficients *a*, *b* and R^2 of the exponential function for predicting the resilient deformations of CRB specimen	119
Table 6.2	Coefficients *a*, *b* and R^2 of the power function for predicting the permanent deformations of CRB specimen	121
Table 6.3	Coefficients *a*, *b* and R^2 of the exponential function for predicting the resilient deformations of HCTCRB specimen	123
Table 6.4	Coefficients *a*, *b* and R^2 of the power function for predicting the permanent deformations of HCTCRB specimen	125
Table 6.5	Coefficients *a* and *b* of the nonlinear function for predicting the resilient modulus of CRB specimen	136
Table 6.6	Coefficients *a* and *b* of the nonlinear function for predicting the resilient modulus of HCTCRB specimen	137
Table 6.7	Coefficients *a*, *b* and R^2 of the nonlinear function for predicting the permanent deformations of the column strip under a wheel with CRB and t_b = 100 mm	149
Table 6.8	Coefficients *a*, *b* and R^2 of the nonlinear function for predicting the permanent deformations of the column strip under a wheel with CRB and t_b = 200 mm	150
Table 6.9	Coefficients *a*, *b* and R^2 of the nonlinear function for predicting the permanent deformations of the column strip under a wheel with HCTCRB and t_b = 100 mm	164

Table 6.10 Coefficients a, b and R^2 of the nonlinear function for predicting the permanent deformations of the column strip under a wheel with HCTCRB and t_b = 200 mm 164

ABBREVIATIONS

AASHTO	American Association of State Highway and Transportation Officials
AC	Asphalt Concrete
AS	Australian Standard
ASTM	American Standard for Testing Materials
Austroads	the association of Australian and New Zealand road transport and traffic authorities
CBR	California Bearing Ratio
CLS	Crushed Lime Stone
CRB	Crushed Rock Base
E	Empirical
FA	Fully Adjusted
FEM	Finite Element Method
HCTCRB	Hydrated Cement Treated Crushed Rock Base
M	Mechanistic
M-E	Mechanistic-Empirical
MDD	Maximum Dry Density
MRWA	MAIN ROADS Western Australia
OMC	Optimum Moisture Content
RC	Reinforced Concrete
RI	Relative Intact
RLT	Repeated Load Triaxial
SG	Specific Gravity
UGM	Unbound Granular Materials

NOTATION

a	=	Regression constant
b	=	Regression constant
c	=	Material parameter or cohesion
C_1	=	Constant
C_2	=	Constant
C_3	=	Constant
C_4	=	Constant
d	=	Material parameter
D	=	Disturbance function
E	=	Young's modulus of elasticity or modulus of cemented materials
E_{ws}	=	Modulus of elasticity of wearing surface layer
E_b	=	Modulus of elasticity of base layer
E_{sb}	=	Modulus of elasticity of subbase layer
E_{sg}	=	Modulus of elasticity of subgrade
E_{su}	=	Secant modulus at ultimate stress of material
F_y	=	Reaction force along y-axis
H	=	Hardening modulus
I_x	=	Moment of inertia around x-axis
k	=	Modulus of elastic foundation
k_a	=	Regression constant
k_b	=	Regression constant
k_c	=	Regression constant
k_1	=	Regression constant
k_2	=	Regression constant
M_r	=	Resilient modulus
M_x	=	Bending moment around x-axis
N	=	Number of cycle of repeated loading
$N_{allowable}$	=	Number of allowable traffic loading

p	=	Mean stress
p_a	=	Atmospheric pressure
p_0	=	Unit reference stress (1 kPa)
q	=	Shear stress
RF	=	Reduction factor
r	=	Radius
S_{mix}	=	Modulus of asphalt concrete (MPa)
t_{ws}	=	Thickness of wearing surface layer
t_{wsn}	=	Neutral thickness of wearing surface layer
t_b	=	Thickness of base layer
t_{sb}	=	Thickness of subbase layer
t_{sg}	=	Thickness of subgrade layer
V_b	=	Volume of binder in asphalt mix
V_y	=	Shearing force along y-axis
β	=	$\sqrt[4]{\frac{k}{4EI_x}}$
δ_p	=	Permanent vertical displacement
ε_p	=	Permanent strain
ε_r	=	Recoverable strain
ε_t	=	Total strain
$\mu\varepsilon$	=	corresponding micro strain
$\emptyset$	=	Internal friction angle
σ_d	=	Deviatoric stress
σ_{xbws}	=	Horizontal stress at bottom fibre of wearing surface layer
σ_1	=	Axial stress along 1-Axis or major principal stress
σ_2	=	Axial stress along 2-Axis or intermediate principal stress
σ_3	=	Axial stress along 3-Axis or minor principal stress or confining stress
θ	=	Bulk stress
θ_x	=	Rotational angle around x-axis of structure

CHAPTER 1

INTRODUCTION

1.1 Background

MAIN ROADS Western Australia (MRWA) generally uses asphaltic concrete, crushed rock base and hydrated cement treated crushed rock base as structural materials in pavement (Siripun et al. 2009). There are three main layers in the pavement structure, these are the wearing surface at the top (asphaltic concrete), and the roadbase and subbase (CRB or HCTCRB) in layers underneath. The foundation for the pavement, the natural soil layer, is subgrade. Traditional design methods are based on experience and the results from simple tests such as the California Bearing Ratio (CBR), angle of shearing resistance, moisture sensitivity, particle size distribution, aggregate durability and deflection. These are static tests that exclude consideration of multidimensional geometry, distribution of displacement, and stress and strain distribution in multilayered pavement structures. In addition, traffic loads are by nature repeated loads, which affect and cause complex behaviour in pavement. Therefore, it is questionable whether the currently used, empirically based approach is suitable in accurately predicting pavement behaviour under repeated loading, and whether the design outcomes based on this approach are cost efficient.

According to the structural behaviour of pavement, traffic loads are transferred vertically from the surface layer to the lower layers, and they also spread out laterally. As the loads are transferred between each layer, the stresses vary. Stresses are at a maximum on the surface layer, they then decrease until reaching minimum stress at the top of the subgrade layer. In order to optimise the pavement design based on this behaviour, layers are arranged with the highest bearing capacity material placed on the top, while the lowest bearing capacity material makes up the bottom layer above the subgrade The design optimisation of the structural pavement is mainly to determine an appropriate

layer thickness and composition. The main design objective is to limit the layer stresses induced by the traffic loads.

There are many factors affecting the deformation behaviour and performance of asphaltic concrete. These are the mode of loading, temperature, stress state, ageing and moisture. Granular materials, which are subjected to repeated load, exhibit two types of deformation, namely resilient deformation and permanent plastic deformation. Resilient deformation can lead to fatigue cracking of the pavement surface, and permanent plastic deformation can lead to failure in the pavement due to excessive rutting.

Over the past 30 years, various research has been conducted, and material models have been developed which are based on elasticity, plasticity, and viscoelasticity. These models and qualities determine rutting, damage, fatigue and thermal cracking. There are numerous recent publications on the mechanistic model of pavement materials, including approaches to pavement analysis and design methods for road pavement (Kim 2009; Desai and Whitenack 2001; Desai 2001; Theyse et al. 1996; Abo-Hashema and Sharaf 2009; Luo et al. 2006; Park et al. 2001; Lacey et al. 2008; Kuo and Chou 2004; Allou et al. 2007; Velasquez et al. 2008; Belay et al. 2008; Abaza 2007; Konrad and Nguyen 2006). However, there is still no development of a fully mechanistic approach for pavement analysis and design. This research aims to develop an advanced analytical approach for pavement structure having thin wearing surface layer which commonly construct in Western Australia. The use of developed approach will obtain a better calculation of rutting, which is an important criterion for road design, than using empirical formulas of the current mechanistic–empirical approach. In this study, mechanistic models were developed based on mechanics of materials and theory of structures. The DSC and finite element method will be applied together for developing a numerical approach to predict permanent deformation of pavement. As a result, the maximum permanent deformation of pavement structure will be calculated based on major properties of pavement materials, such as elastic modulus, thickness of layer and confining stress, which are neglected in empirical

formulae. Eventually, the proposed advanced approach will improve the design method for the flexible pavement in Australia and world-wide.

1.2 Objective and scope

The purpose of this research is mainly to propose an innovative analytical model for mechanistic-empirical pavement design and analysis in Western Australia, concentrating on base course materials. The advanced analytical approach introduces in this research will lead to improvement in design procedure of road pavement. With a more fundamental pavement analysis the research aims to:

I. Evaluate the potential use of the disturbed state concept (DSC) for its potentiality in the modelling of commonly used base course materials in Western Australian roads. Materials such as crushed rock base (CRB) and hydrated cement-treated crushed rock base (HCTCRB), will be examined by studying their behavioural responses under applied cyclic loads using standard laboratory tests.

II. Identify and modify currently used constitutive base course material models to reliably address pavement distresses such as permanent deformation (rutting).

III. Validate the results from tests on a selected (and appropriately modified) constitutive base course material model to provide stress–strain response characteristics under static and cyclic loading in laboratory conditions.

IV. Investigate the behaviour of a typical Western Australian multi-layered pavement structure, using finite element modelling.

V. Establish an advanced pavement analytical approach resulting from investigations into the disturbed state concept and the finite element procedure, with validation from laboratory test results.

VI. Use structural theories as the basis of formulating and using a mechanistic approach which will be able to derive equations for predicting deformation and resilient modulus of base course materials used in pavement structure.

1.3 Significance

The significance of this research is that the outcomes would provide a materials model which exhibits more realistic behaviour; and improvements would be made to the approach in pavement design procedure. Analysis and design of flexible pavement in Western Australia could be more efficient and economical than is the case at present. The results of this study will yield:

- a new understanding of behavior of base course materials, both CRB and HCTCRB, under real stress conditions based on mechanistic characterization using DSC;

- the mechanistic models for behavioural response of base course materials which can be used in mechanistic-empirical and fully mechanistic design;

- a new approach for analysis of flexible pavement having thin wearing surface layer which improves the quality of roads and highways in service for Western Australia and world-wide.

1.4 Research Approach

To achieve the objectives of this research, the study will be carried out using the methodology shown in Figure 1.1.

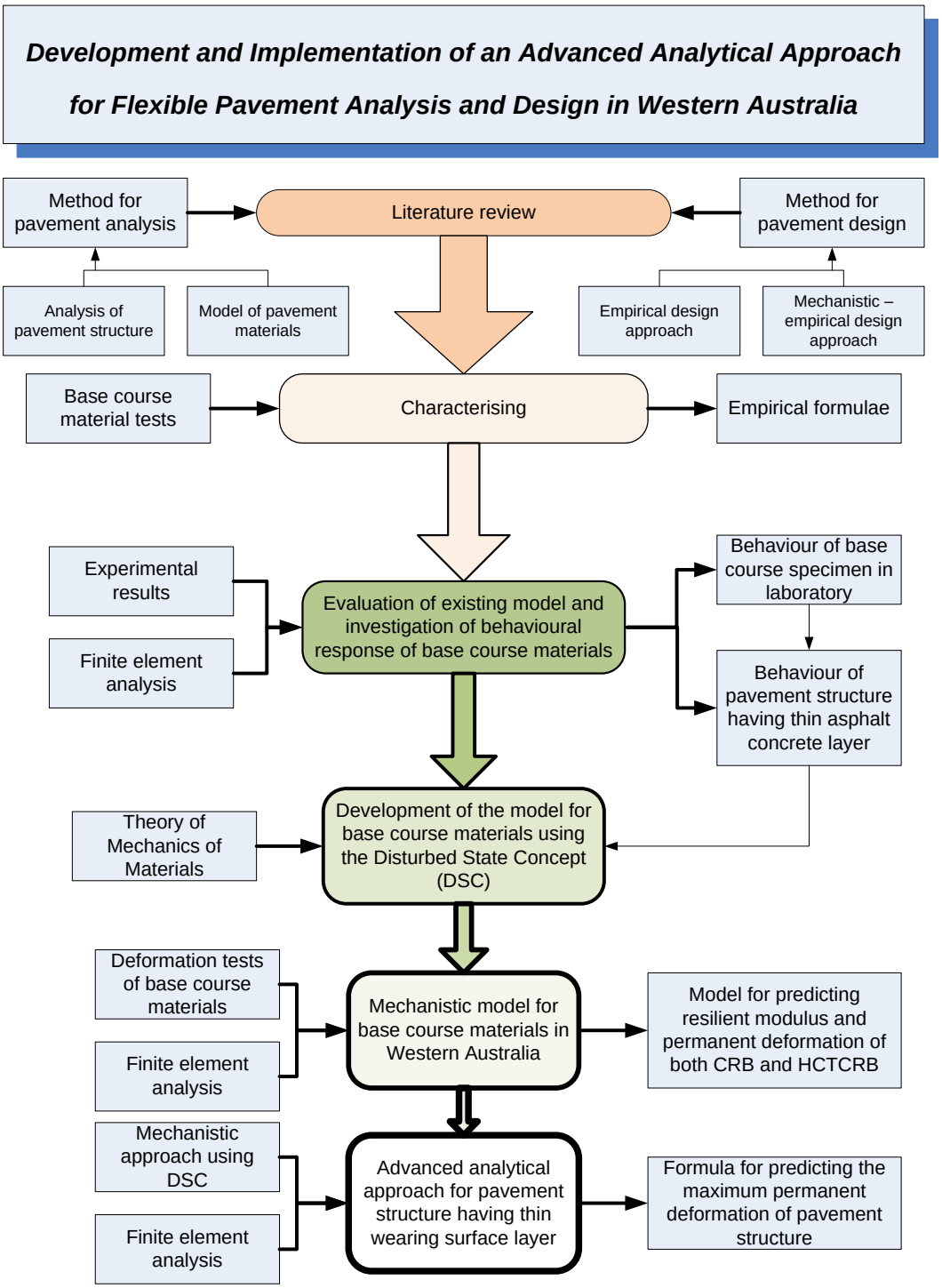

Figure 1.1 Diagram of Research Methodology

Literature review

In the first stage of the research, a detailed review of the literature was conducted to assess the current stage of knowledge available. The review was focussed on literature relevant to material models of flexible pavement and the analysis of pavement structures. It also included the study of the finite element model of structural pavement design.

Characterising behavioural model of base course materials

In the second stage, properties of base course materials and the behaviour of materials under repeated cyclic loading were investigated. In addition, the analysis and design method for structural pavements were studied. Material models which are suitable for road pavement in Western Australia were selected and used as prototypes.

Evaluation of existing model and investigation of behavioural response of base course materials

The third stage was to prove the selected models. Materials specimens were tested in the laboratory and experimental results were compared with finite element simulation. Finally, the structure of road pavement would analysed by finite element method to investigate its behaviour and stresses condition.

Development of the model for base course materials using the Disturbed State Concept (DSC)

The fourth stage is to prove the potential used of DSC for modelling of base course material responses such as resilient modulus and permanent deformation. Theories of the mechanics of materials and DSC will be employed to derive the formulation of the models. This formulation will also be adjusted according to the experimental data obtained. Models for base course materials will be proposed. Furthermore, the procedure for derivation of aforementioned models can be applied to formulate a new analytical approach in the next stage.

Mechanistic model for base course materials in Western Australia

This fifth stage aims to use all knowledge gained previously formulate the mechanistic model of base course material using DSC. This step starts from the deformation concept, which assumes the total deformation of base course specimen is composed of resilient deformation part and permanent deformation part, is introduced then the DSC is applied to eliminate the difference between ideal model and the results from laboratory. Eventually, the mechanistic models for predicting both deformation and resilient modulus of base course material will be founded and the use of these models would give more accurate prediction because major factors that affected on behaviour of material, such as thickness of layer, modulus of base course materials and confining stress in base layer, are the variables in models.

Advanced analytical approach for pavement structure having thin wearing surface layer

The last stage is to introduce a new approach for analysing flexible pavement having thin wearing surface layer by the use of mechanistic models obtained in fifth stage. Because wearing surface of flexible pavement having thin asphalt concrete layer behave like the covering of base layer, a new approach for analysis of pavement structure which consider only the column of pavement structure under a wheel is then proposed. 3-D model of the column of pavement structure under a wheel is analysed by finite element method in which the thickness of layer, modulus of material and confining stress are the variables. The analysis processes are continuously run for 200 cycles of loading and permanent deformation of pavement structure for each case is determined. Finally, all obtained permanent deformation equations are used to formulate a constitutive model for predicting the maximum permanent deformation of pavement structure.

1.5 Thesis outline

This thesis comprises seven chapters as outlined below:

Chapter 1 gives a comprehensive introduction to the research and includes the purpose, scope, methodology and organisation of the study.

Chapter 2 presents relevant current knowledge regarding the base course materials which are commonly used in pavement structures. It includes information on both laboratory and theoretical developments. The mechanical properties of CRB and HCTCRB are presented and the basic concept for the road base analysis and design is described.

Chapter 3 describes the experimental program used in this study. In addition the materials and the procedures for testing are outlined and explained.

Chapter 4 shows the results of main experiments performed in this study, the discussion and summary are also presented, including investigation of stresses distribution in base layers, and stress condition of base course specimens during the test in accordance with Austroads standard.

Chapter 5 explains how to use the results from previous chapter to develop new mechanistic models for predicting behavioural response of base course materials. Furthermore, the new stress stages suitable for conducting cyclic load test of base course specimens are introduced according to the results from finite element analysis.

Chapter 6 introduces a new analytical approach for pavement having thin wearing surface layer that uses DSC applied with finite element method. Mechanistic models for predicting resilient modulus and permanent deformation of base course specimen are derived based on DSC, then they are used in structural analysis with finite element method. Finally, the equations for predicting the maximum permanent deformation of pavement structure, which based on a mechanistic approach that introduces in this chapter, are proposed.

Chapter 7 presents the conclusions reached. The interpretation of all results in this study is briefly covered with consideration given to relevance. Ideas for further research are suggested.

CHAPTER 2
BACKGROUND AND LITERATURE REVIEW

2.1 Background

In Western Australia, flexible pavement is commonly used as wearing surface. However, the thickness of wearing surface layer is generally thin when comparing to the section of structural pavement (Adamson 2011; Main Roads Western Australia 2012). Therefore, a base course layer plays a major role for resisting the traffic loads in pavement structure.

Nowadays, most of road and highway agencies in Western Australia still use crushed rock base (CRB) or hydrated cement treated crushed rock base (HCTCRB) as a road base in road pavement (Main Roads Western Australia 2003a). HCTCRB is manufactured by mixing the original CRB with 2% of general purpose (GP) Portland cement (Australian Standard 1997). Normally, strength of HCTCRB is higher than that of CRB, therefore HCTCRB is classified to be suitable for the highway carrying heavy traffic loading while CRB would be for a base course material of lower traffic loads.

Although HCTCRB suits for heavy traffic loading road pavement, the strength of base layer should not be relatively high because the behaviour of flexible pavement structure would be altered from its assumption, particularly the flexibility such as elastic behaviour is needed to maintain. Consequently, HCTCRB is normally pounded at 7 days of a hydration period then re-mix and re-compact again. In the construction field, before paving the wearing surface layer, both CRB and HCTCRB must be left at the site for evaporation (or dry back) until its moisture content reduces to approximately 85% of its optimum moisture content (OMC) (Main Roads Western Australia 2010).

In 1987, an empirical-mechanistic approach for analysis and design of road pavement was first introduced in Australia by the National Association of Australian State Road Authorities (NAASRA) as an alternative method

(Youdale 1996). In Western Australia however, the mechanistic-empirical method still has been commonly used by most road and highway agencies (Siripun 2010; Jitsangiam and Nikraz 2009) but there is still a lack of in-depth knowledge for some areas in advanced material characterisation and pavement modelling. Although the current pavement design method in the mechanistic-empirical approach is satisfied at a practical level, it should be developed further because it could not entirely govern some realistic behaviour of materials in pavement structure, for example, complex deformation under reliable design modulus. A fully-mechanistic approach, which could take into account realistic material behaviour with reliable pavement modelling for analysis and design of road pavement, is therefore a way forward in pavement engineering.

2.2 Structure of road pavement

Generally, the structure of road pavement comprises of 4 main layers of different materials as seen in Figure 2.1, namely, wearing surface, base, subbase and subgrade.

As aforementioned, most of road in Western Australia is flexible pavement and the wearing surface layer is quite thin. The wearing surface, base, subbase, and subgrade layers are commonly made using asphalt concrete, CRB or HCTCRB, crushed lime stone (CLS), and Perth sand, respectively. For economical purpose, strength of material in each layer is descended from top to bottom layers according to the stress distribution as seen in Figure 2.2.

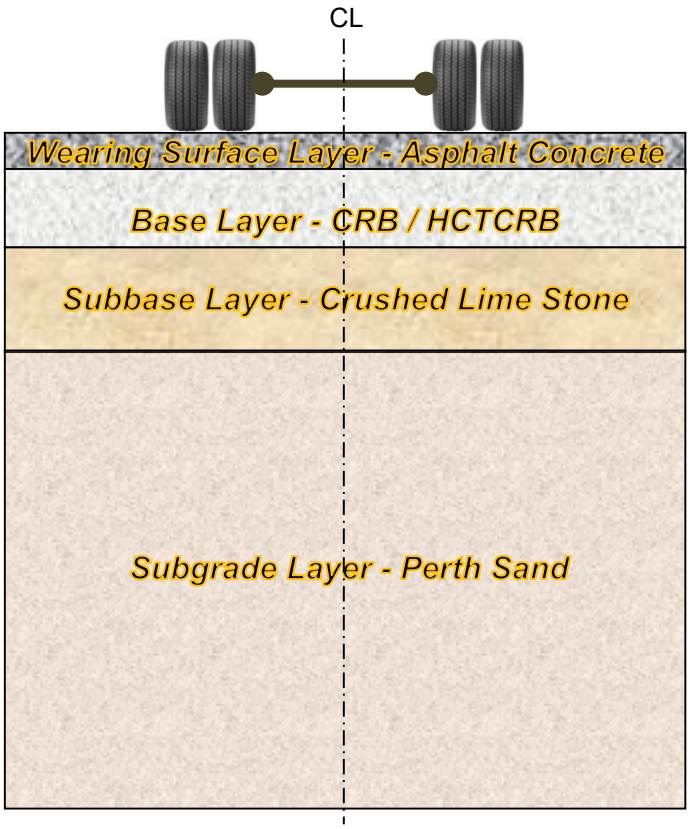

Figure 2.1 A flexible pavement structure in Western Australia

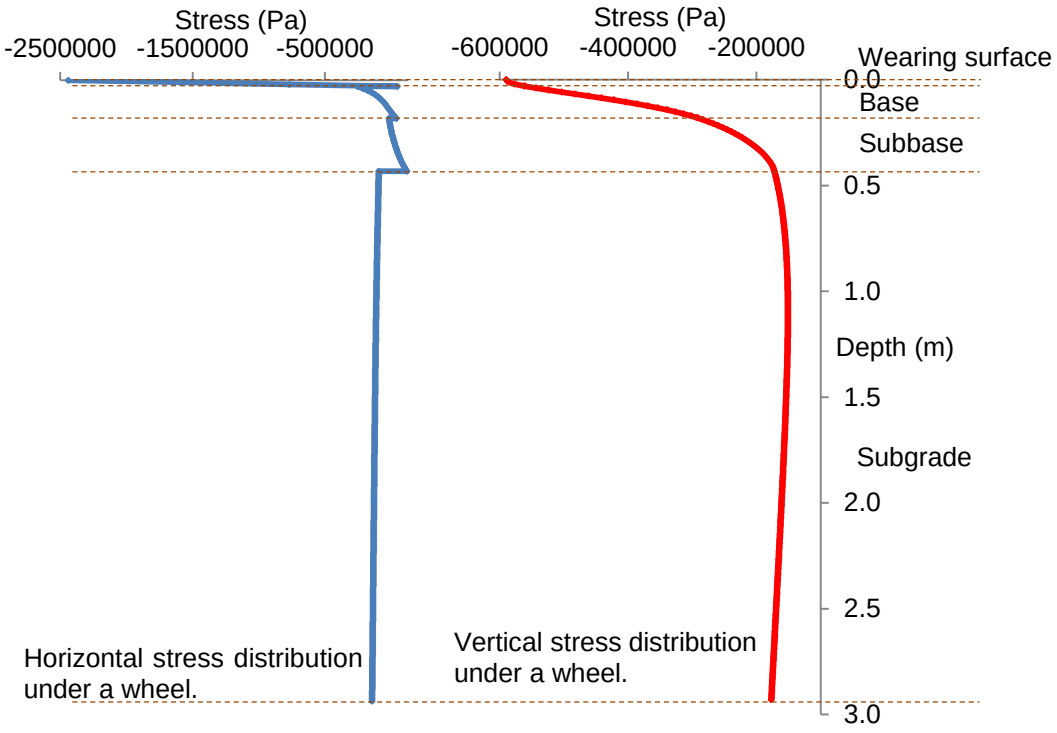

Figure 2.2 Stress distribution under a wheel in pavement structure

2.3 Base course materials

2.3.1 Crushed Rock Base

Crushed rock (as seen in Figure 2.3) is commonly used as base course material by most of road agency around the world (Werkmeister et al. 2004; Hefer and Scullion 2005). Although the composition of CRB would be varied up on the source of manufacturing, its basic aspects should be consistent. Normally, CRB comprises both fine and coarse aggregates which are produced by crushing sound unweathered rock. The mixture of natural sand or clayey sand with crushed rock fragments or crushed rock fragments is classified as fine aggregate and the fragments which are durable, hard, angular and clean are classified as coarse aggregate (Main Roads Western Australia 2010).

Figure 2.3 Dry crushed rock base (CRB)

2.3.2 Hydrated Cement Treated Crushed Rock Base

HCTCRB was prepared by mixing a standard crushed rock base (CRB) (Main Roads Western Australia 2003b) with 2%, by weight, of GP Portland cement following the standard of AS 3972-1997 (Australian Standards 1997). As seen in Figure 2.4, HCTCRB was kept in the range of -1.0% to +2.0% of the optimum

moisture content (OMC) of CRB as stated in MRWA Test Method WA 133.1 (Main Roads Western Australia 1997).

Figure 2.4 Hydrated cement treated crushed rock base (HCTCRB)

2.4 Analysis of pavement structure

There are many theories that have been used for the analysis of pavement structure, one of which is the theory of beams and plates on elastic foundations (Hetenyi 1979; Timoshenko and Woinowsky-Krieger 1959; Ventsel and Krauthammer 2001; Timoshenko 1940b, 1940a). This theory is the most classical, and the method used is the fully mechanistic approach to the analysis of pavement structure, the reason being that analytical models are derived from the flexural behaviour of the structural section. The governing differential equation of beams on elastic foundations is derived from the interaction between the structure and the subgrade reaction, as illustrated in Figure 2.5.

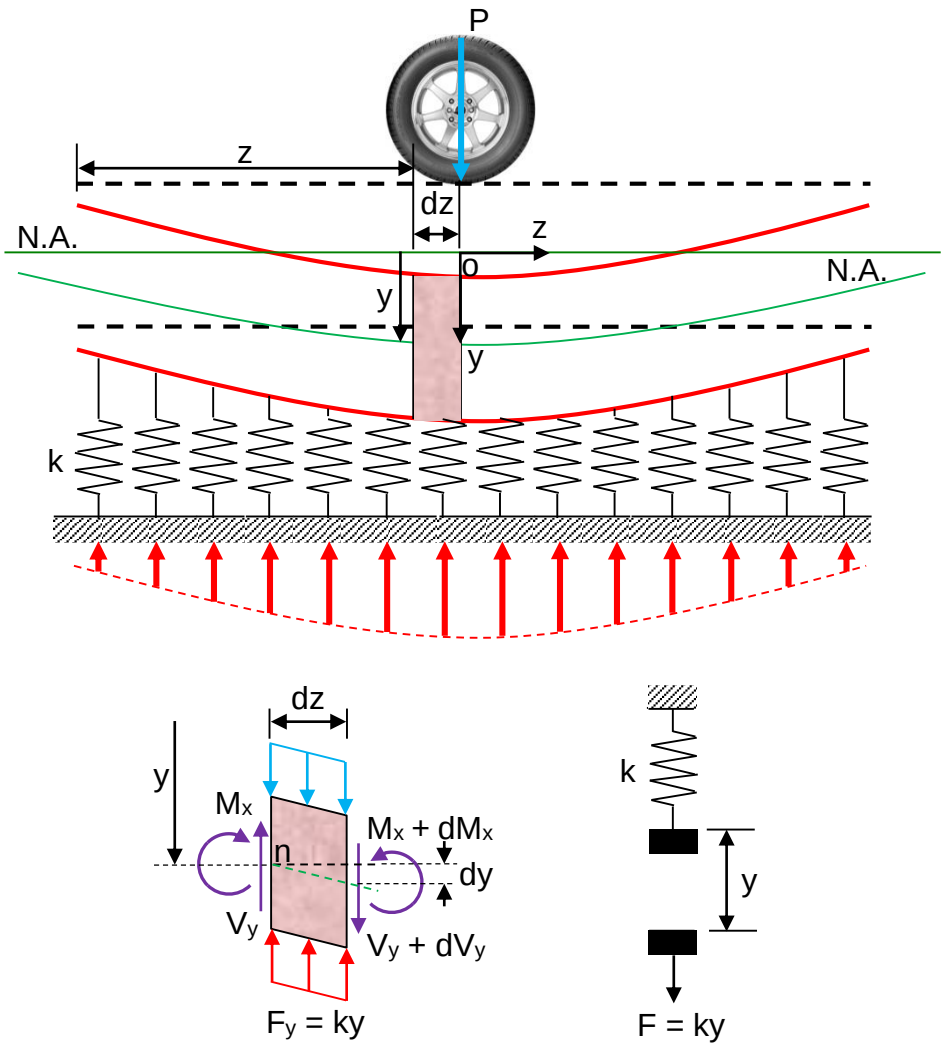

Figure 2.5 Free body diagram of beams on elastic foundations and forces system

The first model to represent the interaction between structure and soil foundation was introduced by Professor Dr Emil Oscar Winkler around 1867 (FRÝBA 1995). Although Winkler's foundation is the simplest model, it has frequently been used as a fundamental model in the development of an advanced model of substructural interaction. Winkler's foundation assumes that the subgrade foundation behaves like an isolated elastic spring in which its ability to resist both tensile and compressive force are identical. Hence, the reaction of the foundation against the applied loading on the structure is in linear proportion to the deflection point. Therefore the mathematical modelling of beams on elastic foundations can be written as Equations (2.1) - (2.4).

$$\frac{dy}{dz} = \theta_x \tag{2.1}$$

$$\frac{d\theta_x}{dz} = \frac{d^2 y}{dz^2} = -\frac{M_x}{EI_x} \tag{2.2}$$

$$\frac{dM_x}{dz} = -EI_x \frac{d^3 y}{dx^3} = V_y \tag{2.3}$$

$$\frac{dV_y}{dz} = -EI_x \frac{d^4 y}{dx^4} = F_y = ky \tag{2.4}$$

The general solution of Equation (2.4) can be expressed as

$$y = e^{\beta z}\left(C_1 \sin\beta z + C_2 \cos\beta z\right) + e^{-\beta z}\left(C_3 \sin\beta z + C_4 \cos\beta z\right) \tag{2.5}$$

where $\beta = \sqrt[4]{\frac{k}{4EI_x}}$, and C_1 , C_2 , C_3 , C_4 are the constants which can be determined using the boundary conditions of the beam.

The distribution of subgrade reactions, deflections, shearing forces, bending moments of an infinite beam resting on elastic foundation can be depicted as seen in Figure 2.6. The theory of beams on elastic foundations has long been used for the analysis and design of railway structures. As mentioned earlier, the theory of plates on elastic foundations has also been used for some time for the analysis and design of road pavement. Although the exact solutions can be obtained by the use of this method, difficulties are still presented in terms of solving the differential equations of pavement structure, as the structural system and traffic loading conditions are complex. Consequently, classical analysis has been replaced by numerical analysis such as the finite element method, as this method is very conveniently able to simulate such complicated structures by using a computer. In the era of computer simulation, the resilient modulus (M_r) is commonly used to represent the elastic property of a material, as the behaviour of the material can be captured far more accurately than by using the static modulus.

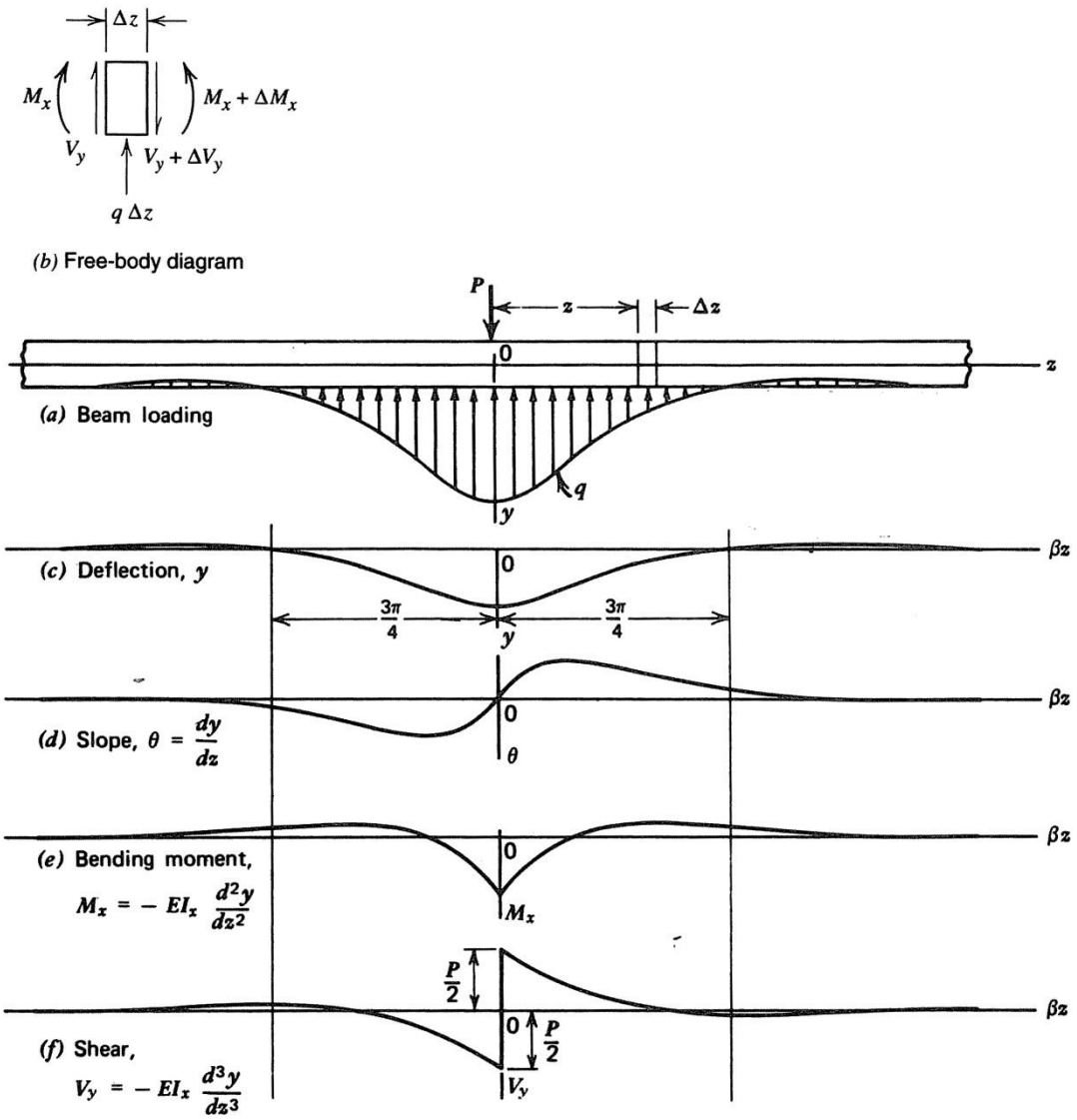

Figure 2.6 Infinite beam on an elastic foundation and loaded at origin (Boresi and Schmidt 2003)

Since traffic load is somewhat of a cyclic force, there are therefore several theories which attempt to explain the response of materials to this type of loading using the resilient modulus concept, one of which is the shakedown approach. For road pavements that contain a thin asphalt concrete layer, the wearing surface may be neglected from the structural system in that the wearing surface functions as a covering. Therefore the composite structural members can be assumed to be made up of unbound granular types of material (UGM), and the structural system can be modelled as stress

dependent, as well as elastic. The plastic aspect can be applied to the material properties by using the Mohr-Coulomb state to define the failure criteria. The shakedown approach is a rational theory which can be used to predict various modes of failure for UGM in the structure of a pavement and the approach has the capability to assess the effects of various design factors (Collins and Boulbibane 1998).

According to Werkmeister's classification (Werkmeister et al. 2005), there are three range of materials responses to cyclic loading (as shown in Figure 2.7), namely (A) plastic shakedown, (B) intermediate response – plastic creep, and (C) incremental collapse. Range A is commonly used as an allowable regime for pavement design as the summation of accumulated strain is relatively small and there is no more permanent strain developed at this level of applied stress. Range B is somewhat of a transition zone, most of the strain rate is nearly constant and the permanent strain can be observed as a linear rise. However, material failure can occur at this applied stress level if the cyclic loadings are continuously performed over a long enough period. Range C is opposite to range A in terms of strain - it is not appropriate for pavement design as the permanent strain rate continuously increases without cessation at this level of applied stress. If range C were used, the road pavement would fail by rutting due to the shear deformation in the layer of UGM.

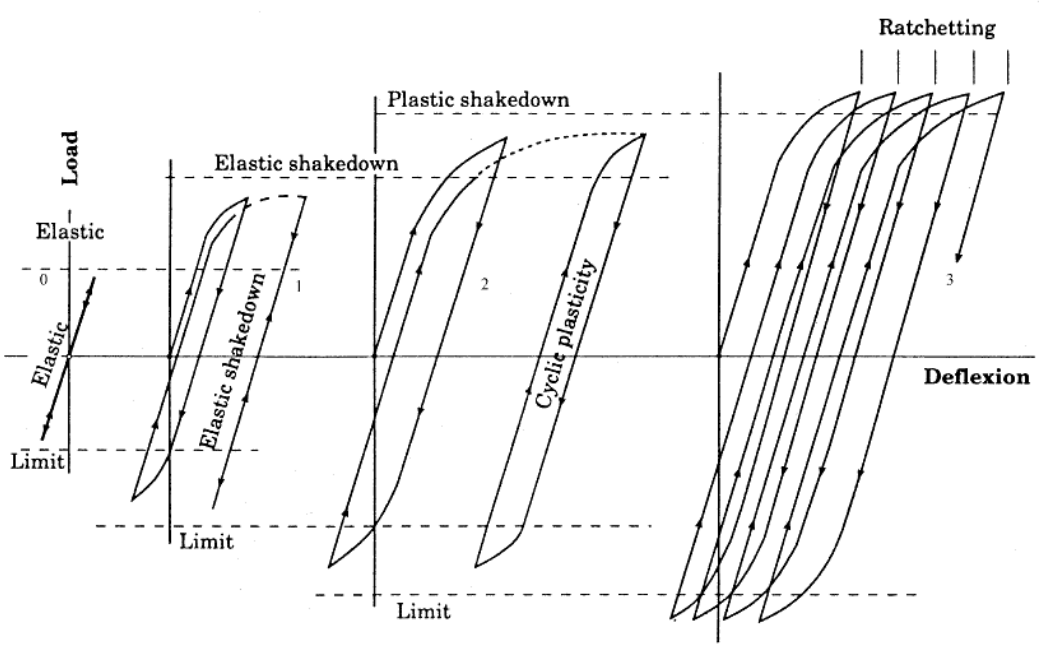

Figure 2.7 Illustration of shakedown concepts (Wong et al. 1997)

Nowadays, most of the approaches to pavement analysis still rely on the elastic materials assumption as it is consistent with the working stresses condition. One of the important elastic properties of materials, widely used by engineers for the analysis of pavement structure, is the resilient modulus (M_r). The resilient modulus is similar to the elastic modulus of materials but there are differences in both purpose and formulation, as seen in Figure 2.8.

The elastic modulus is usually used for analysis of structure subjected to static loading, while the resilient modulus is more suitable for structural systems subjected to cyclic loading, such as road pavement. The elastic modulus can be determined from the slope of the elastic portion of the stress-strain curve obtained from the static load test, as shown in Figure 2.8(b). The resilient modulus is calculated by dividing the deviatoric stress by the recoverable strain as shown in Figure 2.8(a) and can be written as:

$$M_r = \frac{\sigma_d}{\varepsilon_r} \tag{2.6}$$

where σ_d is the deviatoric stress and ε_r is the recoverable strain.

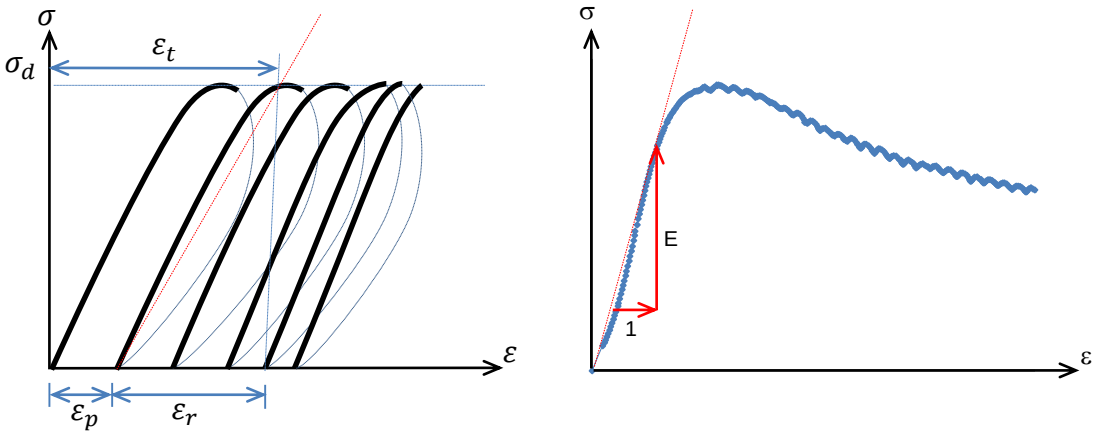

(a) (b)

Figure 2.8 The modulus of materials; (a) resilient modulus and (b) elastic modulus

As design criteria, resultant stress distribution and permanent deformation (rutting) are relatively recent. A number of material models for predicting the resilient modulus and permanent deformation have been developed by engineers over the past 50 years. These are discussed below.

2.4.1 Models for prediction of resilient modulus

The first well-known model, widely used by engineers, is the *K*-*θ* model. This model, which has been in used since 1962, was introduced by Seed et al. (1962). It is a nonlinear model based on a stress-dependent power function. The model uses a curve-fitting approach with regression constants k_1 and k_2 as shown in Equation (2.7).

$$M_r \text{ (MPa)} = k_1 \, \theta^{k_2} \tag{2.7}$$

where σ_1 is the axial stress (kPa), σ_2 is the confining stress (kPa), σ_3 is the confining stress (kPa), and θ is the bulk stress (= $\sigma_1 + \sigma_2 + \sigma_3$).

The shear stress effects in granular materials are neglected in this model which was further developed and later introduced by Uzan (1985). As seen in Equation (2.8) the effect of shear stress on the resilient modulus is taken into account in the model.

$$M_r \text{ (MPa)} = k_a \left(\frac{\theta}{p_0}\right)^{k_b} \left(\frac{\sigma_d}{p_0}\right)^{k_c} \quad (2.8)$$

where σ_d is the deviatoric stress (= σ_1 - σ_3), p_0 is the unit reference stress (1 kPa), and k_a, k_b, k_c are the material constants obtained from the RLT tests.

Although both the *K*-θ and the Uzan model are practical models for the analysis and design of flexible pavement as the resilient modulus can be reasonably predicted, the models are still based on a mechanistic-empirical approach.

2.4.2 Models for prediction of permanent deformation

Similar to the resilient modulus of UGM, an aspect of permanent deformation behaviour is stress dependence. Many models have been formulated to predict permanent deformation, one of which is the model proposed by Lekarp and Dawson (1998). Their model was formulated based on the relationship between the length of the stress path, the ratio of maximum shear stress, and the accumulated permanent axial strain, as seen in Equation (2.9).

$$\frac{\varepsilon_{1,p}\left(N_{ref}\right)}{\left(\frac{L}{p_0}\right)} = a \cdot \left(\frac{q}{p}\right)^{b}_{max} \quad (2.9)$$

where $\varepsilon_{1,p}\left(N_{ref}\right)$ is the accumulated permanent axial strain at a given number of N_{ref} ($N_{ref} > 100$), L is the length of the stress path (kPa), q is the deviatoric stress (kPa), p is the mean normal stress (kPa), $\left(\frac{q}{p}\right)_{max}$ is the maximum stress ratio, a and b are the regression constants.

However, this model is still quite complex when comparing to Sweere's model (SAMARIS 2004), which was introduced through SAMARIS project. Sweere's model is a nonlinear equation based on the number of cyclic loading power functions. This model is developed using a curve-fitting approach, in terms of regression constants as shown in Equation (2.10).

$$\delta_p = a \cdot (N)^b \quad (2.10)$$

where δ_p is the permanent vertical displacement, a and b are regression constants, and N is the number of cycle of repeated loading.

However, Sweere's model is suitable for predicting the permanent deformation of UGM subjected to single applied stress configuration. The reasonable result of prediction would not be obtained by this model as seen in Figure 2.9.

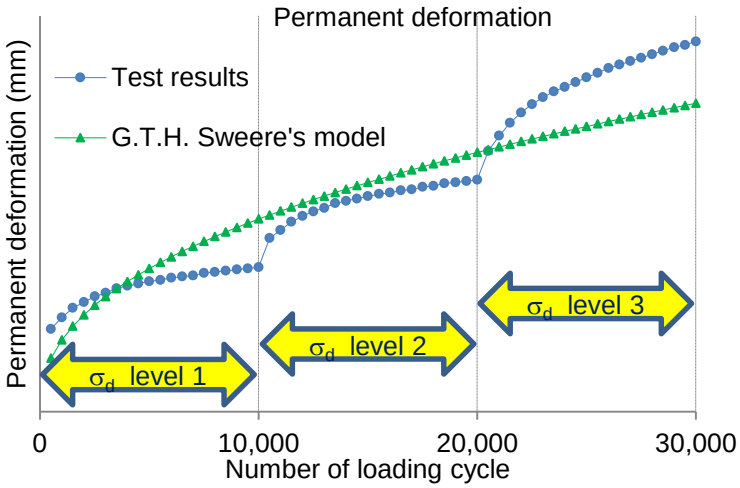

Figure 2.9 Illustration of the permanent deformation testing results and the use of Sweere's model

It can be observed that all models above rely on curve-fitting technics, or mechanistic-empirical approach.

2.4.3 Models for finite element analysis

In a new era of engineering analysis, the finite element method (FEM) is a powerful tool widely used by engineers in many fields of engineering behavioural investigation, including that of structural pavement. Although only approximate solutions can be obtained due to the numerical method being predominantly used (Chandrupatla and Belegundu 2002), analysis results are generally reasonable and acceptable to engineers. In addition to the models outlined in the previous sections, many material modelling approaches have been proposed by researchers for use with the finite element (FE) analysis of pavement structure and these models include the linear elastic, nonlinear elastic, viscoelastic, elastoplastic, and plastic models. There is no particular

model that is superior, as the choice of model depends on the aim of the case of analysis. Although the elastic assumption is the simplest, it has been commonly used up until now by engineers as the working stress conditions under traffic loading can be easily obtained.

In general, there are three types of finite element (FE) modelling that are usually employed for analysis of pavement structure, namely plane strain, axisymmetric, and three dimensional (3-D) model. Cho et al. (1996) investigated the difference of analysis results between these three models and found the axisymmetric approach to be an appropriate model for FE analysis of structural pavement. This model provides reasonable solutions when used for pavement section where the traffic loads are some distance from special boundary conditions such as cracking or edges. As with the 3-D model, the axisymmetric approach gives reasonable stress results consistent with the layered elastic theory when boundary conditions and structural geometry are strictly controlled. This is opposed to the plane strain approach, commonly used by engineers, but ineffective at solving stress distribution issues.

Hadi and Bodhinayake (2003) conducted a preliminary study in 2003 to compare the FE analysis results from ABAQUS/Standard software. The linear and nonlinear elastic materials assumptions regarding pavement structure were compared, along with the effects of static and cyclic loadings on the analysis results. The results indicate that when cyclic loadings were applied to a pavement structure together with nonlinear elastic material, the resultant deflection at the top of the subgrade layer was higher than when the pavement was subjected to static loading, whether linear or nonlinear elastic properties were assumed. This finding implies that a pavement structure may fail before its design life if linear elastic materials and static loadings are used for structural analysis. Moreover, the aforementioned study shows that the real deflections from field measurements were nearly identical to the results from the FE analysis using cyclic loading and a nonlinear elastic assumption.

Taha and Cyrille (2005) proposed a simplified model, using the finite element method to predict the rutting of road pavement. Their model was developed

further from Zarka and Casier's model (Zarka and Casier 1979) which is based on the shakedown theory and still relies on the mechanistic empirical approach. They used the plastic potential of von Mises and Drucker–Prager yield criteria with a linear kinematic hardening to develop the hardening modulus as

$$H = 10^{\left[(c+1)\log\left(\frac{p}{p_a}\right)+\log\left(\sqrt{1+\left(\frac{q}{p}\right)^2}\right)+d\right]}p_a \quad (2.11)$$

where p_a is the atmospheric pressure, c and d are material parameters.

Equation (2.11) is useful for the analysis of flexible pavement using the finite element method as it can be used to determine the hardening modulus of UGM at any mean stress p_{max} and at any $\frac{q}{p}$ which is employed for the calibration of finite element modelling.

The research carried out by Hurrman, et al (2007) reveals that the utilisation of the FEM for pavement analysis, both on a structural scale and a mixture scale, could predict the responsive behaviour of pavement structure which is related to the trinity of material properties, loading condition, and geometry of pavement section. Furthermore, they found that the accurate prediction of σ and ε are compulsory when utilising the mechanistic design approach.

Minkwan, et al (2009) studied the use of nonlinear materials modelling for FE analysis to investigate the differences between axisymmetric and 3-D FE modelling. The commercial program GT-PAVE and ABAQUS were selected and the Uzan model was used to model the UGM response in pavement structure. Their results reveal that critical pavement response can be predicted accurately by using the appropriate model for characterising the nonlinear behaviour of UGM, and that the nonlinear model is suitable for designing airfield pavement when using the results from 3-D finite element analysis. Furthermore, it was found that pavement analysis using an axisymmetric model is more conservative than a 3-D model as the effects of σ_2 on the behavioural responses of materials are ignored, and higher stress and strain are obtained.

2.5 Flexible pavement design

There are currently two types of road pavement commonly used by most road agencies; rigid pavement and flexible pavement. The major difference between these two types of pavement is the wearing surface. The wearing surface in rigid pavement is normally made up of reinforced concrete (RC) whereas asphalt concrete is usually used in the wearing surface of flexible pavement. As stated in the title of this dissertation, this research places its emphasis on flexible pavement, and will not examine rigid pavement in any detail.

The wearing surface is the main part of the pavement structure that can be used for classifying the quality of road used by the motorist. The roughness or smoothness of the pavement is often adopted as a measure for judging the adequacy and condition of a road. The Western Australian road network mostly comprises flexible pavements in which the thickness of the asphalt layer is relatively thin. Therefore the base layer plays a major role in resisting traffic loadings in a structural system, then distributes the stresses to the supportive layers below. A schematic of a pavement structure can be seen in Figure 2.10.

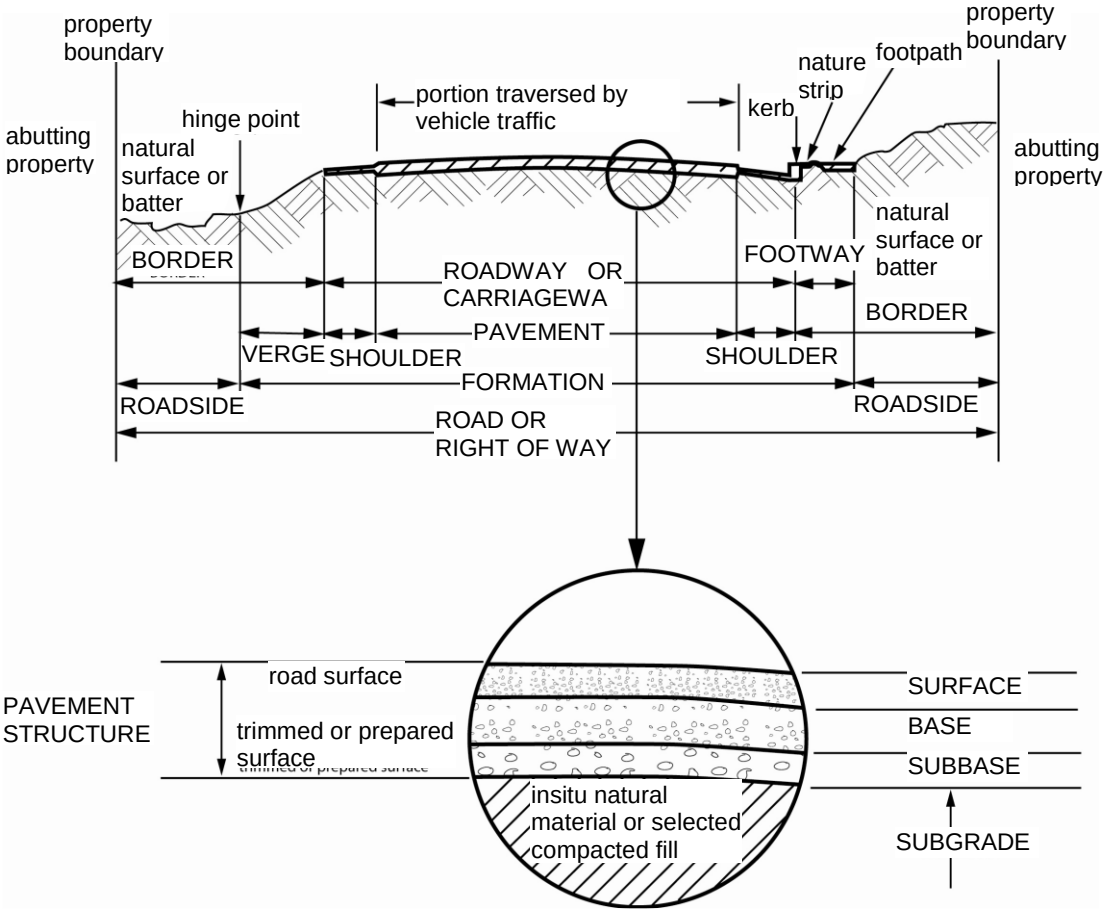

Figure 2.10 Pavement structure and its role in the road formation (AUSTROADS 2008)

The function of the wearing surface layer of pavement is to protect the supportive layer below from environmental effects such as excess water which may penetrate from the surface to the lower layers, while the surface itself is able to carrying traffic loads without failing. The thickness of the wearing surface can be varied from 25 mm for low traffic loads to up to 150 mm or more for heavy traffic loads.

A wearing surface layer is supported by a base course layer which is the main flexural member in pavement structure. It is the base course layer which is fundamental to the effective carrying of traffic loads. Its function is to prevent the resultant stresses and strains that occur when a structural system undergoes excessive deformation and shear failure.

The subbase layer is usually positioned on top of the subgrade, between the base course layer and the subgrade. It provides a more suitable working surface for man and machine than the fragile subgrade. Its main function is to prevent intrusion between the base course layer and subgrade, and it provides additional thickness to the pavement section.

The subgrade behaves like a foundation in a structural system. It is commonly made up of in-situ soil that may comprise compacted fill located during earthworks. If the natural soil should contain unsuitable characteristics it can be stabilised. The stabilised subgrade section is generally considered as a lower subbase layer.

2.5.1 Empirical Approach

The method for the analysis and design of flexible pavement has been continuously developed for over a century. In the past, most road was constructed using gravel and natural soil as the materials in structural pavement. The design criteria were based on the shear strength of selected materials and the empirical (or traditional) approach was widely employed by engineers. The empirical (E) approach is still being used in numerous countries as it is the simplest method, but it may result in costly construction. The use of the empirical approach to design pavement structure is based on finding suitable thicknesses for the layers above the subgrade. The subgrade must provide sufficient strength to prevent failure caused by excessive shear stress, and shear failure must not occur in these layers. These are the fundamental concepts of the California Bearing Ratio (CBR) design method (AASHTO 1993a, 2008; American Society for Testing and Materials 2009, 2007), which relies on the CRB design charts, as shown in Figure 2.11. The shear strength of materials is estimated by the use of the CRB value, and the number of vehicles per day is characterised as traffic load. The guide for the design of pavement structure under various conditions of traffic loading, climate, and materials has been available since the 1960s, in which the results from CBR tests on materials were employed to construct the design charts. Hence, the empirical approach, which only uses experiences or index

properties like the CBR value as the key input factors, concerns only the limitation of overall deflection of pavement structure and the ultimate working shear stresses in materials (Huang 1993).

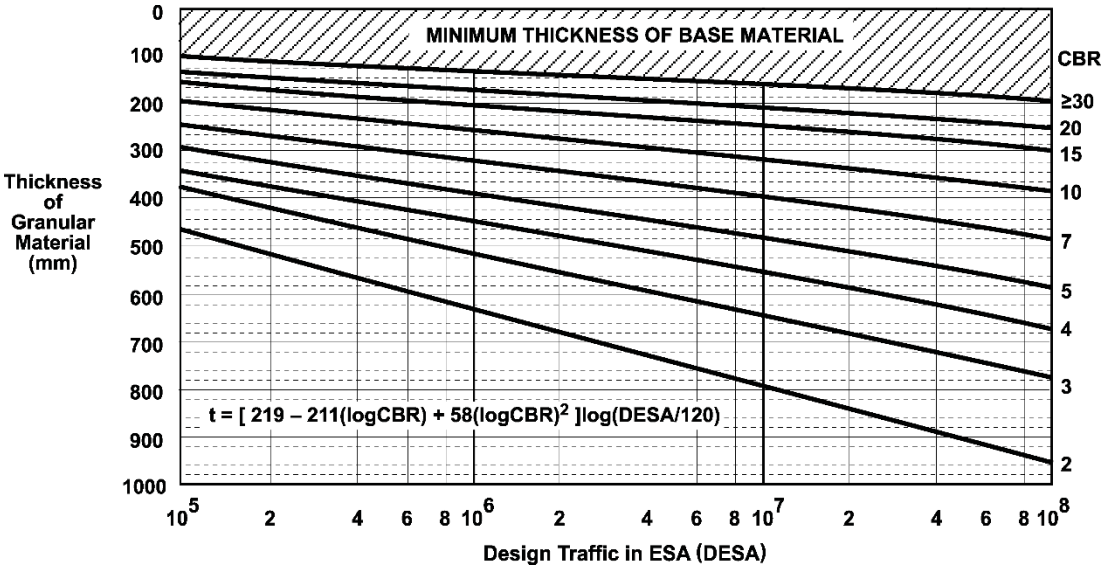

Figure 2.11 Design chart for granular pavements with thin bituminous surfacing (AUSTROADS 2008)

As mentioned above, only the experiences or the results from simple tests such as the CBR value, confined compressive strength (shear strength), aggregate durability, moisture content or particle size distribution - which comes from the static tests, are employed in the empirical approach. Therefore realistic material behaviours such as stress-strain distribution and displacement during cyclic loading, or any consideration of multidimensional geometry in a multilayered structural section are neglected. Wolff and Visser (1994) stated that it is too simple to use only static indices in which the realistic behaviour of pavement structure cannot be explained, as the nonlinear responses of UGM cannot be taken into account in the design formula.

2.5.2 Mechanistic-Empirical Approach

Although the empirical approach, which relies on the soil classification system (AASHTO 1993b), has been used up until now, many engineers have continuously tried to achieve the mechanistic approach over the past 40 years.

Engineers believe that the mechanistic (M) approach to pavement analysis and design should be the most effective solution, and that it can fulfil many requirements by providing such benefits as economical pavement sections, environmentally friendly construction and motorist satisfaction. This explains why many researchers have dedicated their efforts toward developing mechanistic models for pavement materials. Another benefit that mechanistic models provide is the ability to explain the actual behaviour of pavement structure under working conditions where cyclic loadings are applied. All mechanical properties such as the stress-strain relationship, the resilient modulus and the permanent deformation can be determined accurately from sophisticated tests whereby real pavement conditions can be simulated in testing protocols (Collins et al. 1993).

As a completely mechanistic approach has not yet been fully developed, only the mechanistic–empirical (M-E) approach has been in established use up until now. In the M-E approach, both analytical solutions and empirical formulae are employed. The first step in this type of approach is to analyse the pavement structure using a mechanistic model such as the finite element method applied with a multi-layered model in which linear elastic, nonlinear elastic (e.g., the resilient modulus), or elastoplastic models such as the hardening, von Mises, and Mohr-Coulomb models are taken into account (Vermeer 1982). The analytical results from the first step are then adopted and input into the empirical formulae in the next step. The second step is where the resultant stresses and strains are input into the empirical formulae to find permanent deformation, cracking, damage and an allowable number of repeated cyclic loads. A suitable thickness for each layer is finally determined. Although this approach has more advantages than the empirical approach, the predictions of distress, which are calculated by the use of empirical formulae, may be inaccurate due to an anisotropy and non-homogeneity of materials. This includes multidimensional geometry, which strongly depends on stresses, strains, number of load repetitions, time, and environmental factors; elements which are often neglected. The nonlinear elasticity or plasticity of materials, which represents the interaction between traffic loadings and pavement

structure, is adopted in the M-E approach via two input parameters only, i.e., the resilient modulus and the corresponding permanent strain. Figure 2.12 shows the current design criteria for the M-E approach, namely: the horizontal tensile strain in the bottom fibres of the wearing surface layer and in the top fibres of the subgrade (this induces cracking on the surface), and the vertical deformation (both recoverable and permanent deformation) along the vertical section under a wheel load. There are three elements, with the exception of the UGM layer, which are often ignored, but they are considered as essential to the design criteria for pavement structure:

a. the horizontal tensile strain in the bottom fibres of the wearing surface layer
b. the horizontal tensile strain in the bottom fibres of the base or subbase layer that uses cemented materials
c. the vertical compressive strain in the top fibres of the subgrade

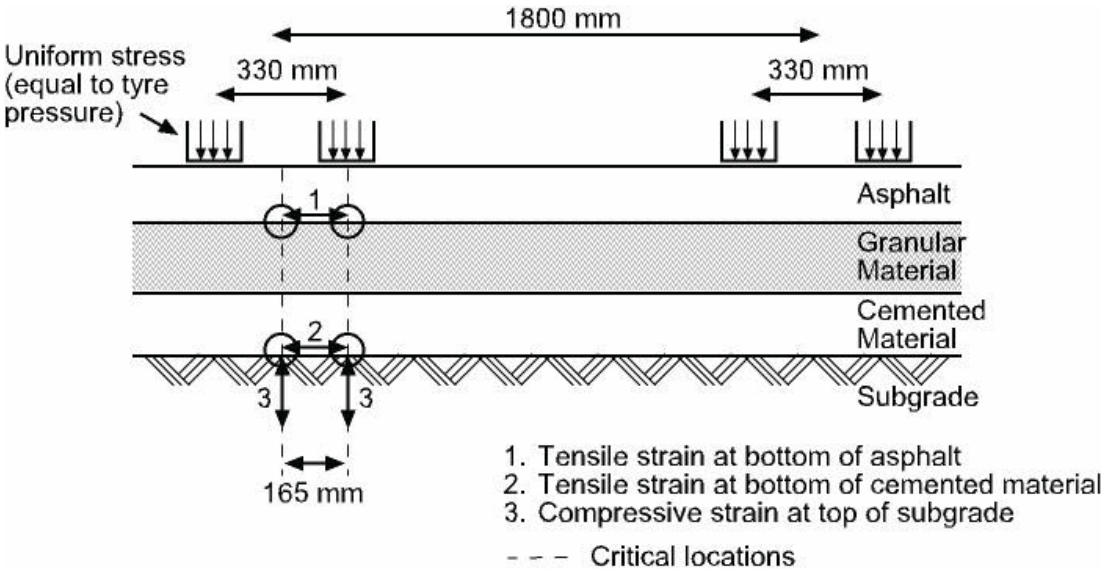

Figure 2.12 Structural model of flexible pavement and its design criteria (AUSTROADS 2008)

Since 1992, the M-E approach, which uses the resilient modulus as an input parameter, has been widely used by several road agencies in Australia (Youdale 2009). In addition, several computer programs have become effective tools for pavement analysis and design. These include CIRCLY, HIPAVE, ILLI-PAVE, MICH-PAVE, etc. CIRCLY (Mincad Systems 2012) which

are widely used for analysis and design of pavement structure in Australia and its algorithm is taken to be a mechanistic approach which is used by pavement engineers. The procedure used in CIRCLY can be illustrated in Figure 2.13 and can be explained as:

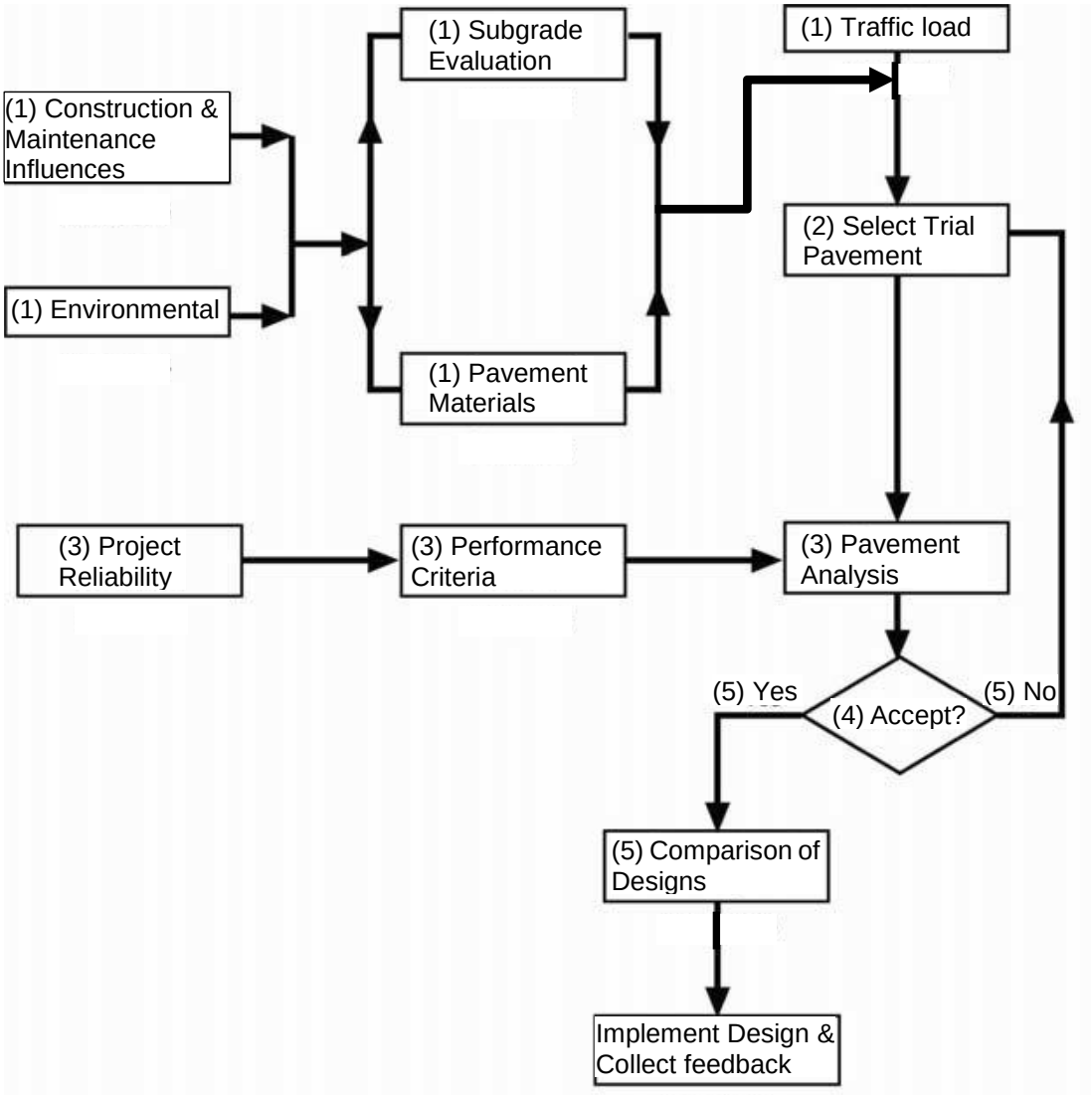

Figure 2.13 Mechanistic-Empirical design procedure for flexible pavement (AUSTROADS 2008)

Step 1 Determine the input parameters such as material properties, environmental effects, traffic load conditions, etc.

Step 2 Assume a preliminary structural section of road pavement.

Step 3 Find the number of allowable traffic load by analysing the preliminary pavement section.

Step 4 Compare the results from Step 3 based on the design criteria

Step 5 If the results in Step 4 are not satisfy, re-design the pavement structure by using the previous results as guide and repeat Step 2 to 5 until all results are acceptable.

However, the method suggested by Austroads (AUSTROADS 2008) which uses the CIRCLY program, should be considered as a mechanistic-empirical approach as the theory of structural mechanics is employed only for the analysis of pavement structure but the design steps still rely on empirical formulae. The number of allowable load repetitions (or traffic loadings) which is the design criterion, is calculated by the use of empirical formulae that come from the experimental results or experiences. The intention of these formulae is:

- to prevent fatigue in asphalt concrete materials,

$$N_{allowable} = RF\left[\frac{6918\left(0.856V_b + 1.08\right)}{\mu\varepsilon S_{mix}^{0.36}}\right]^5 \quad (2.12)$$

- to prevent the fatigue occurs in cemented materials,

$$N_{allowable} = RF\left[\frac{\frac{113000}{E^{0.804}}+191}{\mu\varepsilon}\right]^{12} \quad (2.13)$$

- to limit the total permanent deformation,

$$N_{allowable} = \left[\frac{9300}{\mu\varepsilon}\right]^7 \quad (2.14)$$

where $N_{allowable}$ is the number of allowable traffic load, RF is the reduction factor, V_b is the volume of binder in asphalt mix (%), S_{mix} is the modulus of asphalt concrete (MPa), E is the modulus of cemented materials (MPa), and $\mu\varepsilon$ is the corresponding micro strain.

Furthermore, as stated in the Austroads guide, this method suits the analysis of structural pavement, where the thickness of the wearing surface layer is at least 40 mm. For pavement with a thin wearing surface layer (< 40 mm), as

commonly constructed in Western Australia, the results from the structural analysis would be inaccurate if the method recommended by Austroads to be employed. Therefore the model for analysis of such pavement structures should be accurately and appropriately formulated.

2.6 Disturbed state concept (DSC)

The DSC was introduced by Professor Desai from the University of Arizona, USA (Desai 2001). The main idea of the DSC is that the responsibility to the loading of a material can be expressed towards the interactions between its components. With the material microstructure consideration, the material self-adjustment causing from decay (Xin et al. 1992) or growth (healing) are formulated through the reference material states in the formed of the relatively intact (RI) or “continuum” state and the fully adjusted (FA) state (Figure 2.14). The behaviour of materials exhibited through the interacting mechanisms of components in a mixture can be expressed in terms of the responses of the components connected through a coupling function, called the disturbance function (D) (Desai 2001). The disturbance of material at an initial state, before the application of an external load, was set up to be zero. Alternatively, in the case that the material has initial anisotropy, microcracking, and flaws, the initial disturbance was set up to be nonzero. The disturbance can be expressed in any functions of engineering terms such as stress, modulus, void, area, mass, velocity.

It is believed that a versatile and unified approach for constitutive modelling of materials can be provided by the DSC. The advantages of the DSC are (Desai 2001; Kim 2009):

1. The DSC provides a systematic hierarchical basis for behavioural characterization of the material because it involves both the RI (continuum) and FA states.
2. The DSC presents a simplified approach with a lower number of parameters because its nature is unified and hierarchical.

3. Most of its parameters have physical meanings and can be determined based on standard laboratory tests.

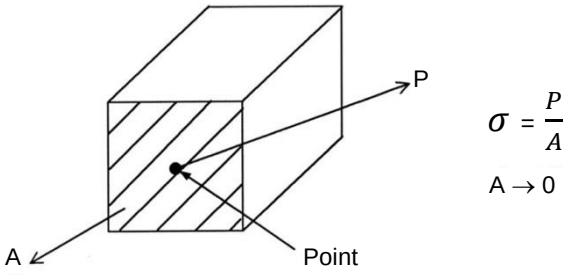

(a) Local

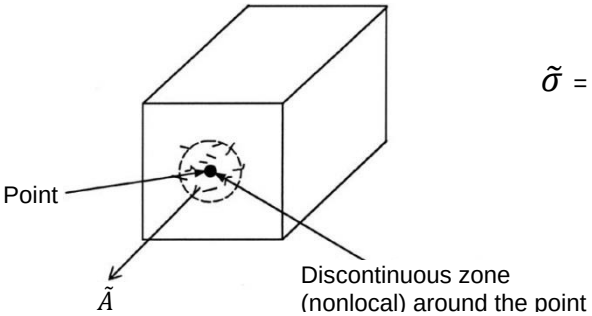

(b) Nonlocal

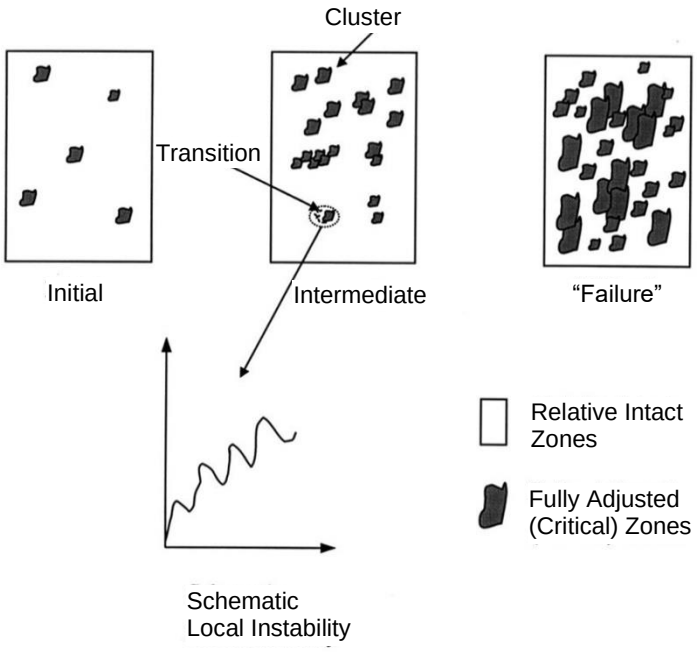

(c) Relative intact and fully adjusted clusters in DSC

Figure 2.14 Definitions of stress. (Desai 2001)

4. The coupled responses, including related factors such as elastic, plastic, and creep stains, microcracking and fracture, softening and healing under mechanical and environmental (for example, thermal and moisture) loadings, are included in the model of material which is obtained by the DSC.
5. The DSC can be applied to both interfaces and joints, and solids (bound and unbound materials).
6. The DSC has been validated and applied to a wide range of materials such as soils, rocks, concrete, asphalt concrete, and alloys (solders).
7. The DSC can be easily applied to the numerical method for engineering analysis such as the finite element method.

2.6.1 Relative Intact (RI) State

The RI state is the defined material state which is the first condition of the material with respect to other subsequent material condition to which the material is subjected to external loading. For example, the linear elastic response of a continuum without micro cracks can define the RI response with respect to the nonlinear elastic response affected by microcracking and the elastoplastic behaviour without friction can define the RI response with respect to the elastoplastic behaviour with friction.

2.6.2 Fully Adjusted (FA) State

For the DSC, it is considered that the FA material possesses strength properties and certain deformation, and the material can also stiffen or gain strength during loading. Therefore, the DSC allows for characterising both stiffening (healing) and degradation (damage or decay) in material responses (Figure 2.15). In general, the FA state can be determined based on the ultimate disturbance, D_u (Figure 2.16), because the FA state cannot be measured in the laboratory. The FA state is supposed to occur in the ultimate range and because the measurement system would stop to operate when a test specimen is “collapsed” from an engineering viewpoint. An approximation procedure must be used for determining the material response at the FA state.

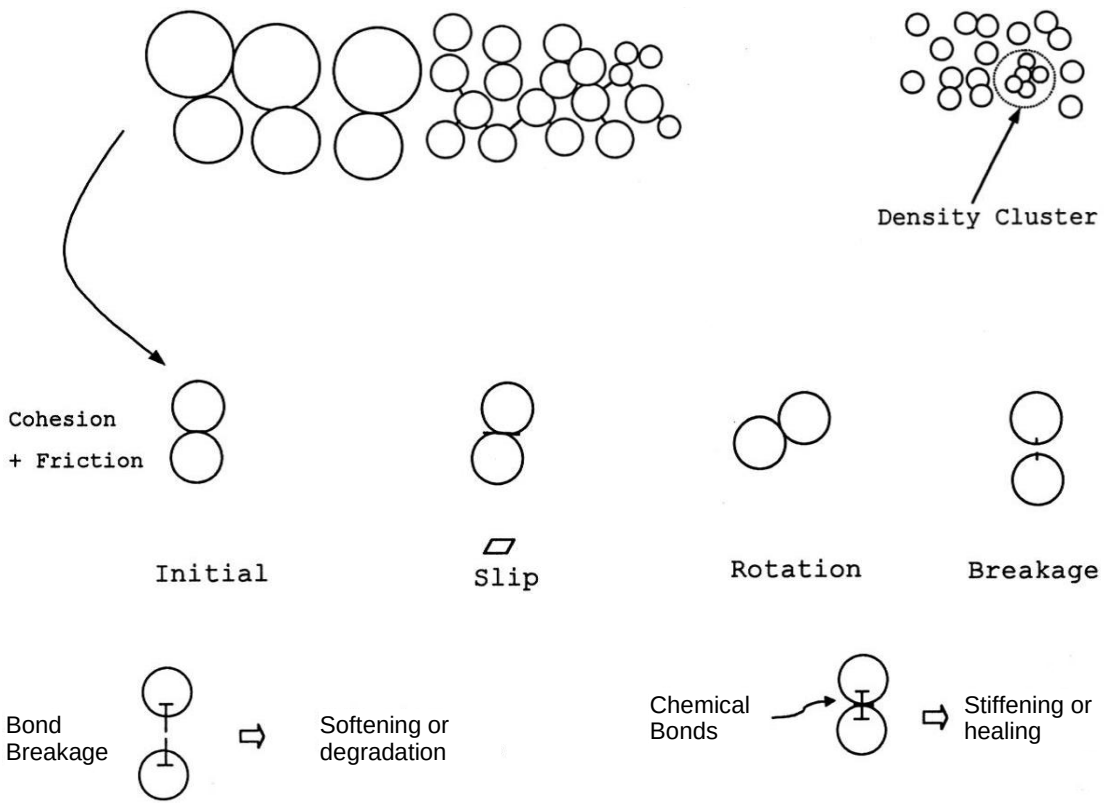

Figure 2.15 Particle motions, degradation or softening, and healing (Desai 2001)

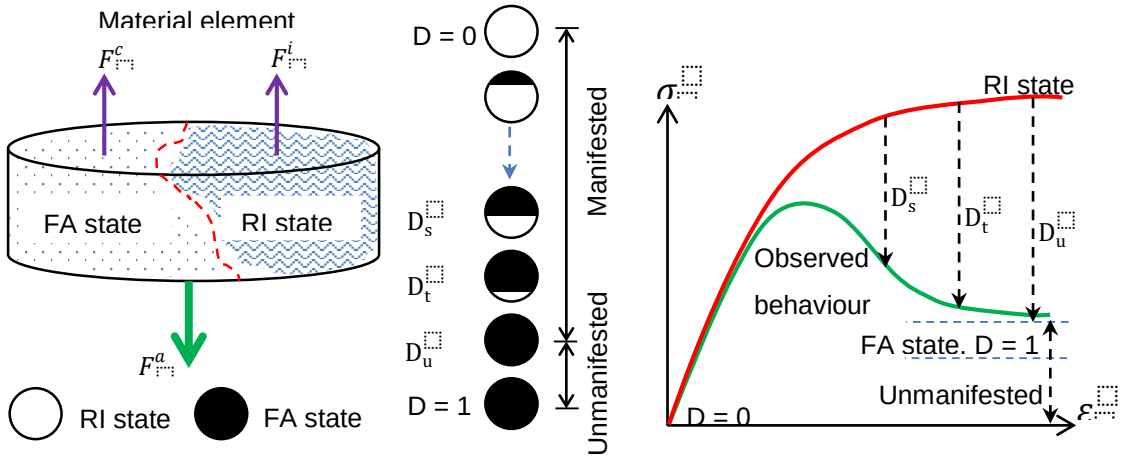

Figure 2.16 Illustration of the fundamental concept of the DSC (Desai 2001)

2.6.3 Formulation of DSC equation

When considering the material element which is based on equilibrium of forces, the element composed of the clusters of particles in the RI and FA states (Figure 2.16) which can be expressed in equation (2.15).

$$F^a = F^i + F^c \tag{2.15}$$

where F^a is the observed force, F^i is the force in the relative intact part and F^c is the force in the fully adjusted part.

When dividing both sides of equation (2.15) by the total area, A (assuming thickness to be unity), also the corresponding area of the RI part and the FA part, A^i and A^c respectively, it can be formulated as;

$$\frac{F^a}{A} = \left(\frac{F^i}{A^i}\right) \cdot \left(\frac{A^i}{A}\right) + \left(\frac{F^c}{A^c}\right) \cdot \left(\frac{A^c}{A}\right) \tag{2.16}$$

or

$$\sigma^a = \sigma^i \cdot \left(\frac{A^i}{A}\right) + \sigma^c \cdot \left(\frac{A^c}{A}\right) \tag{2.17}$$

where σ^a is the observed stress, σ^i is the stress in the relative intact part, σ^c is the stress in the fully adjusted part and A = $A^i + A^c$.

However, the disturbance function can be defined as;

$$D = \frac{A^c}{A} \tag{2.18}$$

And $\frac{A^i}{A} = \frac{(A - A^c)}{A} = 1 - \frac{(A^c)}{A} = 1 - D$ (2.19)

By substituting Equations (2.18) and (2.19) into Equation (2.17) yields

$$\sigma^a = (1 - D) \cdot \sigma^i + D \cdot \sigma^c \tag{2.20}$$

Equation (2.20) could be a general equation for the DSC in a stress form and this equation can also be used to predict the response of the material for analysis and design of structural members.

The disturbance function can be the ratio of interested factors with respect to the FA state. The preceding disturbance function can be expressed in terms of material properties which can be measured from laboratory tests. For instance, if the DSC is used to predict the stress-strain relationship, the disturbance function can be calculated by

$$D = \frac{\left(\sigma^{i} - \sigma^{a}\right)}{\left(\sigma^{i} - \sigma^{c}\right)} \tag{2.21}$$

Over the past two decades, the DSC has been applied with many kinds of materials in an effective manner to model their responses corresponding to their properties, loadings, and oriented conditions. Over a range of DSC-related studies, they reveal that the DSC can be effectively applied to model the behaviour of materials for engineering analysis and design purpose.

Desai and Whitenack (2001) demonstrated the use of DSC for constitutive modelling of materials and interfaces. In their study, cyclic fatigue failure were calculated by using an approximate procedure based on the DSC. The results indicate that the DSC can provide a unified methodology for fracture leading to softening and fatigue failure, microcracking and stress-deformation.

To characterize the influence of parameters in a material model based on the DSC, Desai and Chen (2006) studied the determination of parameters in the unified disturbed state concept constitutive model by using an optimization procedure and then comparing the result with the use of an averaged procedure. The optimized parameters were calculated from the experimental results of multiaxial tests on sand under different densities, stress paths and initial mean pressures. The cyclic behaviour in a boundary value problem was predicted by using a finite element procedure with the optimized parameters. The results reveal that their proposed optimization procedure can improve predictions of the stress-strain and volume change behaviour.

To satisfy the need for unified and mechanistic constitutive models for pavement materials, Desai (2007) introduced the DSC, which is a modelling approach that includes various responses, such as microcracking and fracture, softening and healing, creep, plastic, elastic, etc, within a single unified and

coupled framework. The DSC can be applied to a wide range of pavement materials with validations. Various forms of distress, such as permanent deformations (rutting), microcracking and fracture, thermal cracking, and healing, could be evaluated based on the DSC. A number of problems were analysed by using the DSC with the finite-element (FE) procedure, both in two- and three-dimensional examples. The results showed that the material model, which is based on the DSC and was applied in the FE procedure, provides the novel and unique approaches for pavement analysis. However, further research and applications, including validation with respect to simulated and field behaviour of pavements, need to be performed.

A study by Sane et al. (2008) modelled a tills by using the DSC. The numerical model was performed to simulate and predict the behaviour of the tills with the validation process of comparing what predicted with the experimental results. DSC parameters were calculated from shear and creep tests and were applied to a finite-element simulation. The results from the shear tests reveal that when 85% of the mass reached a fully adjusted state, failure and resulting motion began, and that plastic strain was mostly measured from the time at the starting of loading was started. The gravity-induced motion of a 5000-m long and 100-m thick slab of ice coupled to an underlying 1.5-m thick layer of till setting on a 4° inclination was predicted with the pore-water pressure in the till at 90% of a load. After the peak shear stress, at a shear strain of around 0.75 and induced shear stress around 23 kPa in the till, the critical disturbance at which failure occurs was observed. The occurrence of critical disturbance observed in the laboratory tests compares very well with the numerical prediction of critical disturbance, particularly when the displacement showed a sharp change in rate. After the till underwent plastic strain, failure and initiation of motion could be predicted by the DSC, and it was more accurate than the use of the Mohr-Coulomb model.

To investigate the influence of the material model on the load-deformation behaviour of foundations, Akhaveissy et al. (2009) characterized the constitutive behaviour of soils by predicting the load-deformation behaviour including the bearing capacity of foundations using a nonlinear finite element

method. A Generalized Plasticity Model (GPM) with a non-associated flow rule, and the DSC with the Hierarchical Single-Surface (HISS) plasticity model with an associated flow rule, were employed for calculation. It was found that the behaviours of foundations predicted using both models were in good agreement with the experimental data. These results indicate that the DSC/HISS has certain advantages over the GPM.

2.7 Summary

This chapter discussed the existing knowledge regarding road pavement analysis and design approaches utilised by engineers and researchers. It was panted out that engineers and researchers have attempted to formulate a full mechanistic approach towards the analysis and design of pavement structure but it has not yet been achieved. Although the full mechanistic approach consumes computational effort, the effort is offset by the benefits and the approach is still being developed by engineers around the world. In the present research, a mechanistic approach is proposed by using Disturbed State Concept as a tool for modelling of material behaviour. It is believed that the use of the mechanistic approach to pavement design would lead to a more efficient structure and more economical construction.

CHAPTER 3
LABORATORY WORKS

3.1 Introduction

This chapter presents the mechanical properties of crushed rock base (CRB) and hydrated cement treated crushed rock base (HCTCRB). The mechanical properties included the shear strength parameters investigated through a static triaxial test, and resilient modulus and permanent deformation resulted from a repeated load triaxial test. All laboratory works were conducted in the Geomechanics and Pavement laboratory, Department of Civil Engineering, Curtin University. Details of materials, test methods and laboratory results are described in the following sections.

3.2 Materials and Test Methods

3.2.1 Materials

3.2.1.1 Crushed Rock Base (CRB)

The standard Crushed Rock Base (CRB), used in this study was sampled and collected from a stockpile area of a local quarry (Gosnells Quarry). The basic properties of the material were checked for compliance with the specifications of CRB (Main Roads Western Australia 2003a).

3.2.1.2 Cement

A bagged type of general purpose (GP) Portland cement (Australian Standard 1997), the product of Cockburn Cement (Cockburn cement 2006), was used as a stabilising agent. The chemical compositions of this cement are shown in Table 3.1.

(a) (b)

Figure 3.1 Physical aspects of crushed rock; (a) dry crushed rock and (b) wet crushed rock

3.2.1.3 Hydrated Cemented Crushed Rock Base (HCTCRB)

HCTCRB was prepared by mixing a standard crushed rock base (CRB) with GP cement, approximately 2% by weight of dry CRB, at the optimum moisture content (OMC) of CRB obtained from the MRWA Test Method WA 133.1 (Main Roads Western Australia 1997). The materials were then blended at least 10 minutes, until their colour and texture could be visibly uniform. Then the mixture was placed in sealed plastic bags and kept for 7 days at controlled room temperature of 25 °C. Once achieved the hydration period of 7 days, the hydrated mixture was put in the same mixer again in order to break the cementitious bonds. This process is called “remixing process”, HCTCRB was obtained after finishing this step.

Table 3.1 Chemical composition of Cockburn GP Cement (Cockburn Cement 2007)

Parameter	Method	Units	Typical	Range	AS3972 Limits
Chemical Properties					
SiO_2	XRF	%	20.2	19.8-20.6	-
Al_2O_3	XRF	%	4.9	4.6-5.2	-
Fe_2O_3	XRF	%	2.8	2.6-3.0	-
CaO	XRF	%	63.9	63.1-64.7	-
MgO	XRF	%	2	1.5-2.5	3.5% max
SO_3	XRF	%	2.4	2.1-2.7	-
LOI	AS2350.2	%	2.5	2.1-2.9	-
Chloride	ASTM C114	%	0.015	0.005-0.025	-
Na_2O Equivalent	XRF	%	0.5	0.4-0.6	-
Physical Properties					
Fineness Index	AS2350.8	m^2/kg	400	375-425	-
Normal Consistency	AS2350.3	%	29.5	28.5-30.5	-
Setting Times					
Initial	AS2350.4	mins	135	105-150	45 mins min
Final	AS2350.4	mins	195	165-225	6 hrs max
Soundness	AS2350.5	mm	1	0-2.0	5 mm max
Compressive Strengths					
3 Day	AS2350.11	MPa	38	35-41	-
7 Day	AS2350.11	MPa	48	44-52	35 MPa
28 Day	AS2350.11	MPa	60	56-64	45 MPa

Figure 3.2 Mixing machine uses for HCTCRB manufacturing

Figure 3.3 Physical aspects of HCTCRB

3.2.2 Compaction tests

The modified compaction test, according to WA133.1 (Main Roads Western Australia 2007) was performed to obtain the maximum dry density (MDD) and the optimum moisture content (OMC) of test materials. The OMC and MDD of materials can be graphically determined from a compaction curve, i.e. a relationship of dry density values over the range of moisture contents. For each of moisture content value, material sample was compacted into five equal layers in a standard cylinder mould, 105 mm in diameter and 115 mm in height. Each layer was subjected to a 25-blow of a 4.9-kg rammer and 450 mm in drop height.

(a) (b)

Figure 3.4 Compaction test illustrations; (a) some equipment and (b) compacted sample

3.2.3 Preparation of specimen for static and repeated load triaxial tests

All test specimens for static and repeated load triaxial tests were prepared at 100% of their optimum moisture contents (OMCs) in standard cylinder mould, 100 mm in diameter and 200 mm in height. Each specimen was compacted by dividing material into eight equal layers using the modified compaction method (Main Roads Western Australia 2007). Better bonding between layers was created by scratching the surface of each layer before adding material for the next layer.

Once complete compaction, the cylinder sample was carefully extruded from the mould using a hydraulic extruder. Then the porous stone discs were attached to the top and the bottom ends of the specimen. Consequently, the specimen was placed on the bottom platen of the triaxial cell, and the top load platen was also put on top of the specimen. Finally, the specimen with the top and the bottom platens were wrapped by a rubber membrane and sealed by the rubber o-rings fasten at top and bottom platens.

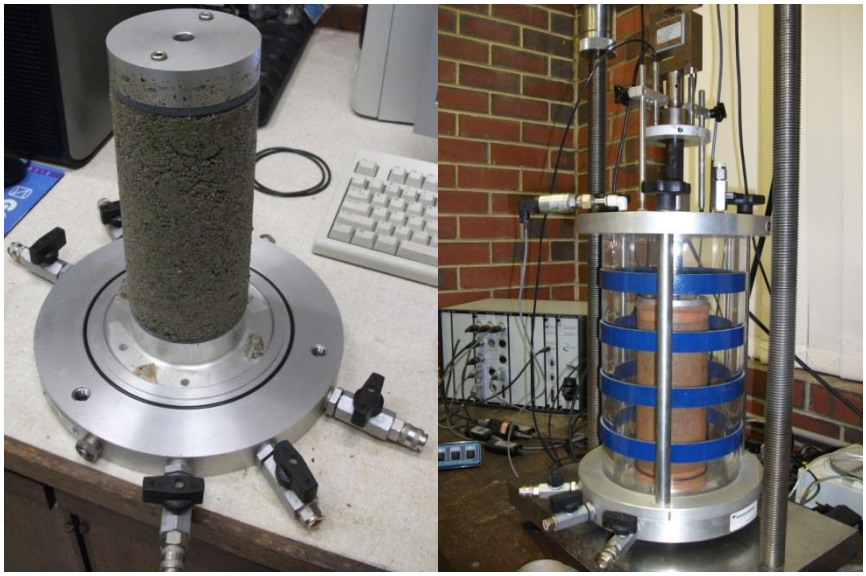

(a) (b)

Figure 3.5 (a) Test specimen on the base of the triaxial cell and (b) RLT test set-up on the universal testing machine (UTM-14P)

3.2.4 Static triaxial test

Static triaxial tests, under drained conditions with no suction measurement during tests, were performed to determine the shear strength parameters, i.e. cohesion (c) and the internal friction angle (ϕ) values of CRB and HCTCRB. In this study, the materials' responses were collected from a set of three constant confining pressures of 0, 25 and 100 kPa for HCTCRB, and 0, 50 and 200 kPa for CRB. A monotonic load applied to test samples at constant strain rate of 1 mm/minute.

3.2.5 Repeated load triaxial (RLT) test

The resilient modulus (M_r) and permanent deformation (PD) were measured, using a repeated load triaxial (RLT) test in accordance with Austroads standard test method AG:PT/T053 (Austroads 2007). The tests were conducted under drained conditions, samples were not saturated and suction measurement was not performed.

The RLT test apparatus comprises a computer with software, a control and data acquisition system (CDAS), a triaxial cell connected with a load actuator, and a confining pressure and linear variable differential transducer (LVDT), as shown in Figure 3.6. The applied stresses and sample information were defined through the interfacing of the computer with the testing software. The cyclic axial stresses and confining stresses were produced from a pneumatic control system capable of accurately applying a defined stress. Two external linear variable differential transducers (LVDTs) were attached to the top of the triaxial cell to measure the axial deformations of the specimens. The repeated vertical force waveform, lasting for a period of 3 s, comprised a load pulse width of 1 s with rise and fall times of up to 0.3 s, as shown in Figure 3.7. During the test, the actual values of deviator stresses, confining stresses, and sample deformations were measured and acquired by CDAS and then transferred to a computer. These values enabled the determination of the resultant stresses and strains in the samples.

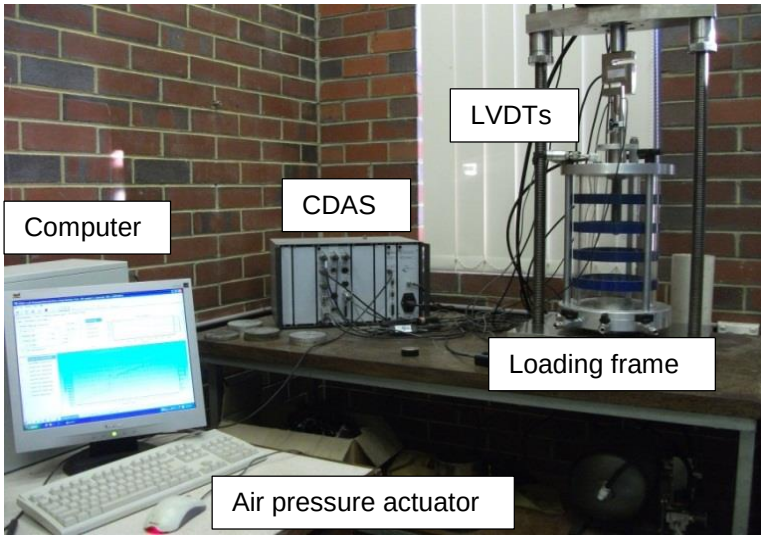

Figure 3.6 RLT test apparatus

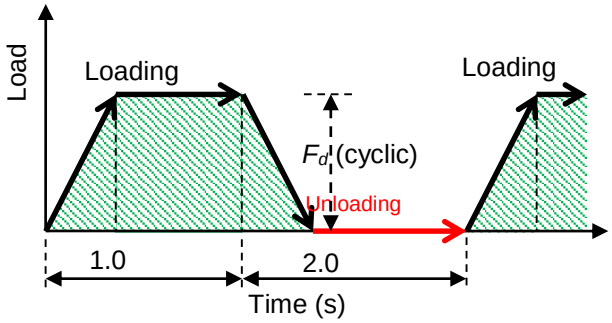

Figure 3.7 The waveform of the vertical deviator stress

3.2.5.1 Permanent deformation tests

Permanent deformation tests were performed at a constant confining pressure (σ_3) of 50 kPa throughout the tests. Each sample was subjected to three stages of deviator stresses (σ_d), 350, 450 and 550 kPa. At each stress stage, the machine applied 10,000 cycles of a vertical force to a sample.

3.2.5.2 Resilient modulus tests

The resilient modulus test was performed with the applied stress condition of 66 stress stages of different deviator and confining stresses to simulate sophisticated traffic loadings. The stress ratio between deviator stress and confining stress (σ_d/σ_3) varied from 2 at the first stage to 25 at the final stage. The deviator stresses varied from 100–600 kPa, while the confining stresses ranged from 20–150 kPa. One thousand loading cycles of pre-conditioning was carried out prior to the tests. The aim of the process was to allow the end caps to bed-in to the specimen and to ensure that the applied stresses and resilient strains became stable under the imposed stress conditions. Subsequently, 66 stress stages were applied to each specimen in order to conduct the resilient modulus test. At each stress stage, a minimum of fifty loading cycles was applied to the specimen. Each stage terminated when the standard deviations of the last six values of the resilient moduli were less than 5%, or until two hundred loading cycles were reached. The stages then continued in order until all given stress stages were completed.

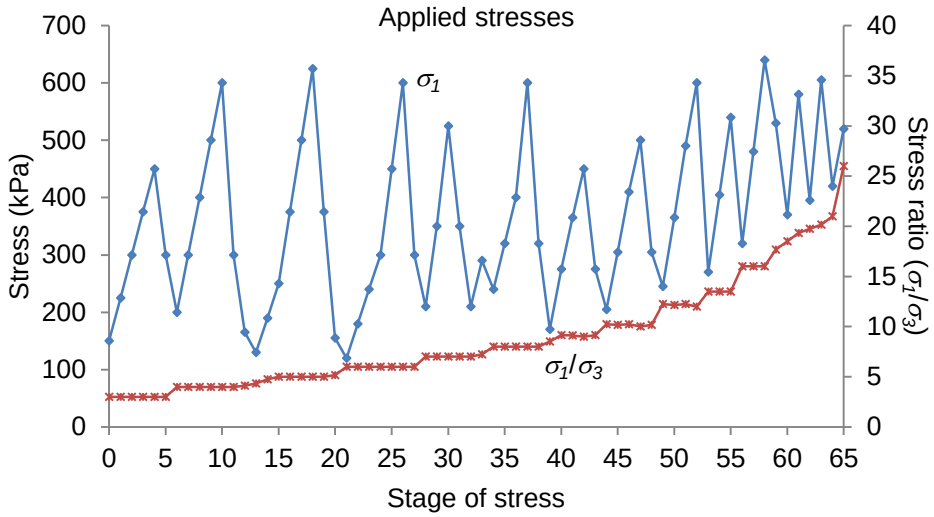

Figure 3.8 The applied stresses for finding the resilient modulus in accordance with the Austroads-AG:PT/T053

3.3 Test Results

3.3.1 Modified compaction tests

The maximum dry density (MDD) and the optimum moisture content (OMC) of crushed rock are 2.309 t/m^3 and 5.9% respectively, as shown in Figure 3.9. The compaction curve of HCTCRB (see Figure 3.10) shows that MDD and OMC of HCTCRB are 2.369 t/m^3 and 5.4% respectively.

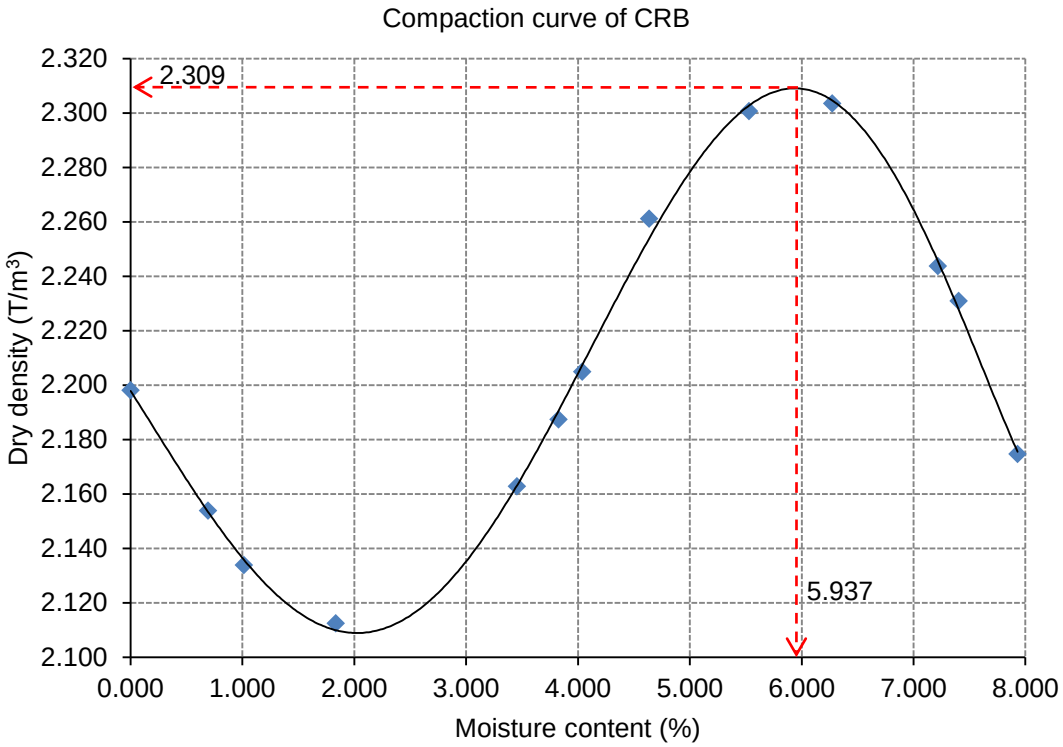

Figure 3.9 Results from the modified compaction tests of CRB

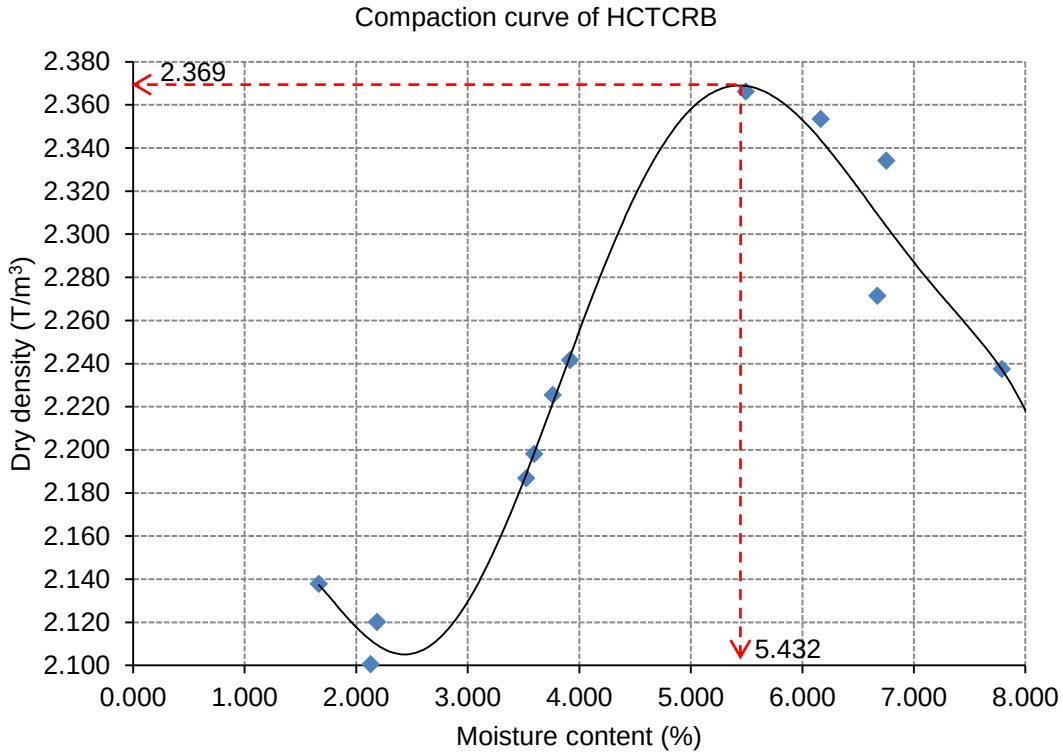

Figure 3.10 Results from the modified compaction tests of HCTCRB

3.3.2 Static triaxial tests

The stress-strain curves resulted from static triaxial tests for CRB and HCTCRB are shown in Figure 3.11 and Figure 3.12, respectively. These results indicate that the peak stress of these materials increases with higher confining stress (σ_3). As can be seen in these figures, the peak stress at 0 kPa of confining pressure, i.e. unconfined compression strength (UCS), of CRB and HCTCRB are 0.31 and 0.41 MPa respectively. HCTCRB may be classified as an unbound granular material as its UCS laid within a threshold of unbound granular materials, i.e. UCS is less than 1 MPa.

The materials also gained higher elastic modulus (tangential modulus) with greater confining pressure. Figure 3.13 shows of the relationship between elastic modulus and confining pressure for both materials, and the correlations between these terms are also expressed in Equation (3.1) for CRB and (3.2) for HCTCRB. The elastic modulus of HCTCRB was 2-3 times higher than that of CRB.

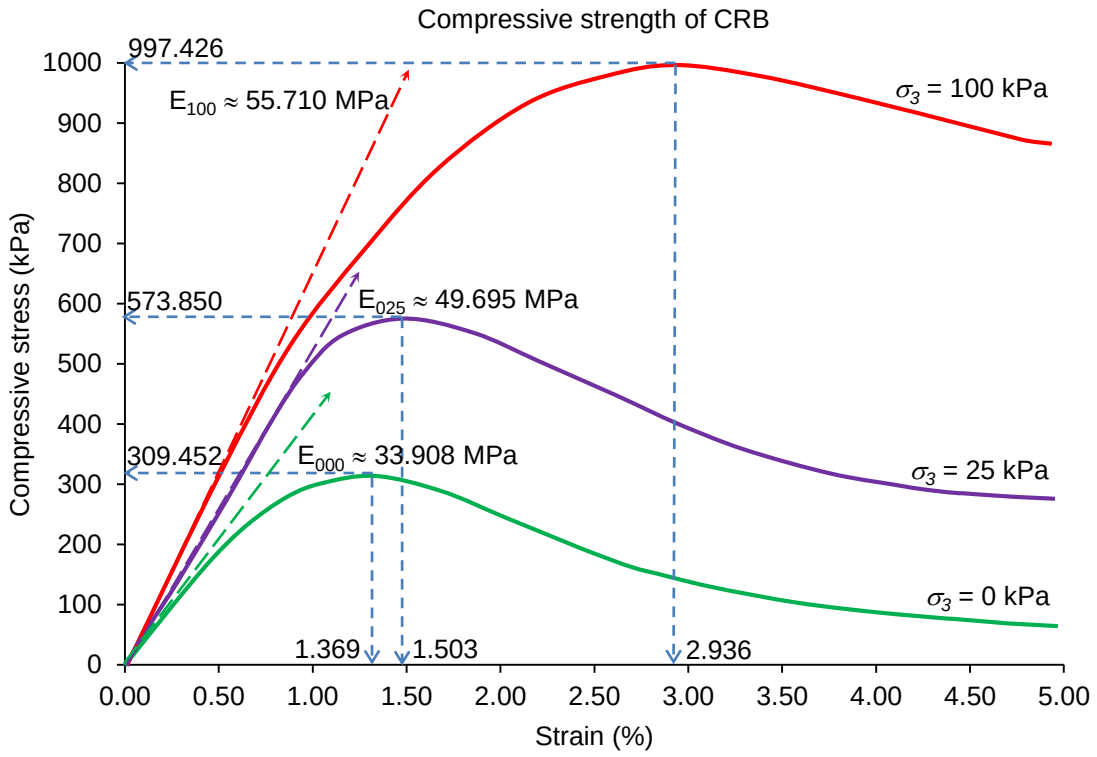

Figure 3.11 Results from the static triaxial tests of CRB specimen

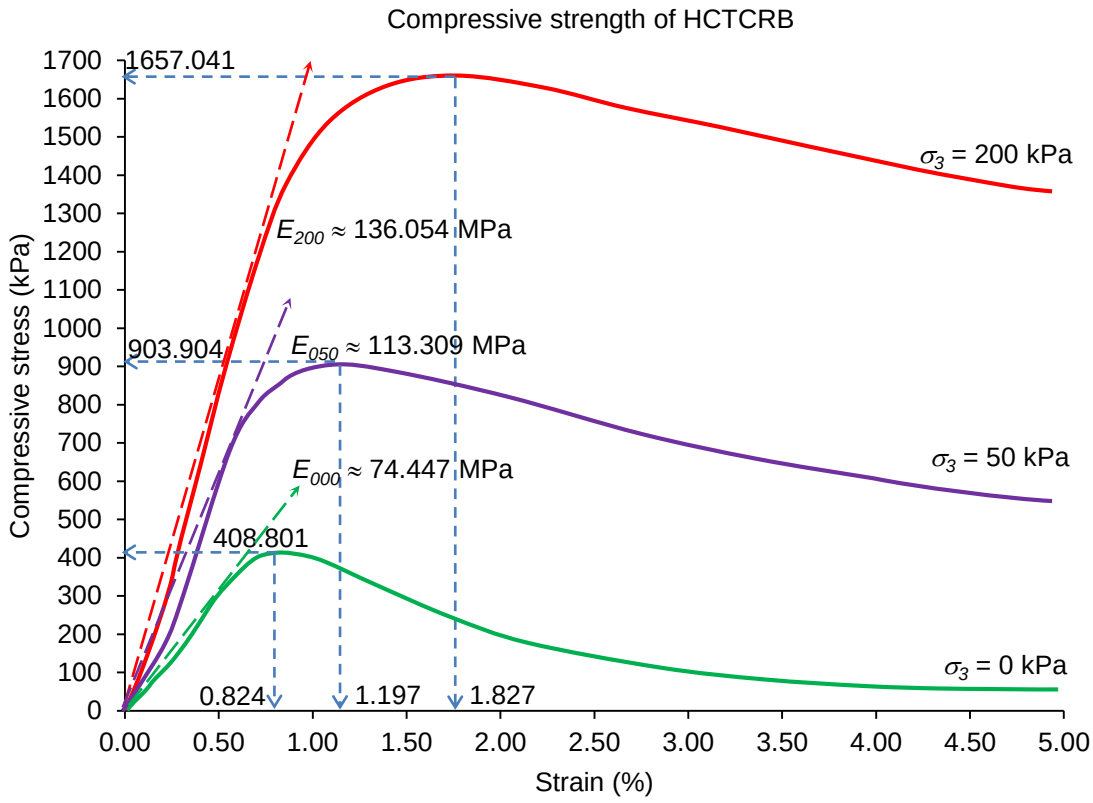

Figure 3.12 Results from the static triaxial tests of HCTCRB specimen

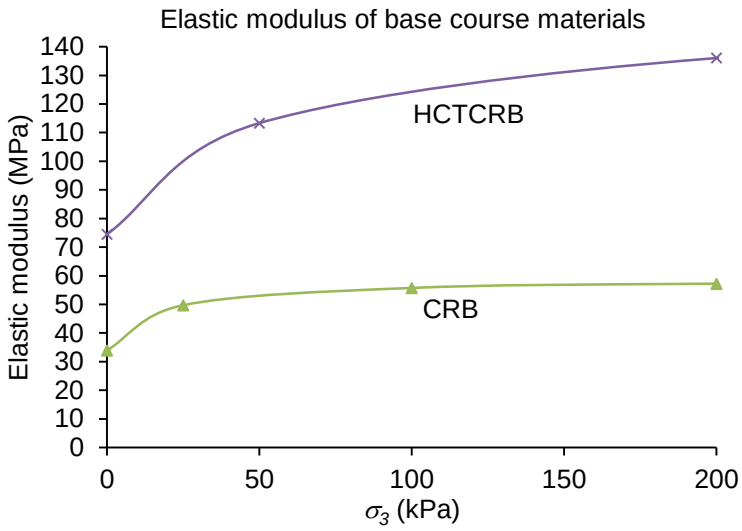

Figure 3.13 Trends of estimated elastic modulus of base course materials

$$E = \frac{\left[(58.88)\left(\sigma_3\right)+493.30\right]}{\left(\sigma_3+14.55\right)} \quad \text{for CRB} \tag{3.1}$$

$$= \frac{\left[(151.00)\left(\sigma_3\right)+3609.00\right]}{\left(\sigma_3+48.48\right)} \quad \text{for HCTCRB} \tag{3.2}$$

Figure 3.14 and Figure 3.15 show the failure mechanism of CRB and HCTCRB specimen, respectively. Both materials obviously failed by excessive shear stress, which is similar to cohesive soil failure. Hence, the Mohr-Coulomb failure theory, which is widely used for explanation of cohesive soil behaviour, was selected to explain failure mechanism of the two materials.

Consequently, Mohr-Coulomb failure envelopes for CRB and HCTCRB were constructed and illustrated in Figure 3.16 and Figure 3.17, respectively. The cohesion (*c*) and the internal friction angle (∅) of CRB were 91.0 kPa and 44.4° respectively. For HCTCRB, values of *c* and ∅ were 145.7 kPa and 41.9° respectively. This is as expected as adding cement to produce HCTCRB would modify the shear strength characteristics of CRB by increasing its cohesion but reducing the angle of internal friction. This is because HCTCRB sample generally has a smoother, more rounded surface, while CRB particles has sharp edges and corners. However, the plane of failure of specimens could be incorporated in to a design aid in a form of video to demonstrate the failure mechanism, it could be useful for engineers in investigating behaviour of specimens from beginning of load test until failure obviously exhibits.

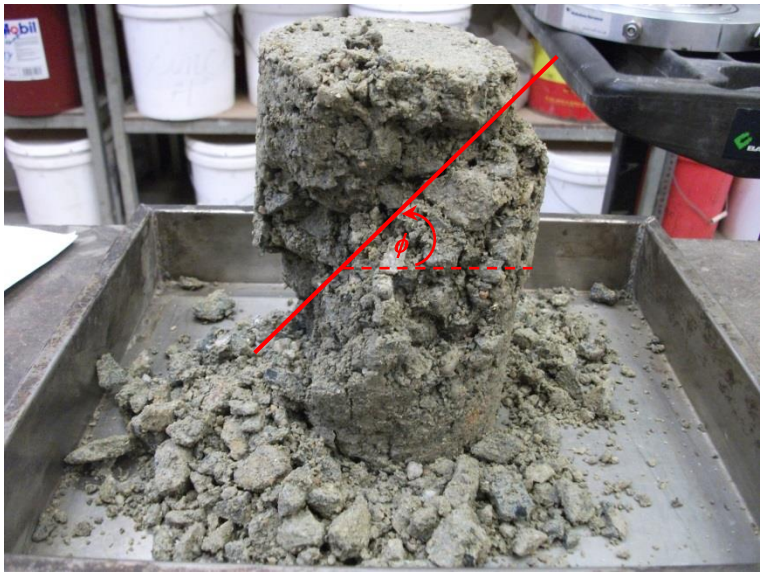

Figure 3.14 Failure mechanism of CRB specimen after static triaxial test

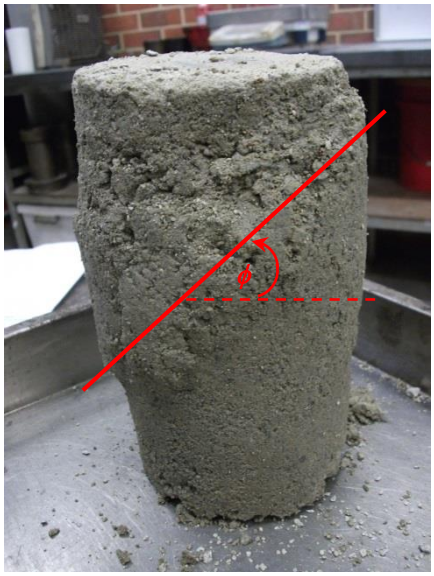

Figure 3.15 Failure mechanism of HCTCRB specimen after static triaxial test

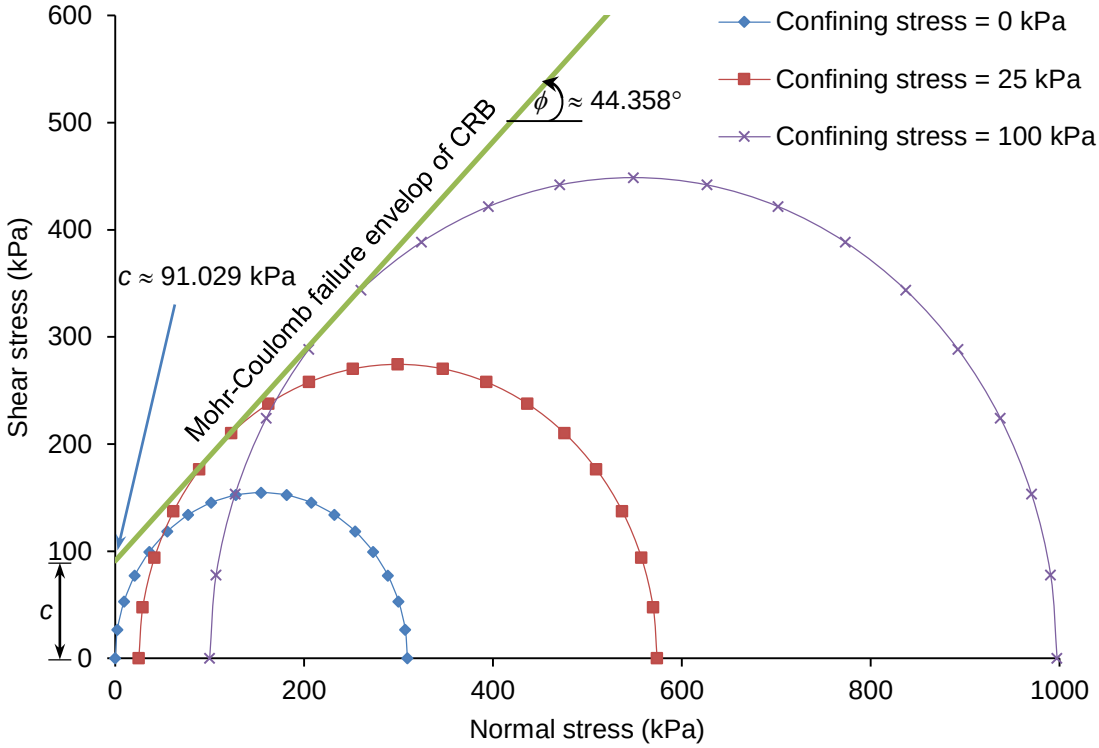

Figure 3.16 Mohr-Coulomb failure envelop of CRB

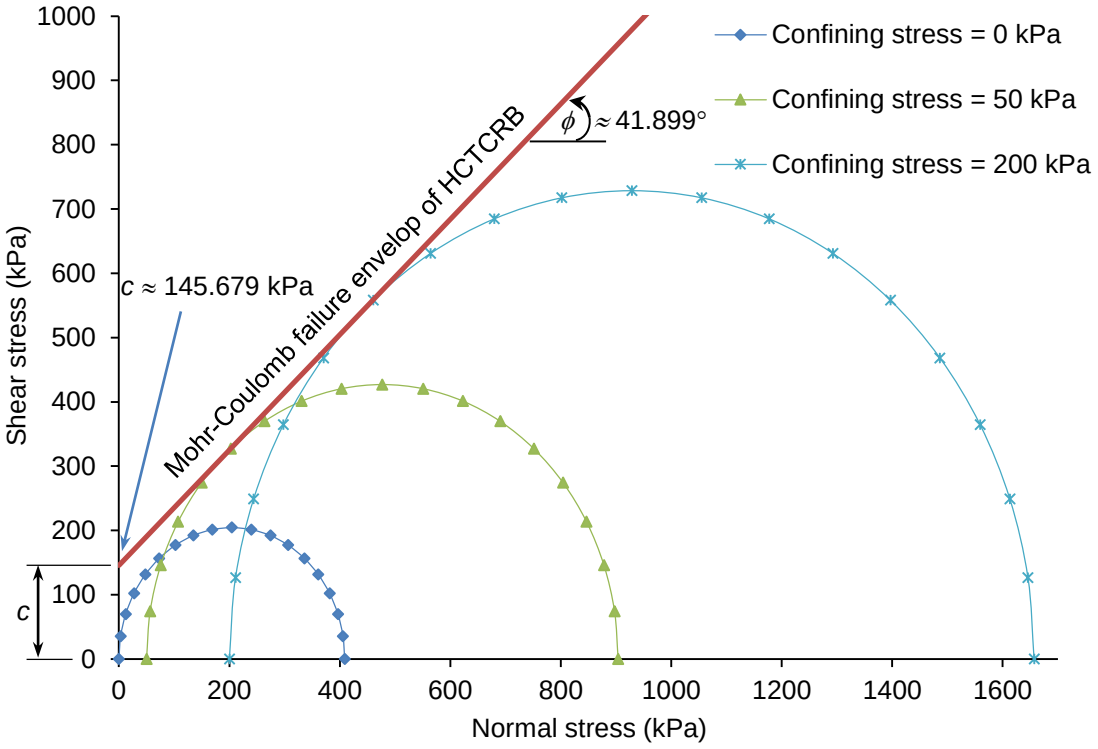

Figure 3.17 Mohr-Coulomb failure envelop of HCTCRB

The failure envelopes of the test materials were plotted on p-q space and compared with a set of applied stresses which was specified for conducting the resilient modulus test, as shown in Figure 3.18. It can be seen that several applied stress stages located beyond the ultimate strength of material, particularly for CRB. The comparison between all applied stresses for conducting the resilient modulus test and failure envelop of materials reveals that the applied stresses suggested by the Austroads – AG:PT/T053 standard are not suitable for all base or sub-base materials. In order to obtain the appropriate results, the stress intensity and stress stages applied in the RLT test should be determined based on the actual strength of material which is being tested.

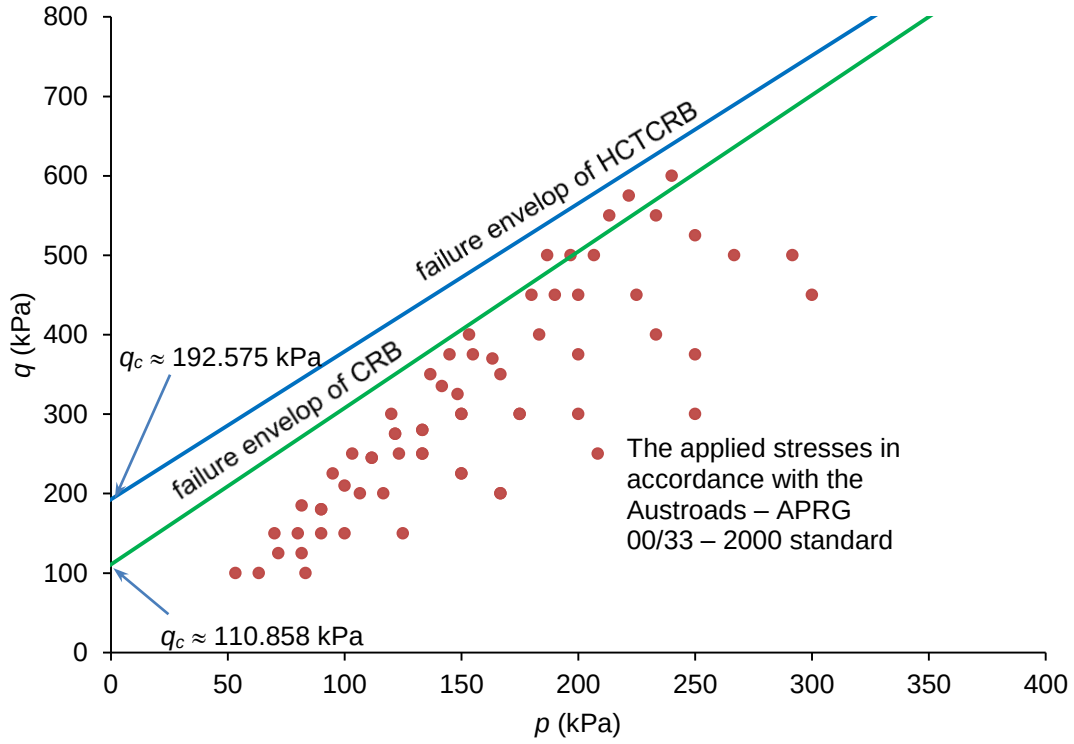

Figure 3.18 *p-q* diagram of base course materials and the applied stresses in accordance with the Austroads AG:PT/T053

3.3.3 Repeated load triaxial (RLT) tests

3.3.3.1 Resilient modulus

The resilient modulus values over 66 stress stages for CRB and HCTCRB are shown in Figure 3.19. Resileint moduli of HCTCRB, which are much higher than that of CRB, varied from 300 kPa – 940 kPa, while the resilient modulus of CRB ranged between 100 kPa - 300kPa. Both materials show the stress dependency behaviour i.e. resilient modulus value changes with the variation in the applied deviator and confining stresses. The test results were further evaluated in term of bulk stress, which is called k-θ model. This evaluation, see Figure 3.20, showed that the resilient properties of both materials are nonlinearly dependent of the bulk stress.

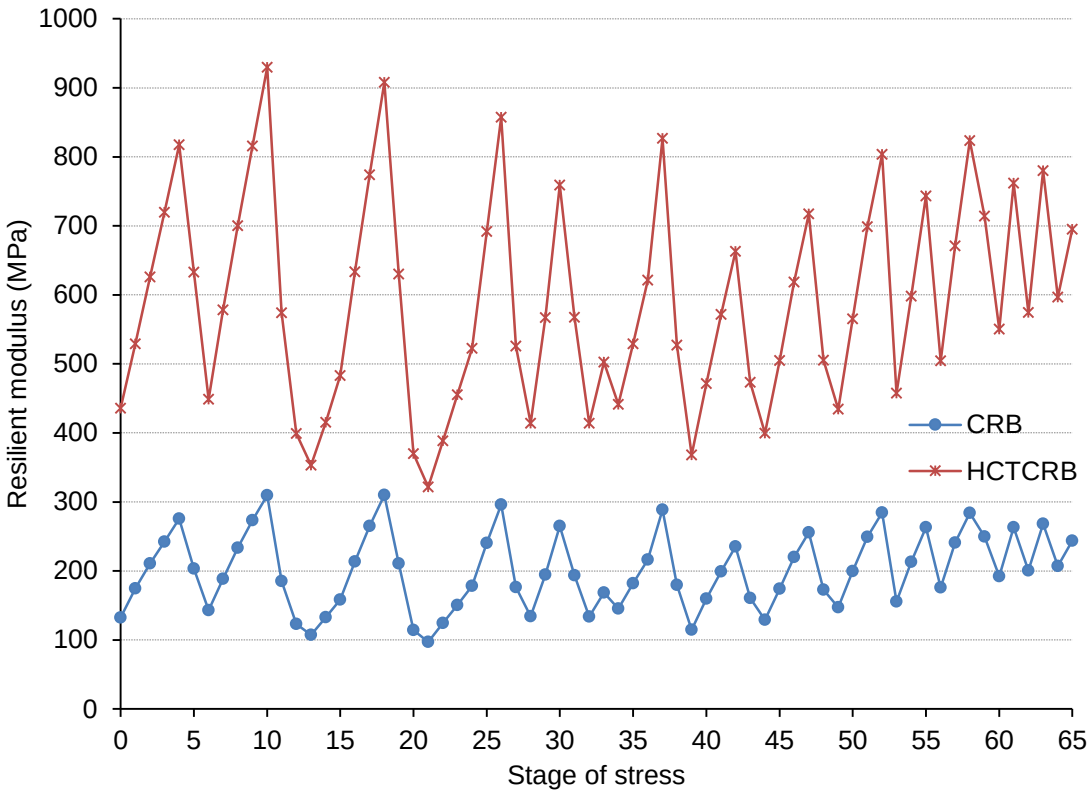

Figure 3.19 Resilient modulus test results for CRB and HCTCRB

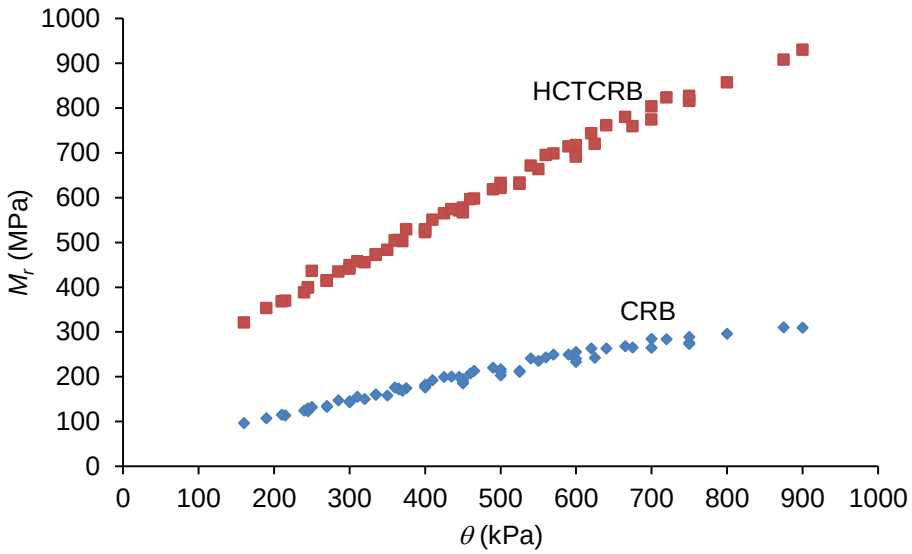

Figure 3.20 Relationship between the resilient modulus and the bulk stress of base course materials (k-θ model)

3.3.3.2 Permanent deformation

HCTCRB also showed better performance, in terms of permanent deformation, than CRB. The permanent deformation at the end of test for HCTCRB and CRB were 0.36 and 3.6 mm, respectively, as shown in Figure 3.21. The permanent deformations of both materials were dependent of the number of loading cycles and the intensity of deviator stress. At each stage, the permanent deformation increased dramatically at initial cycles, and then the incremental rate decayed during the remaining cycles.

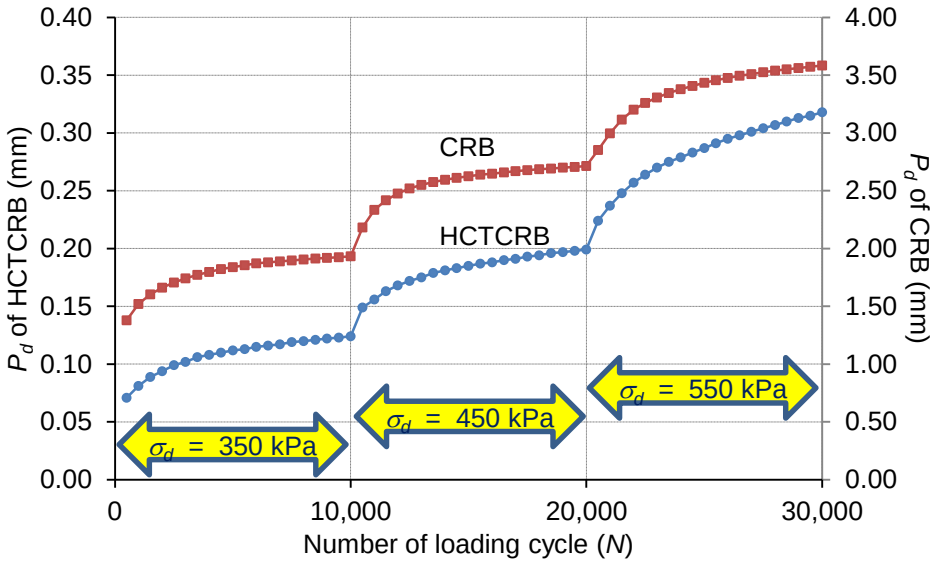

Figure 3.21 Relationship between the permanent deformation, the applied stress and number of load repetition of base course materials

3.4 Summary

HCTCRB showed superior performance to CRB in terms of UCS, resilient modulus and permanent deformation. These results indicate that HCTCRB technique can improve the strength of the original material. However the unbound property of the stabilised material is still retained even though 2% cement was added to CRB.

Based on the comparison between the applied stresses for RLT tests and failure envelopes of the test materials, further analyses of induced stress in flexible pavement model and RLT specimen model were carried out. The analyses aimed to define the suitable set of applied stresses for use in the RLT tests. The details of the analyses and outcomes are described in Chapter 4.

CHAPTER 4
APPLICATION OF DSC FOR MODELLING OF MATERIAL RESPONSES

4.1 Introduction

This chapter presents the application of the disturbed state concept (DSC) for modelling the behaviour of CRB and HCTCRB from mechanical tests as presented in Chapter 3. These include stress-strain relationship resulted from the static triaxial test, and resilient modulus and permanent deformation from the cyclic load test i.e. repeated load triaxial (RLT) test. All given models of base course materials from this chapter are based on empirical-mechanistic approach and they are the fundamental formulae that have to be employed by an advanced analytical approach for pavement analysis and design, which will be proposed in the following chapter.

4.2 DSC model of stress-strain relation of base course materials

The Mohr-Coulomb failure envelopes of cohesive soils are usually non -linear (Lamb and Whitman 1979). Nevertheless, fundamental concept for determining the trend of tangential slope (ϕ_t) of failure envelope can be estimated as demonstrated in Figure 4.1, where σ_3 and σ_{1u} are the confining stress applied on a testing specimen and the ultimate stress of materials, respectively.

The determination of ϕ_t, it can be expressed in Equations (4.1) - (4.3), where σ^a is the observed stress, σ^i is the stress in the relative intact part, σ^c is the stress in the fully adjusted part and $A = A^i + A^c$. Based on the experimental results in the present work, the trends of ϕ_t of the materials are as shown in Figure 4.2. Eventually, the equations for predicting ϕ_t can be simplified as shown in Equations (4.4) and (4.5).

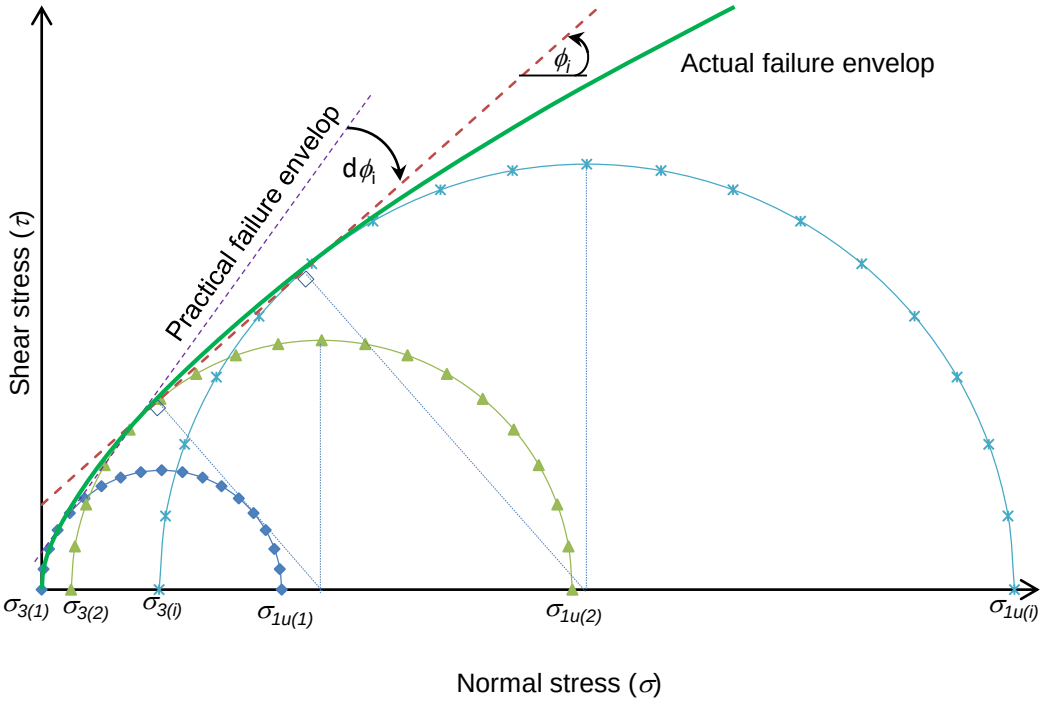

Figure 4.1 Fundamental concept of Mohr-Coulomb failure envelop for modelling of base course materials using DSC

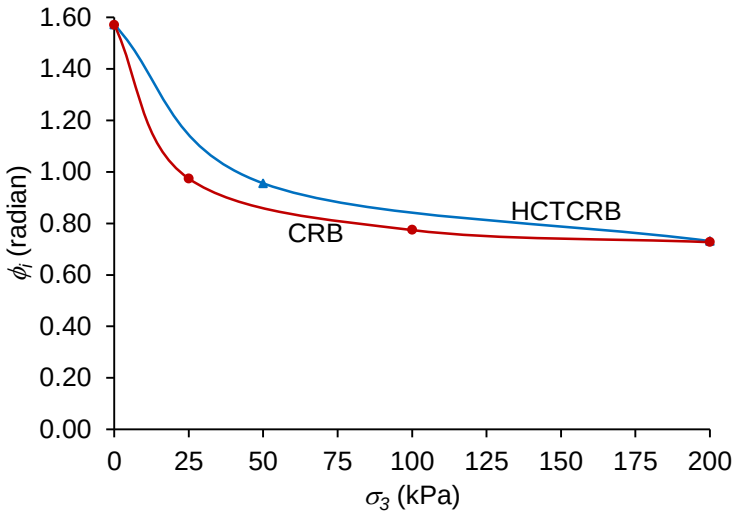

Figure 4.2 Trends of tangential slope of Mohr-Coulomb failure envelop

$$\emptyset_i = \sin^{-1}\left[\frac{\left(\sigma_{1u(i)}-\sigma_{3(i)}\right)-\left(\sigma_{1u(i-1)}-\sigma_{3(i-1)}\right)}{\left(\sigma_{1u(i)}+\sigma_{3(i)}\right)-\left(\sigma_{1u(i-1)}+\sigma_{3(i-1)}\right)}\right] \quad (4.1)$$

$$d\emptyset_i = \emptyset_{i-1} - \emptyset_i \quad (4.2)$$

$$\frac{d\emptyset_i}{d\sigma_{3(i)}} = \frac{d\emptyset_{i-1}}{d\sigma_{3(i)}} - \frac{d\emptyset_i}{d\sigma_{3(i)}} \tag{4.3}$$

$$= \frac{d}{d\sigma_{3(i)}} \sin^{-1}\left[\frac{\left(\sigma_{1u(i-1)}-\sigma_{3(i-1)}\right)-\left(\sigma_{1u(i-2)}-\sigma_{3(i-2)}\right)}{\left(\sigma_{1u(i-1)}+\sigma_{3(i-1)}\right)-\left(\sigma_{1u(i-2)}+\sigma_{3(i-2)}\right)}\right]$$

$$- \frac{d}{d\sigma_{3(i)}} \sin^{-1}\left[\frac{\left(\sigma_{1u(i)}-\sigma_{3(i)}\right)-\left(\sigma_{1u(i-1)}-\sigma_{3(i-1)}\right)}{\left(\sigma_{1u(i)}+\sigma_{3(i)}\right)-\left(\sigma_{1u(i-1)}+\sigma_{3(i-1)}\right)}\right]$$

$$\emptyset_i = \frac{\left(0.674\cdot\sigma_3 + 19.75\right)}{\left(\sigma_3 + 12.58\right)} \quad \text{, for CRB} \tag{4.4}$$

$$= \frac{\left(0.615\cdot\sigma_3 + 43.41\right)}{\left(\sigma_3 + 27.63\right)} \quad \text{, for HCTCRB} \tag{4.5}$$

The stress-strain relationships of CRB and HCTCRB specimens (cf. Figure 4.4 and Figure 4.5) can be expressed in the form of exponential function as follows;

$$\sigma = \frac{a\cdot\varepsilon}{e^{b\varepsilon}} \mp \frac{c\cdot\varepsilon}{e^{d\varepsilon}} \quad \text{, for } 0 \le \varepsilon \le \varepsilon_u \tag{4.6}$$

$$\sigma = \frac{a\cdot\varepsilon}{e^{b\varepsilon}} \mp \frac{c\cdot\varepsilon}{e^{d\varepsilon}} - f\cdot\langle\varepsilon-\varepsilon_y\rangle^2 \quad \text{, for } 0 \le \varepsilon \le \varepsilon_u \tag{4.7}$$

where *a*, *b*, *c*, *d*, *f* are constant, σ is the axial stress, and ε is the axial strain.

Consequently, the constants (*a*, *b*, *c*, *d* and *f*) can be determined using a trial and error method (Desai 2001), based on the average of 3 testing results by omitting the maximum and minimum results (totally, 5 specimens were tested), as:

$$a = \left[\frac{\sigma_{1u}}{\varepsilon_u}\right]\cdot e \tag{4.8}$$

$$b = \frac{1}{\varepsilon_u} \tag{4.9}$$

$$c = \left[\frac{5.5}{6.5}\right]\cdot\left[\frac{\sigma_{1u}}{\varepsilon_u}\right]\cdot e \tag{4.10}$$

$$d = \frac{\left\{\left[\frac{\varepsilon_c}{\varepsilon_u}\right]\cdot\left[e^{1-\left(\frac{\varepsilon_c}{\varepsilon_u}\right)}\right]\cdot\sigma_{1u}-\sigma_{1c}\right\}}{\left(\varepsilon_c-\varepsilon_u\right)^2} \tag{4.11}$$

Then, fully plastic RI (as depicted in Figure 4.3) applied in conjunction with Equations (4.6) and (4.7), the disturbance function (*D*) can be expressed as:

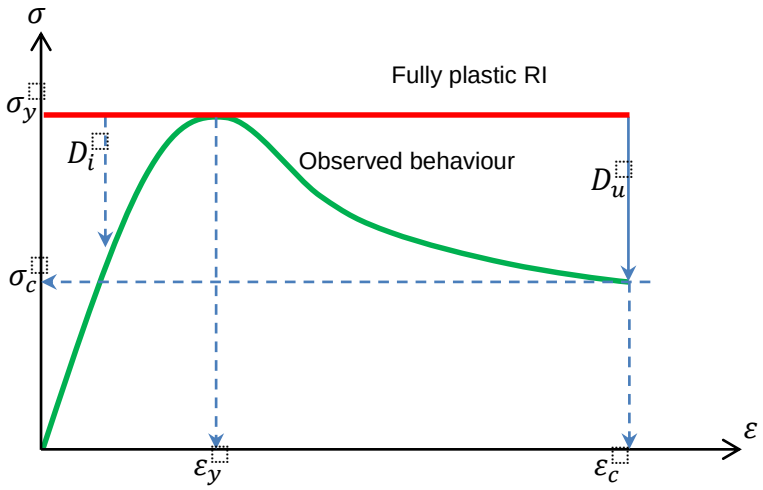

Figure 4.3 Representation of the DSC modelling for the stress-strain relationship using fully plastic RI

$$D = D_u \left\{ 1 - \left[\frac{\varepsilon e^{1-\frac{\varepsilon}{\varepsilon_u}}}{\varepsilon_u} \right] \left[1 - \left(\frac{5.5}{6.5} \right) e^{-\frac{4.5\varepsilon}{\varepsilon_u}} \right] + \left[\left(\frac{\varepsilon_c}{\varepsilon_u} \right) e^{1-\left(\frac{\varepsilon_c}{\varepsilon_u} \right)} - \left(\frac{\varepsilon_c}{\varepsilon} \right) \left(\frac{\sigma_{1c}}{\sigma_{1u}} \right) \right] \frac{\langle \varepsilon - \varepsilon_u \rangle^2}{(\varepsilon_c - \varepsilon_u)^2} \right\} \quad (4.12)$$

where σ_{1u} is the ultimate compressive stress, σ_{1c} is the stress at fully adjusted state, σ_3 is the confining stress, ε_u is the strain at the point of ultimate compressive stress, ε_c is the strain at the point of fully adjusted state, and $D_u = \frac{\sigma_{1u}}{\sigma_{1u} - \sigma_{1c}}$

Based on the stress-strain relationships of CRB and HCTCRB, the variables $\sigma_{1c(i)}$, $\varepsilon_{u(i)}$ and $\varepsilon_{c(i)}$ of the materials can be expressed in term of $\sigma_{3(i)}$ as shown in Equations (4.13) - (4.18).

$$\sigma_{1c(i)} = \frac{\left(1533 \cdot \sigma_{3(i)} + 5743\right)}{\left(\sigma_{3(i)} + 114.9\right)} \quad \text{, for CRB} \tag{4.13}$$

$$= \frac{\left(2573 \cdot \sigma_{3(i)} + 6205\right)}{\left(\sigma_{3(i)} + 206.8\right)} \quad \text{, for HCTCRB} \tag{4.14}$$

$$\varepsilon_{u(i)} = \left(0.016459 \cdot \sigma_{3(i)} + 1.250117\right) \quad \text{, for CRB} \tag{4.15}$$

$$= \left(0.004828 \cdot \sigma_{3(i)} + 0.880036\right) \quad \text{, for HCTCRB} \tag{4.16}$$

$$\varepsilon_{c(i)} = \left(0.016459 \cdot \sigma_{3(i)} + 5.000000\right) \quad \text{, for CRB} \tag{4.17}$$

$$= \left(0.004828 \cdot \sigma_{3(i)} + 5.000000\right) \quad \text{, for HCTCRB} \tag{4.18}$$

And $\sigma_{1u(i)}$ can be determined by rearranging Equation (4.1), as:

$$\sigma_{1u(i)} = \frac{\sin \emptyset_i}{\left(1 - sin\emptyset_i\right)} \left[\sigma_{3(i)} - \left(\sigma_{1u(i-1)} + \sigma_{3(i-1)}\right)\right] + \frac{1}{\left(1 - sin\emptyset_i\right)} \left[\sigma_{3(i)} + \left(\sigma_{1u(i-1)} - \sigma_{3(i-1)}\right)\right] \tag{4.19}$$

To sum up, the back-prediction process of stress-strain relationship starts from the calculation of ϕ using Equations (4.4) and (4.5), then the variables, $\sigma_{1u(i)}$, $\sigma_{1c(i)}$, $\varepsilon_{u(i)}$ and $\varepsilon_{c(i)}$, are calculated. After that, the disturbance functions (*D* and D_u) are determined and the stress-strain curve is finally constructed. The examples of the use of the DSC to back-predict the stress-strain curve of CRB and HCTCRB are illustrated in Figure 4.4 and Figure 4.5, respectively.

For CRB specimen as shown in Figure 4.4, the ultimate strength are 309.452, 573.850 and 997.426 kPa for σ_3 = 0, 20 and 100 kPa respectively. For HCTCRB specimen as shown in Figure 4.5, the ultimate strength are 408.801, 903.904 and 1657.041 kPa for σ_3 = 0, 50 and 200 kPa respectively. These results indicate that the ultimate strength (σ_{1u}) of base course materials is influenced by the confining stress (σ_3) i.e, higher σ_3 provides higher σ_{1u}.

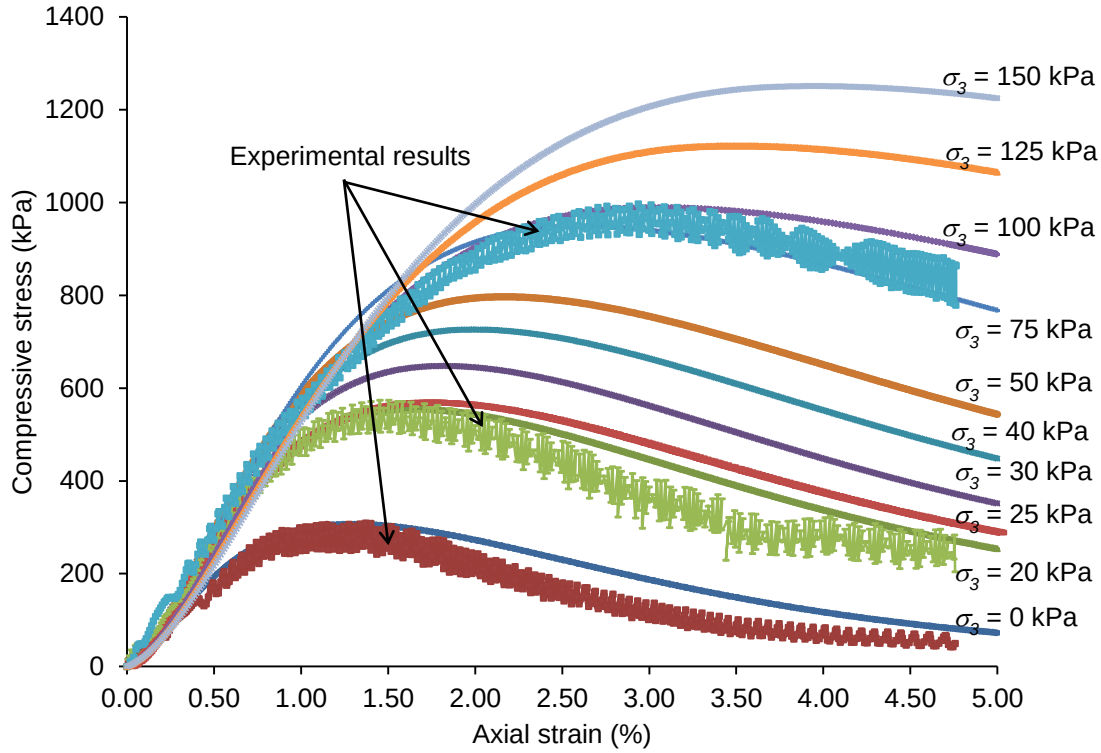

Figure 4.4 Prediction of stress-strain curves of CRB using DSC equation

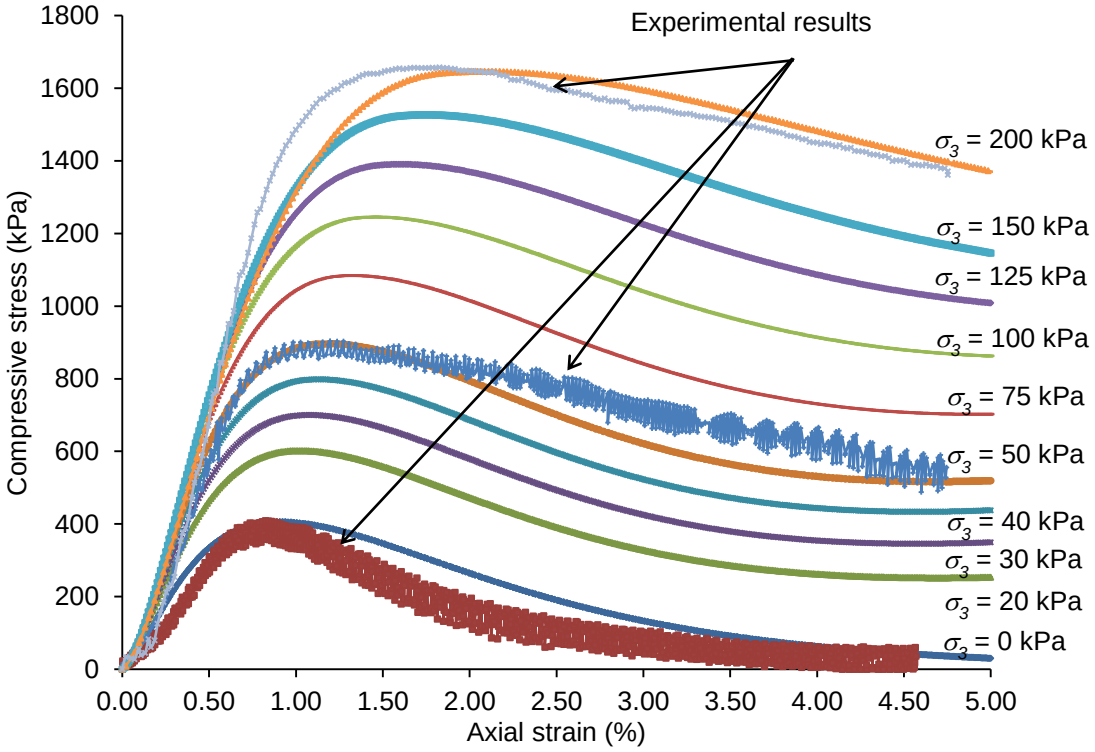

Figure 4.5 Prediction of stress-strain curves of HCTCRB using DSC equation

4.3 DSC model of resilient moduli-applied stresses relation of base course materials

The DSC equation for predicting the resilient modulus can be initially formulated by dividing DSC equation in the stress form, as given in Equation (2.20) with resilient strain (ε_r), as:

$$\frac{\sigma^a}{\varepsilon_r} = \frac{(1-D)\sigma^i}{\varepsilon_r} + \frac{D\sigma^c}{\varepsilon_r} \tag{4.20}$$

or

$$M_r^a = (1-D)M_r^i + DM_r^c \tag{4.21}$$

To predict the resilient modulus using the DSC, the disturbance function is formulated as;

$$D = \frac{\left(M_r^i - M_r^a\right)}{\left(M_r^i - M_r^c\right)} \tag{4.22}$$

The resilient modulus test results of CRB and HCTCRB (cf. section 3.3.3.1) were plotted against stress ratio (σ_1/σ_3) at each level of σ_3, as shown in Figure 4.6 and Figure 4.7, respectively. In this study, it was assumed that the relationships between the resilient moduli and the applied stresses of the materials were linearly dependent, therefore, the equation for predicting the resilient modulus can be defined as:

$$M_r^a = \left(\frac{\sigma_1}{\sigma_3}\right) c_1 + c_2 \tag{4.23}$$

where c_1 , c_2 are constants, σ_1 is the axial stress (kPa), and σ_3 is the confining stress (kPa).

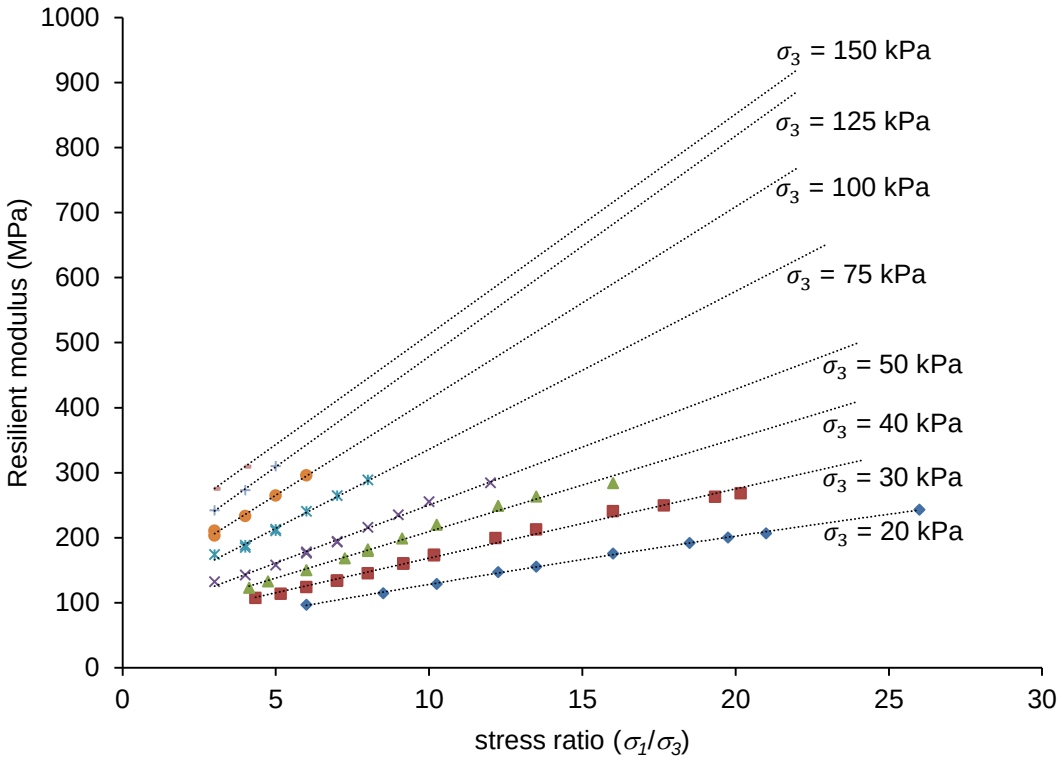

Figure 4.6 Relationship between the resilient moduli and the applied stresses of CRB specimen

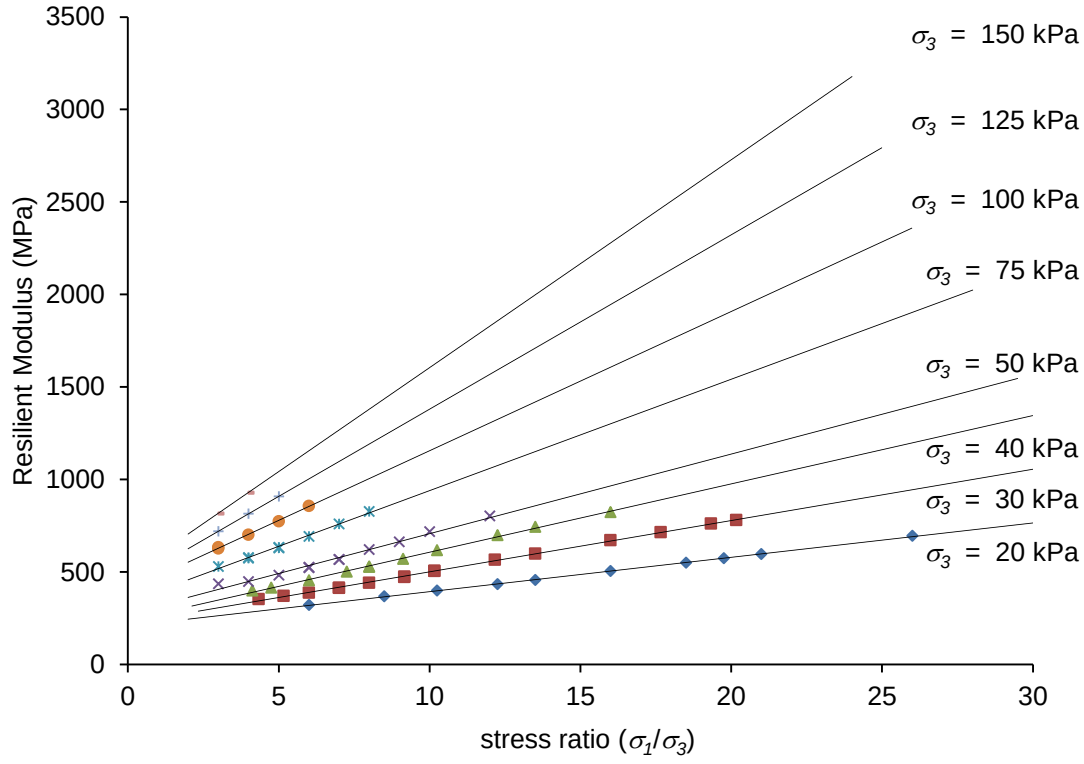

Figure 4.7 Relationship between the resilient moduli and the applied stresses of HCTCRB specimen

Consequently, the relative intact which is linear elastic, as depicted in Figure 4.8, was chosen to formulate the constitutive model of resilient modulus. Then the constants were determined using the trial and error method (Desai 2001), based on the average of 3 testing results by omitting the maximum and minimum results (totally, 5 specimens were tested), and yielded;

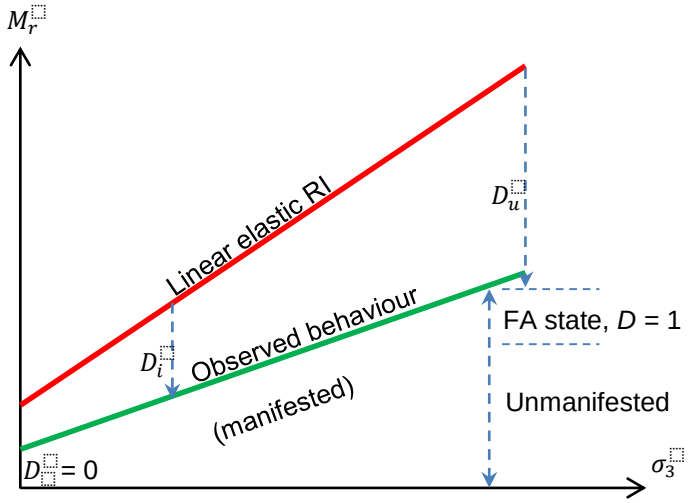

Figure 4.8 Representation of fundamental DSC concept for predicting the resilient moduli of base course specimen

$$c_1 = (0.220)(\sigma_3) + 3.300 \quad \text{for CRB} \tag{4.24}$$

$$= (0.675)(\sigma_3) + 6.750 \quad \text{for HCTCRB} \tag{4.25}$$

$$c_2 = (1.100)(\sigma_3) + 33.000 \quad \text{for CRB} \tag{4.26}$$

$$= (2.400)(\sigma_3) + 165.000 \quad \text{for HCTCRB} \tag{4.27}$$

By applying linear elastic RI together with Equations (4.22) - (4.27), the disturbance function (D) of the materials can be expressed as:

$$D = \frac{(1.100)(\sigma_3)+33.000}{(1.320)(\sigma_3)+36.300} \quad \text{for CRB} \tag{4.28}$$

$$= \frac{(2.400)(\sigma_3)+165.000}{(3.075)(\sigma_3)+171.750} \quad \text{for HCTCRB} \tag{4.29}$$

Substituting Equations (4.28) and (4.29) into Equation (4.21), DSC formulae of resilient modulus for both materials are:

$$M_r^a = \left[\frac{(0.220)(\sigma_3)+3.300}{(1.320)(\sigma_3)+36.300}\right](M_r^i) + \left[\frac{(1.100)(\sigma_3)+33.000}{(1.320)(\sigma_3)+36.300}\right](M_r^c) \quad (4.30)$$

for CRB

$$M_r^a = \left[\frac{(0.675)(\sigma_3)+6.750}{(3.075)(\sigma_3)+171.750}\right](M_r^i) + \left[\frac{(2.400)(\sigma_3)+165.000}{(3.075)(\sigma_3)+171.750}\right](M_r^c) \quad (4.31)$$

for HCTCRB

Equations (4.30) - (4.31) show that the disturbed function is a function of confining stress (σ_3) and the relative intact resilient modulus is a function of stress ratio $\left(\frac{\sigma_1}{\sigma_3}\right)$.

Figure 4.9 and Figure 4.10 show the use of the *K*-θ model and the DSC equation to back predict the resilient moduli of CRB and HCTCRB. Based on the experimental results in this study, the regression parameters for the *K*-θ model of CRB and HCTCRB were k_1 = 2.422, 11.372 and k_2 = 0.721, 0.645 respectively. The *K*-θ model for each of the materials are shown in Equations (4.32) and (4.33).

$$M_r = 2.422\theta^{0.721} \quad \text{for CRB} \quad (4.32)$$

$$M_r = 11.372\theta^{0.645} \quad \text{for HCTCRB} \quad (4.33)$$

The comparison results revealed that the proposed DSC equation for prediction of the resilient modulus provided promising results as all the predicted values were fitted well with the experimental data.

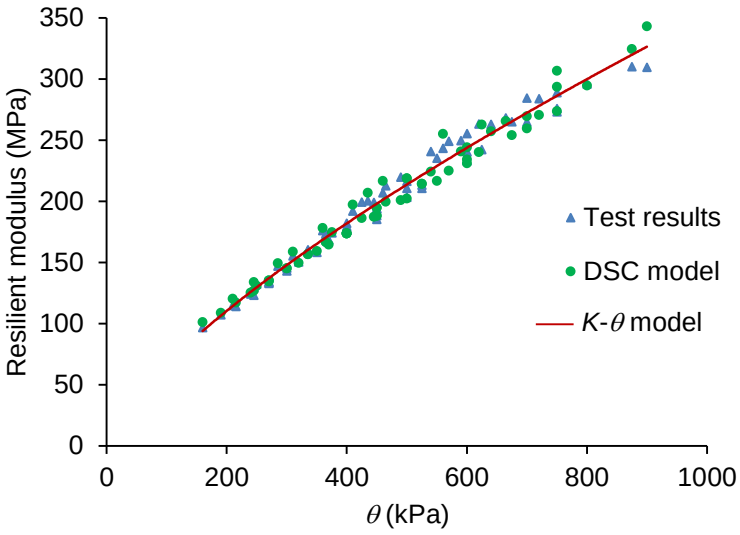

Figure 4.9 Prediction of the resilient moduli of CRB by the use of DSC equation (R^2 = 0.951)

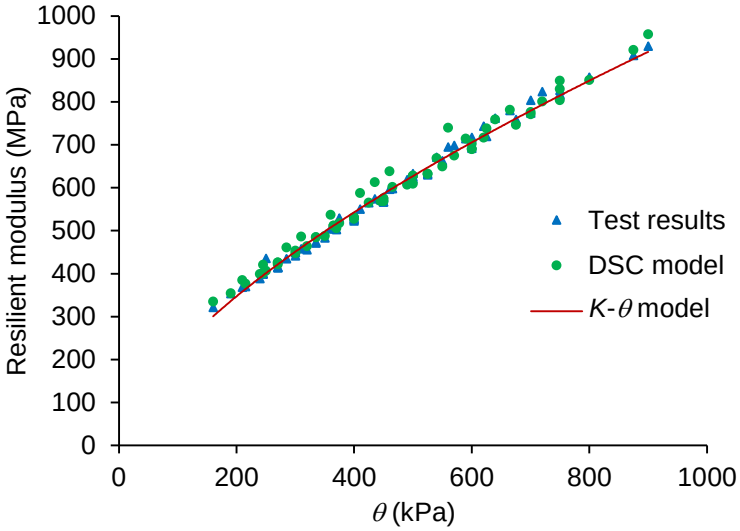

Figure 4.10 Prediction of the resilient moduli of HCTCRB by the use of DSC equation (R^2 = 0.928)

4.4 DSC model of permanent deformation of base course materials

Permanent deformation of road pavement i.e. rutting, particularly along the wheel path, is a result of both the prevailing load and the material having insufficient stability to resist the traffic loads and environmental conditions (Austroads 2004). According to the Austroads standard (Austroads 2010), only

permanent deformation of subgrade is one of the design criteria apart from tensile strains at the bottom of asphalt surface and cemented layer. However, the permanent deformation of base course layer is not included as part of the design criteria. This standard only suits for the road having asphalt surface at least 40 mm thick. Thus, addition of permanent deformation in base course layer is worthy of consideration for the pavement analysis and design because most of the roads in Western Australia are constructed with thin asphalt surface of around 30 mm thick.

CRB and HCTCRB behave similar to the unbound granular materials, the permanent deformation would thus be produced by the compaction and densification of granular aggregates. Figure 4.11 demonstrates the deformation behaviour of unbound granular materials subjected to a certain magnitude of cyclic loading. During the course of repeated loading, permanent strain of the material increases at a diminishing rate. Eventually, both permanent and recoverable strains become constant. This fundamental concept was used to derive the equation for predicting permanent strain based on the DSC.

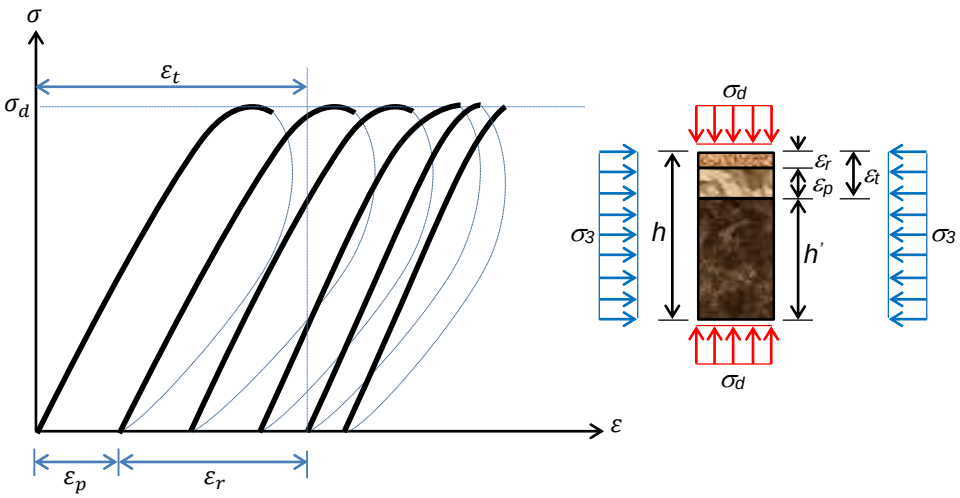

Figure 4.11 Representation of strain in base course specimen subjected to cyclic loading

The (total) strain of pavement materials comprises two parts, i.e. the recoverable part or “resilient strain”, and unrecoverable part so called “permanent strain “, as shown in Equation (4.34).

$$\varepsilon_t = \varepsilon_r + \varepsilon_p \tag{4.34}$$

where ε_t is the total strain, ε_r is the recoverable strain and ε_p is the permanent strain.

The resilient strain (ε_r), the results form repeated load triaxial tests and the results from static triaxial tests were used for finding the relationship between permanent deformation and applied stresses by rearranging Equations (4.30) and (4.31) to a form of stress and strain relationship, as:

$$\frac{\sigma_d^a}{\varepsilon_r} = \left[\frac{(0.220)(\sigma_3)+3.300}{(1.320)(\sigma_3)+36.300}\right]\left[\frac{\left(\frac{\sigma_1}{\sigma_3}\right)}{(1.320)(\sigma_3)+36.300}\right] + \left[\frac{(1.100)(\sigma_3)+33.000}{(1.320)(\sigma_3)+36.300}\right]\left[\frac{\left(\frac{\sigma_3}{\sigma_3}\right)}{(1.320)(\sigma_3)+36.300}\right] \tag{4.35}$$

for CRB

$$\frac{\sigma_d^a}{\varepsilon_r} = \left[\frac{(0.675)(\sigma_3)+6.750}{(3.075)(\sigma_3)+171.750}\right]\left[\frac{\left(\frac{\sigma_1}{\sigma_3}\right)}{(3.075)(\sigma_3)+171.750}\right] + \left[\frac{(2.400)(\sigma_3)+165.000}{(3.075)(\sigma_3)+171.750}\right]\left[\frac{\left(\frac{\sigma_3}{\sigma_3}\right)}{(3.075)(\sigma_3)+171.750}\right] \tag{4.36}$$

for HCTCRB

where $M_r^c = (1.320)(\sigma_3) + 36.300$ for CRB, $M_r^c = (3.075)(\sigma_3) + 171.750$ for HCTCRB, $\varepsilon_r = \frac{\sigma_3}{(1.320\sigma_3 + 36.300)}$ for CRB, $\varepsilon_r = \frac{\sigma_3}{(3.075\sigma_3 + 171.750)}$ for HCTCRB, and $M_r^i = (M_r^c)\left(\frac{\sigma_1}{\sigma_3}\right)$.

The permanent strain can then be calculated by deducting the resilient strain from the total strain as:

$$\varepsilon_p = \varepsilon_t - \varepsilon_r \tag{4.37}$$

$$\varepsilon_p = \left[\frac{(\sigma_1)(\sigma_3 + 14.55)}{(58.88)(\sigma_3) + 493.30}\right] - \left[\frac{\sigma_3}{(1.32)(\sigma_3) + 36.30}\right] \quad \text{for CRB} \tag{4.38}$$

$$\varepsilon_p = \left[\frac{(\sigma_1)(\sigma_3 + 48.48)}{(151.00)(\sigma_3) + 3609.00}\right] - \left[\frac{\sigma_3}{(3.075)(\sigma_3) + 171.750}\right] \quad \text{for HCTCRB} \tag{4.39}$$

Figure 4.12 depicts an example of the CRB cases showing the calculated strains (total, resilient and permanent parts) in relation with the confining pressure (σ_3) over the range of vertical stresses (σ_1). Similarly, Figure 4.13 shows an example of the HCTCRB cases.

Eventually, the DSC equation for predicting the permanent deformation of the test materials, derived from trial and error method (Desai 2001) based on the average of 3 testing results by omitting the maximum and minimum results (totally, 5 specimens were tested), is expressed as:

$$\delta_p^a = \delta_p^i + \delta_p^c = (a_0^i)(N)^{b_0^i + \sum_{m=1}^{n}(a_m^c)(N)^{b_m^c}} \tag{4.40}$$

where δ_p^a is the observed permanent deformation, δ_p^i is the permanent deformation in the relative intact part, δ_p^c is the permanent deformation in the fully adjusted part, a^i and b^i are the regression constants of power equation in relative intact part, a^c and b^c are the constants of power equation in fully adjusted part, $a_m^c = \frac{\delta_{p(N=10000)}^i}{(10^{4b})(2)(m+1)}$, $b_m^c = \frac{1}{2} log\left[\frac{(2)(m+1)(2.25)\delta_p^{\sigma_3}}{\delta_{p(N=10000)}^i}\right]$ for CRB, $b_m^c = \frac{1}{2} log\left[\frac{(2)(m+1)\delta_p^{\sigma_3}}{\delta_{p(N=10000)}^i}\right]$ for HCTCRB

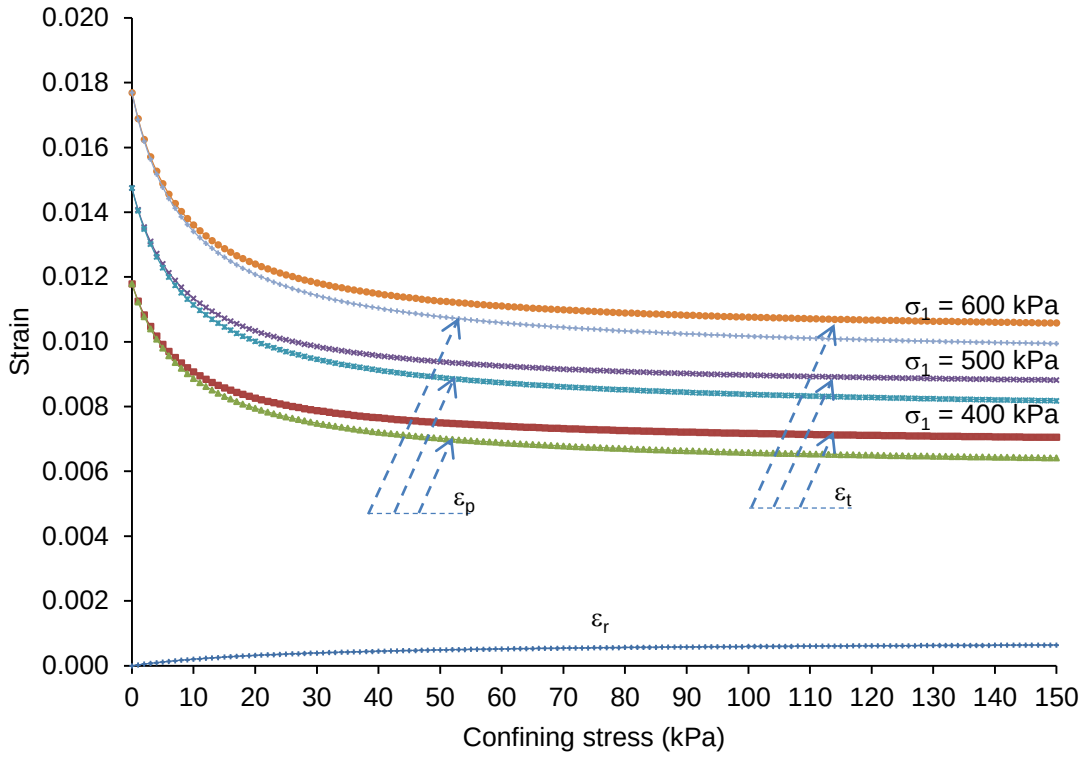

Figure 4.12 Trends of strain of CRB specimen

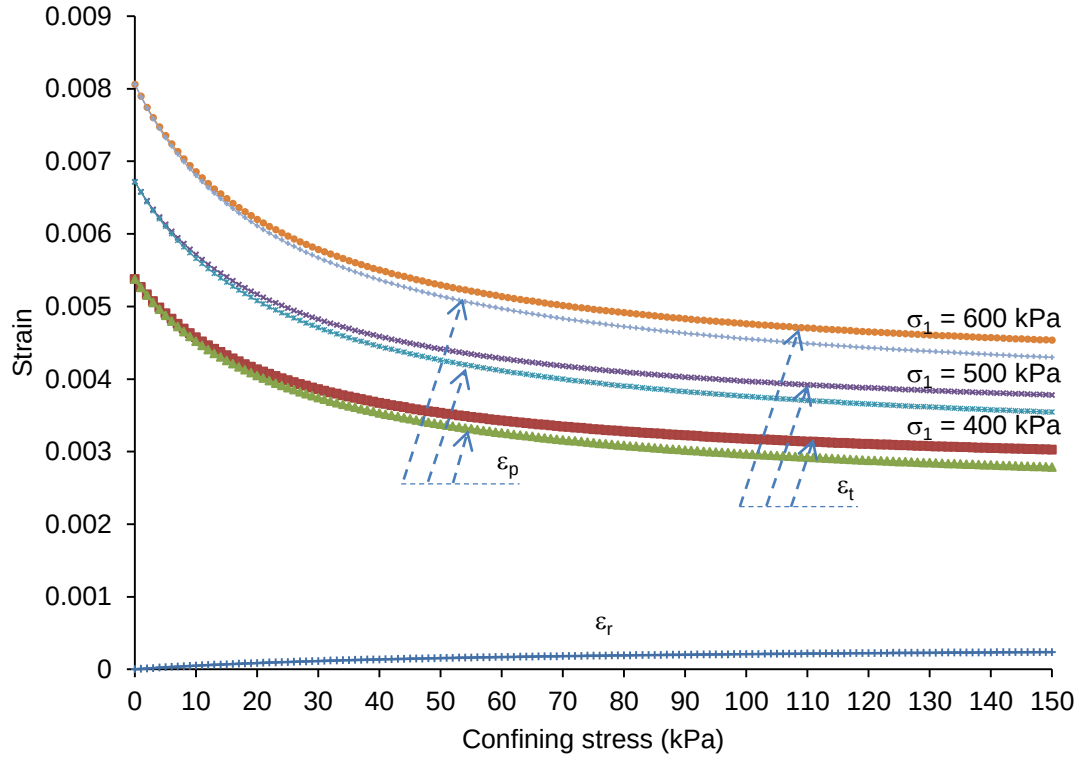

Figure 4.13 Trends of strain of HCTCRB specimen

In this study, the model suggested by G.T.H. Sweere from SAMARIS (2004) was adopted to predict the permanent deformation of the test materials and then compare with the DSC model. The Sweere's model, as shown in Equation (4.41), is a power function dependent of the number of cyclic loading, and the constants *a* and *b* are determined by the regression analysis of the test result. Based on the permanent deformation test results presented in section 3.3.3.2, the Sweere's model for CRB and HCTCRB are expressed in Equations (4.42) and (4.43), respectively.

$$\delta_p = (a)(N)^{(b)} \quad (4.41)$$

$$\delta_p = \left(182.018 \times 10^{-3}\right)(N)^{\left(279.759 \times 10^{-3}\right)} \quad \text{for CRB} \quad (4.42)$$

$$\delta_p = \left(3.203 \times 10^{-3}\right)(N)^{\left(428.369 \times 10^{-3}\right)} \quad \text{for HCTCRB} \quad (4.43)$$

Figure 4.14 and Figure 4.15 show the permanent deformation results in comparison with the predicted values obtained from the two models of CRB and HCTCRB, respectively. The Sweere's model is dependent of the number of loading cycles and only applicable for single stress tests. Thus it is not suitable for prediction the multi-stage test results.

Contrary, the DSC model is capable of predicting the results from the multi-stage tests. Figure 4.14 and Figure 4.15 also show that the predicted values at the end of each stage compare well with the test results. However a significant difference between the test results and the prediction was found during the initial period of each stage.

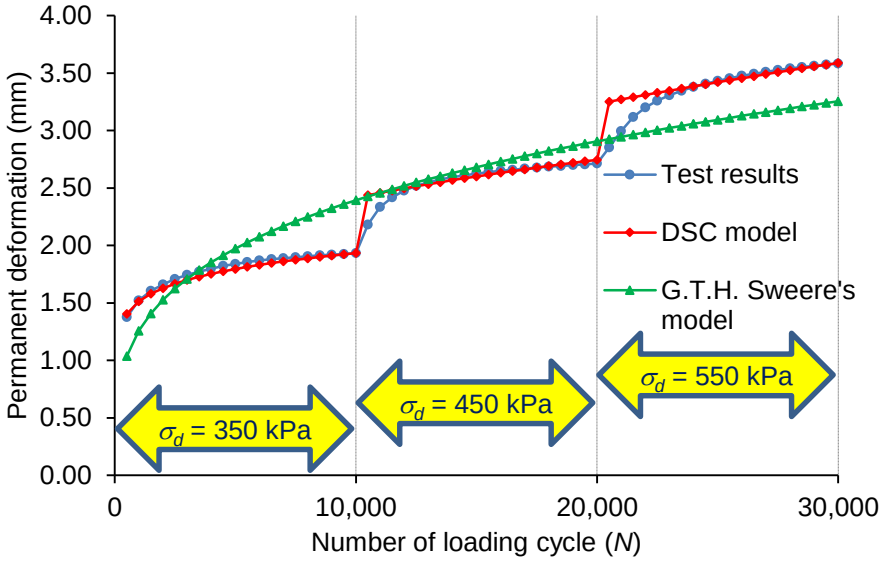

Figure 4.14 Prediction of the permanent deformation of CRB by the use of DSC equation

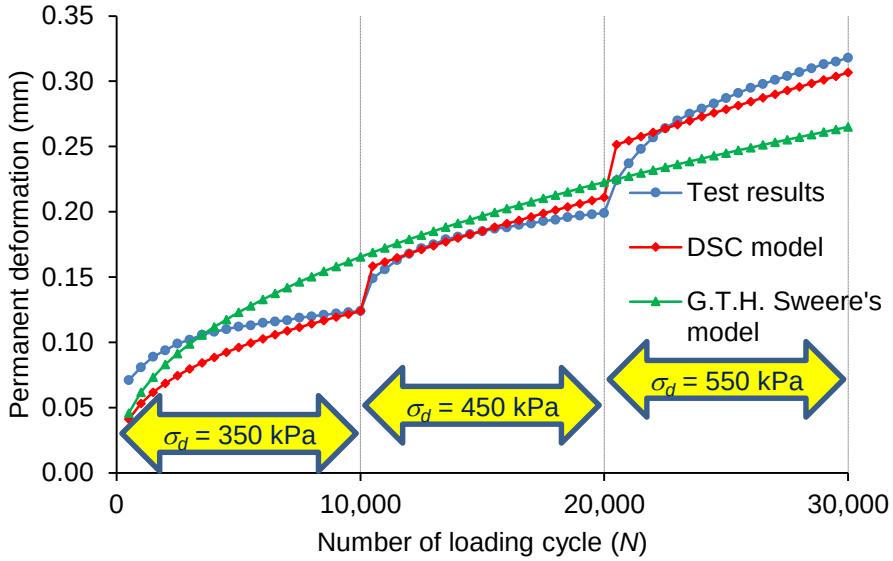

Figure 4.15 Prediction of the permanent deformation of HCTCRB by the use of DSC equation

4.5 Summary

In this chapter, the results from basic laboratories in accordance with Austroads standard were shown and interpreted. The results from static triaxial tests were used to define the failure envelop of base course materials and the RLT tests were conducted to determine the resilient moduli and the permanent

deformations of materials. These results indicated that both compressive strength and modulus of HCTCRB were higher than that of CRB, under either the static or cyclic loading condition. Consequently, the permanent deformations of HCTCRB were lower than the permanent deformations of CRB. Then the Disturbed State Concept was employed to model the behavioural responses of base course materials, for both the static and cyclic loading condition. The use of all proposed DSC models gave the predicted values which compared well with the experimental results, for both static load triaxial and repeated load triaxial tests. Furthermore, all DSC models given by this chapter will be adopted as the fundamental formulae using in the advanced analytical approach for design of flexible pavement having thin wearing surface layer, which will be introduced in Chapter 6.

CHAPTER 5
ANALYSIS OF STRESSES IN PAVEMENT MATERIALS

5.1 Introduction

Stress conditions in a model of thin-surfaced flexible pavement which is usually constructed in Western Australia were determined in conjunction with stress conditions in a RLT test sample using the finite element analysis. These analyses were to evaluate the suitability of applied loading conditions of the standard RLT protocol (Voung and Brimble 2000; Austroads 2007) with respect to the compatibility between induced stresses in a RLT test sample and a pavement model. A commercial finite element analysis program, namely ABAQUS (Dassault Systèmes Simulia Corporation 2010), was adopted for these series of analyses. All aforementioned steps are described in the following sections.

5.2 Finite element analysis

Finite element analysis (FEA) was performed to determine the stress conditions of thin-surfaced flexible pavement subjected to the standard axle load (i.e., the equivalent standard axle load, ESAL) and the RLT test specimen under a series of applied standard test loads. The finite element analysis of this task was based on an elastic material assumption which can be explained next.

5.2.1 Modelling of multi-layer flexible pavement

5.2.1.1 Classification of a pavement structure having a thin wearing surface

Road pavement in Western Australia is generally constructed with a thin wearing surface layer. However, the design guide issued by Austroads (Austroads 2004) only covers the analysis and design of road pavement having a relatively thick wearing surface layer $(t_{ws} \geq 40\ mm)$ of which the tensile stresses and the tensile strains occur at the bottom fibre. This tensile-

induced behaviour was used as an intrinsic behaviour of a corresponding thin surface pavement in this study. Parametric analysis in conjunction with finite element analysis corresponding to a variation of pavement performance-related parameters was performed to determine stress-strain conditions in pavement. The finite element analysis was relied on an assumption of the plane strain approach with considering the wheel configuration of standard axle loads and the pavement structure as shown in Figure 5.1.

The pavement structure for finite element analysis can be modelled, according to assumptions and conditions as follows:

1. For ESAL of the Austroads' pavement design guide, the maximum wheel loading of ESAL is 20 kN, being over a circular area of 92.1 mm radius (*r*), by which 750 kPa is the applied stress of this condition.
2. Side supports represent a roller-based condition, while bottom supports are fixed, and the thickness of the section was set to be 184.2 mm (2*r*).
3. The interaction between layers was set to be fully fixed (no slip) and quadratic element (CPE8R) was used for all analyses.
4. The self-weight of each layer was calculated by the use of the specific gravity (SG) of 2.4, 2.3, 1.9, and 1.8 kN/m^3 for asphalt concrete, crushed rock base (including HCTCRB), crushed lime stone, and Perth sand, respectively.
5. Because the maximum stresses are commonly located beneath a wheel therefore the stresses along the section under a wheel was assumed to be a critical section and used to be representative results from the analysis.

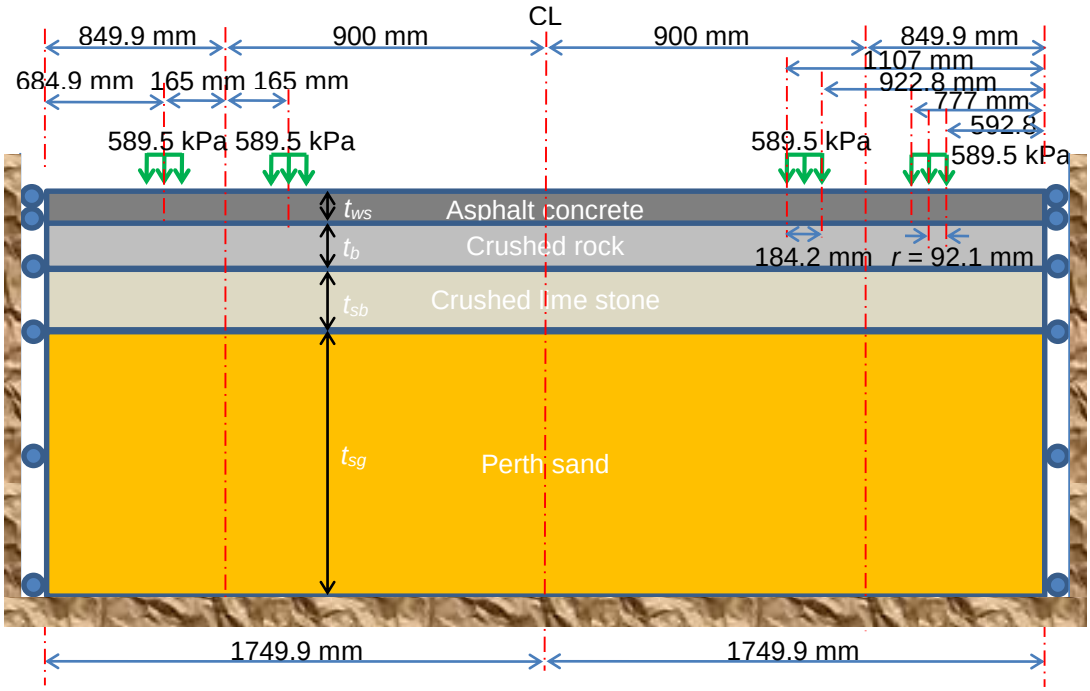

Figure 5.1 Structural section of road pavement uses as finite element model for analysis using ABAQUS

A series of the values of essential material properties, e.g. thickness of layer, modulus of elasticity, Poison's ratio, which were used for the analysis in ABAQUS are shown in Table 5.1. The thickness of wearing surface (t_{ws}) used in this study is varied between 10 to 150 mm, which is the range that tensile stress at bottom fibre of wearing surface layer can vanish. The thickness of base and subbase layers (t_b and t_{sb}) are varied between 100 to 200 mm and 150 to 250 mm, respectively, which are commonly used for construction of road pavement in Western Australia. In order to keep subgrade layer behaves as a half space of elastic material, the thickness of subgrade layer (t_{sg}) is fixed at 2500 mm which is larger than t_{sb} at least 10 times. As well as elastic modulus and Poison's ratio of each layer, they also come from the properties of pavement materials which are commonly used in Western Australia namely, elastic modulus can be varied from 1000 to 5000 MPa (E_{ws}), 250 to 450 MPa (E_{sb}) and 30 to 70 MPa (E_{sg}) for asphalt concrete, crushed lime stone and Perth sand, respectively. For base course materials, elastic modulus is varied from 200 to 800 MPa, which covered the common range of elastic modulus of both crushed rock base (CRB) and hydrated cement treated crushed rock base (HCTCRB). The effect of material properties on the horizontal stresses at

bottom fibre of wearing surface layer (σ_{xbws}) was investigated by varying the elastic modulus values of materials and the thicknesses of each layer, as shown in Table 5.2. In order to determine the point that σ_{xbws} = 0, t_{ws} was varied between 10 – 150 mm because the horizontal tensile stresses at bottom fibre of wearing surface layer was vanished within this range. Nevertheless, only the effect of the strength of material on σ_{xbws} is shown because the horizontal stresses in wearing surface layer are slightly affected by the change in the thickness of base and subbase layer.

Due to the variation in the material properties of pavement materials, each model was abbreviated as;

WSTV – (WS)(B)(SB)(SG)E(*i*)

where WS means wearing surface layer, B means base layer, SB means subbase layer, SG means subgrade layer, TV means the thickness is varied, E(*i*) means elastic modulus, *i* = 200, 350 and 800 MPa for base layer, *i* = 250, 350 and 450 MPa for subbase layer and *i* = 30, 50, and 70 MPa for subgrade.

Table 5.1 Material data for finite element analysis of pavement structure

Materials	Thickness (mm)	Modulus of Elasticity (MPa)	Poison's ratio
Asphalt concrete	10,20,30,…,150	1000,3000,5000	0.40
CRB / HCTCRB	100,150,200	200,350,800	0.35
Crushed Lime Stone	150,200,250	250,350,450	0.35
Perth Sand	2500	30,50,70 (no tension)	0.45

Then the results from the finite element analysis were used to define the pavement structure having thin wearing surface layer and no tensile stress occurrence at its bottom fibre. Hereafter, the thickness of the wearing surface layer which is the inflection point of σ_{xx} (from compressive to tensile stress) at bottom fibre of the wearing surface layer can be called "***the neutral thickness of wearing surface layer*** $(\boldsymbol{t_{wsn}})$".

Table 5.2 Cases of investigation on the effect of material properties on σ_{xbws} of pavement structure

Layer / Case	Wearing surface		Base		Subbase		Subgrade	
	E_{ws} (MPa)	t_{ws} (mm)	E_b (MPa)	t_b (mm)	E_{sb} (MPa)	t_{sb} (mm)	E_{sg} (MPa)	t_{sg} (mm)
WSTV-WSE1000	1000	10-150	350	150	250	200	50	2500
WSTV-WSE3000	3000	10-150	350	150	250	200	50	2500
WSTV-WSE5000	5000	10-150	350	150	250	200	50	2500
WSTV-BE200	3000	10-150	200	150	250	200	50	2500
WSTV-BE350	3000	10-150	350	150	250	200	50	2500
WSTV-BE800	3000	10-150	800	150	250	200	50	2500
WSTV-SBE250	3000	10-150	350	150	250	200	50	2500
WSTV-SBE350	3000	10-150	350	150	350	200	50	2500
WSTV-SBE450	3000	10-150	350	150	450	200	50	2500
WSTV-SGE30	3000	10-150	350	150	250	200	30	2500
WSTV-SGE50	3000	10-150	350	150	250	200	50	2500
WSTV-SGE70	3000	10-150	350	150	250	200	70	2500

5.2.1.2 Investigation of stress distribution in base course layer

Since a base course layer behaves like a main flexural member in the pavement structure having a thin wearing surface layer, therefore the stress distribution in this layer must be investigated first. The obtained results from finite element analysis of pavement structures as shown in Table 5.2 were used to determine the thickness of a wearing surface layer, which is classified as a “thin” layer ($t_{ws} \leq t_{wsn}$) then the structures were modelled and analysed using ABAQUS. The analysis results were then employed to formulate a mechanistic model of base course materials.

The examples of the results from finite element analysis in the form of stress contour and stress distribution along a depth section of a wheel path, are illustrated in Figure 5.2 and Figure 5.3.

Figure 5.2 indicates that the maximum vertical and the maximum horizontal stresses are located under a wheel path. The maximum vertical stress and the maximum horizontal stress occur at top fibre and at bottom fibre of wearing surface layer, respectively.

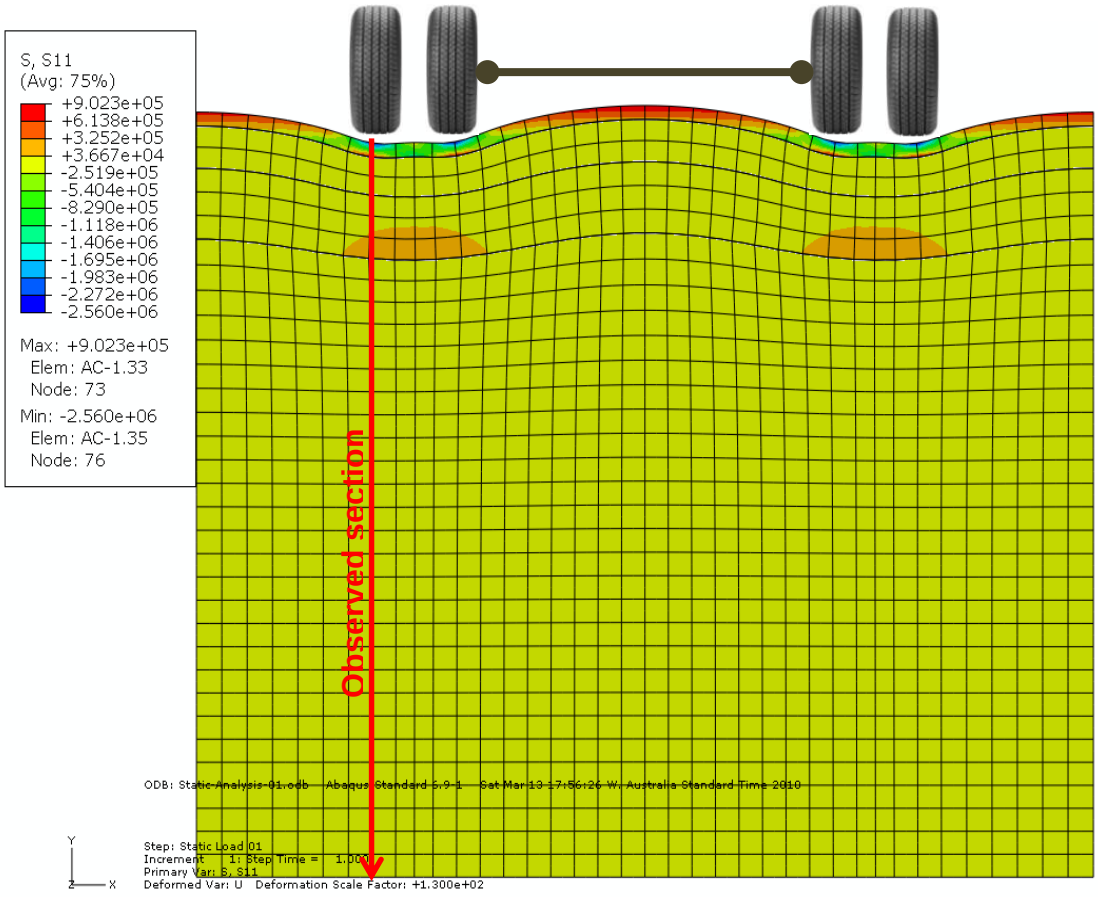

Figure 5.2 Example of the result from finite element analysis using ABAQUS

Figure 5.3 reveals that the distribution of horizontal stress in each layer is almost a linear line. The obtained horizontal stresses as seen in this figure will be adopted as the confining stresses that apply to the specimen of base course materials in RLT test and they will be also adopted for calculating the average value of confining stress uses in an advanced analytical approach, which will be shown in Chapter 6. These analysis results indicate that the horizontal stress along the depth of each layer is varied between -2.50 to 1.00 MPa, -450 to 50 kPa, -200 to 100 kPa and -90 to -150 kPa for wearing surface, base, subbase and subgrade layer, respectively.

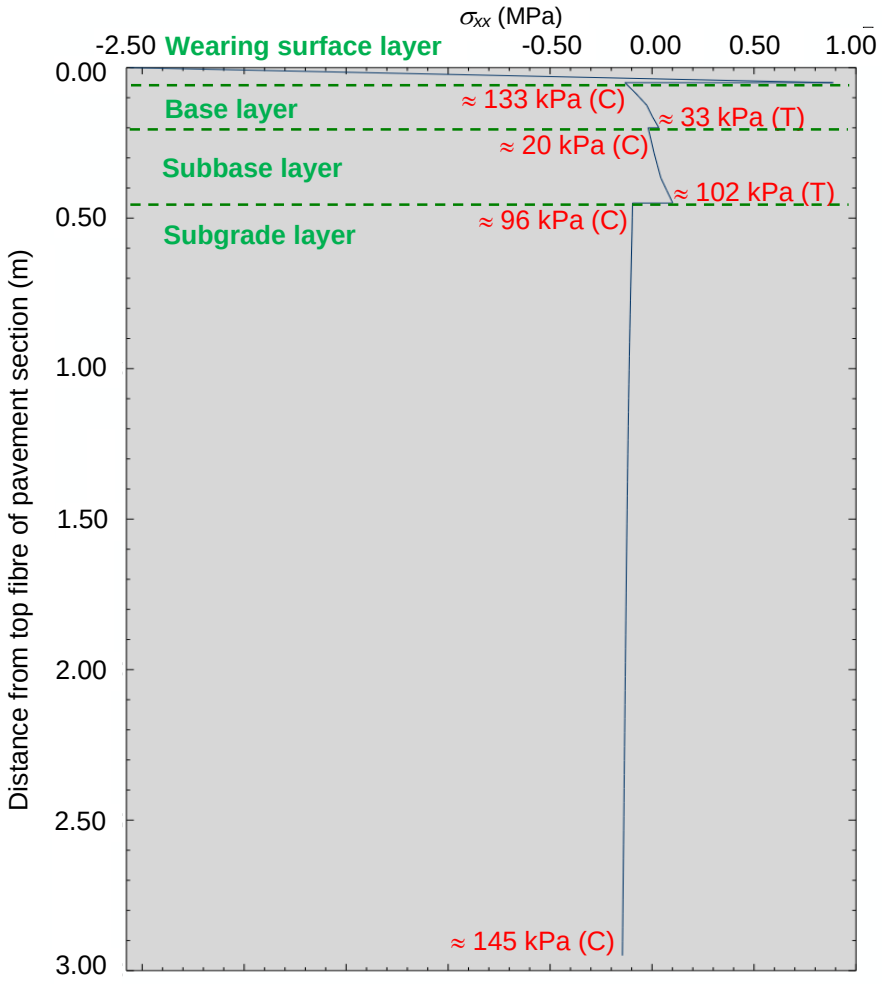

Figure 5.3 Example of the distribution of horizontal stresses (x-direction) under a wheel along the depth of pavement section

5.2.2 Analysis of specimen in RLT test

The resilient modulus of a base course material is generally obtained from the RLT tests and then used in the further sections of this study as an input parameter for the finite element analysis and the Disturbed concept analysis. It is therefore necessary to assure that induced stress conditions in a RLT test specimen under standard-applied cyclic loading are in correspondence with those in the real pavement. In this step, the stress conditions in base course specimen were determined and compared against the stress conditions in pavement structure based on the finite element analysis.

Consequently, the standard test specimen of 100 mm in diameter and 200 mm in height for the RLT test was also analysed by ABAQUS based on the 3D assumption, as shown in Figure 5.4.

Mesh size was set to 5.0 mm and the quadratic 3D stress (C3D20R), which is a 20-node quadratic brick, was used for analysis.

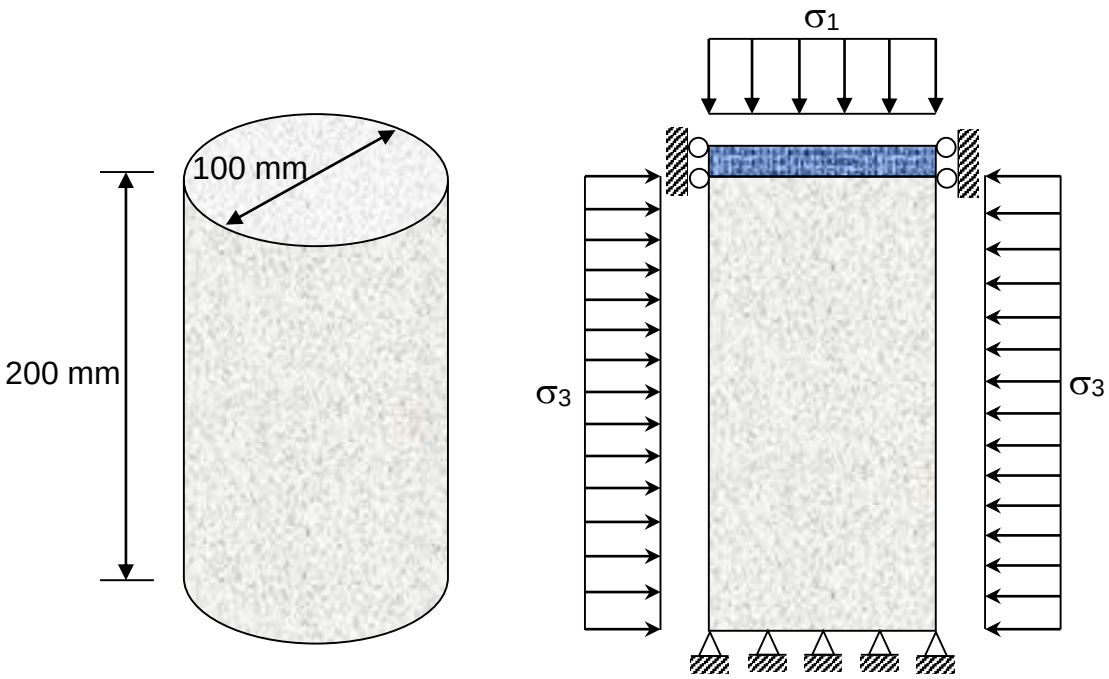

Figure 5.4 Configuration of finite element model of specimen in RLT test

5.3 Analysis of pavement structure

5.3.1 Classification of pavement structure having thin wearing surface layer

The effect of strength of wearing surface layer (E_{ws}) on the horizontal stresses at its bottom fibre (σ_{xbws}) was investigated first, and the results are illustrated in Figure 5.5. It was found that the neutral thickness of wearing surface layer (t_{wsn}) reduced with an increase in strength of asphalt wearing surface, i.e. t_{wsn} is around 21, 29, and 67 mm for the case of E_{ws} is 5000, 3000, and 1000 MPa, respectively.

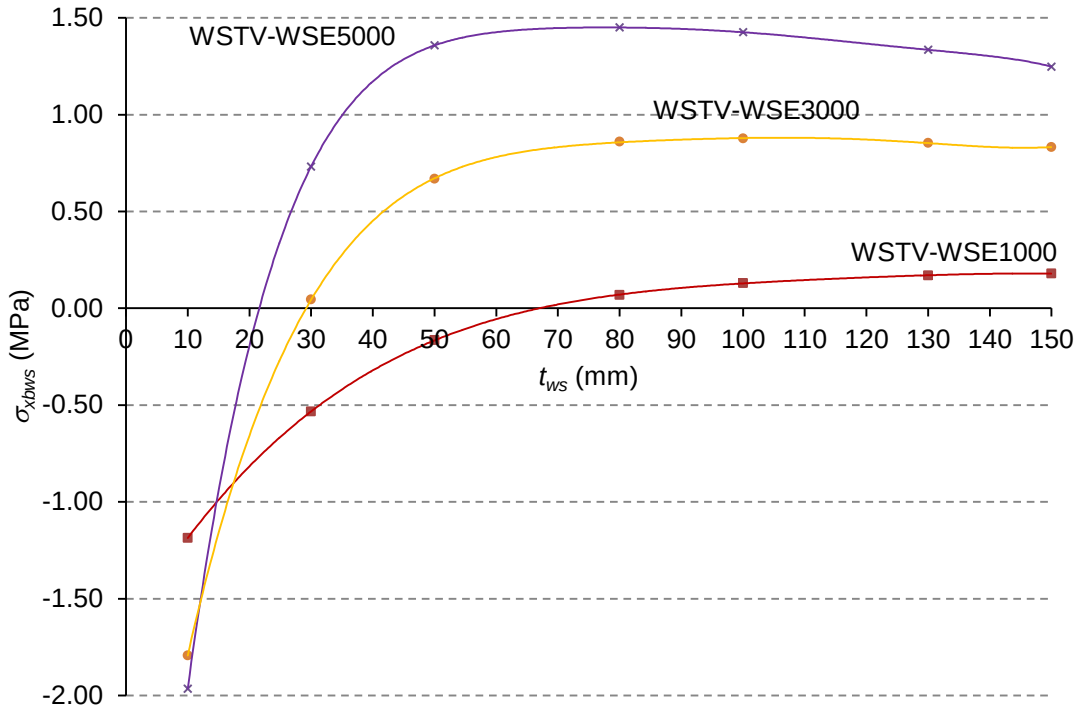

Figure 5.5 Effect of strength of wearing surface layer on horizontal stresses at the bottom fibre of itself

Then the effect of variation in strength of base layer (E_b) on σ_{xbws} was evaluated. The analysis results as illustrated in Figure 5.6 revealed that higher E_b induced the lower value of t_{wsn}, i.e., t_{wsn} values were around 19, 29, and 55 mm for E_b of 800, 350, and 200 MPa, respectively.

Subsequent analyses on the effect of strength of subbase layer (E_{sb}) on σ_{xbws} show that σ_{xbws} was insignificantly affected by the value of E_{sb}, as shown in Figure 5.7. The values of t_{wsn} were almost identical, at around 29 mm, while (E_{sb}) had been varied.

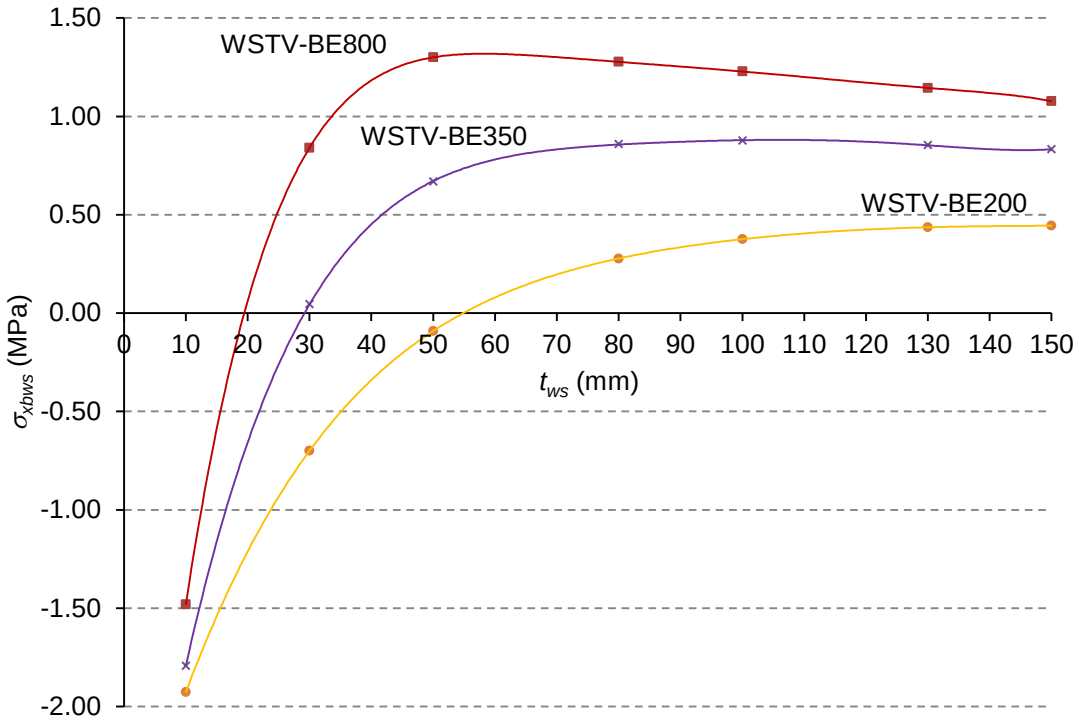

Figure 5.6 Effect of strength of base layer on horizontal stresses at the bottom fibre of wearing surface layer

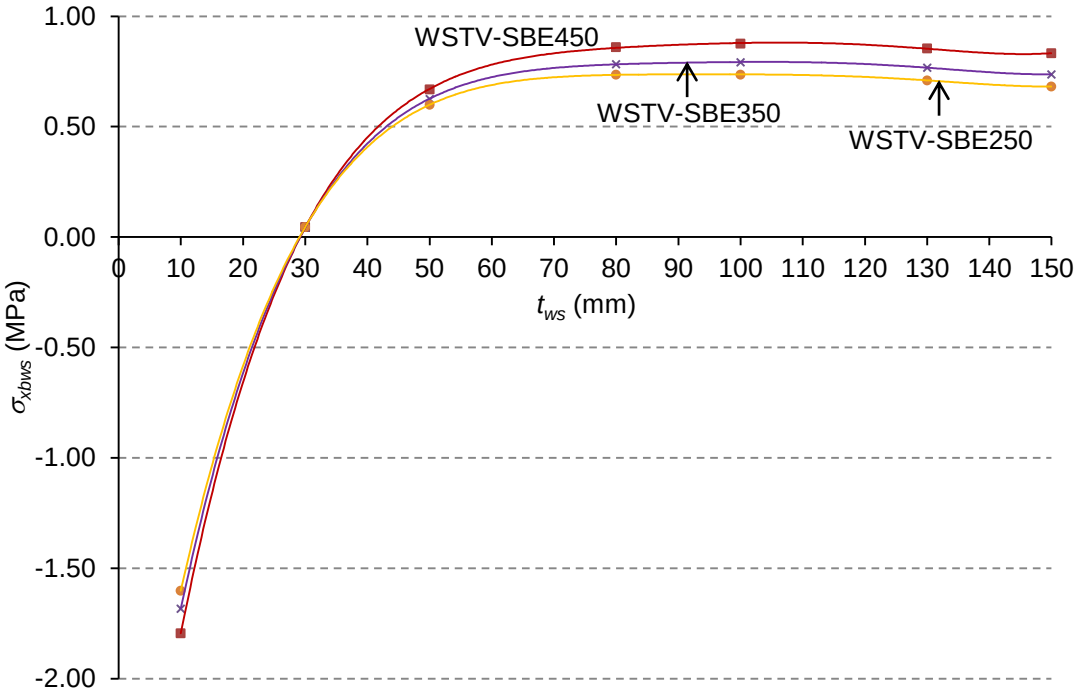

Figure 5.7 Effect of strength of subbase layer on horizontal stresses at the bottom fibre of wearing surface layer

Lastly, the investigation was done to examine changes in σ_{xbws} over the range of subgrade strength (E_{sg}). The results illustrated in Figure 5.8, show that σ_{xbws} slightly increased while the value of E_{sg} decreased. Values of t_{wsn} were around 29, 30, and 31 mm for the case of E_{sg} varied from 70, 50, and 30 MPa, respectively.

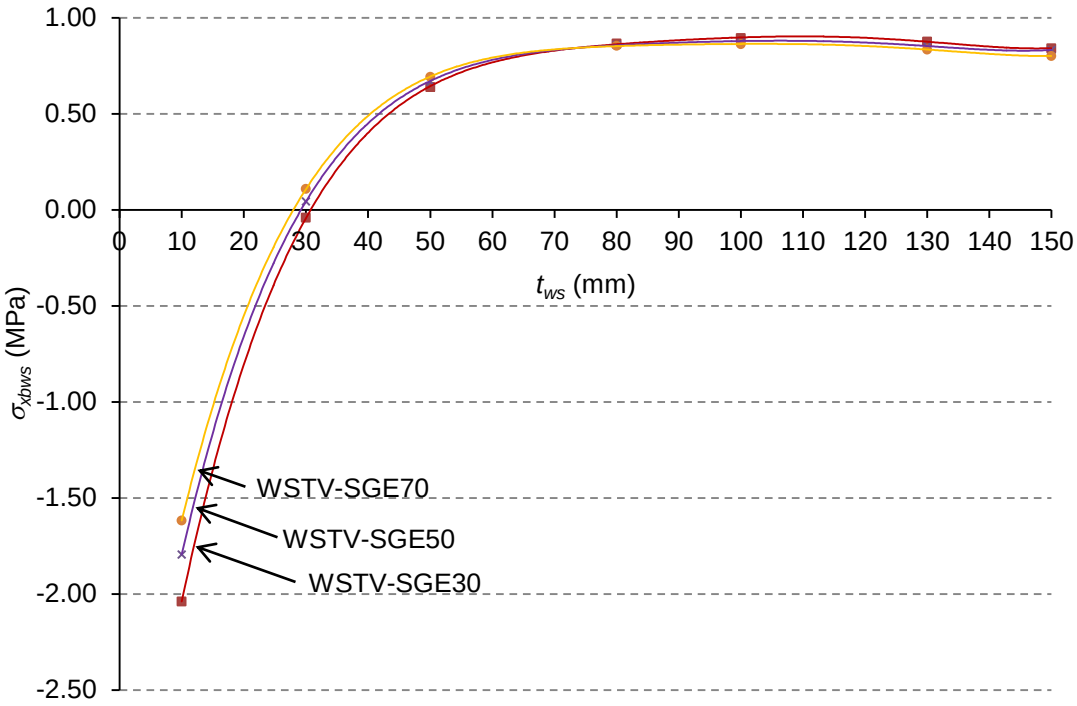

Figure 5.8 Effect of strength of subgrade on horizontal stresses at the bottom fibre of wearing surface layer

Then, a regression technique was employed to formulate polynomial equations for predicting σ_{xbws}, which can be expressed as a general equation as:

$$\sigma_{xbws} = a \cdot t_{ws}^6 + b \cdot t_{ws}^5 + c \cdot t_{ws}^4 + d \cdot t_{ws}^3 + e \cdot t_{ws}^2 + f \cdot t_{ws} + g$$

where the coefficients *a*, *b*, *c*, *d*, *e*, *f* and *g* for each case of investigation are shown in Table 5.3.

Table 5.3 Coefficients of polynomial equation for predicting σ_{xbws}

Case	Coefficients						
	a ($\times 10^{-6}$)	b ($\times 10^{-6}$)	c ($\times 10^{-3}$)	d	e ($\times 10^{3}$)	f ($\times 10^{3}$)	g ($\times 10^{6}$)
WSTV-WSE1000	0.000	-5.000	-4.900	3.051	-0.602	52.978	-2.000
WSTV-WSE3000	0.000	400.000	-202.300	41.223	-4.179	213.073	-4.000
WSTV-WSE5000	-8.000	4.600	-1125.000	146.060	-10.580	407.978	-5.000
WSTV-BE200	0.000	-100.000	-57.300	13.717	-1.707	113.998	-3.000
WSTV-BE350	0.000	400.000	-202.300	41.223	-4.179	213.073	-4.000
WSTV-BE800	-6.000	4000.000	-991.200	130.440	-9.508	361.894	-4.000
WSTV-SBE250	0.000	300.000	-170.000	35.593	-3.689	190.046	-3.000
WSTV-SBE350	0.000	300.000	-181.700	37.709	-3.880	199.307	-3.000
WSTV-SBE450	0.000	400.000	-202.300	41.223	-4.179	213.073	-4.000
WSTV-SGE30	0.000	400.000	-221.100	44.953	-4.542	231.390	-4.000
WSTV-SGE50	0.000	400.000	-202.300	41.223	-4.179	213.073	-4.000
WSTV-SGE70	0.000	300.000	-182.000	37.722	-3.878	199.196	-3.000

Finally, the polynomial equations for predicting σ_{xbws} can be used to derive the equation for predicting t_{wsn}. Figure 5.9, for instance, illustrates the surface of t_{wsn} for wearing surface layer having elastic modulus of 3000 MPa. By applying a regression technique, an equation for calculation of t_{wsn} in this case can be established as;

$$t_{wsn} = \left(-10.26 \times 10^{-6}\right) \cdot E_b^2 + \left(-238.60 \times 10^{-6}\right) \cdot t_b^2 + \left(157.50 \times 10^{-6}\right) \cdot E_b \cdot t_b + \left(43.27 \times 10^{-3}\right) \cdot E_b + \left(16.68 \times 10^{-3}\right) \cdot t_b + 10.10, \left[R^2 = 0.999\right] \quad (5.1)$$

Equation (5.1) can be used to classify the road pavement having thin wearing surface layer in particular case of E_{ws} = 3000 MPa, E_{sb} = 250 MPa, t_{sb} = 250 mm, E_{sg} = 50 MPa, and t_{sg} = 2500 mm.

According to the analysis results in this section, the structural behaviour of road pavement, especially for thin wearing surface pavement, strongly depends on the strength and thickness of both wearing surface and base course layers. It was also found that one of pavement having wearing surface thickness up to 70 mm can be classified as thin surface pavement.

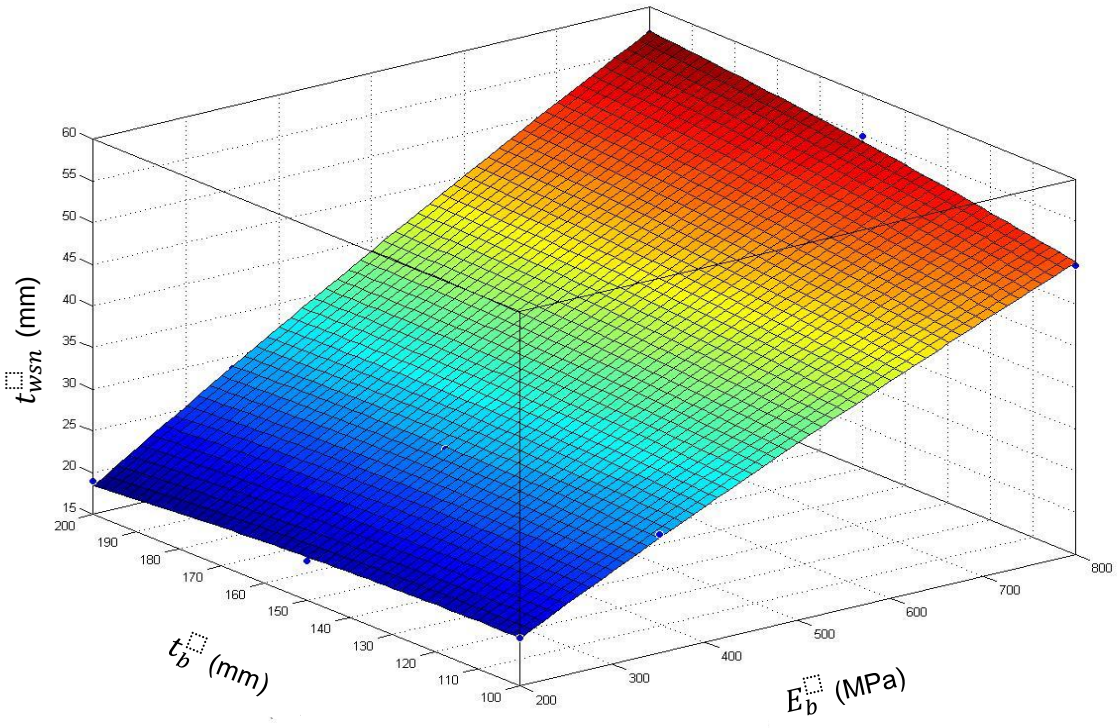

Figure 5.9 Surface of σ_{xbws} = 0 in which E_{ws} = 3000 MPa, E_{sb} = 250 MPa, t_{sb} = 250 mm, E_{sg} = 50 MPa, and t_{sg} = 2500 mm

5.3.2 Investigation of stress distribution in base course layer

Figure 5.10 - Figure 5.15 depict the stress distribution in base layer of WSTV-BE200, in which the thickness of the base layer is varied from 100-200 mm. It can be seen that the horizontal stresses (σ_{xx}) varied from 30-450 kPa (compression) and the vertical stresses (σ_{yy}) ranged from 230-600 kPa (compression) which resulted in the variation of stress ratios $\left(\frac{\sigma_{yy}}{\sigma_{xx}}\right)$ from 1.25-10. These analysis results can be adopted to determine the appropriate stress stages for cyclic load test of base course materials. The stress distributions of the other cases are illustrated in Appendix C.

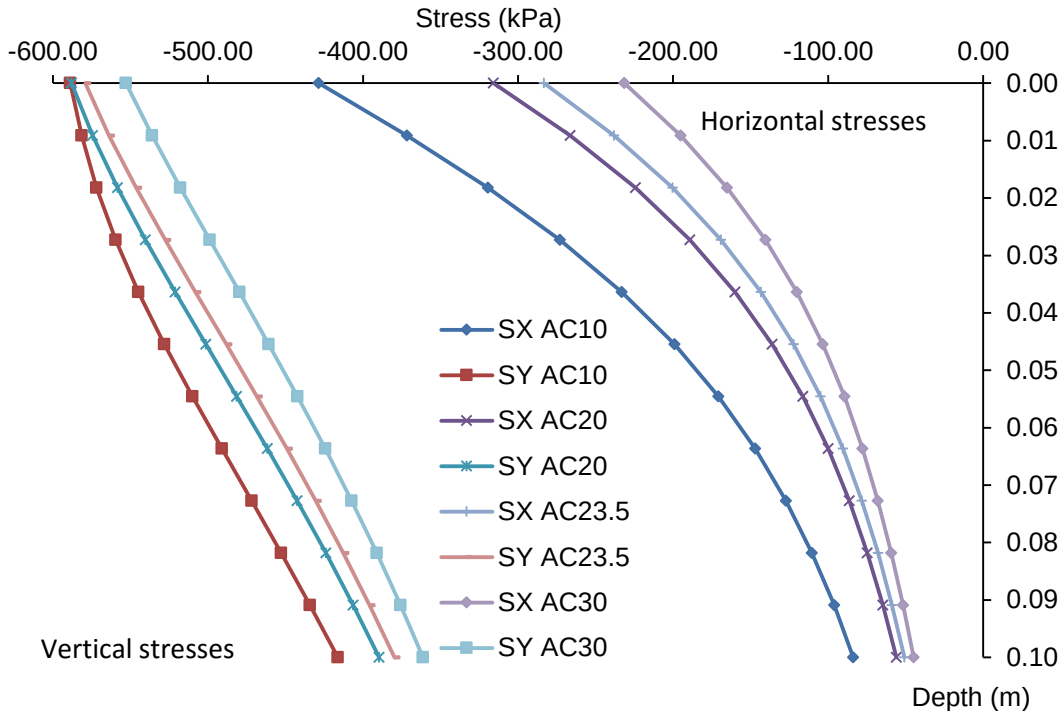

Figure 5.10 Stress distribution in the base layer of WSTV-BE200 with t_b reduced to 100 mm and $t_{ws} \leq t_{wsn}$

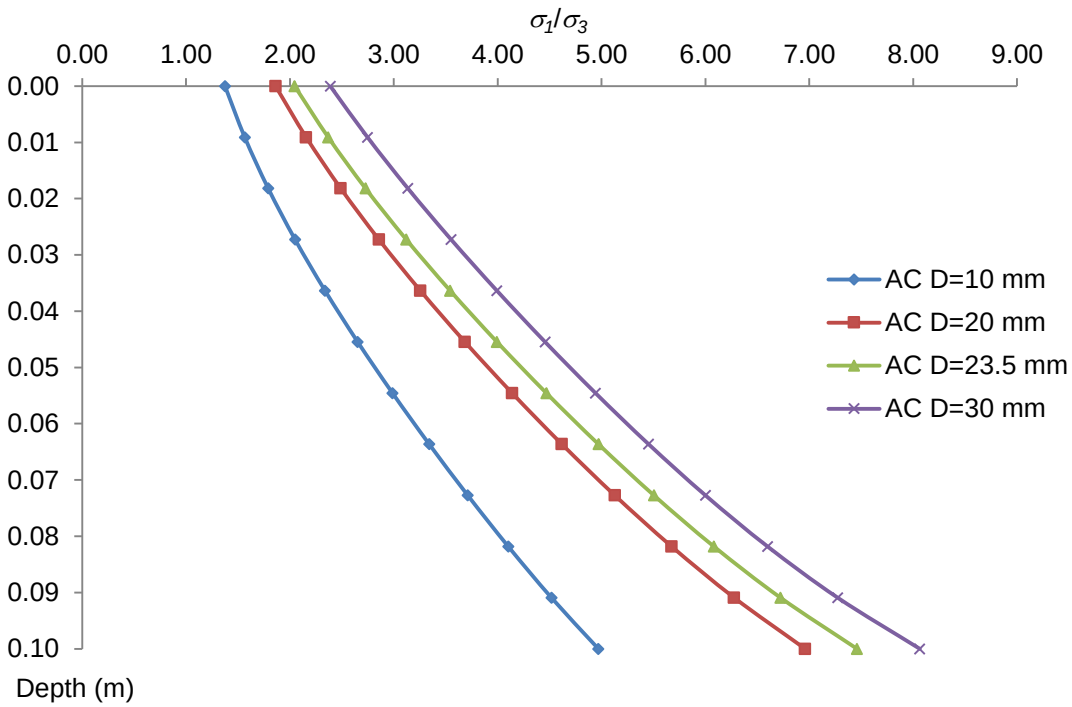

Figure 5.11 Ratio of stress distribution in the base layer in case of WSTV-BE200 with t_b reduced to 100 mm and $t_{ws} \leq t_{wsn}$

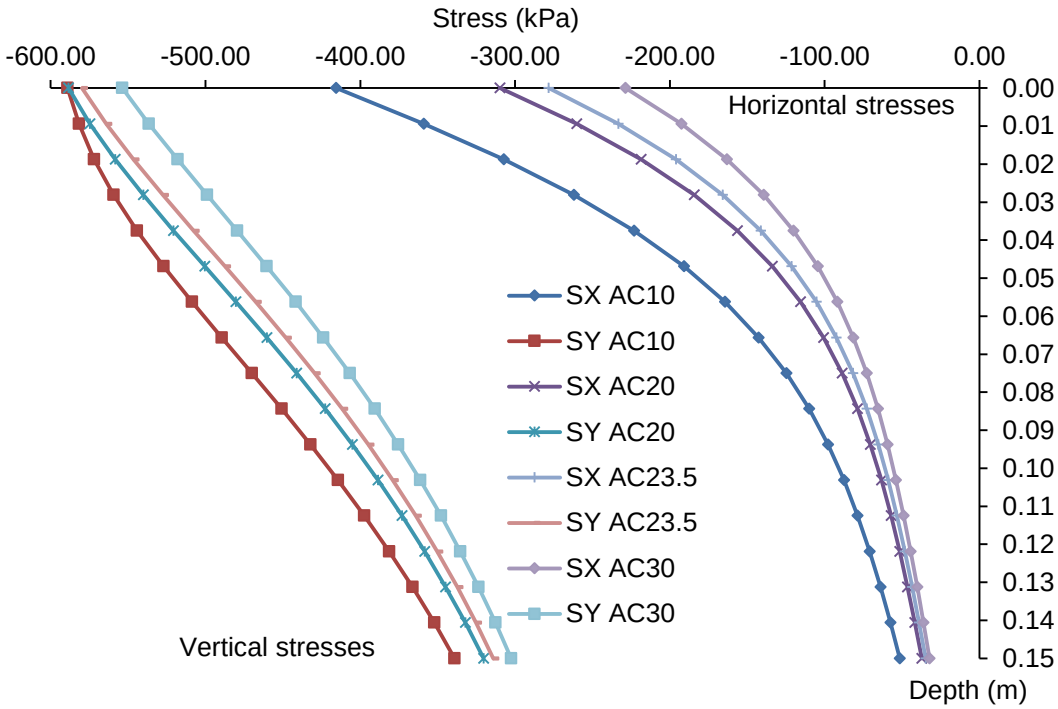

Figure 5.12 Stress distribution in the base layer of WSTV-BE200 with $t_{ws} \leq t_{wsn}$

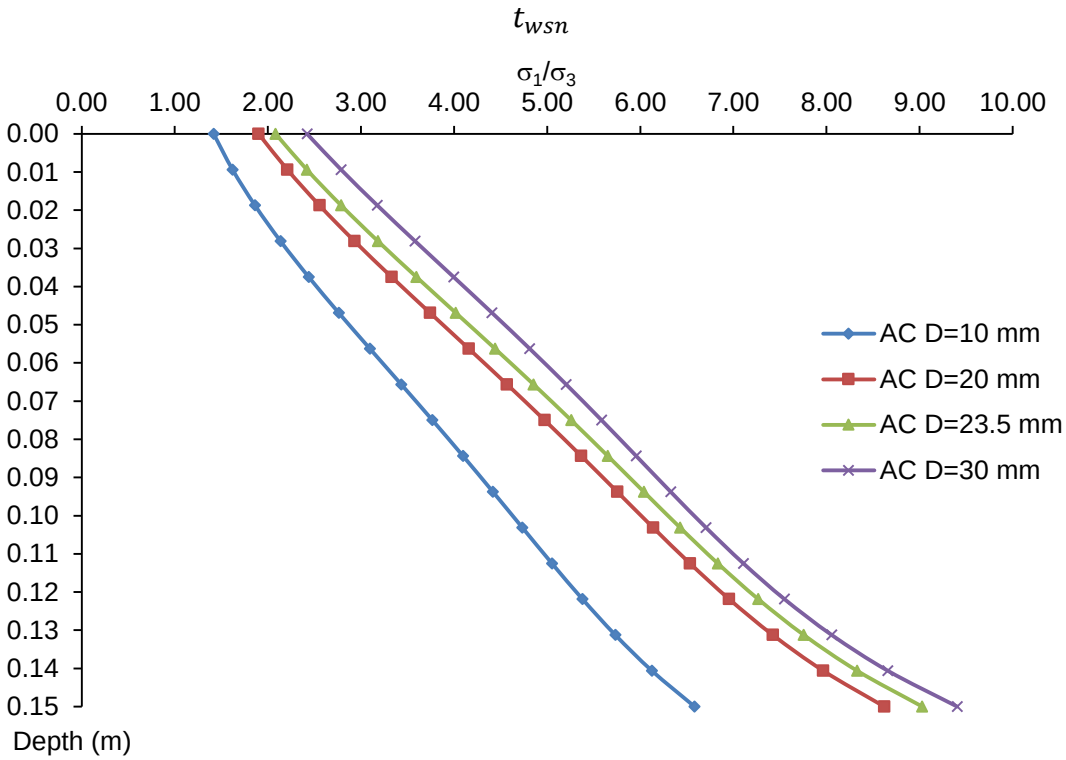

Figure 5.13 Ratio of stress distribution in the base layer of WSTV-BE200 with $t_{ws} \leq t_{wsn}$

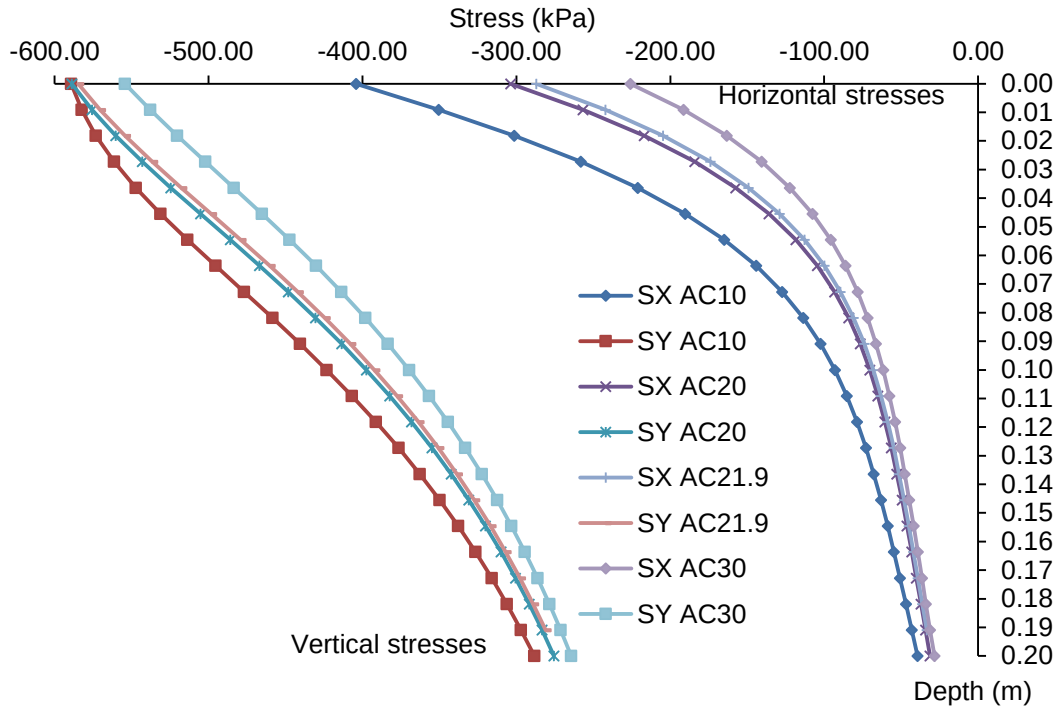

Figure 5.14 Stress distribution in the base layer of WSTV-BE200 with t_b increased to 200 mm and $t_{ws} \leq t_{wsn}$

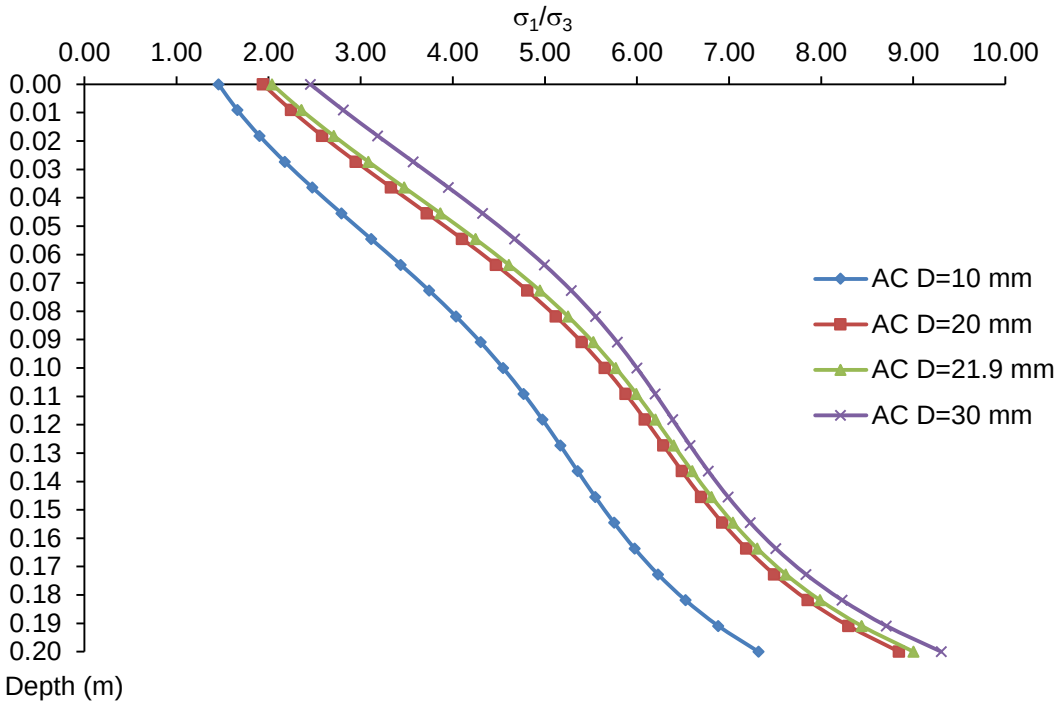

Figure 5.15 Ratio of stress distribution in the base layer of WSTV-BE200 with t_b increased to 200 mm and $t_{ws} \leq t_{wsn}$

5.4 Analysis of specimen in RLT test

Figure 5.16 shows an example of the distribution of induced stress in an RLT specimen model. The results were then plotted on p-q space, as shown in Figure 5.17. It was found that the maximum principal stresses in the specimen were more than the applied stresses (σ_1 and σ_3) specified by Austroads (Austroads 2007). Moreover, some applied stresses located beyond the Mohr-Coulomb failure envelopes of test materials; this may cause the failure of test specimen during RLT test.

Furthermore, the tensile stresses were generated in the RLT specimen model when the stress ratio (σ_1/σ_3) is higher than 12.5. As a consequence, a significant error may occur in design process when pavement engineers use the resilient moduli obtained from the standard testing protocol which the applied stress ratio beyond 12.5. Thus the applied stresses used in the RLT test should be revised to appropriately represent the stresses distribution in pavement structure.

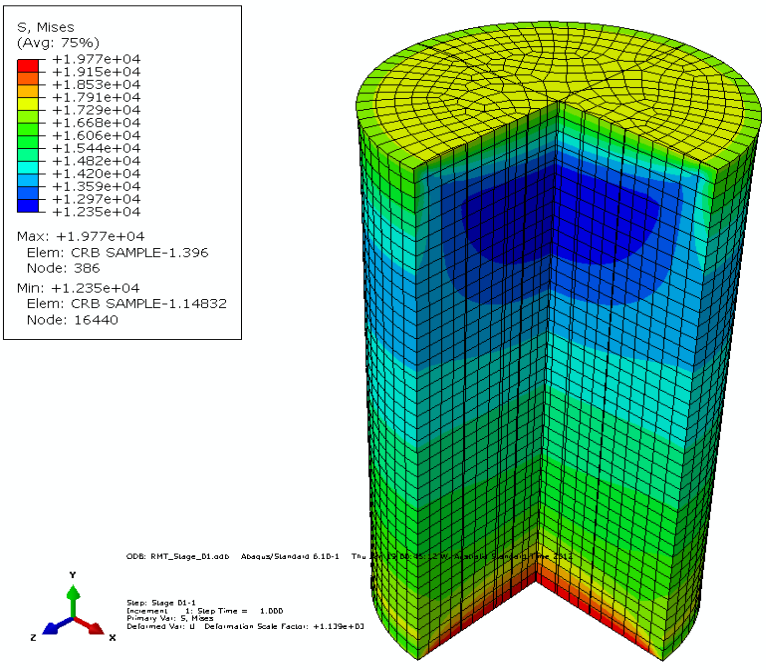

Figure 5.16 Example of the result from finite element analysis of the specimen in RLT test

Based on the results from finite element analysis as seen in Figure 5.16, the maximum principal stresses commonly occurred around bottom surface of specimen, which was the support area. By employing the failure envelope as shown in Figure 5.17, it can be implied that the specimen already failed during the test is being performed. This indicates that the assumption using by Austroads for conducting the RLT test cannot represent the stress conditions occur in testing specimen because the applied stresses (σ_1 and σ_3) in accordance with Austroads standard are not the principal stresses occur in base course materials, both CRB and HCTCRB.

Therefore, the obtained results would be more accurate if the resultant stresses occur in testing specimen are not exceed the failure envelope of material. This means the applied stresses which suit for each material have to be investigated.

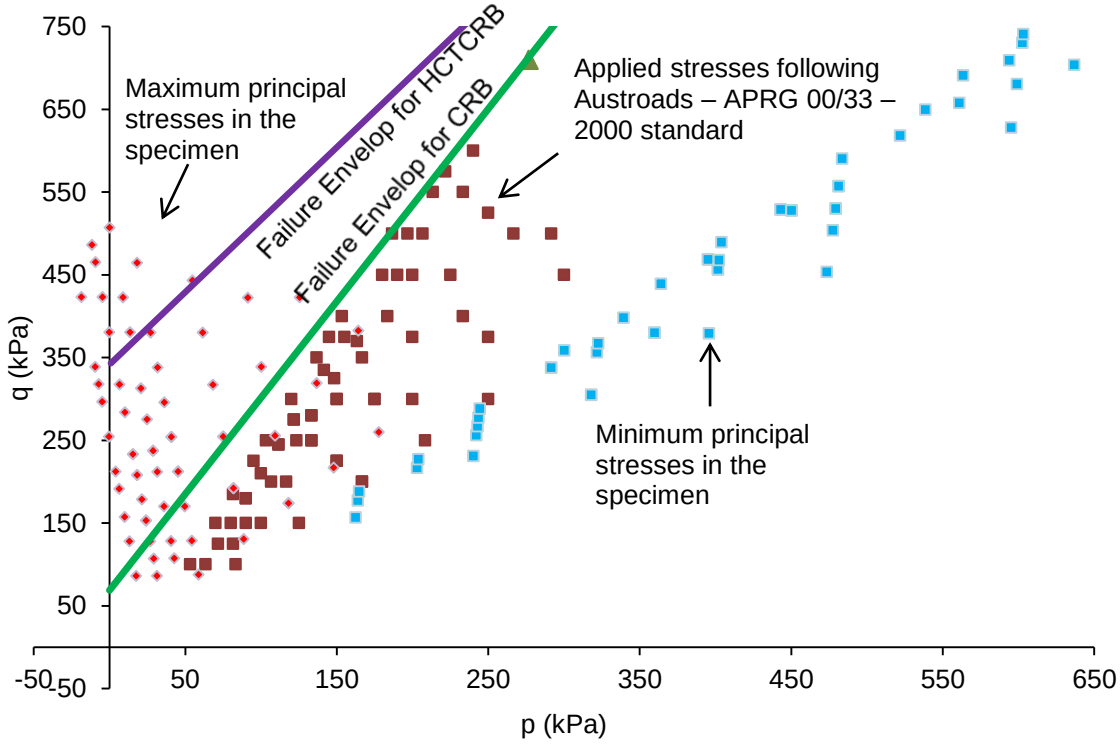

Figure 5.17 p-q diagram of the applied stresses according to Austroads

5.5 Modification of the applied stresses for RLT test of base course materials

This section presents determination of suitable stress regime for the resilient modulus test of CRB and HCTCRB. The results from FEM analysis of both pavement structure and the RLT test specimen were compared and used to determine the appropriated stress stages to be adopted for the resilient modulus test.

5.5.1 Results from finite element analysis

Examples of the induced stresses in base course layer are shown in Figure 5.18 - Figure 5.26. It was found that the stresses in base course layer depended on the strength and thicknesses of base and subbase layer. Horizontal stresses along the depth of base course layer varied from 0 to 800 kPa, excluded the tensile stress. Therefore the major principal stress (σ_1) that suits for the resilient modulus test should be in this range.

Mohr-Coulomb failure envelope and the stress condition along the depth of base layer were plotted on p-q diagram as shown in Figure 5.27. It was found that some stresses underwent beyond failure envelope. Some tensile stresses were found when the strength of base course materials was around 800 MPa and higher. This was because the analyses were done based on an elastic assumption, therefore the tensile stress in material was allowed and the base course layer might act as a flexural member.

The finite element analysis of standard RLT specimen showed that the tensile stresses occurred in specimen when the stress ratio (σ_1/σ_3) was higher than 12.5. Therefore the new loading regime for resilient modulus test must be limited at the stress ratio of 12.5 and the resultant stresses in the specimen should be below the failure envelope of the test material.

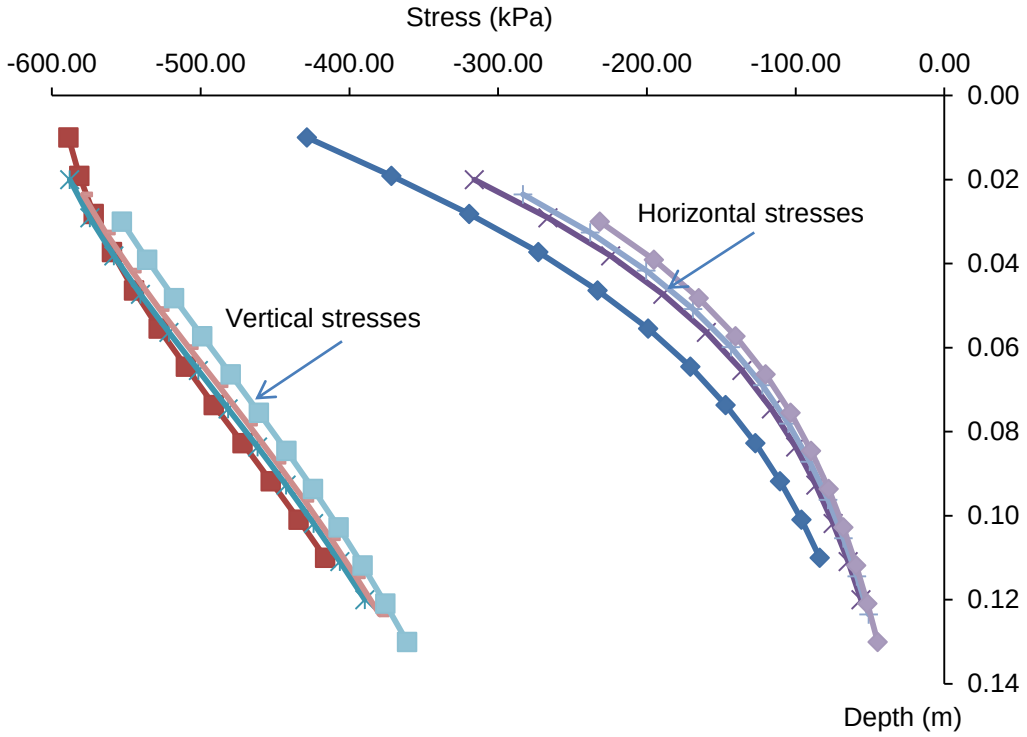

Figure 5.18 Stress distribution along the depth of base layer in WSTV-BE200 with t_b reduced to 100 mm

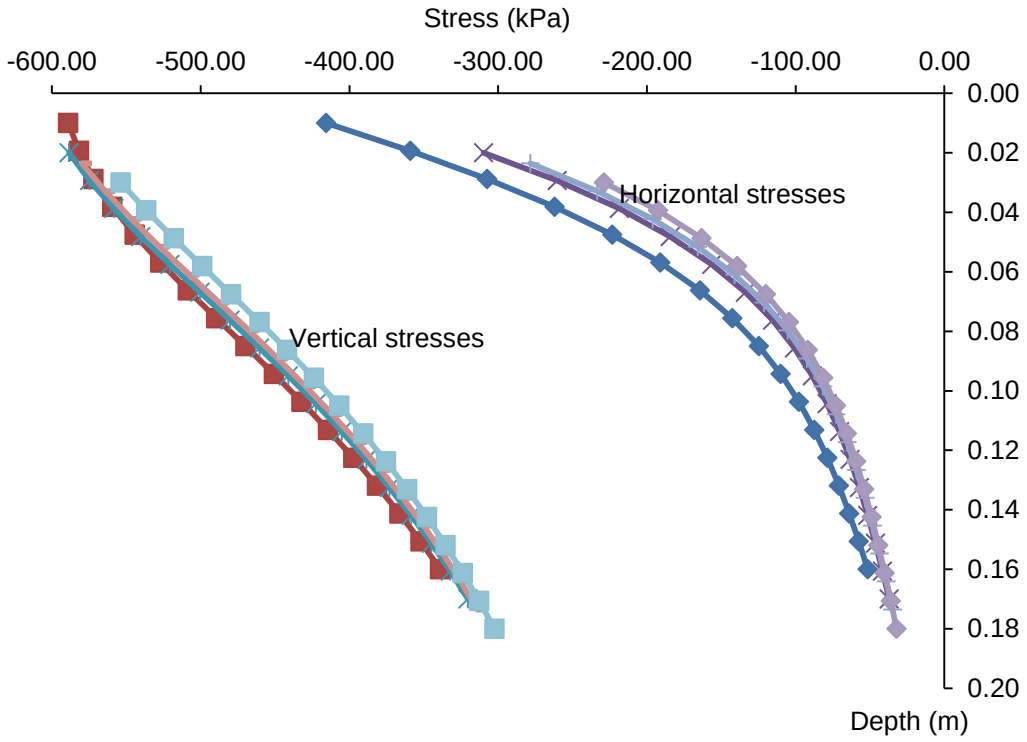

Figure 5.19 Stress distribution along the depth of base layer in WSTV-BE200

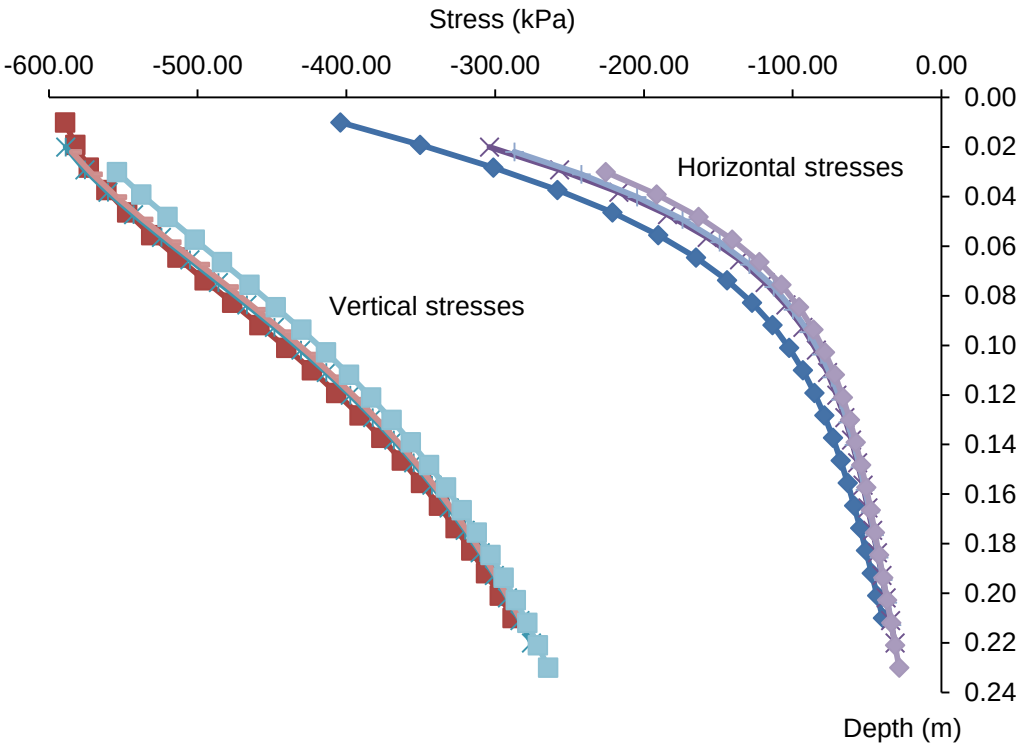

Figure 5.20 Stress distribution along the depth of base layer in WSTV-BE200 with t_b increased to 200 mm

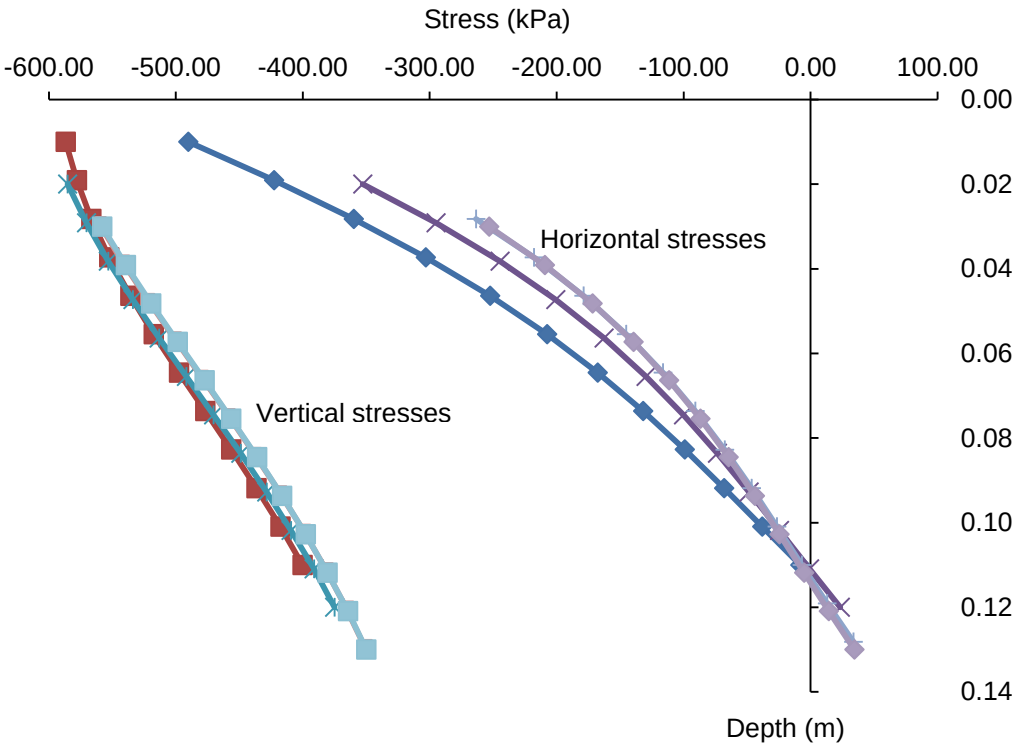

Figure 5.21 Stress distribution along the depth of base layer in WSTV-BE350 with t_b reduced to 100 mm

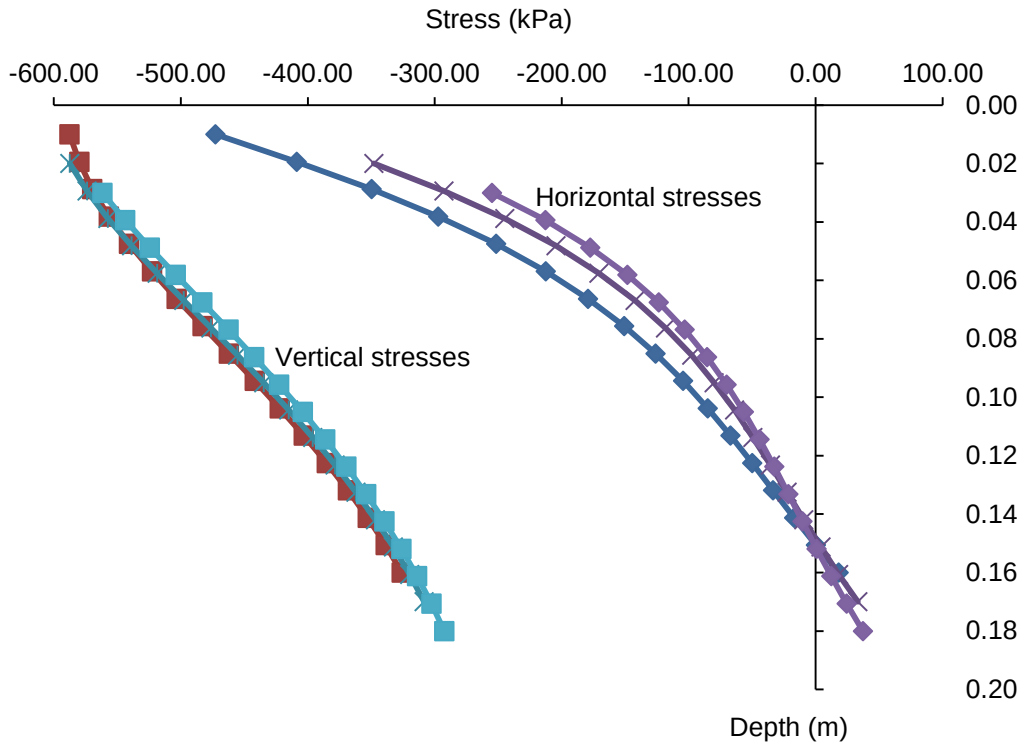

Figure 5.22 Stress distribution along the depth of base layer in WSTV-BE350

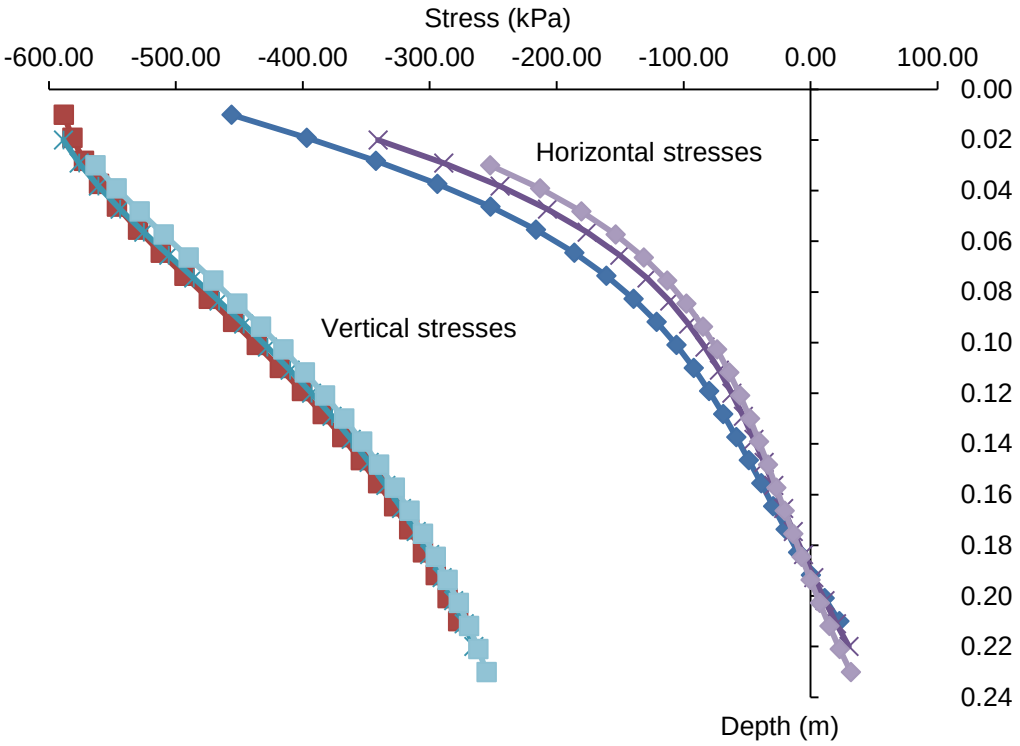

Figure 5.23 Stress distribution along the depth of base layer in WSTV-BE350 with t_b increased to 200 mm

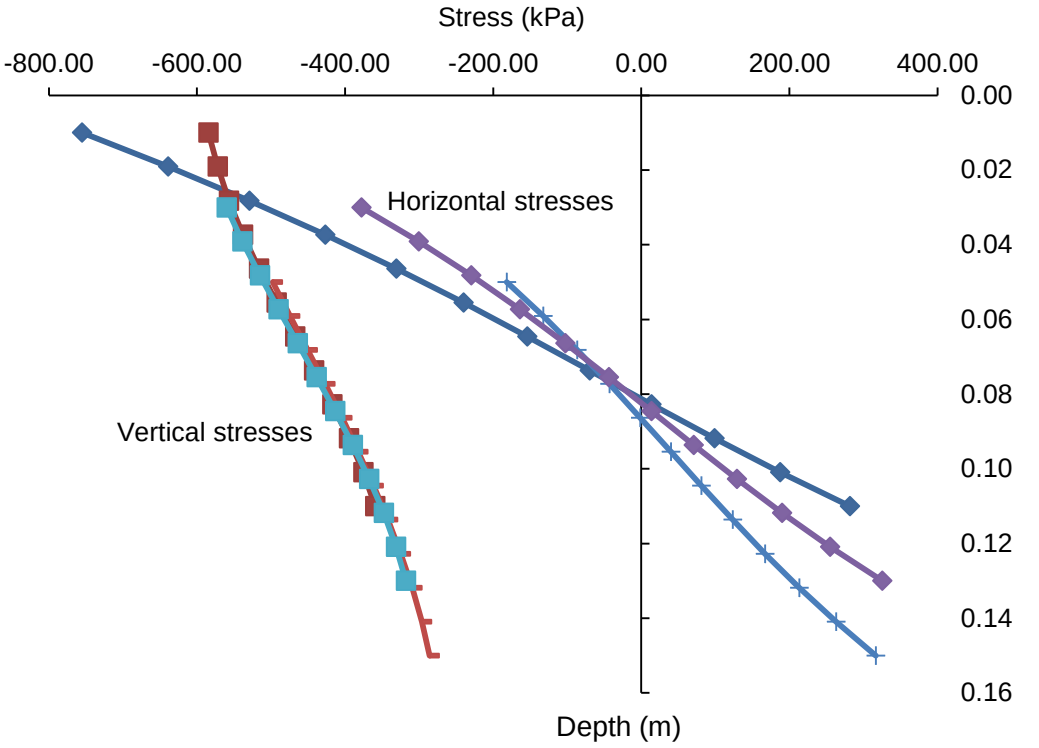

Figure 5.24 Stress distribution along the depth of base layer in WSTV-BE800 with t_b reduced to 100 mm.

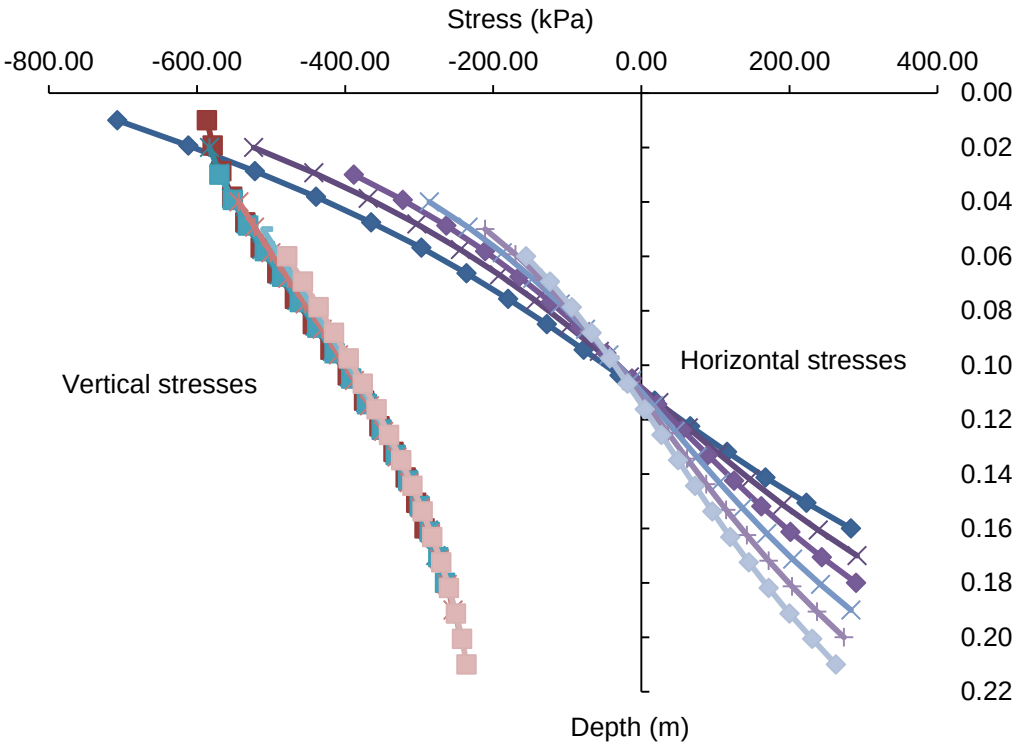

Figure 5.25 Stress distribution along the depth of base layer in WSTV-BE800

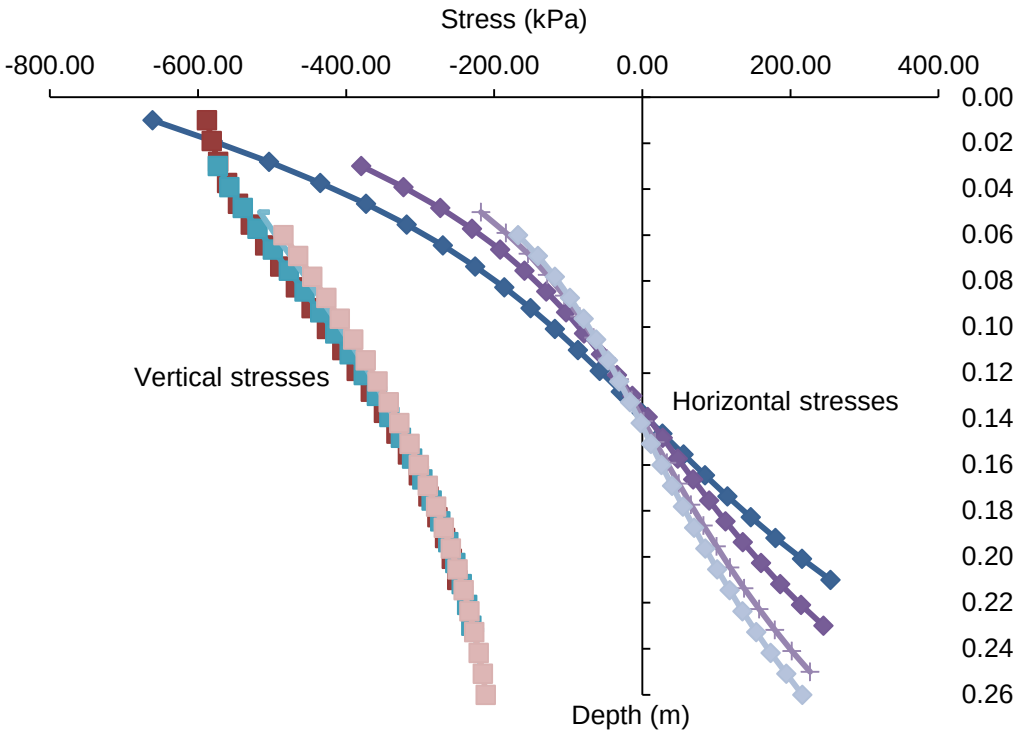

Figure 5.26 Stress distribution along the depth of base layer in WSTV-BE800 with t_b increased to 200 mm

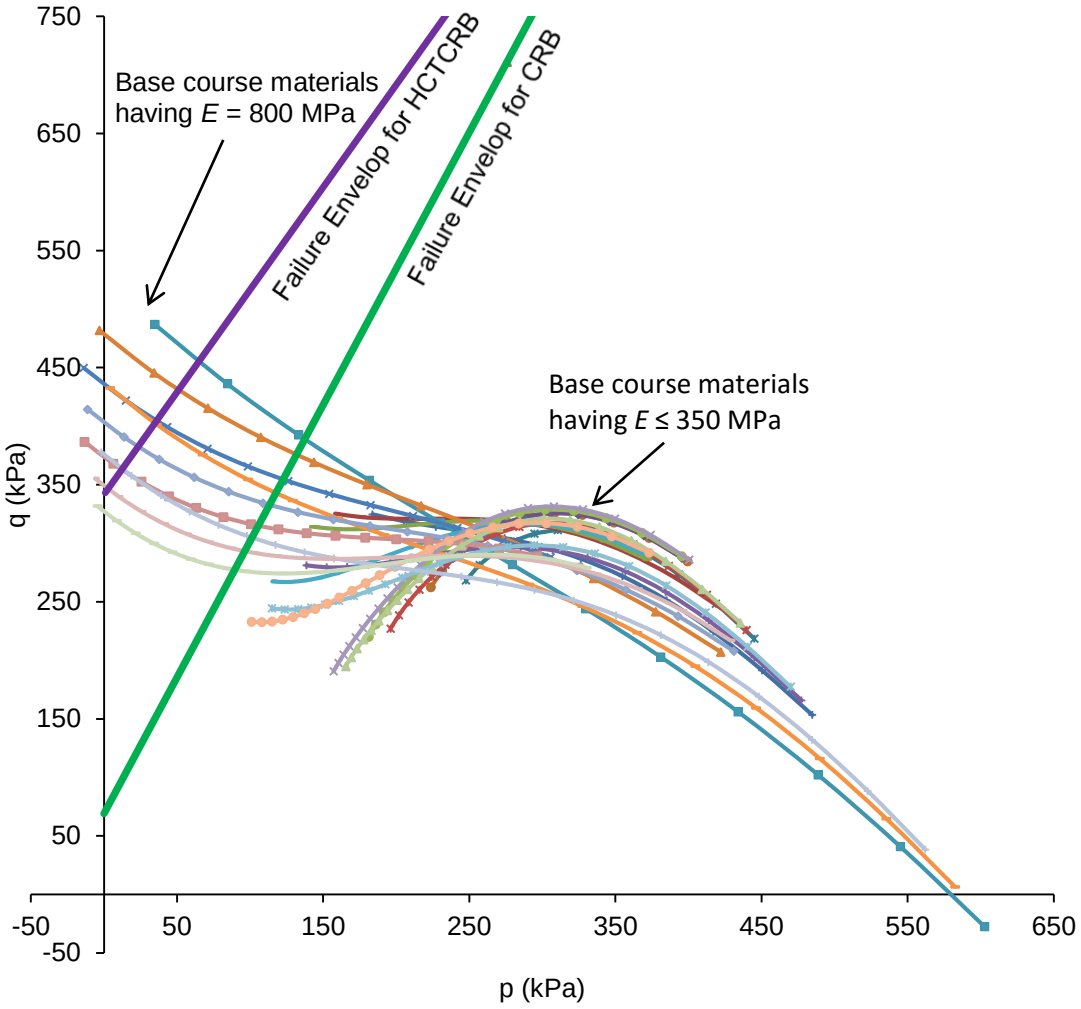

Figure 5.27 p-q diagram of stress distribution in base course layer of pavement structure

5.5.2 New loading regime

The applied stresses suitable for the resilient modulus test should be in the shaded area as shown in Figure 5.28. This was done by a trial and error method under the following criteria:

- The resultant stresses must scatter around the stress conditions that occur along the depth of base layer, as seen Figure 5.28.
- The major principal stress (σ_1) should not more than 800 MPa.
- The stress ratio (σ_1/σ_3) should be limited at 12.5.
- The resultant stresses in the specimen should be below the failure envelope of the test material.

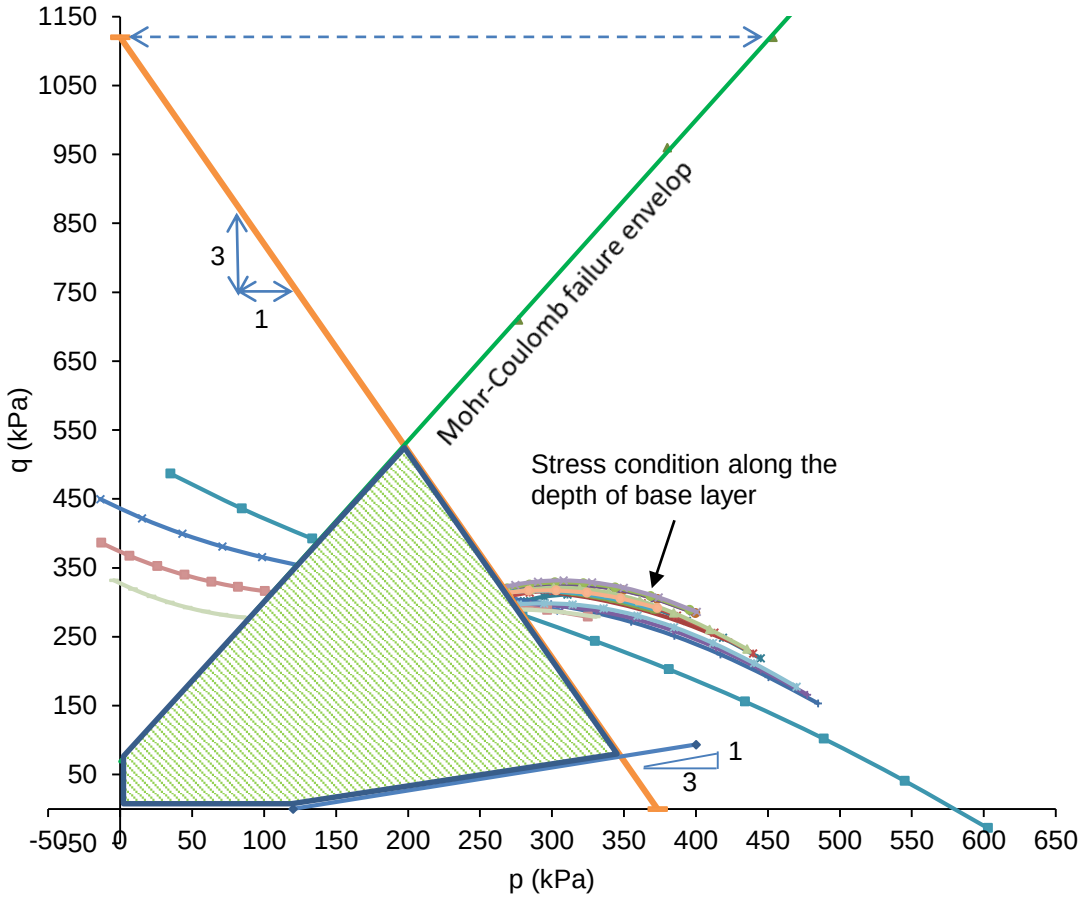

Figure 5.28 Area for determination of the applied stress stages for resilient modulus test of base course materials

The suitable applied stresses can be expressed in a form of relationship between stress ratio and confining stress as shown in Equation (5.2), and its curve can be illustrated as shown in Figure 5.29 and Figure 5.30.

$$\left(\frac{\sigma_1}{\sigma_3}\right) = 12.5e^{m_1\,\sigma_3} \tag{5.2}$$

where $m_1 = 0.0024\ln(M_{re}) - 0.0217$ and M_{re} = an expected resilient modulus of base course material.

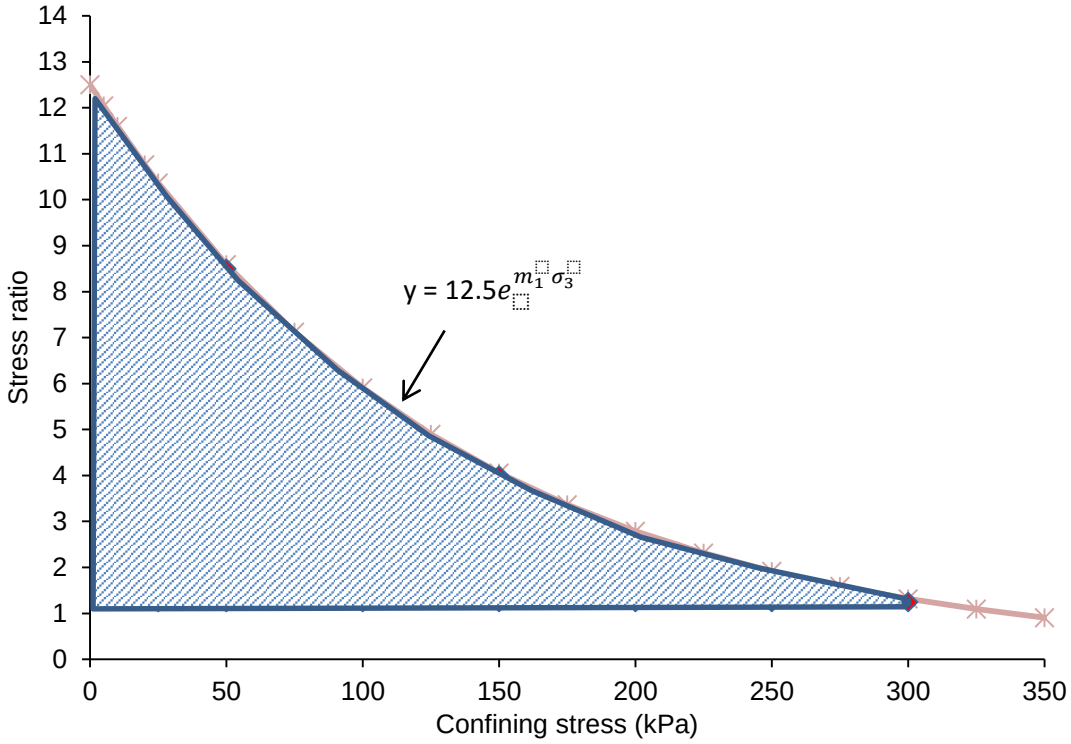

Figure 5.29 The area for determining the applied stresses in term of the relationship between stress ratio and confining stress

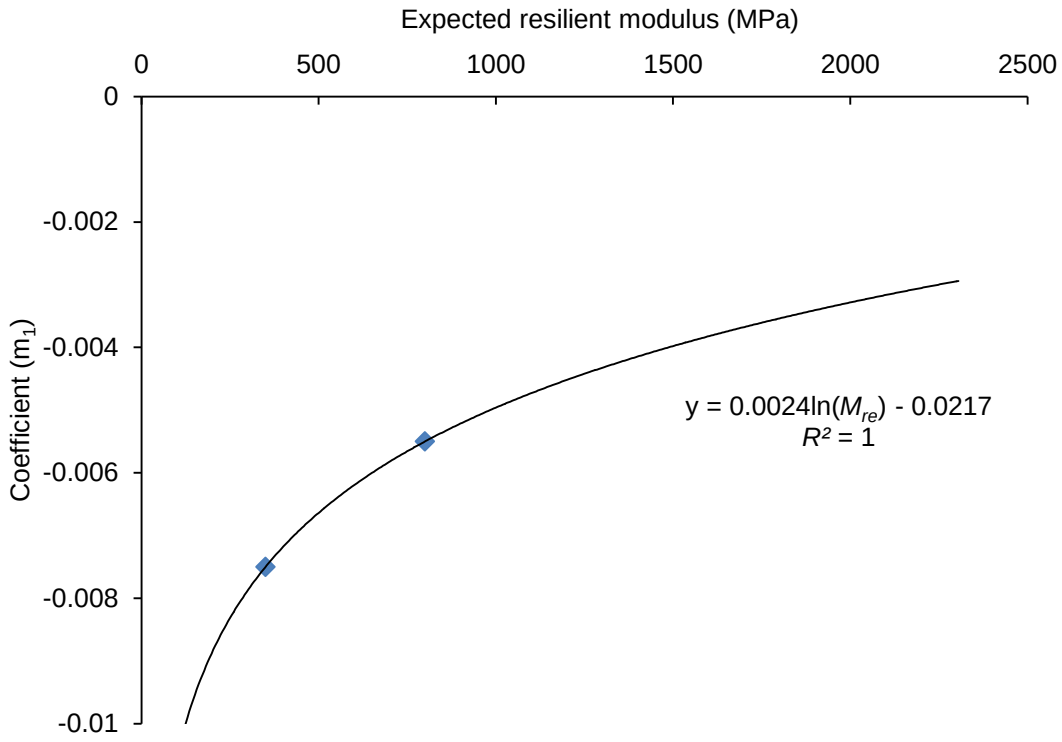

Figure 5.30 Relationship between m_1 and the expected resilient modulus

Because the applied stress regime in this section is proposed for flexible pavement having thin asphalt concrete layer, thus the surcharge weight on top of base course layer is quite small in comparison with the weight of base course layer and the underlying layers. According to the results in section 5.3.2, it can be found that the stress ratio along the depth of base layer start around 1.25 at the top fibre of base layer (cf. Figure 5.10 - Figure 5.15), which is the point of maximum stress, therefore the stress ratio for RLT test can start from 1.25 at higher confining stress.

Table 5.4 shows an example of the applied stresses which are retrieved from the area under the curves in Figure 5.31.

Figure 5.32 and Figure 5.33 reveal that maximum principal stresses found in the RLT specimen model were well below the failure envelope when subjected to the proposed stress regime. It was also found that some maximum principal stresses in the RLT specimen model were closed to stresses in the base course layer of the pavement model. Thus the resilient modulus test results,

analysed using the proposed stress regime, would be more reliable than the results from the Austroads standard test method.

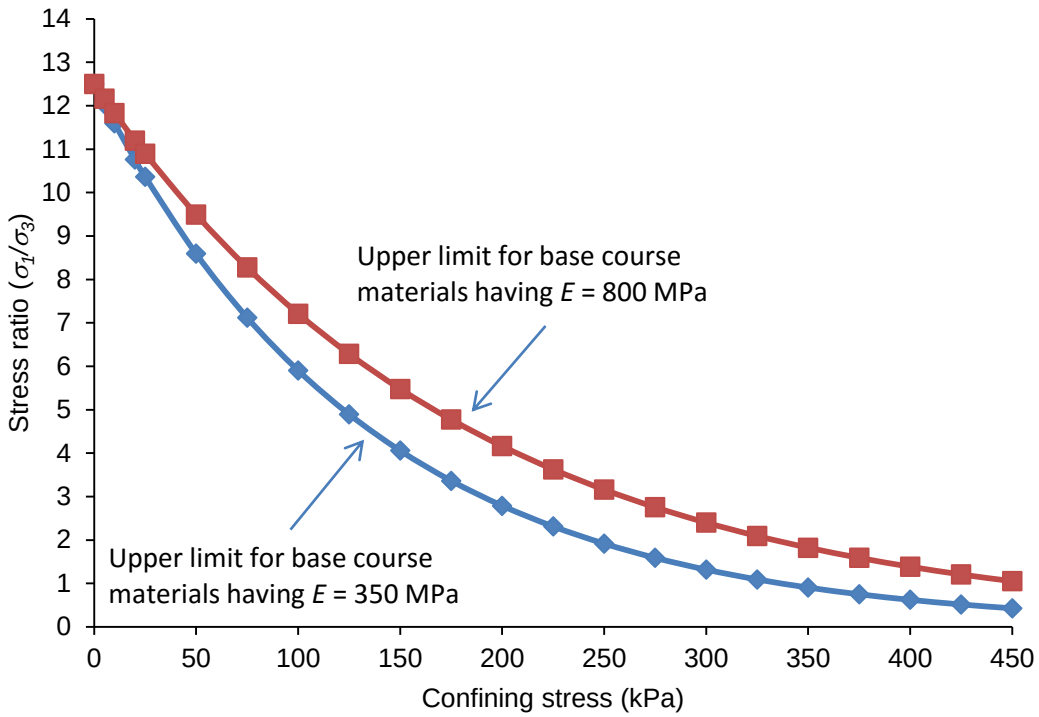

Figure 5.31 Example of the proposed upper limit of the applied stresses for resilient modulus test

Table 5.4 Example of the applied stresses from the area under the upper limit

M_r = 350 MPa (for CRB)				M_r = 800 MPa (for HCTCRB)			
Stage no.	Stress ratio	Confining stress (kPa)	Axial stress (kPa)	Stage no.	Stress ratio	Confining stress (kPa)	Axial stress (kPa)
1	2	25	50	1	2	25	50
2	3	25	75	2	3	25	75
3	4	25	100	3	4	25	100
4	5	25	125	4	5	25	125
5	2	50	100	5	2	50	100
6	3	50	150	6	3	50	150
7	4	50	200	7	4	50	200
8	5	50	250	8	5	50	250
9	6	50	300	9	6	50	300
10	7	50	350	10	7	50	350
11	8	50	400	11	8	50	400
12	8.5	50	425	12	9	50	450
				13	9.5	50	475
13	2	100	200	14	2	100	200
14	3	100	300	15	3	100	300
15	4	100	400	16	4	100	400
16	5	100	500	17	5	100	500
17	5.5	100	550	18	6	100	600
				19	7	100	700
18	2	150	300	20	2	150	300
19	3	150	450	21	3	150	450
20	4	150	600	22	4	150	600
				23	5	150	750
				24	5.5	150	825
21	1.5	200	300	25	1.5	200	300
22	2	200	400	26	2	200	400
				27	3	200	600
				28	4	200	800
23	1.25	250	312.5	29	1.25	250	312.5
24	1.5	250	375	30	1.5	250	375
				31	2	250	500
				32	3	250	750
25	1.25	300	375	33	1.25	300	375
				34	1.5	300	450
				35	2	300	600
				36	1.25	350	437.5
				37	1.5	350	525
				38	1.25	400	500

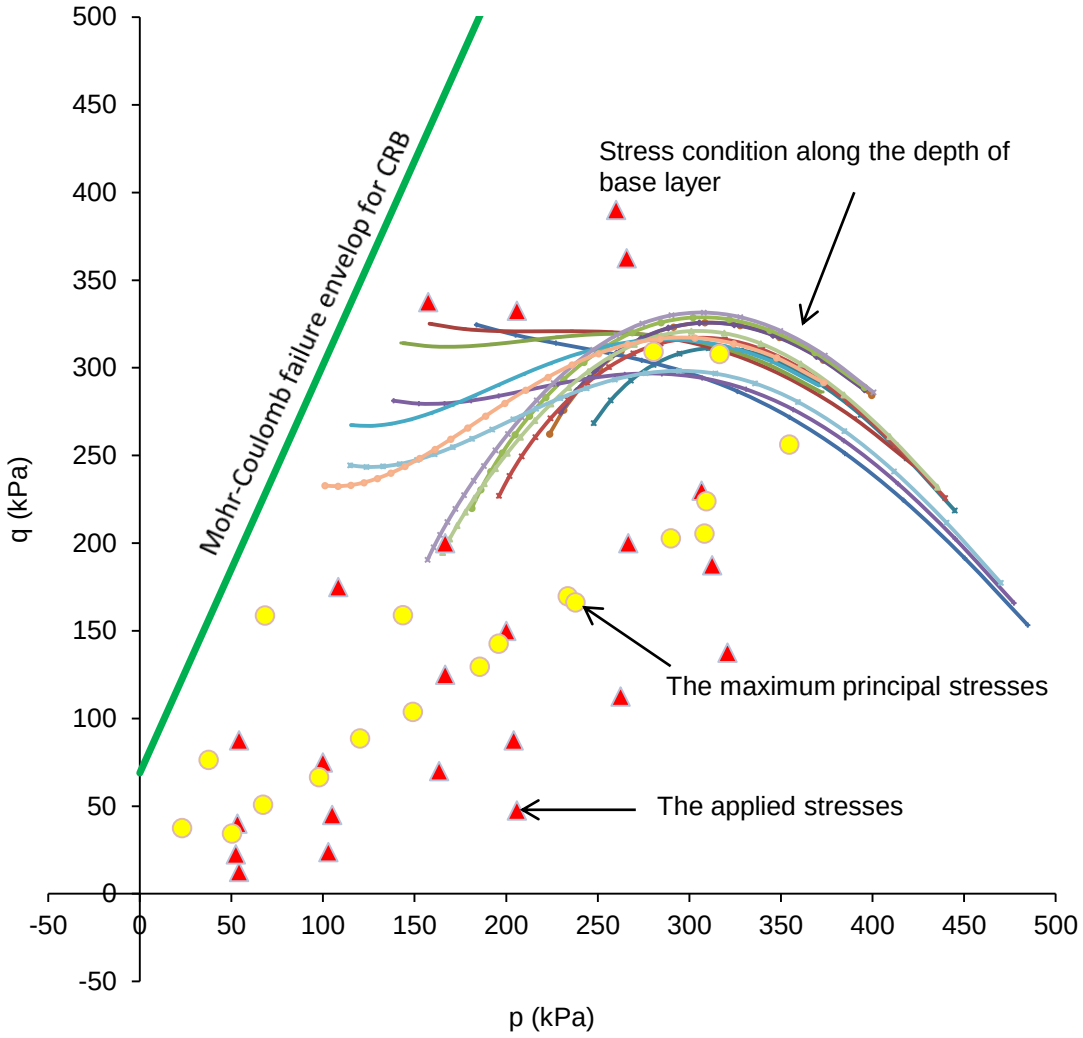

Figure 5.32 Example of the results from 3D finite element analysis of CRB using the proposed applied stresses

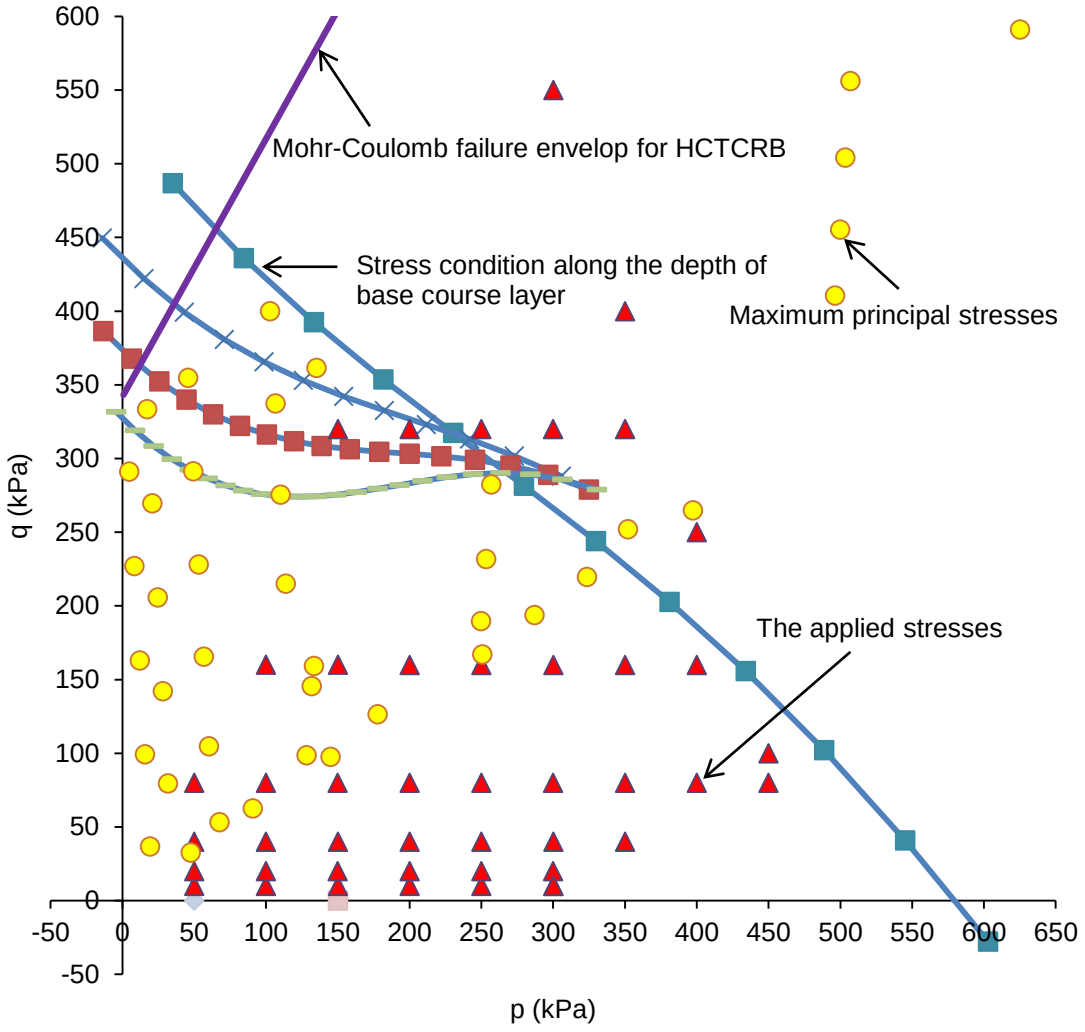

Figure 5.33 Example of the results from 3-D finite element analysis of HCTCRB using the proposed applied stresses

5.6 Summary

The finite element analysis was employed to check the stress distribution, in pavement structure model subjected to the equivalent standard axle load and RLT specimen subjected to the applied stresses in accordance with the Austroads standard. The comparison of occurrence stresses in pavement model and the RLT specimen model revealed that the applied stresses in the RLT test protocol do not suit all base course materials. This is because some stress stages can cause the induced stress in RLT test sample to be beyond the failure envelope of the material. Therefore the applied stresses in the RLT

test have been modified to correctly represent the stress conditions in a pavement structure. Consequently, the proposed applied stresses and stress stages for conducting the RLT test were presented for CRB and HCTCRB. Analysis using the proposed applied stresses showed that some maximum principal stresses in the RLT specimen model were scattered around the stress conditions along the depth of base layer in the pavement model. Hence, the use of the proposed stress regime in conducting the resilient modulus test of base course materials provides the results which are more realistic in the resultant stresses and deformations of the test specimen than the results from the Austroads standard test method.

CHAPTER 6
ADVANCED ANLYTICAL APPROACH FOR FLEXIBLE PAVEMENT IN WESTERN AUSTRALIA

6.1 Introduction

Application of the disturbed state concept (DSC) for modelling the response of CRB and HCTCRB subjected to the static and cyclic loadings was presented in Chapter 4. In this chapter, The DSC was further adopted to establish a new concept for pavement analysis and design. The advanced modellings of base course materials and a new analysis concept obtained from this chapter, which rely on empirical-mechanistic approach, can be used for analysis and design of flexible pavement having thin asphalt surface.

6.2 Deformation concept

A new concept for analysis of pavement structure introduced in this chapter was based on the load-deformation behaviour of base course materials. Both laboratory and finite element analysis results were used to establish the equations which represented the response of material subjected to repeated loading. Firstly, the base course materials, CRB and HCTCRB, were characterised in term of resilient deformation and permanent deformation.

Consequently, the base course specimens were modelled and analysed by finite element method using ABAQUS, to determine the deformation responses. The first loop (N = 1) of analysis adopted an elastic modulus from Equation (3.1) and (3.2) for CRB and HCTCRB respectively. On the next loop, the elastic modulus was replaced by the resilient modulus calculated from Equations (2.6) and (4.34). Then the resilient deformation obtained from laboratory tests and finite element analyses were compared. Certainly, the resilient deformations determined by the two methods were not identical therefore the disturbance function (D) was adopted for adjustment of these values.

The deformation concept can be illustrated as a flow chart shown in Figure 6.1. Details for finite element analysis of the specimen are as same as described in Section 5.2.2 while the process to determine function *D* can be explained concisely as;

Step 1 model a base course specimen in RLT test for a 3D finite element analysis, as state in section 5.2.2, by using elastic modulus (*E*) which is calculated by Equation (3.1) or (3.2).

Step 2 apply axial stress (σ_1) and confining stress (σ_3) on the model then start analysing the specimen in ABAQUS. Then the maximum deformation obtained from finite element analysis is adopted as the total deformation (δ_t) of the specimen.

Step 3 since the total deformation of material (δ_t) is composed of the resilient deformation part (δ_e) and the permanent deformation part (δ_d), as expressed in Equation (2.6), therefore the theoretical resilient deformation (δ_r^e) can be calculated by $\delta_r^e = \delta_t - \delta_d^a$, where δ_d^a is the actual permanent deformation which obtained from laboratory test.

Step 4 record the different value between the theoretical resilient deformation and the actual resilient deformation ($\delta_r^e - \delta_r^a$). This value will be brought to establish a constitutive formula for predicting function *D*.

Step 5 calculate the resilient modulus (M_r) for using in the next loop of analysis by $M_r = \frac{(\sigma_1 - \sigma_3)}{\left(\frac{\delta_r^a}{200\ mm}\right)}$. Consequently, the value of M_r will always be changed in accordance with the number of load repetition (*N*).

Step 6 repeat Step 1 - 5 by using M_r, which is obtained from Step 5, instead of *E*.

Step 7 after *N* = 200, function *D* will be found by applying regression analysis to determine a curve fitting of $\delta_r^e - \delta_r^a$ data with respect to *N*.

After analysing RLT specimen for all cases of σ_1 and σ_3, the constitutive model for calculating D will be determined by using regression analysis. Finally, D which is a function of σ_1, σ_3 and N will be established. This function D will be used as a model for predicting the deformation response of base course materials and determined the maximum permanent deformation, which is located under a wheel, of pavement structure and it is a major criterion for design purpose.

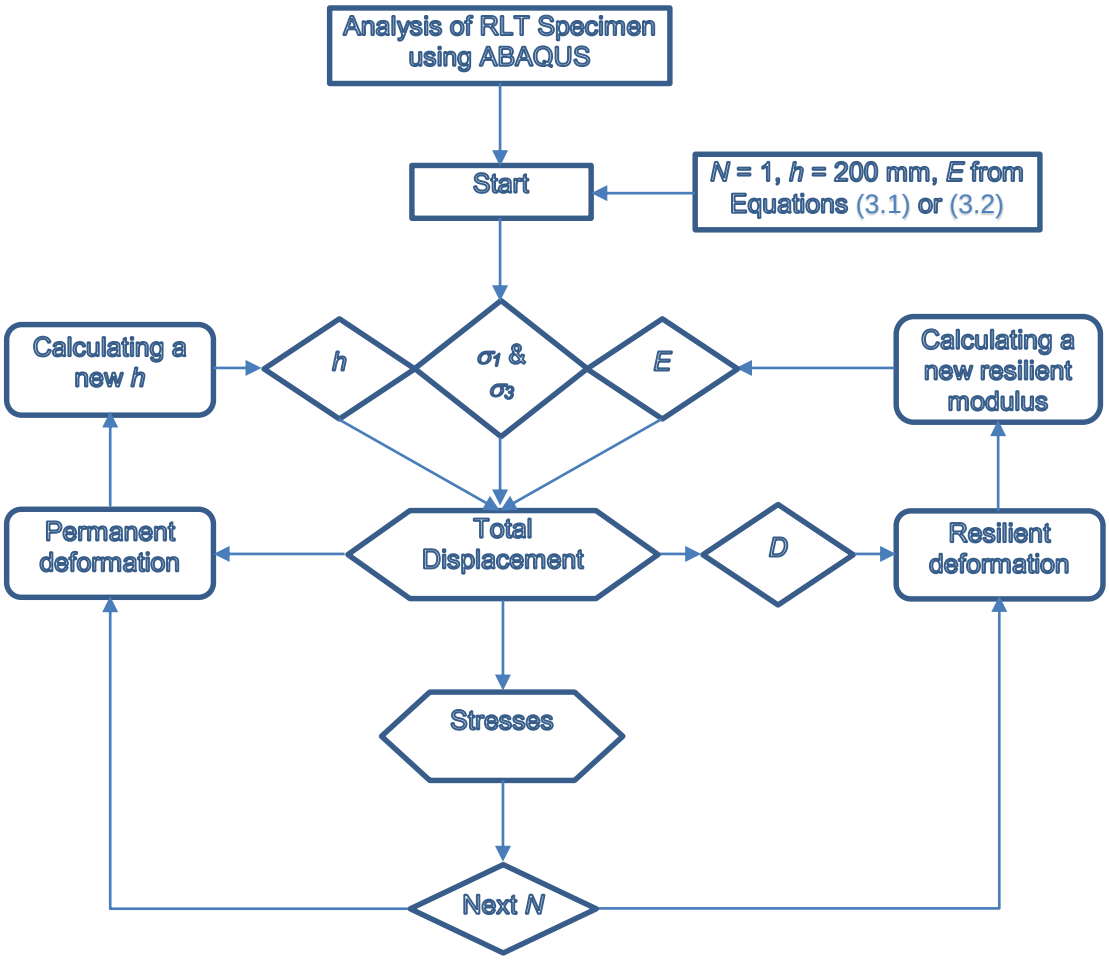

Figure 6.1 The algorithm for finding the disturbance function (D) of base course materials

6.3 Column-Strip Model

For the design purpose, engineers generally determine the maximum stress, the maximum deformation and that critical location in structural system. Consequently, the deformation concept introduced in this chapter was used for analysing column strip under a wheel of pavement structure whereas the maximum stress and the maximum deformation occur there. According to Austroads standard, they assume that all wheels of vehicle contact on the surface of road pavement as a circular area with radius (r) equal to 92.1 mm, therefore this value was adopted as a radius of the column strip used in analysis.

The Column-Strip model as shown in Figure 6.2 was analysed by ABAQUS using a 3D finite element model. Since the analysis results of the pavement structure as shown in section 5.3 indicated that a base layer plays a major role as a main load carrying layer in the thin surface flexible pavement, therefore the deformation concept was applied in base layer only. Consequently, the configurations (i.e. material property, thickness, applied stress conditions) of base layer were varied while such properties of the other layers were fixed. In addition, all contact surfaces between layer were firmly attached to each other (no slip and no separation) and all supports underneath the subgrade layer were pinned.

A series of finite element analysis (FEA) of the 3D model was done by applying material properties, structural configurations and the stress conditions which occurred in the pavement structure model as shown in section 5.3 namely the column-strip model comprises of 4 layers namely wearing surface, base, subbase and subgrade layer. The thickness of wearing surface layer was varied between 10-70 mm, which was a range of thickness that behaves as a thin surface layer. The thickness of base layer was varied between 100-200 mm. The thickness of subbase and subgrade were fixed at 250 mm and 2500 mm, respectively.

Elastic modulus of wearing surface was varied between 1000-5000 MPa, which was a common range of elastic modulus of the asphalt concrete. Elastic

modulus of subbase and subgrade layers were constant at 250 MPa and 50 MPa, respectively. The resilient modulus (M_r), however, was only employed for base course materials. Function *D*, which was determined in section 6.2, was used to determine the resilient strain (ε_r) of base layer then M_r of base course materials was calculated by the use of ε_r , which was always changed in accordance with *N*.

For applied loadings, the maximum wheel pressure of 750 kPa was employed to apply on top of wearing surface. All confining stresses (σ_3) applied around each layer of the column-strip were uniformly distributed. As aforementioned, the confining stress conditions come from analysis results of pavement structure in section 5.3 then σ_3 was varied, depend on t_{ws}, E_{ws}, t_b and E_b in wearing surface layer. For base layer, σ_3 was applied at 50, 100 and 200 kPa. For subbase and subgrade layers, σ_3 was applied at 50 and 100 MPa respectively.

Eventually, the analyses resulted in the relationship between the permanent deformations and applied stresses. Finally the proposed mechanistic-empirical approach, for finding the permanent deformation in flexible pavement having thin wearing surface, can be achieved.

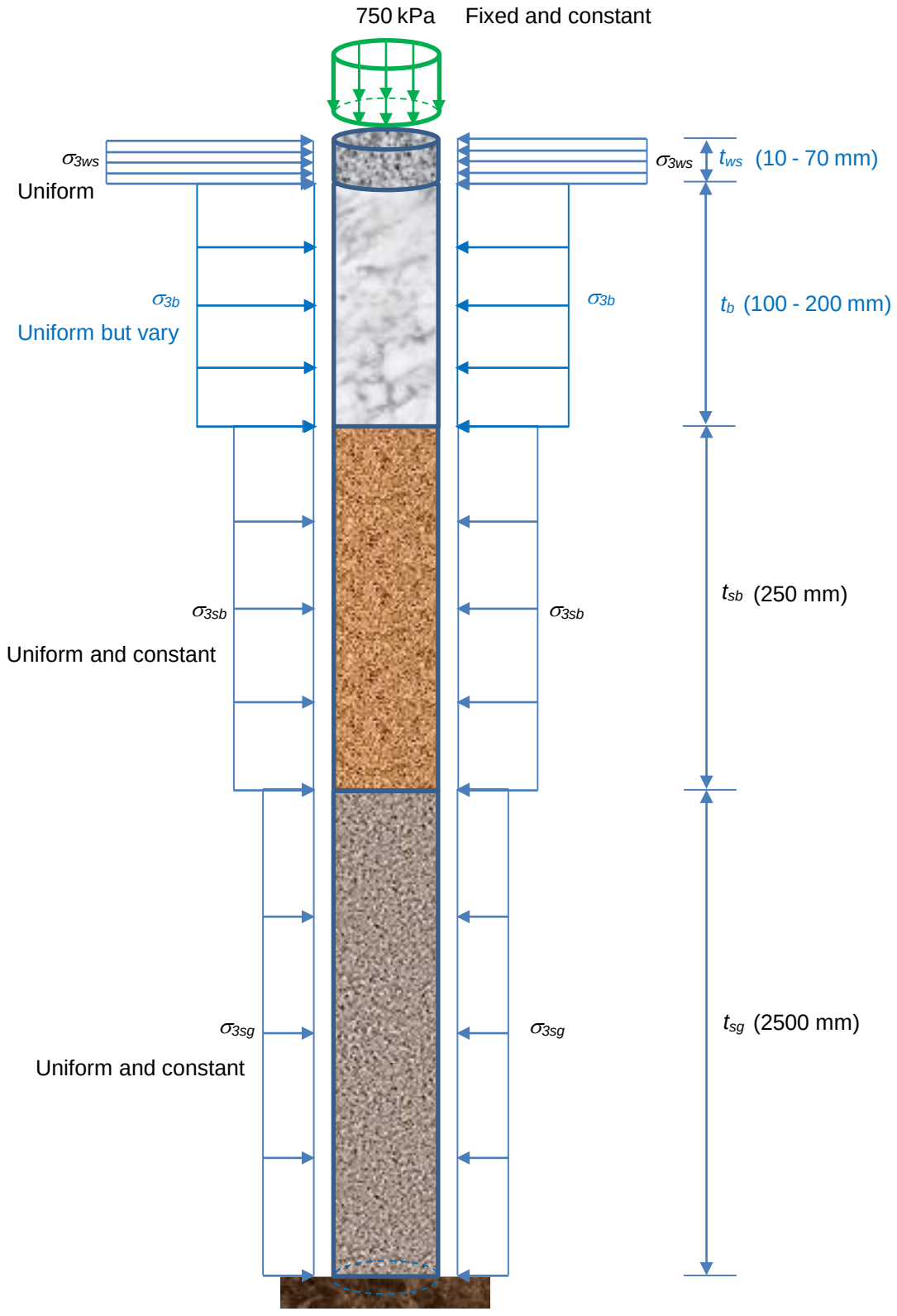

Figure 6.2 Column strip under a wheel of flexible pavement structure having thin asphalt concrete layer

6.4 Results from deformation tests

The relationships between number of loading repetition (*N*) and deformations (both resilient (δ_r^a) and permanent deformation(δ_d^a)) were from the permanent deformation test according to the Austroads, AG:PT-T053. A series of the deformation tests for CRB and HCTCRB was performed by applying 9 sets of cyclic vertical stress (σ_1) and constant confining stress (σ_3), namely σ_d = 350, 450 and 550 kPa and σ_3 = 50, 100 and 200 kPa. Ten thousand cycles of loading applied to the specimen for each set of σ_1 and σ_3. All experimental results from these tests are shown next.

6.4.1 Deformation of crushed rock base (CRB)

6.4.1.1 Resilient deformation of CRB

Figure 6.3 to Figure 6.5 are the resilient deformations of CRB specimen which obtained from the deformation tests, the dot lines show the curve fitting lines and the solid lines show the test results. The results as seen in these figures indicate that the resilient deformation (δ_r^a) of CRB nonlinearly reduced while the number of loading (*N*) increased. However, the reduction rate of δ_r^a decreased continuously, thus the exponential function (ae^b) was selected to calculate δ_r^a values.

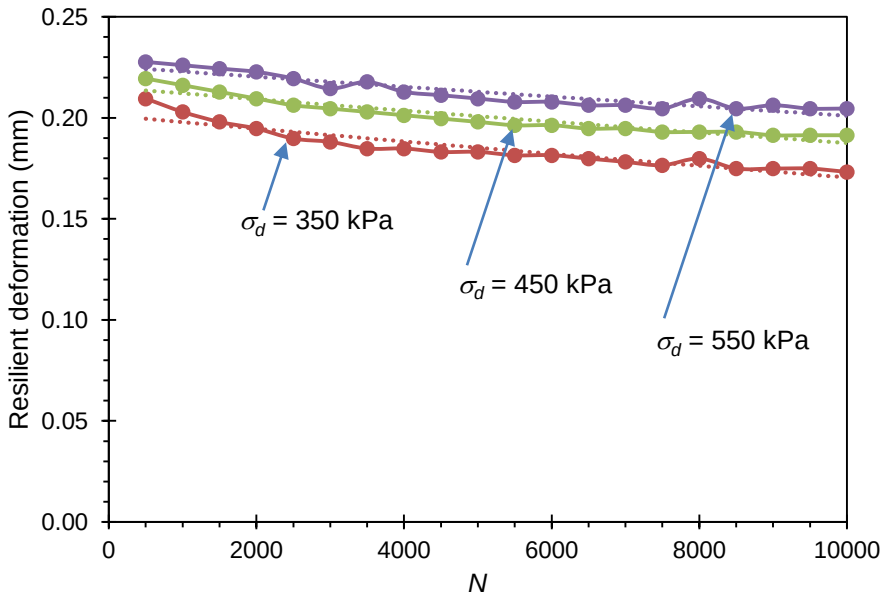

Figure 6.3 Resilient deformation of CRB, σ_3 = 50 kPa

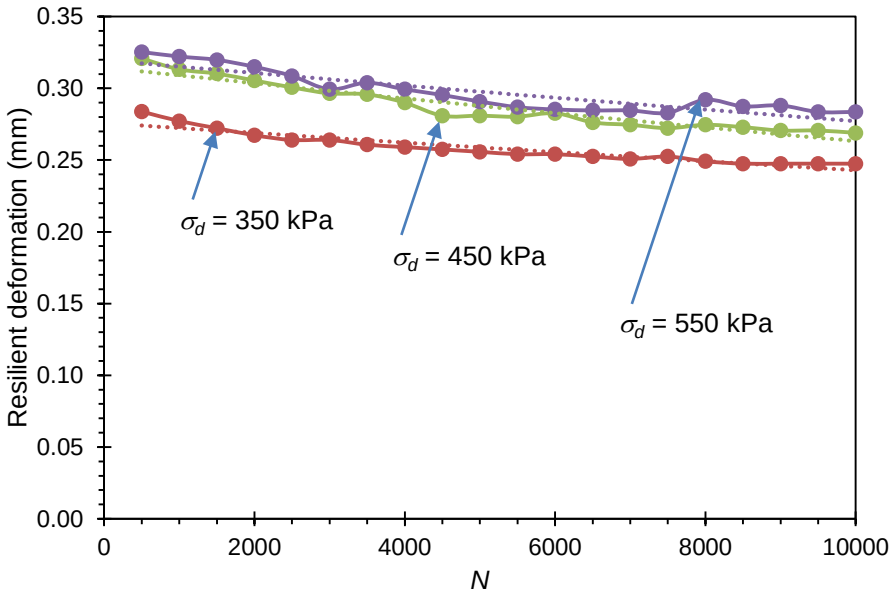

Figure 6.4 Resilient deformation of CRB, σ_3 = 100 kPa

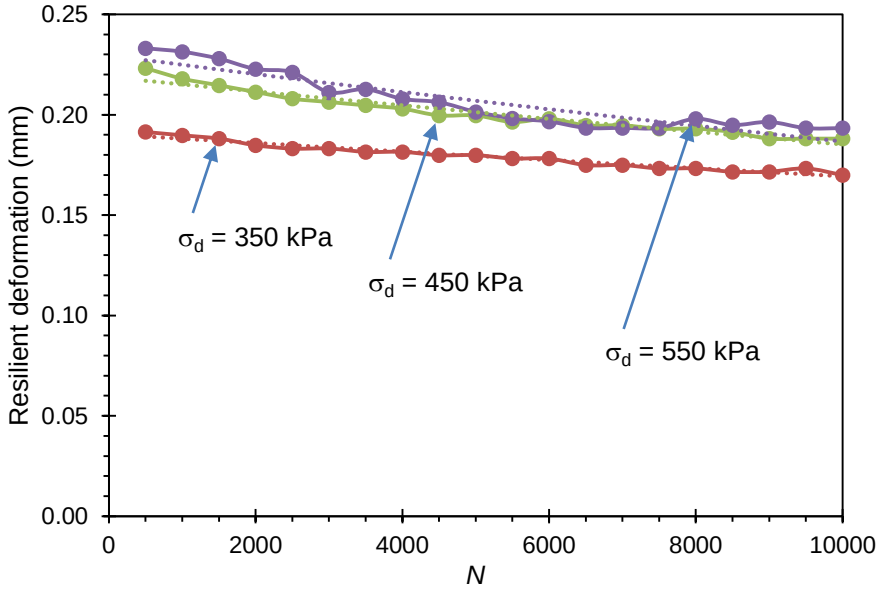

Figure 6.5 Resilient deformation of CRB, σ_3 = 200 kPa

By employing the regression analysis, coefficients *a* and *b* in the function $\delta_r^a = ae^b$, as represented by the dot lines, can be found as expressed in Table 6.1.

Table 6.1 Coefficients *a*, *b* and R^2 of the exponential function for predicting the resilient deformations of CRB specimen

σ_3 (kPa)	Variables	σ_d (kPa)		
		350	450	550
50	*a*	0.201185	0.215030	0.225474
	b	-0.000016	-0.000014	-0.000012
	R^2	0.873	0.909	0.864
100	*a*	0.275812	0.314607	0.319656
	b	-0.000013	-0.000018	-0.000014
	R^2	0.893	0.917	0.808
200	*a*	0.190279	0.218725	0.229566
	b	-0.000012	-0.000017	-0.000021
	R^2	0.962	0.950	0.860

6.4.1.2 Permanent deformation of CRB

The test results shown in Figure 6.6 - Figure 6.8 are the permanent deformations of CRB specimen (the solid lines are testing results and the dot lines are fitting curves). These figures indicated that the permanent deformations (δ_d^a) of CRB specimen increased with decremented rates while the number of loading (*N*) increased. Thus the power function (aN^b) was adopted to represent the δ_d^a values.

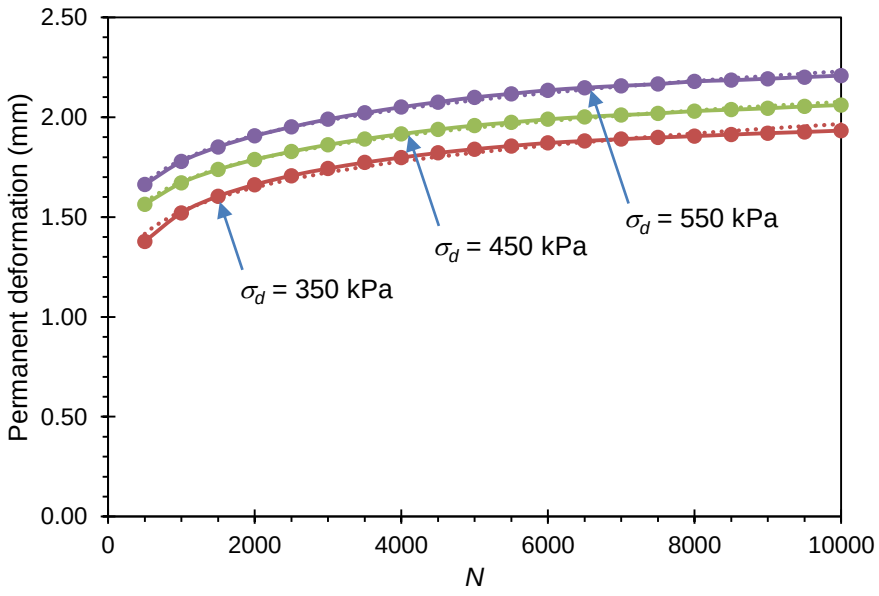

Figure 6.6 Permanent deformation of CRB, σ_3 = 50 kPa

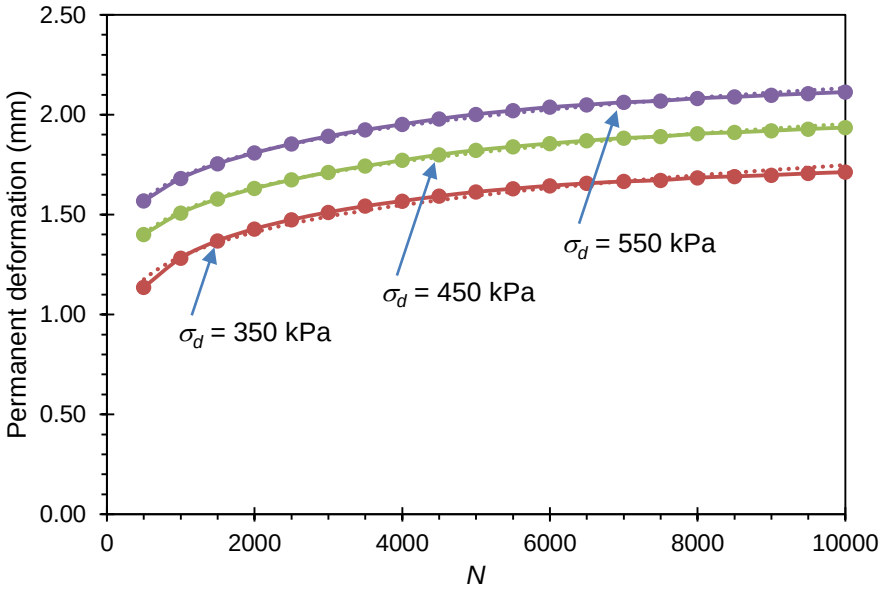

Figure 6.7 Permanent deformation of CRB, σ_3 = 100 kPa

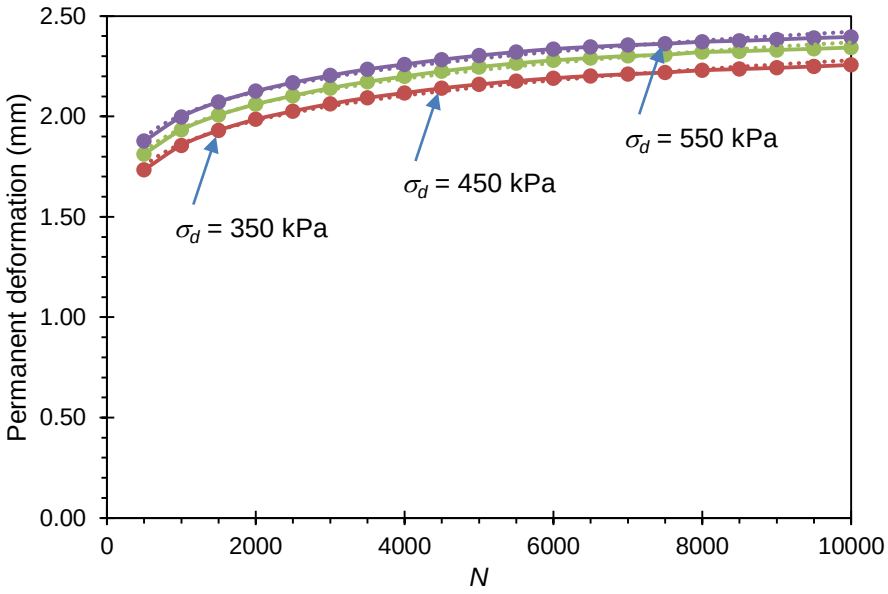

Figure 6.8 Permanent deformation of CRB, σ_3 = 200 kPa

By applying the regression analysis, coefficients *a* and *b* in the function $\delta_d^a = aN^b$ (as represented by the dot lines) can be found as seen in Table 6.2.

Table 6.2 Coefficients *a*, *b* and R^2 of the power function for predicting the permanent deformations of CRB specimen

σ_3 (kPa)	Variables	σ_d (kPa)		
		350	450	550
50	*a*	0.716784	0.881909	0.915923
	b	0.109544	0.092987	0.096576
	R^2	0.984	0.997	0.996
100	*a*	0.516897	0.705464	0.837154
	b	0.132268	0.110592	0.101569
	R^2	0.983	0.997	0.996
200	*a*	1.016758	1.064323	1.139425
	b	0.087666	0.086869	0.081854
	R^2	0.993	0.994	0.992

6.4.2 Deformation of hydrated cement treated crushed rock base (HCTCRB)

6.4.2.1 Resilient deformation of HCTCRB

The resilient deformations of HCTCRB specimen (as depicted by the solid lines) obtained from the deformation tests are illustrated in Figure 6.9 - Figure 6.11. Similar to that of CRB, the decrease in values of δ_r^a with number of loading were represented by the exponential function (ae^b), which is shown by the dot line.

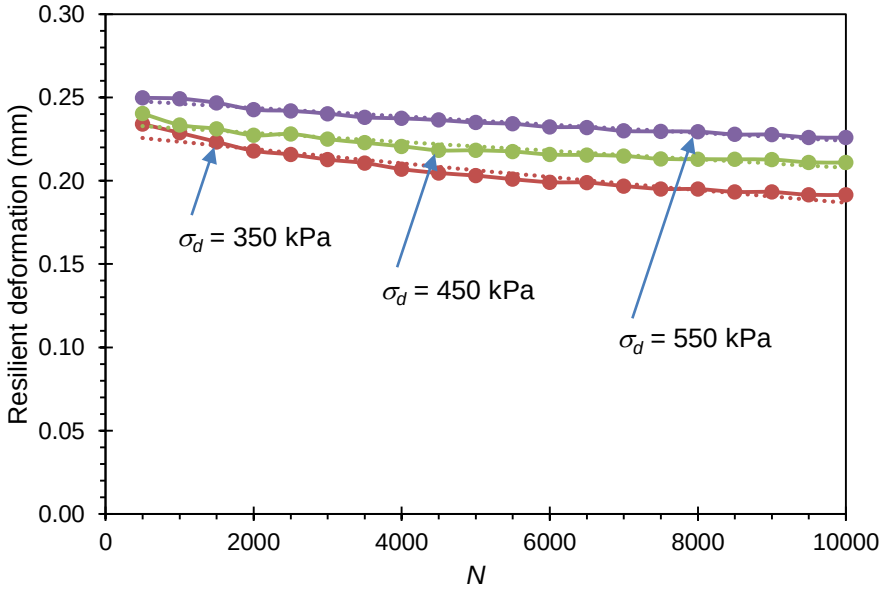

Figure 6.9 Resilient deformation of HCTCRB, σ_3 = 50 kPa

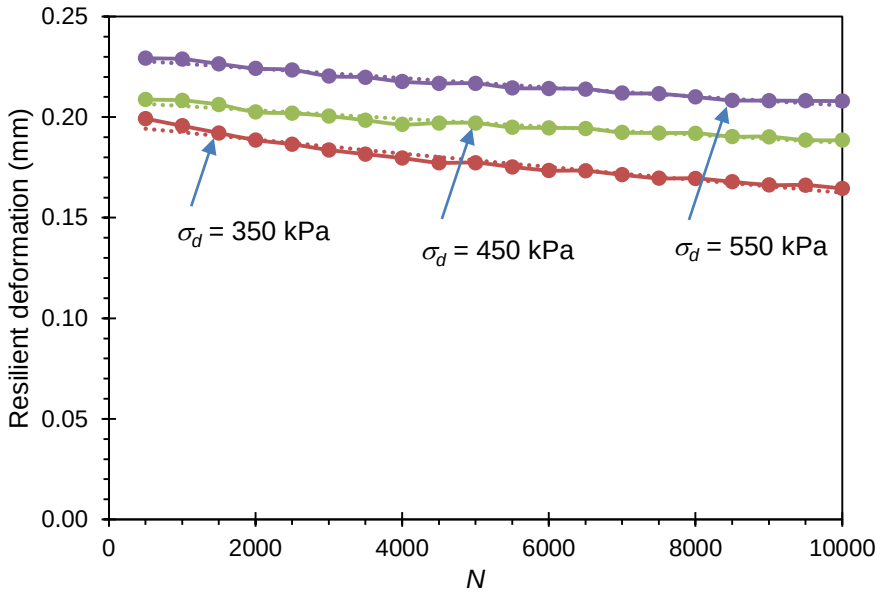

Figure 6.10 Resilient deformation of HCTCRB, σ_3 = 100 kPa

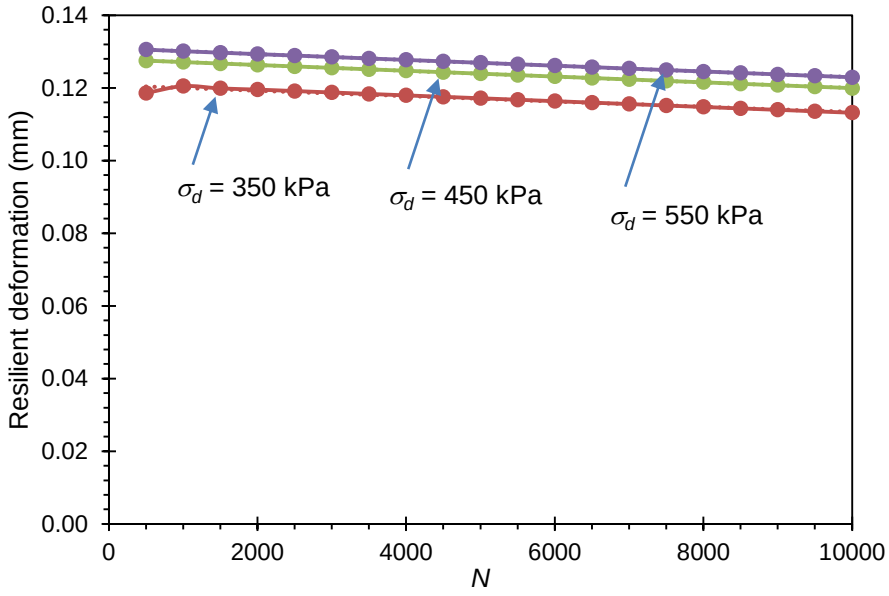

Figure 6.11 Resilient deformation of HCTCRB, σ_3 = 200 kPa

Coefficients *a* and *b* in the function $\delta_r^a = ae^b$ (as shown by the dot lines) were also determined by the regression analysis, they can be expressed as seen in Table 6.3.

Table 6.3 Coefficients *a*, *b* and R^2 of the exponential function for predicting the resilient deformations of HCTCRB specimen

σ_3 (kPa)	Variables	σ_d (kPa)		
		350	450	550
50	*a*	0.227901	0.234256	0.248955
	b	-0.000020	-0.000012	-0.000010
	R^2	0.932	0.905	0.966
100	*a*	0.196149	0.207655	0.229035
	b	-0.000019	-0.000010	-0.000011
	R^2	0.964	0.952	0.972
200	*a*	0.120773	0.127960	0.130954
	b	-0.000006	-0.000006	-0.000006
	R^2	0.960	1.000	1.000

6.4.2.2 Permanent deformation of HCTCRB

Figure 6.12 - Figure 6.14 show the permanent deformations of HCTCRB specimen, the solid lines are represented the test results and the dot lines are represented the curve fitting lines. These figures indicate that the permanent deformations (δ_d^a) of HCTCRB specimen nonlinearly increased with the number of loading cycles (*N*). However, the increased rate of δ_d^a reduced gradually then the power function (aN^b) was adopted for predicting δ_d^a values of HCTCRB.

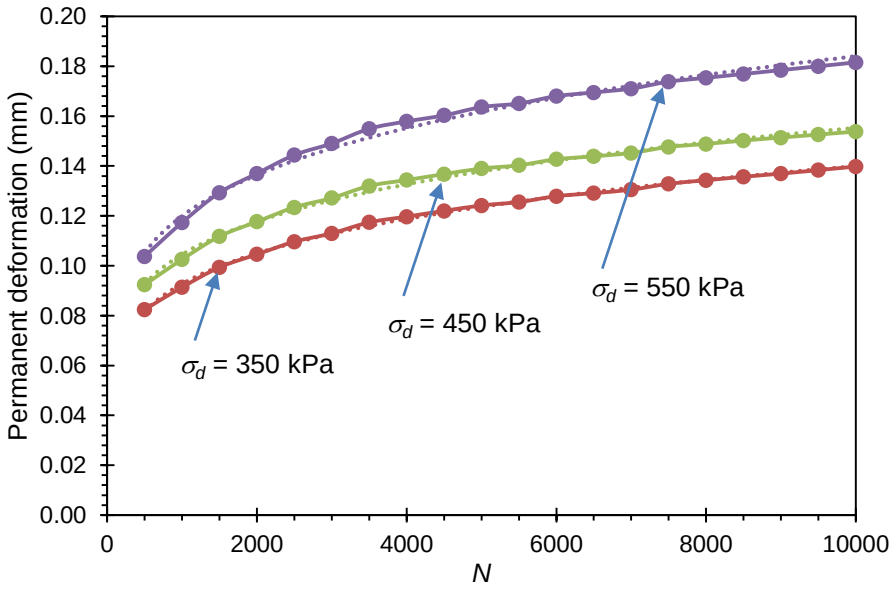

Figure 6.12 Permanent deformation of HCTCRB, σ_3 = 50 kPa

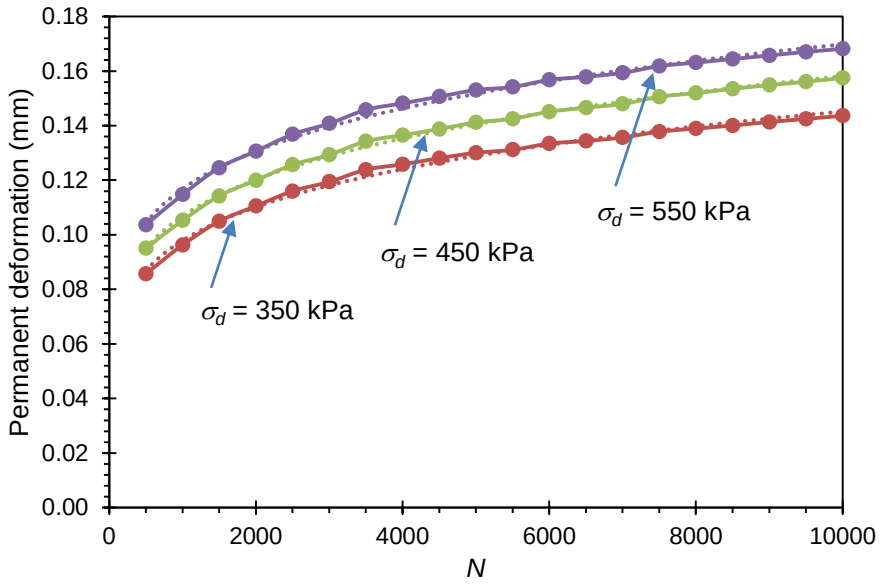

Figure 6.13 Permanent deformation of HCTCRB, σ_3 = 100 kPa

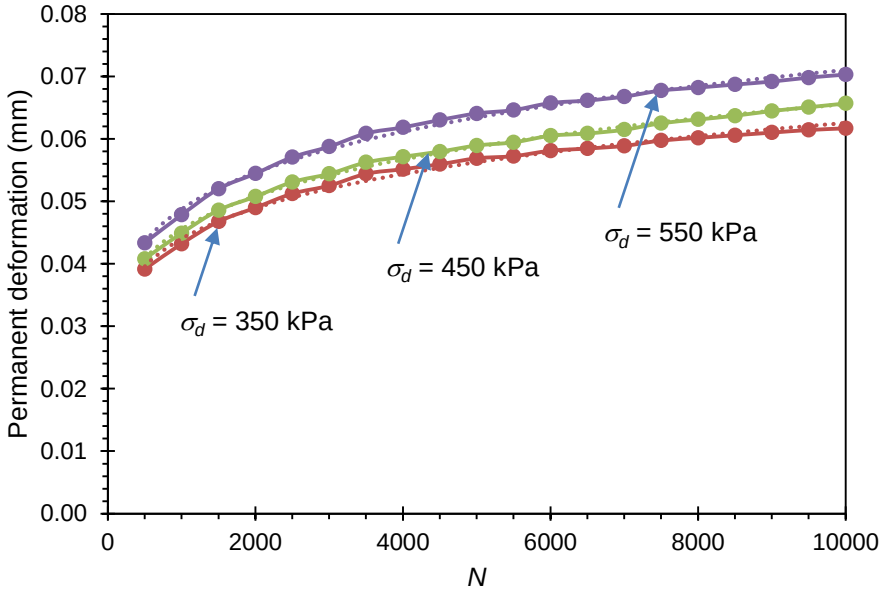

Figure 6.14 Permanent deformation of HCTCRB, σ_3 = 200 kPa

Eventually, coefficients *a* and *b* in the function $\delta_d^a = aN^b$ (as represented by the dot lines) were determined by the regression analysis, they can be expressed as shown in Table 6.4.

Table 6.4 Coefficients *a*, *b* and R^2 of the power function for predicting the permanent deformations of HCTCRB specimen

σ_3 (kPa)	Variables	σ_d (kPa)		
		350	450	550
50	*a*	0.026996	0.031848	0.033161
	b	0.178641	0.172013	0.186053
	R^2	0.998	0.996	0.993
100	*a*	0.029983	0.032948	0.037978
	b	0.171242	0.170302	0.162605
	R^2	0.994	0.998	0.996
200	*a*	0.015314	0.015234	0.015743
	b	0.152780	0.158479	0.163610
	R^2	0.993	0.998	0.995

6.5 Results from finite element analysis of base course specimen

Base course specimens for RLT tests were modelled and analysed using ABAQUS. Due to limitation of computer, analyses were done up to 200 cycles of repeated loading (*N* = 200) only. This step aims to find the resilient deformation part from FEA according to assumption as expressed in Figure 4.11 and Equation (4.34), namely

$$\delta_r^e = \delta_t - \delta_d^a \tag{6.1}$$

where δ_r^e is the resilient deformation calculated from elastic analysis of base course specimen, δ_t^e is the total deformation of base course specimen obtained from FEA and δ_d^a is the permanent deformation of base course specimen calculated from test results by using equations as explained in Section 6.4.1 and 6.4.2 for CRB and HCTCRB respectively.

6.5.1 Analysis results of CRB specimen

After each loop *N* of analysis, the total deformation (δ_t), is the maximum deformation obtained from FEA based on elastic assumption, was substituted into Equation (6.1). Then values of δ_r^e were determined as shown in Figure 6.15 - Figure 6.17. These figures indicate that δ_r^e values were not equal to δ_r^a resulted from the permanent deformation tests.

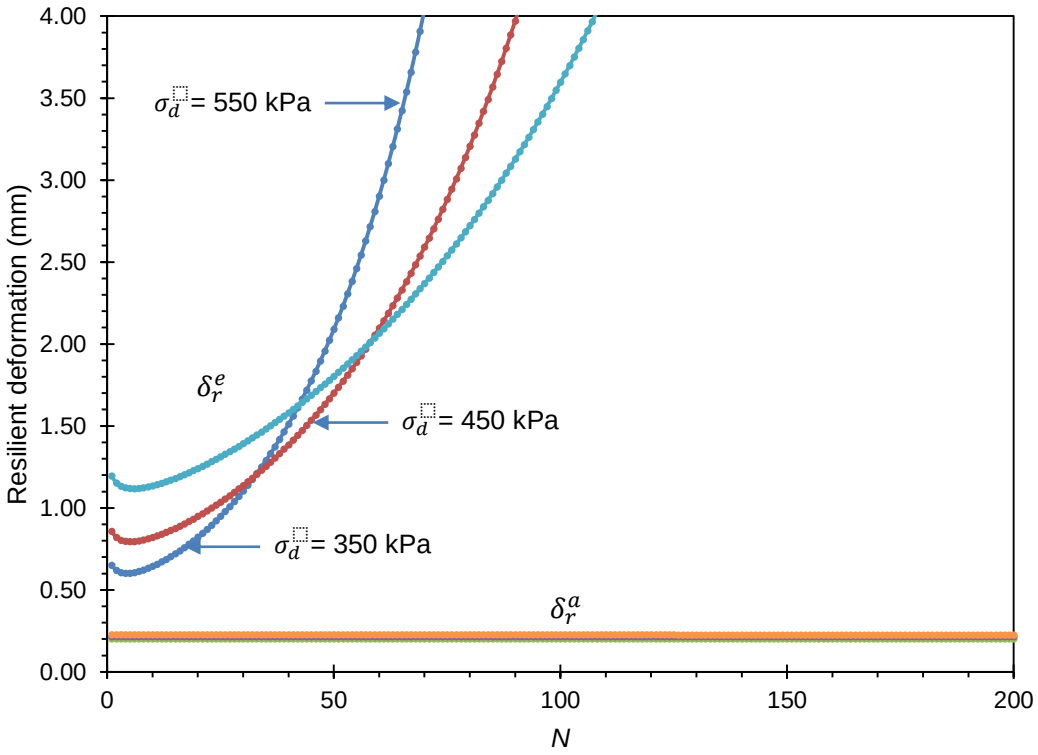

Figure 6.15 Resilient deformation of CRB, σ_3 = 50 kPa

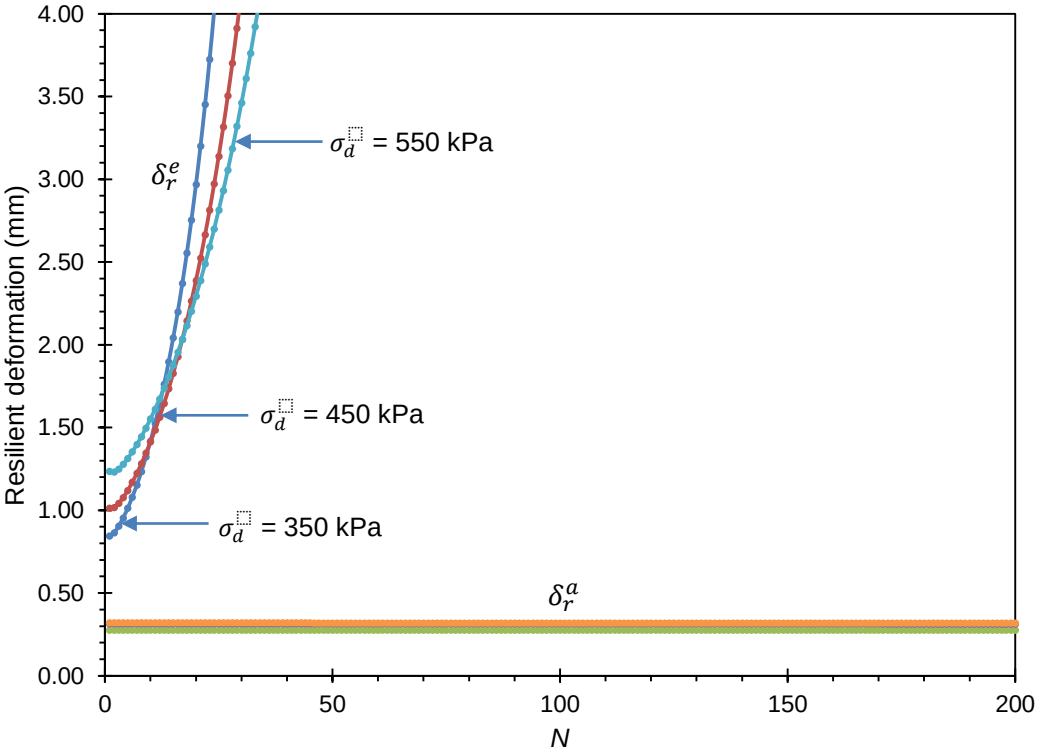

Figure 6.16 Resilient deformation of CRB, σ_3 = 100 kPa

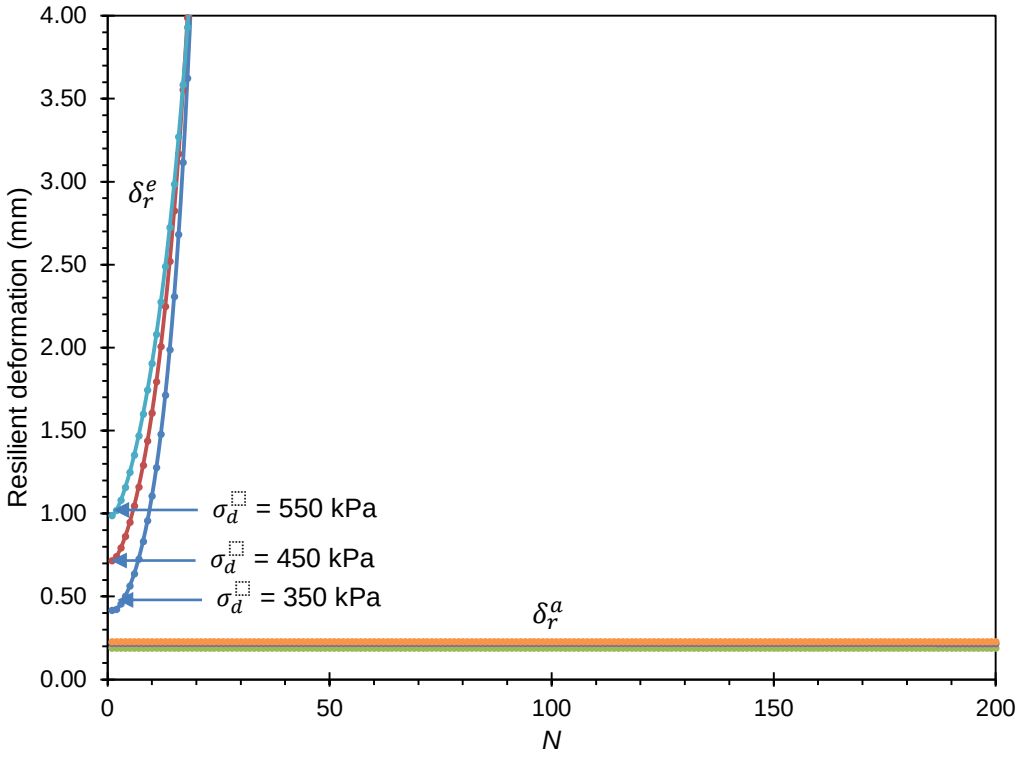

Figure 6.17 Resilient deformation of CRB, σ_3 = 200 kPa

6.5.2 Analysis results of HCTCRB specimen

It can be seen in Figure 6.18 - Figure 6.20 that δ_r^e and δ_r^a of HCTCRB are also totally different.

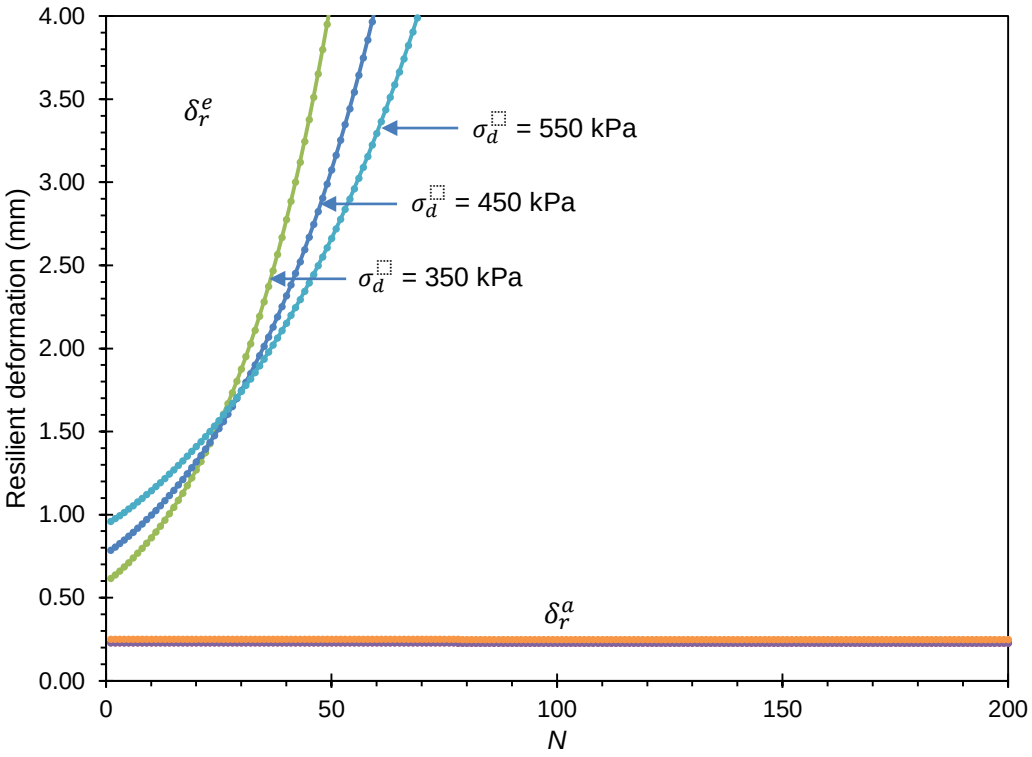

Figure 6.18 Resilient deformation of HCTCRB, σ_3 = 50 kPa

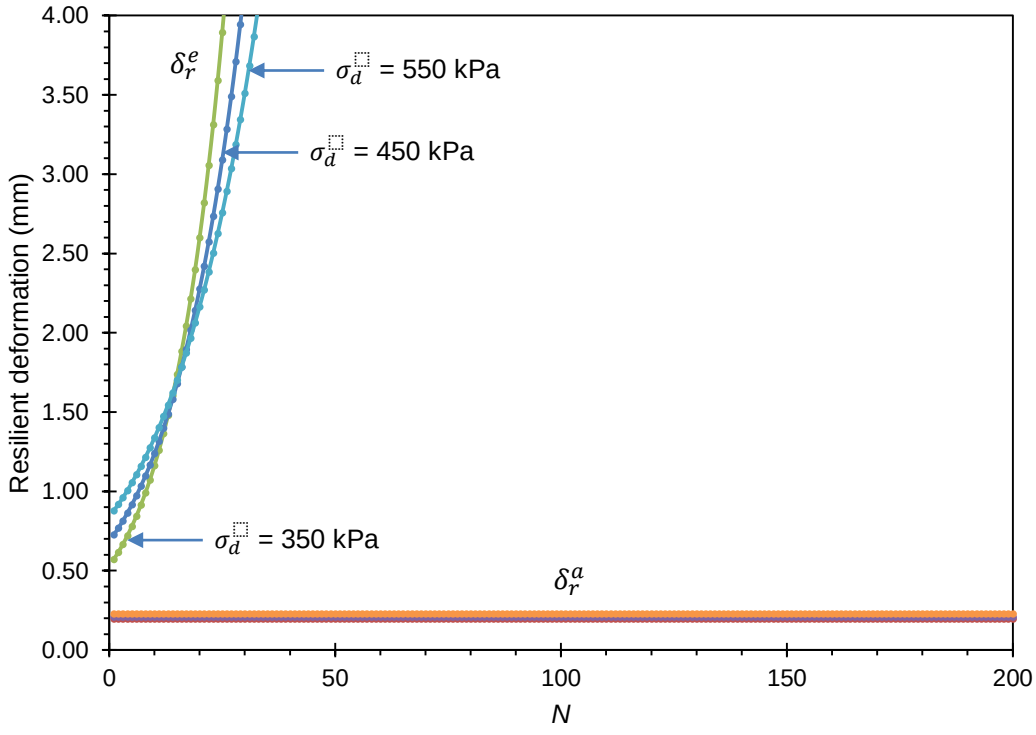

Figure 6.19 Resilient deformation of HCTCRB, σ_3 = 100 kPa

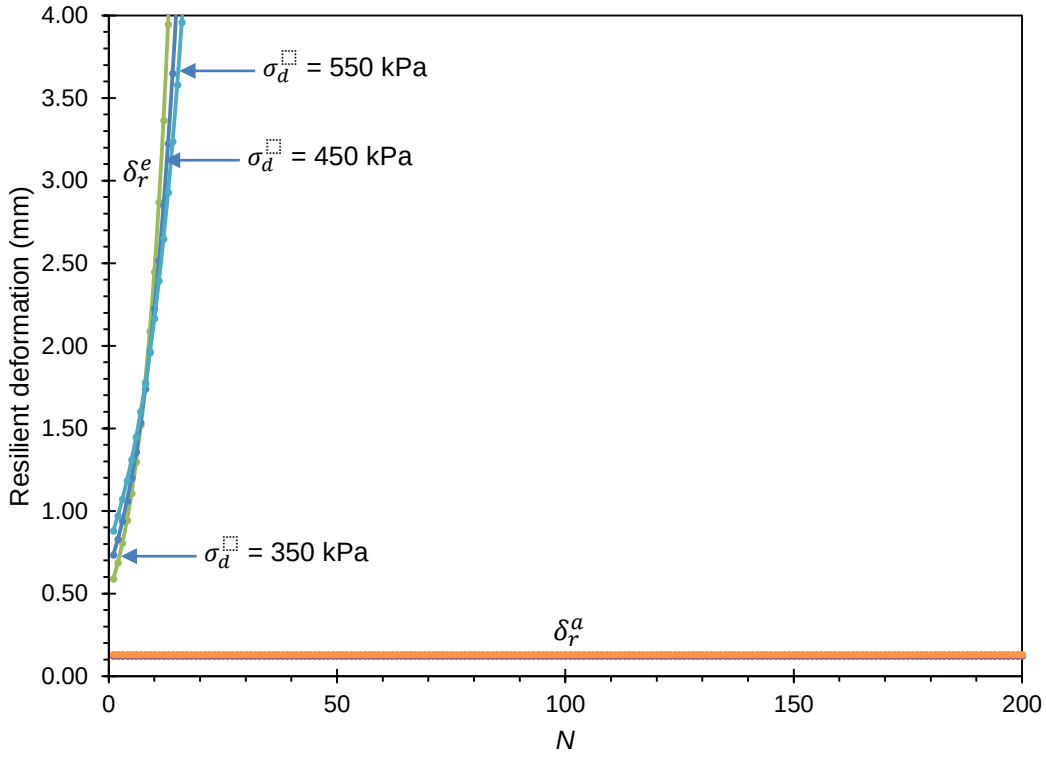

Figure 6.20 Resilient deformation of HCTCRB, σ_3 = 200 kPa

6.5.3 Disturbance function for resilient deformation of base course materials

As described in Section 6.5.1 and 6.5.2, values of δ_r^e and δ_r^a were not identical therefore the disturbance function (*D*) was employed to eliminate these difference.

$$D = \frac{(\delta_r^e - \delta_r^a)}{(\delta_r^e - \delta_r^c)} \quad (6.2)$$

where δ_r^e is assumed to be the resilient deformation in relative intact part and δ_r^c is the resilient deformation at *N* = 10,000 which calculated using equations as explained in Section 6.4.1.1 and 6.4.2.1 for CRB and HCTCRB respectively.

And the resilient deformation can be back calculated using the following equation.

$$\delta_r = (1 - D) \cdot \delta_r^i + D \cdot \delta_r^c \quad (6.3)$$

6.5.3.1 Disturbance function for CRB specimen

Based on Equations (6.2) and (6.3), *D* can be determined and illustrated in Figure 6.21 to Figure 6.23. These curves can be fitted by using rational equations as expressed below.

- For σ_3 = 50 kPa, as shown in Figure 6.21

$$D = \frac{(0.1694N - 2.442)}{(N - 2.809)}, \quad R^2 = 0.999 \tag{6.4}$$

For σ_d = 350 kPa

$$D = \frac{(0.1351N - 2.984)}{(N - 3.292)}, \quad R^2 = 0.999 \tag{6.5}$$

For σ_d = 450 kPa

$$D = \frac{(0.1033N - 3.808)}{(N - 4.073)}, \quad R^2 = 1.000 \tag{6.6}$$

For σ_d = 550 kPa

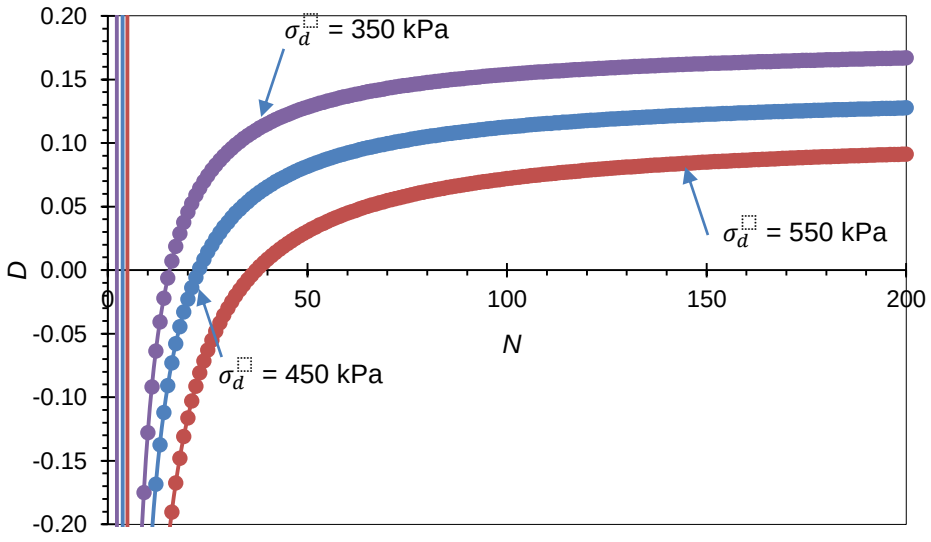

Figure 6.21 Disturbance function of CRB, σ_3 = 50 kPa

- For σ_3 = 100 kPa, as shown in Figure 6.22

$$D = \frac{(0.3875N - 1.381)}{(N - 1.873)}, \quad R^2 = 0.996 \tag{6.7}$$

For σ_d = 350 kPa

$$D = \frac{(0.2465N - 1.090)}{(N - 1.781)}, \quad R^2 = 0.990 \tag{6.8}$$

For σ_d = 450 kPa

$$D = \frac{(0.2331N - 1.661)}{(N - 2.104)}, \quad R^2 = 0.999 \tag{6.9}$$

For σ_d = 550 kPa

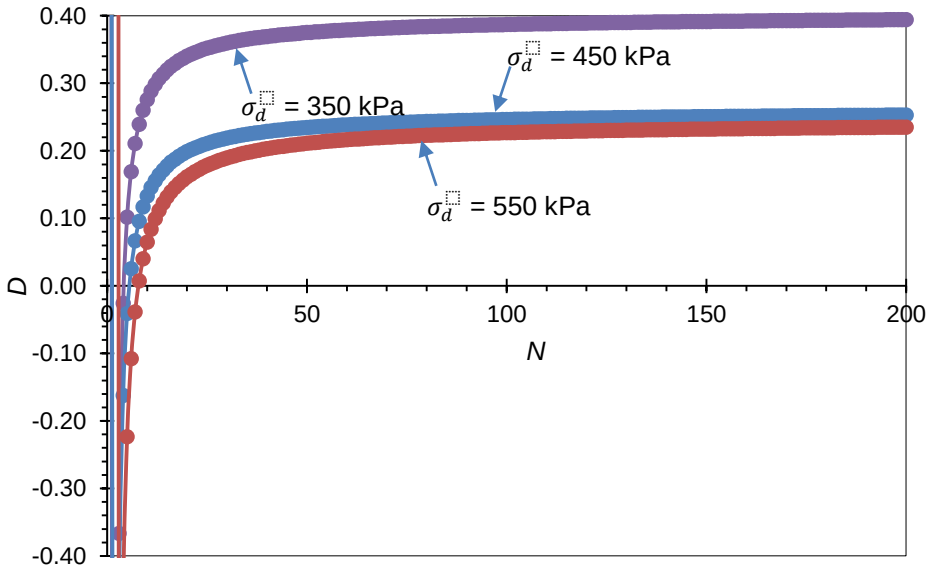

Figure 6.22 Disturbance function of CRB, σ_3 = 100 kPa

- For σ_3 = 200 kPa, as shown in Figure 6.23

$$D = \frac{(0.5951N - 2.131)}{(N - 2.330)}, \quad R^2 = 0.991 \tag{6.10}$$

For σ_d = 350 kPa

$$D = \frac{(0.4393N - 1.786)}{(N - 2.119)}, \quad R^2 = 0.998 \tag{6.11}$$

For σ_d = 450 kPa

$$D = \frac{(0.3328N - 1.553)}{(N - 2.014)}, \quad R^2 = 1.000 \tag{6.12}$$

For σ_d = 550 kPa

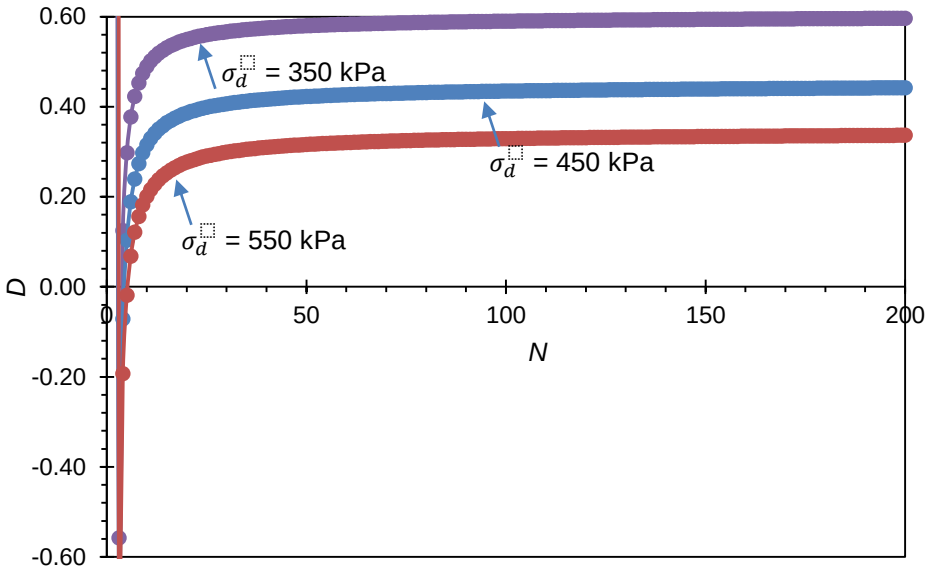

Figure 6.23 Disturbance function of CRB, σ_3 = 200 kPa

6.5.3.2 Disturbance function for HCTCRB specimen

Similarly a set of parameter *D* for HCTCRB can be determined using Equations (6.2) and (6.3). Figure 6.24 to Figure 6.26 illustrate *D* over the range of σ_3 and σ_d. These curves can be represented by rational equations as shown below.

- For σ_3 = 50 kPa, as seen in Figure 6.24

$$D = \frac{(0.1817N - 0.2644)}{(N - 1.091)}, \quad R^2 = 0.999 \tag{6.13}$$

For σ_d = 350 kPa

$$D = \frac{(0.2024N - 0.3381)}{(N - 1.142)}, \quad R^2 = 0.997 \tag{6.14}$$

For σ_d = 450 kPa

$$D = \frac{(0.1751N - 0.3400)}{(N - 1.171)}, \quad R^2 = 0.996 \tag{6.15}$$

For σ_d = 550 kPa

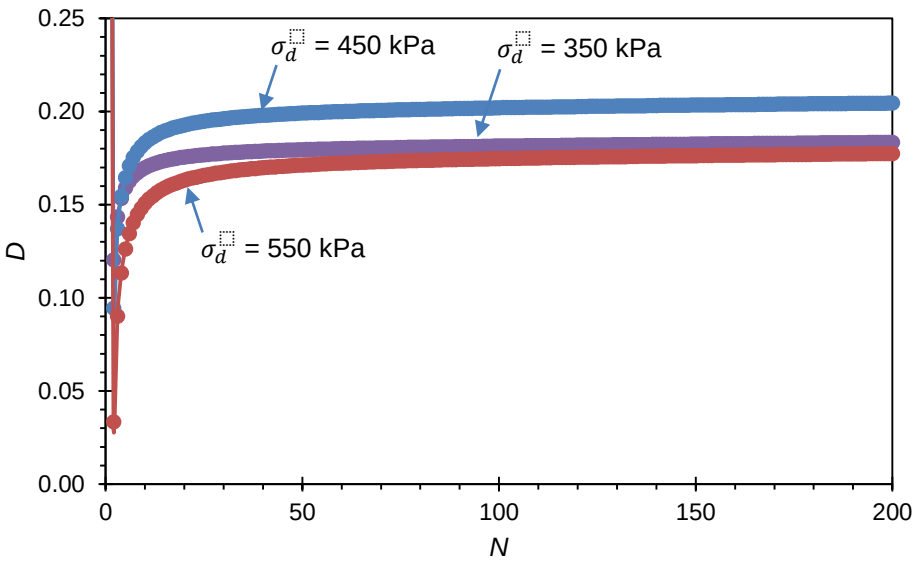

Figure 6.24 Disturbance function of HCTCRB, σ_3 = 50 kPa

- For σ_3 = 100 kPa, as seen in Figure 6.25

$$D = \frac{(0.3298N - 0.4219)}{(N - 1.100)}, \quad R^2 = 0.998 \tag{6.16}$$

For σ_d = 350 kPa

$$D = \frac{(0.3911N - 0.5338)}{(N - 1.148)}, \quad R^2 = 0.996 \tag{6.17}$$

For σ_d = 450 kPa

$$D = \frac{(0.3284N - 0.4766)}{(N - 1.153)}, \quad R^2 = 0.996 \tag{6.18}$$

For σ_d = 550 kPa

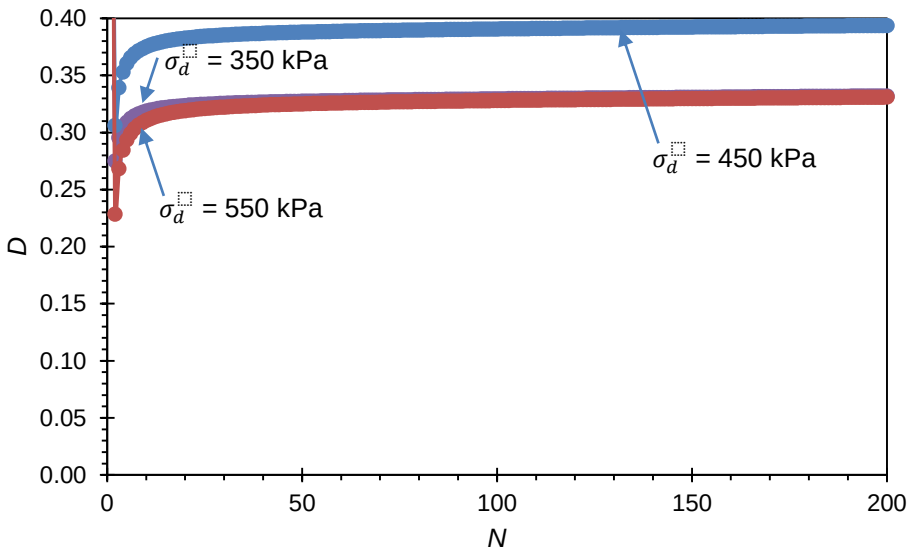

Figure 6.25 Disturbance function of HCTCRB, σ_3 = 100 kPa

- For σ_3 = 200 kPa, as seen in Figure 6.26

$$D = \frac{(0.7395N - 0.8255)}{(N - 1.087)}, \quad R^2 = 0.995 \tag{6.19}$$

For σ_d = 350 kPa

$$D = \frac{(0.6806N - 0.7763)}{(N - 1.097)}, \quad R^2 = 0.995 \tag{6.20}$$

For σ_d = 450 kPa

$$D = \frac{(0.6362N - 0.7465)}{(N - 1.112)}, \quad R^2 = 0.995 \tag{6.21}$$

For σ_d = 550 kPa

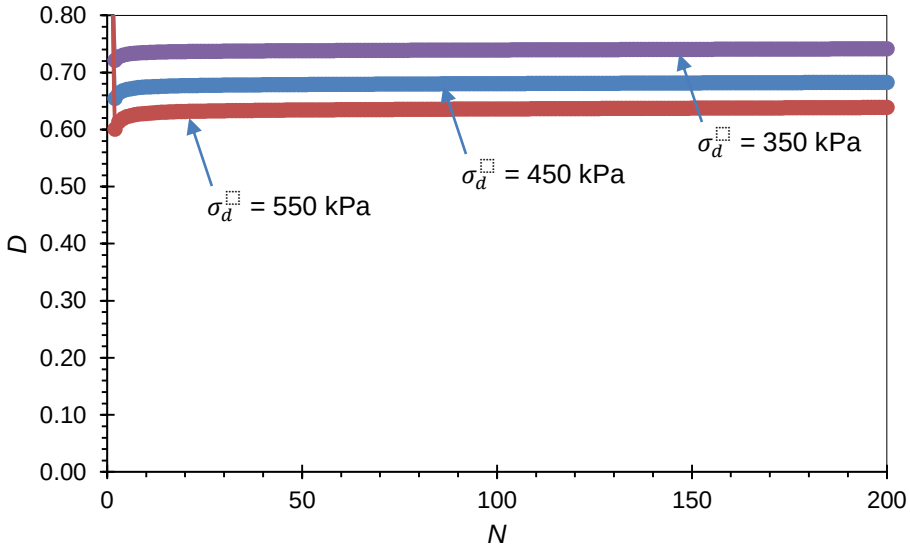

Figure 6.26 Disturbance function of HCTCRB, σ_3 = 200 kPa

The disturbance function (*D*) can be expressed in a constitutive form as shown in Equation (6.22) to represent Equation (6.4) to (6.21). All coefficients *a*, *b*, *c* and *d* of the function can be calculated by curve fitting method and shown below.

$$D = \frac{(aN+b)}{(cN+d)} \tag{6.22}$$

where

$$a = -0.3178 - 978.5 \times 10^{-6}\sigma_3 + 1611 \times 10^{-6}\sigma_d \tag{6.23}$$

For CRB

$$= -0.6834 - 276.0 \times 10^{-6}\sigma_3 + 2495 \times 10^{-6}\sigma_d \tag{6.24}$$

For HCTCRB

$$b = -4.614 - 2588.0 \times 10^{-6}\sigma_3 + 6273 \times 10^{-6}\sigma_d \tag{6.25}$$

For CRB

$$= 0.5362 - 57.19 \times 10^{-6}\sigma_3 + 2343 \times 10^{-6}\sigma_d \tag{6.26}$$

For HCTCRB

$$c = 1 \text{ for both CRB and HCTCRB} \tag{6.27}$$

$$d = -4.954 - 2721.0 \times 10^{-6}\sigma_3 + 6185 \times 10^{-6}\sigma_d \tag{6.28}$$

For CRB

$$= -1.165 - 324.3 \times 10^{-6}\sigma_3 + 180 \times 10^{-6}\sigma_d \quad (6.29)$$

For HCTCRB

6.5.4 Equation for predicting the resilient modulus of base course materials

Resilient modulus M_r of base course materials is calculated by dividing the deviator stress (σ_d) with resilient strain (ε_r^a). The resilient deformation (δ_r^a) derived from the permanent deformation tests as described in section 6.4 can be transformed to the resilient strain (ε_r^a). Consequently, both δ_r^a and ε_r^a are in the form of (ae^b). Thus M_r which is a reciprocal of ε_r^a can be expressed in the form of (ae^{bN}). M_r of CRB and HCTCRB, in unit of Pascal, can be predicted using a nonlinear equation (ae^{bN}) as follow.

6.5.4.1 Equation for predicting the resilient modulus of CRB

For the resilient modulus of CRB specimen, which can be calculated by an equation $M_r = ae^{bN}$, coefficients *a* and *b* can be found as shown in Table 6.5.

Table 6.5 Coefficients *a* and *b* of the nonlinear function for predicting the resilient modulus of CRB specimen

σ_3 (kPa)	Variables	σ_d (kPa)		
		350	450	550
50	*a* (x 10^6)	347.938	418.546	487.861
	b (x 10^{-6})	16.000	14.000	12.000
100	*a* (x 10^6)	253.796	286.071	344.120
	b (x 10^{-6})	13.000	18.000	14.000
200	*a* (x 10^6)	367.881	411.476	479.165
	b (x 10^{-6})	12.000	17.000	21.000

6.5.4.2 Equation for predicting the resilient modulus of HCTCRB

Similar to CRB specimen, M_r of HCTCRB specimen can be predicted by using the function $M_r = ae^{bN}$ with coefficients *a* and *b* are as shown in Table 6.6.

Table 6.6 Coefficients *a* and *b* of the nonlinear function for predicting the resilient modulus of HCTCRB specimen

σ_3 (kPa)	Variables	σ_d (kPa)		
		350	450	550
50	*a* (x 10^6)	307.151	384.195	441.847
	b (x 10^{-6})	20.000	12.000	10.000
100	*a* (x 10^6)	356.872	433.411	480.276
	b (x 10^{-6})	19.000	10.000	11.000
200	*a* (x 10^6)	579.600	703.345	839.990
	b (x 10^{-6})	6.000	6.000	6.000

By using curve fitting method, the resilient modulus and all coefficients can be written in a constitutive form as shown below,

$$M_r = ae^{bN} \tag{6.30}$$

where

$$a = 287.6 \times 10^6 + (743.4 \times 10^3)(\sigma_3) + (6.959 \times 10^3)(\sigma_d) \tag{6.31}$$

For CRB

$$a = -3.680 \times 10^6 + (1.102 \times 10^6)(\sigma_3) + (1.650 \times 10^6)(\sigma_d) \tag{6.32}$$

For HCTCRB

$$b = 8.417 \times 10^{-6} + (9.842 \times 10^{-9})(\sigma_3) + (121.7 \times 10^{-6})(\sigma_d) \tag{6.33}$$

For CRB

$$b = 32.68 \times 10^{-6} - (33.87 \times 10^{-9})(\sigma_3) - (38.83 \times 10^{-9})(\sigma_d) \tag{6.34}$$

For HCTCRB

6.6 Investigation the behaviour of pavement structure having thin wearing surface using advanced analytical approach based on DSC

This section aims to introduce a new analytical approach for pavement having thin asphalt surface based on the disturbed state concept, as derived in previous section. In this study, analyses using ABAQUS were done for a pavement column model subjected to 200 cycles of repeated wheel load. A multi-layer pavement structure was modelled as a circular column subjected to a wheel load of 20 kN which was transformed to a distributed load of 750 kPa, as seen in Figure 6.2. The contact area between the wheel and wearing surface was a circle having radius (*r*) of 92.1 mm then it was used as a radius of pavement column under the distributed wheel load.

The support at bottom of subgrade layer of the column was constrained all directions. The interfaces between each layer of the pavement were bound, i.e. no slip and no separation. In horizontal (radial) direction, the column was bounded by confining pressure (σ_3). All σ_3 applied around each layer in the pavement column was uniformly distributed. The magnitudes of σ_3 were the average values of σ_x obtained from analysis results of 2D pavement structure as shown in section 5.3. However, the magnitude of σ_3 applied around wearing surface layer was varied, depended on the parameters, t_{ws}, E_{ws}, t_b and E_b . For base course layer, three levels of σ_3 namely 50, 100 and 200 kPa was applied. The values of σ_3 applied to subbase and subgrade layers were constant at 50 and 100 kPa respectively.

The results from the pavement structure analysis in section 5.3.1 revealed that stresses and deformation of pavement structure are greatly dependent on the properties of wearing surface and base course layers. The contribution from subbase and subgrade were negligibly small. Thus, only properties of materials such as thicknesses and elastic modulus of the wearing surface and the base course materials were varied in this series of pavement structural analysis. The variation of these parameters was limited by the condition that the bottom fibre of wearing surface layer did not undergo in tension. The thicknesses of wearing surface layer (t_{ws}) were ranged from 10 – 70 mm.

There were three levels of elastic modulus of wearing surface (E_{ws}), i.e. 1000, 3000 and 5000 MPa. For the base course layer, two values of thickness (t_b) of 100 and 200 mm, which are commonly used in Western Australia, were employed in the model. The resilient modulus (M_r) of base course material was dependent of the applied σ_d and σ_3 as explained previously section. The thickness and elastic modulus of subbase layer were held constant at 250 mm and 250 MPa, respectively. For subgrade layer, the thickness and elastic modulus were fixed at 2500 mm and 50 MPa respectively. Based on the variation explained above, the analyses were done for 78 cases CRB as a base course layer and 90 cases of base course layer using HCTCRB. The advantage of using these material properties is that the results from finite element analysis of the column-strip model will be consistent with the analysis results of pavement structure having thin wearing surface layer.

Due to the variation in the material properties of the wearing surface and the base course layer, each model was abbreviated as;

WS·E(*i*)·T(*j*) - B·CS(*k*)·T(*l*)

where WS means wearing surface layer, B means base layer, T(*j*) means thickness of wearing surface, *j* = 10, 20, …, 70 mm, E(*i*) means elastic modulus of wearing surface layer, *i* = 1000, 3000, and 5000 MPa, CS(*k*) means confining stress applied around base layer, *k* = 50, 100, and 200 kPa, T(*l*) means thickness of base layer and *l* = 100 and 200 mm.

6.6.1 Investigation of structural pavement column using CRB as base course material

In this section, CRB was adopted as a base course material used in the column-strip model for finite element analysis, therefore Equations (6.30), (6.31) and (6.33) were employed for computing the resilient modulus of base layer. After all cases of analysis as aforementioned were done, the permanent deformation obtained by each case of analysis was eventually formulated in a constitutive form. The constitutive formula given by this section can be used

for predicting the maximum permanent deformation of pavement structure having thin wearing surface layer by engineers in design procedure.

The analysis result as shown in Figure 6.27 to Figure 6.44 revealed that the permanent deformation of the pavement structure can be also expressed by nonlinear equation $P_d = aN^b$ as same as mentioned in section 6.4. The results obtained in this section can be analysed further to find the effect of each factor on permanent deformation as described below.

Figure 6.27 - Figure 6.29 show analysis results for the case that CRB was adopted as a base course material, confining stress (σ_3) applied around base layer was 50 kPa and thickness of base layer (t_b) was 100 mm. It can be seen obviously that P_d nonlinearly increased with *N* and it also gradually increased with the thickness of wearing surface layer (t_{ws}).

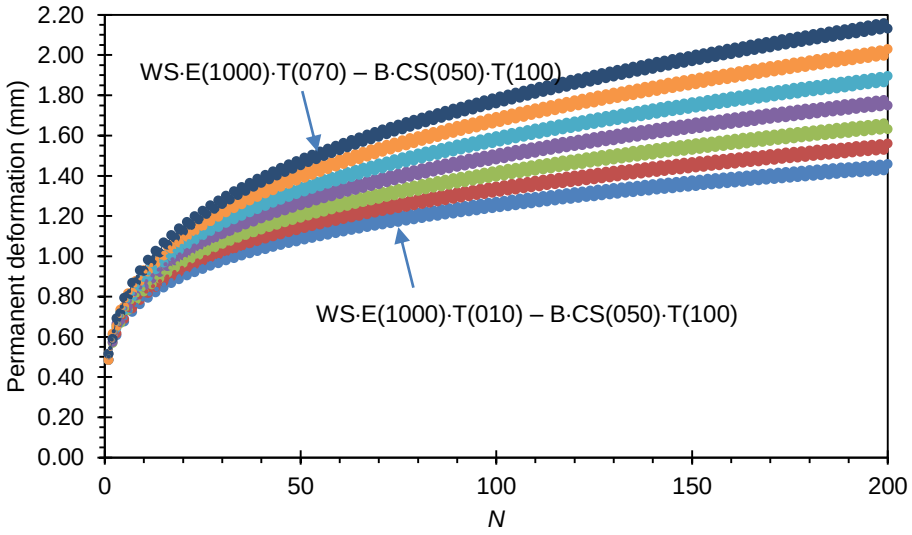

Figure 6.27 Permanent deformation on structural column of pavement in case of WS·E(1000)·T(*j*) – B·CS(050)·T(100) with CRB

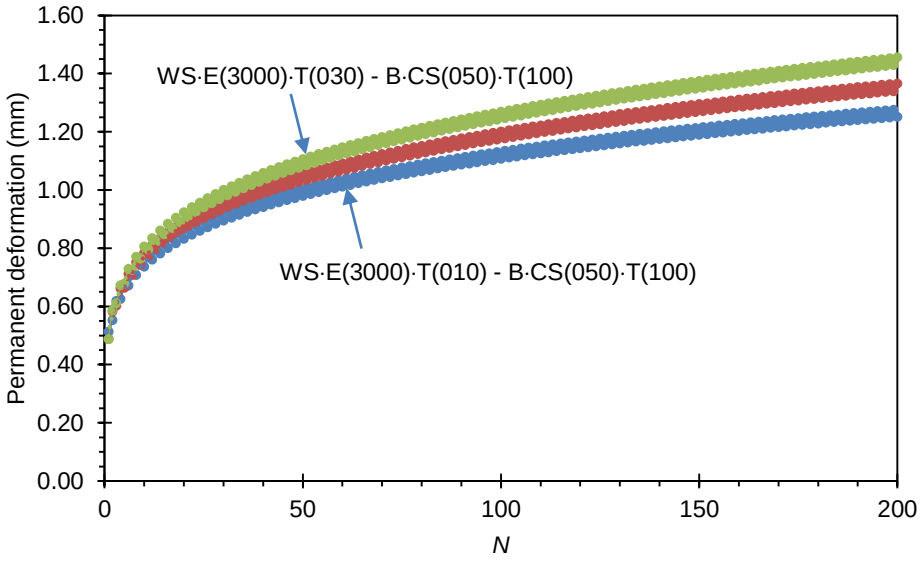

Figure 6.28 Permanent deformation on structural column of pavement in case of WS·E(3000)·T(*j*) – B·CS(050)·T(100) with CRB

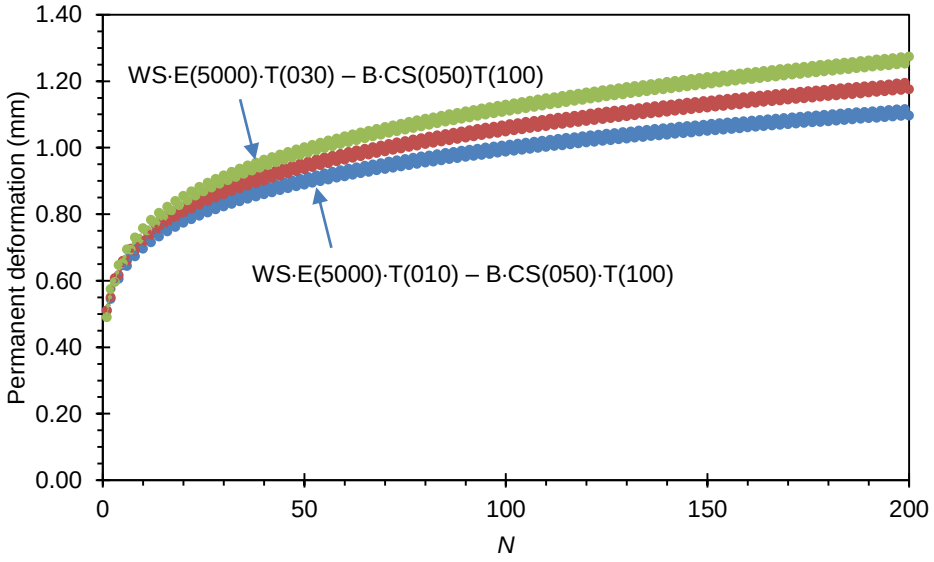

Figure 6.29 Permanent deformation on structural column of pavement in case of WS·E(5000)·T(*j*) – B·CS(050)·T(100) with CRB

Figure 6.30 - Figure 6.32 show analysis results for the case that σ_3 = 50 kPa was applied around CRB base layer and t_b = 200 mm. These figures also indicate that P_d nonlinearly increased with *N* and it gradually increased with t_{ws} too. However, the permanent deformation of each case is higher than that case of t_b = 100 mm.

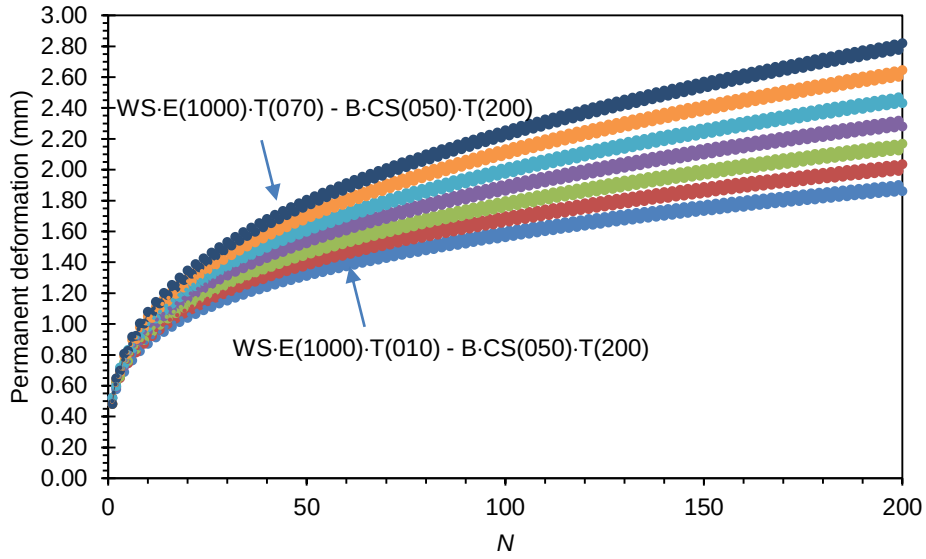

Figure 6.30 Permanent deformation on structural column of pavement in case of WS·E(1000)·T(*j*) – B·CS(050)·T(200) with CRB

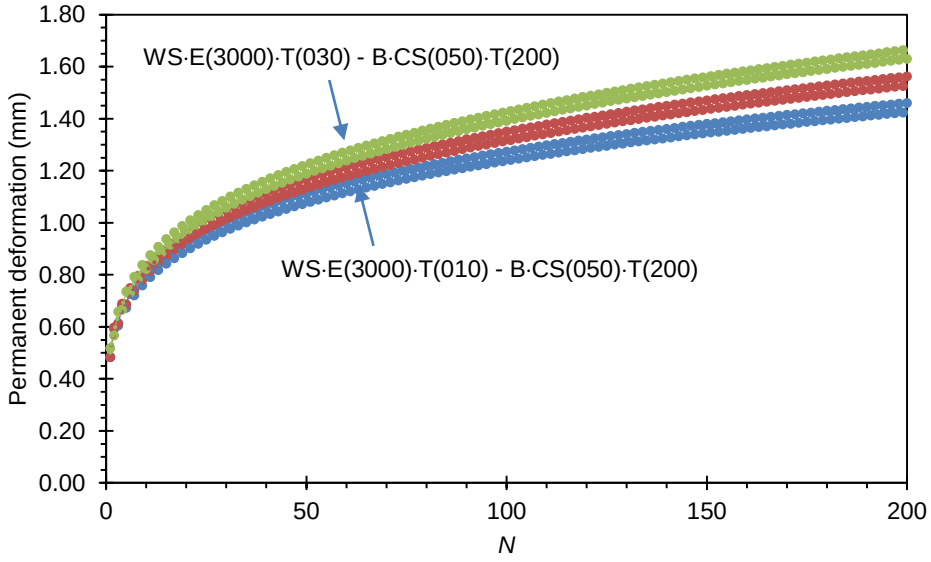

Figure 6.31 Permanent deformation on structural column of pavement in case of WS·E(3000)·T(*j*) – B·CS(050)·T(200) with CRB

Figure 6.33 - Figure 6.35 show analysis results for the case that CRB was adopted as a base course material, σ_3 = 100 kPa was applied around base layer and t_b = 100 mm. It can be seen obviously that P_d nonlinearly increased with *N* and it also gradually increased with t_{ws}.

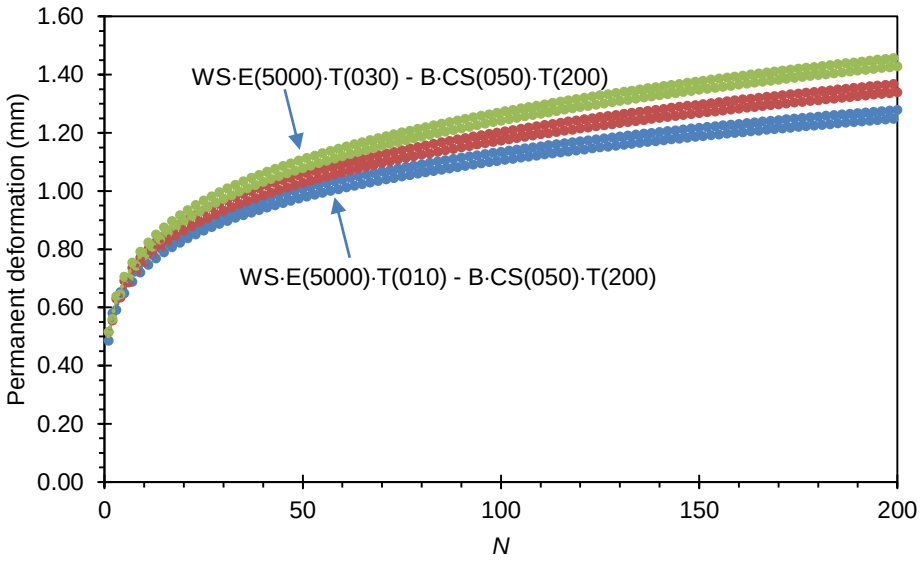

Figure 6.32 Permanent deformation on structural column of pavement in case of WS·E(5000)·T(*j*) – B·CS(050)·T(200) with CRB

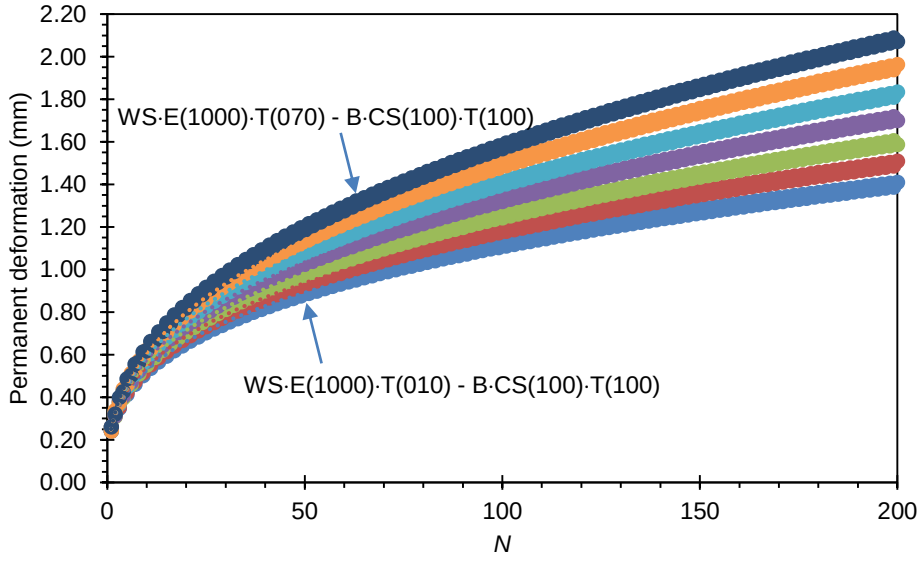

Figure 6.33 Permanent deformation on structural column of pavement in case of WS·E(1000)·T(*j*) – B·CS(100)·T(100) with CRB

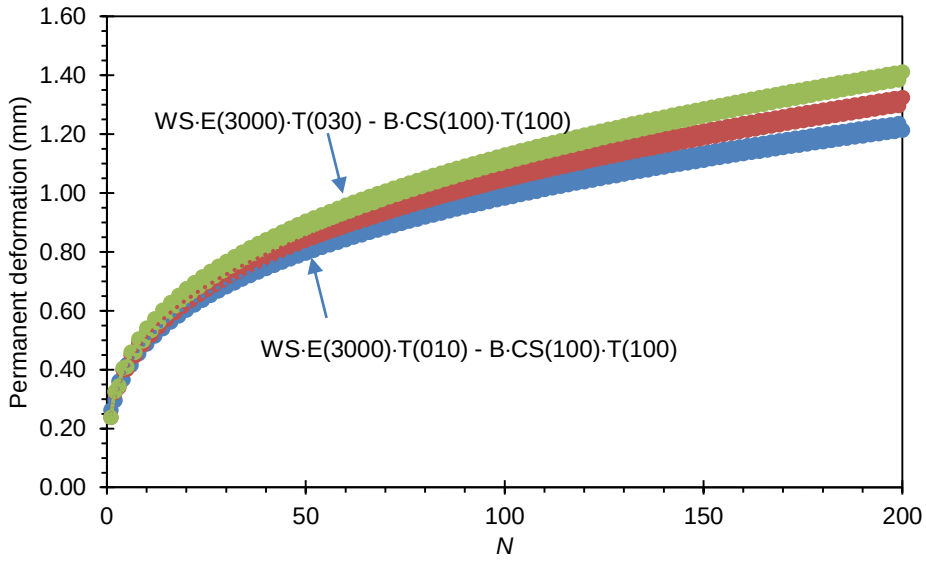

Figure 6.34 Permanent deformation on structural column of pavement in case of WS·E(3000)·T(*j*) – B·CS(100)·T(100) with CRB

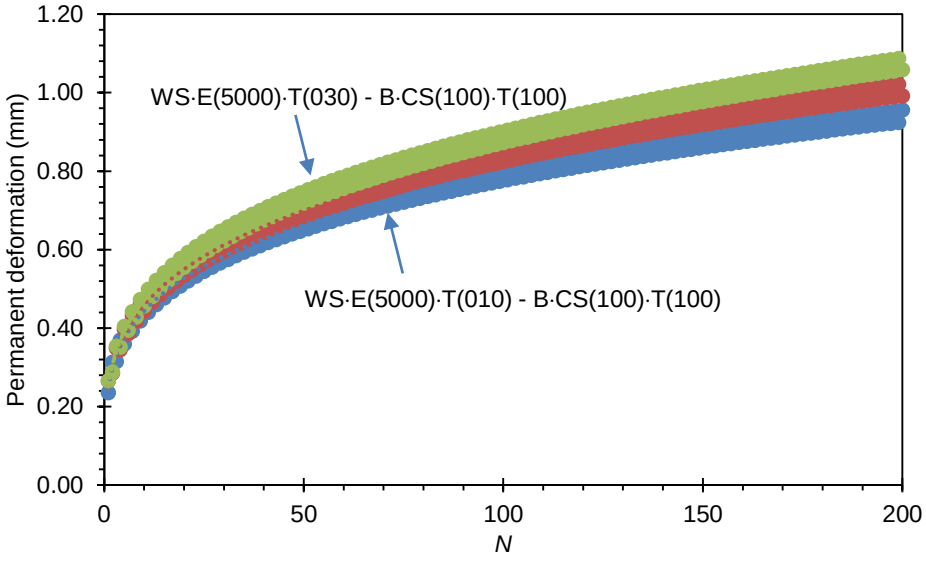

Figure 6.35 Permanent deformation on structural column of pavement in case of WS·E(5000)·T(*j*) – B·CS(100)·T(100) with CRB

Figure 6.36 - Figure 6.38 show analysis results for the case that σ_3 = 100 kPa was applied around CRB base layer and t_b = 200 mm. These figures also indicate that P_d nonlinearly increased with *N* and it gradually increased with t_{ws} too. However, the permanent deformation of each case is higher than that case of t_b = 100 mm.

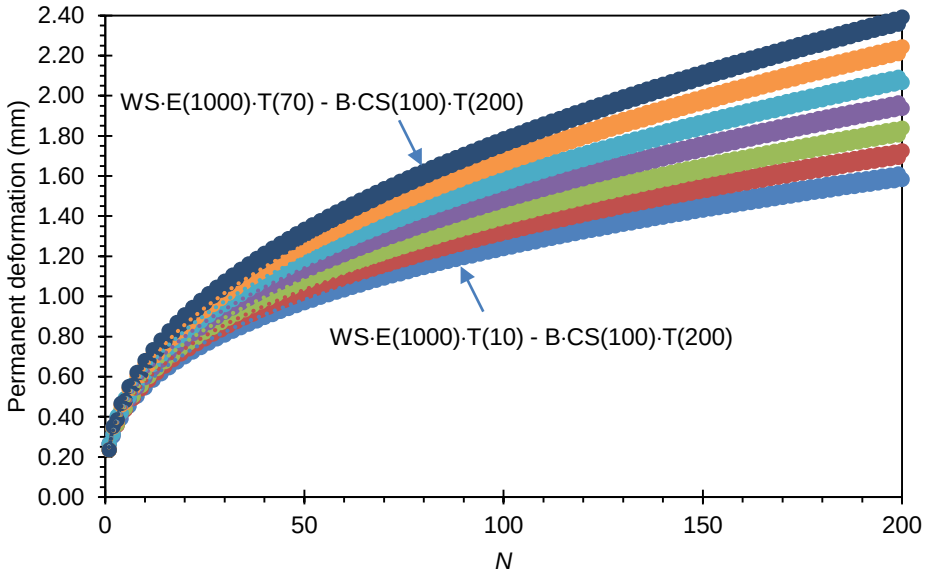

Figure 6.36 Permanent deformation on structural column of pavement in case of WS·E(1000)·T(*j*) – B·CS(100)·T(200) with CRB

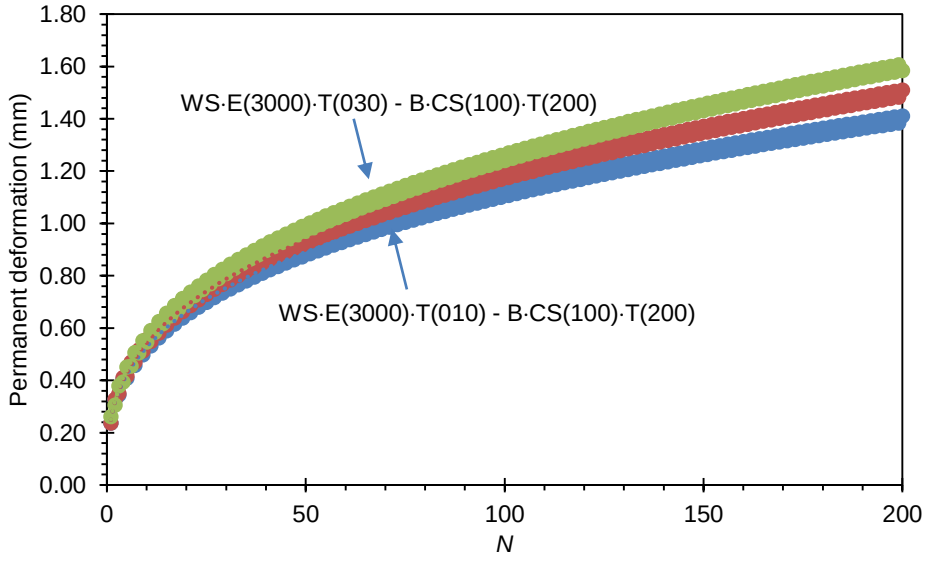

Figure 6.37 Permanent deformation on structural column of pavement in case of WS·E(3000)·T(*j*) – B·CS(100)·T(200) with CRB

Figure 6.39 - Figure 6.41 show analysis results for the case that CRB was adopted as a base course material, σ_3 = 200 kPa was applied around base layer and t_b = 100 mm. It can be obviously seen that P_d nonlinearly increased with *N* and it also gradually increased with t_{ws}.

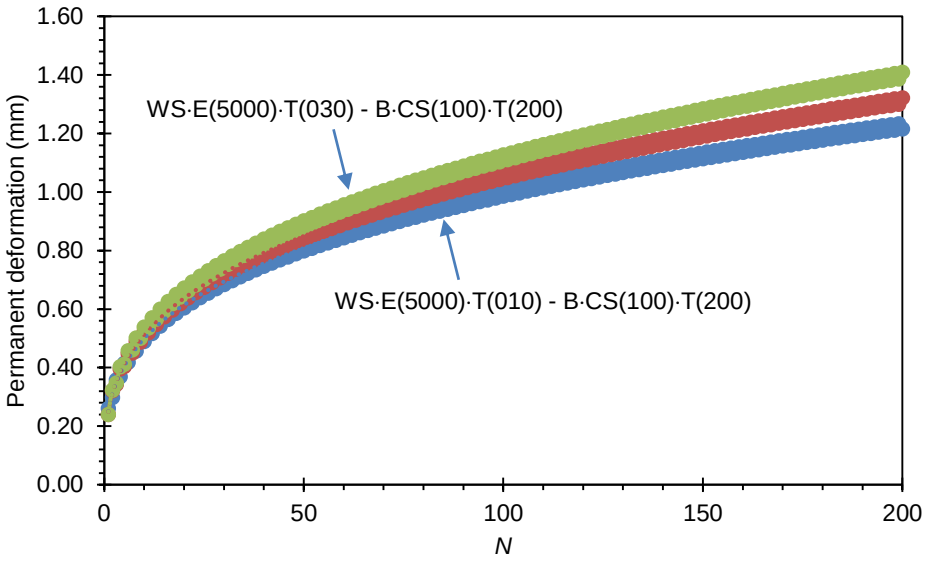

Figure 6.38 Permanent deformation on structural column of pavement in case of WS·E(5000)·T(*j*) – B·CS(100)·T(200) with CRB

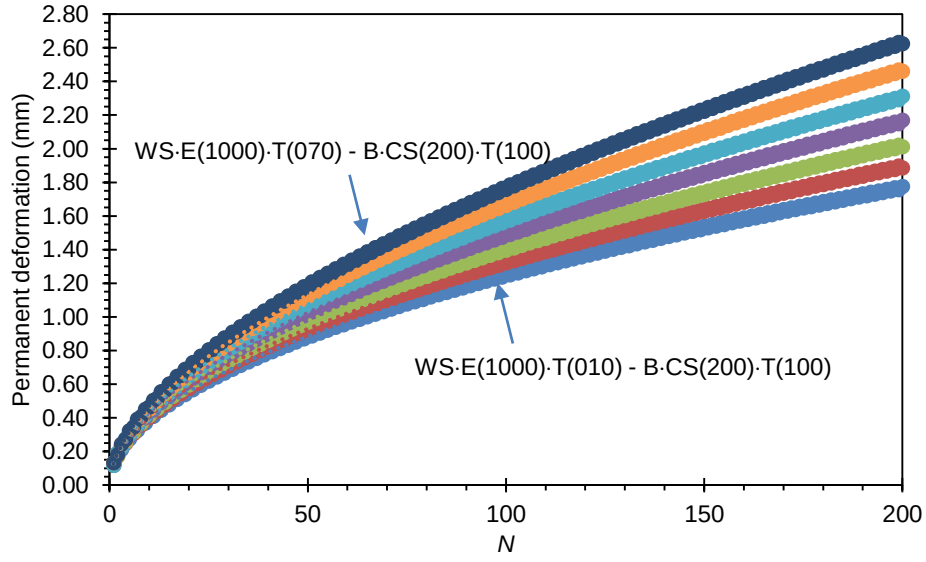

Figure 6.39 Permanent deformation on structural column of pavement in case of WS·E(1000)·T(*j*) – B·CS(200)·T(100) with CRB

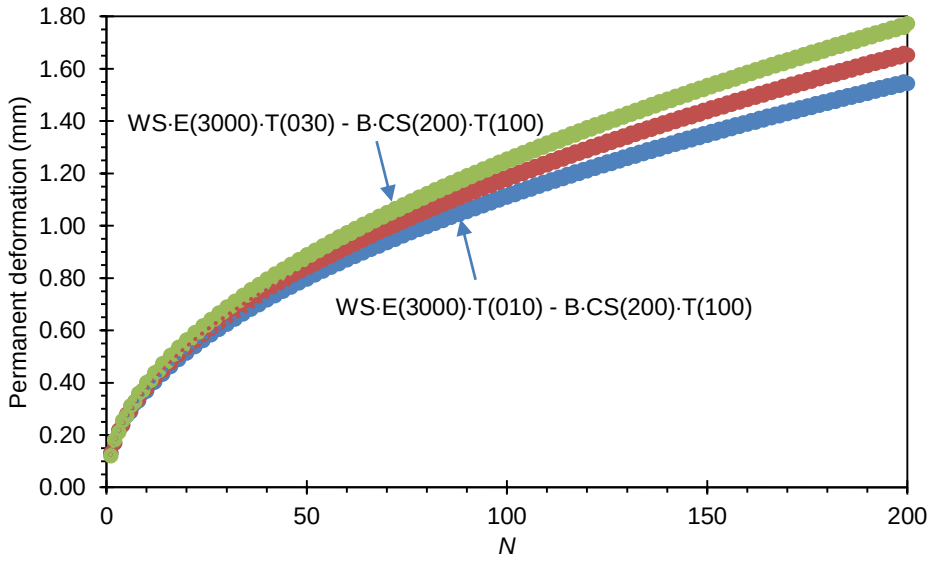

Figure 6.40 Permanent deformation on structural column of pavement in case of WS·E(3000)·T(*j*) – B·CS(200)·T(100) with CRB

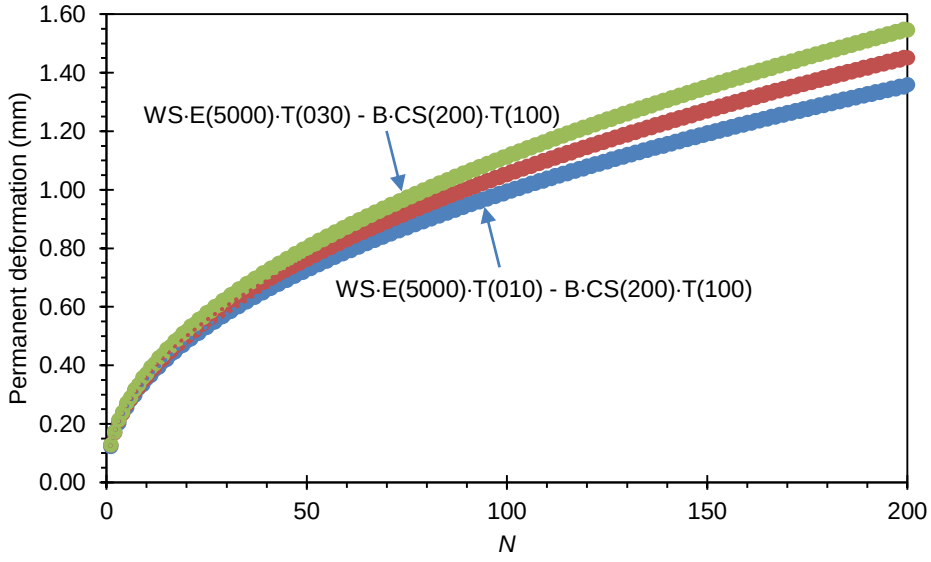

Figure 6.41 Permanent deformation on structural column of pavement in case of WS·E(5000)·T(*j*) – B·CS(200)·T(100) with CRB

Figure 6.42 - Figure 6.44 show analysis results for the case that σ_3 = 200 kPa was applied around CRB base layer and t_b = 200 mm. These figures also indicate that P_d nonlinearly increased with *N* and it gradually increased with t_{ws} too. However, the permanent deformation of each case is higher than that case of t_b = 100 mm.

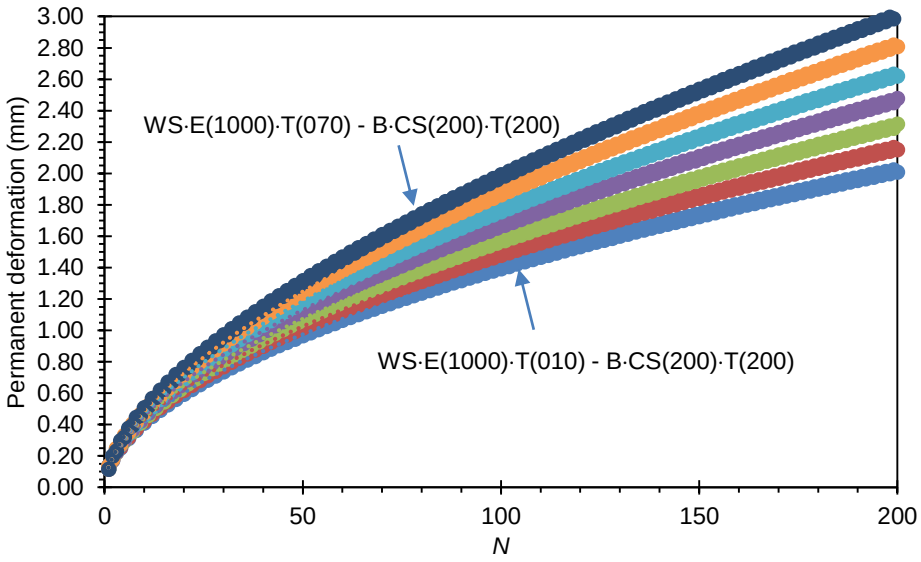

Figure 6.42 Permanent deformation on structural column of pavement in case of WS·E(1000)·T(*j*) – B·CS(200)·T(200) with CRB

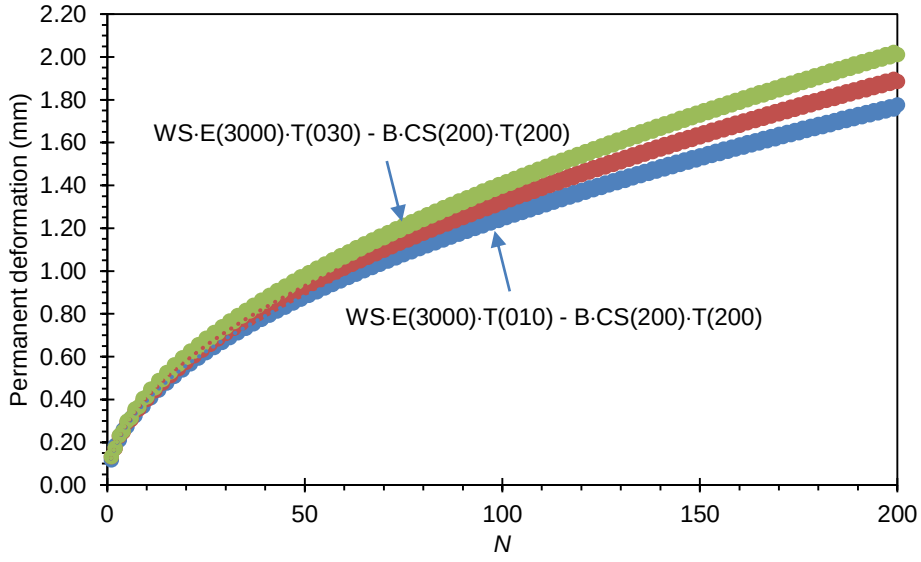

Figure 6.43 Permanent deformation on structural column of pavement in case of WS·E(3000)·T(*j*) – B·CS(200)·T(200) with CRB

Finally, coefficients *a* and *b* for all cases that CRB was adopted as a base course material can be summarised in a table form as seen in Table 6.7 and Table 6.8 for t_b = 100 mm and t_b = 200 mm, respectively.

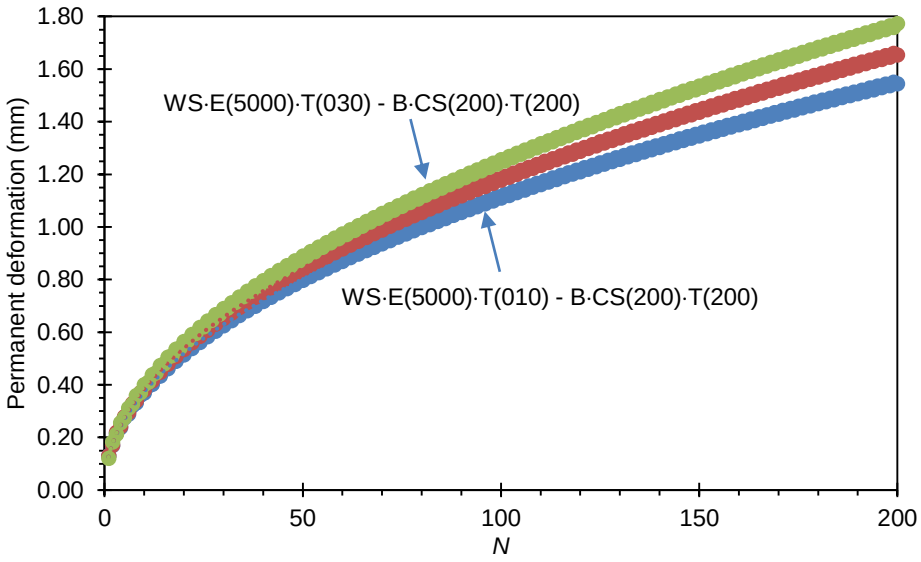

Figure 6.44 Permanent deformation on structural column of pavement in case of WS·E(5000)·T(*j*) – B·CS(200)·T(200) with CRB

Table 6.7 Coefficients *a*, *b* and R^2 of the nonlinear function for predicting the permanent deformations of the column strip under a wheel with CRB and t_b = 100 mm

Wearing surface		σ_3 applied around base layer (thickness of base layer = 100 mm)								
E	Thickness	50 MPa			100 MPa			200 MPa		
(MPa)	(mm)	*a*	*b*	R^2	*a*	*b*	R^2	*a*	*b*	R^2
1000	10	0.499	0.200	0.995	0.249	0.326	0.999	0.124	0.501	1.000
	20	0.498	0.214	0.997	0.249	0.339	0.999	0.125	0.512	1.000
	30	0.501	0.225	0.997	0.251	0.350	0.999	0.126	0.524	1.000
	40	0.500	0.238	0.997	0.250	0.362	0.999	0.124	0.539	1.000
	50	0.499	0.250	0.998	0.249	0.376	0.999	0.124	0.551	1.000
	60	0.498	0.264	0.998	0.249	0.389	0.999	0.125	0.562	1.000
	70	0.501	0.275	0.998	0.251	0.399	1.000	0.126	0.574	1.000
3000	10	0.501	0.175	0.995	0.251	0.299	0.997	0.125	0.474	1.000
	20	0.499	0.188	0.996	0.249	0.314	0.998	0.125	0.488	1.000
	30	0.499	0.200	0.997	0.249	0.326	0.998	0.125	0.501	0.999
5000	10	0.501	0.150	0.994	0.249	0.251	0.992	0.125	0.450	1.000
	20	0.500	0.163	0.996	0.251	0.262	0.993	0.125	0.463	1.000
	30	0.499	0.175	0.997	0.251	0.274	0.994	0.125	0.475	1.000

Table 6.8 Coefficients *a*, *b* and R^2 of the nonlinear function for predicting the permanent deformations of the column strip under a wheel with CRB and t_b = 200 mm

Wearing surface		σ_3 applied around base layer (thickness of base layer = 200 mm)								
E	Thickness	50 MPa			100 MPa			200 MPa		
(MPa)	(mm)	*a*	*b*	R^2	*a*	*b*	R^2	*a*	*b*	R^2
1000	10	0.501	0.250	0.996	0.251	0.349	0.998	0.126	0.524	0.999
	20	0.498	0.264	0.997	0.249	0.364	0.998	0.126	0.537	0.999
	30	0.498	0.276	0.997	0.249	0.376	0.998	0.124	0.552	1.000
	40	0.501	0.286	0.998	0.251	0.387	0.999	0.124	0.564	1.000
	50	0.501	0.300	0.998	0.251	0.399	0.999	0.126	0.574	1.000
	60	0.498	0.314	0.998	0.249	0.414	0.999	0.126	0.587	1.000
	70	0.498	0.326	0.999	0.249	0.426	0.999	0.124	0.602	1.000
3000	10	0.499	0.201	0.994	0.249	0.326	0.998	0.124	0.501	1.000
	20	0.498	0.214	0.995	0.249	0.339	0.998	0.125	0.512	1.000
	30	0.501	0.224	0.996	0.251	0.349	0.994	0.126	0.524	1.000
5000	10	0.499	0.176	0.992	0.251	0.300	0.998	0.125	0.474	1.000
	20	0.500	0.188	0.994	0.249	0.314	0.998	0.125	0.488	1.000
	30	0.501	0.200	0.995	0.249	0.326	0.999	0.125	0.501	1.000

Nevertheless, coefficients *a* and *b*, both in Table 6.7 and Table 6.8, can be expressed in a constitutive form by classifying the case of σ_3 and t_b as shown below;

For the case which t_b = 100 mm and σ_3 = 50 kPa, coefficients *a* and *b* can be written in the forms as

$$a = 0.499 + \left(68.33 \times 10^{-6}\right)\left(t_{ws}\right) - \left(0.467 \times 10^{-6}\right)\left(E_{ws}\right) \left(2.214 \times 10^{-6}\right)\left(t_{ws}^2\right) + \left(0.204 \times 10^{-9}\right)\left(E_{ws}^2\right) -\left(41.87 \times 10^{-9}\right)\left(t_{ws}\right)\left(E_{ws}\right)$$

For $t_{ws} \leq 30$ mm (6.35)

$$b = 0.219 - \left(2.514 \times 10^{-3}\right)\left(t_{ws}\right) + \left(6.288 \times 10^{-6}\right)\left(E_{ws}\right)$$

For $t_{ws} \leq 30$ mm (6.36)

For the case which t_b = 200 mm and σ_3 = 50 kPa, coefficients *a* and *b* can be written in the forms as

$$a = 0.504 - \left(0.269 \times 10^{-3}\right)\left(t_{ws}\right) - \left(2.426 \times 10^{-6}\right)\left(E_{ws}\right) \left(3.395 \times 10^{-6}\right)\left(t_{ws}^2\right) + \left(0.232 \times 10^{-9}\right)\left(E_{ws}^2\right) + \left(58.66 \times 10^{-9}\right)\left(t_{ws}\right)\left(E_{ws}\right) \quad \text{For } t_{ws} \leq 30 \text{ mm} \tag{6.37}$$

$$b = 0.278 - \left(3.769 \times 10^{-3}\right)\left(t_{ws}\right) + \left(6.187 \times 10^{-6}\right)\left(E_{ws}\right) \quad \text{For } t_{ws} \leq 30 \text{ mm} \tag{6.38}$$

For the case which t_b = 100 mm and σ_3 = 100 kPa, coefficients *a* and *b* can be written in the forms as

$$a = 0.251 - \left(0.133 \times 10^{-3}\right)\left(t_{ws}\right) - \left(0.602 \times 10^{-6}\right)\left(E_{ws}\right) + \left(3.200 \times 10^{-6}\right)\left(t_{ws}^2\right) + \left(96.39 \times 10^{-12}\right)\left(E_{ws}^2\right) + \left(8.367 \times 10^{-9}\right)\left(t_{ws}\right)\left(E_{ws}\right) \quad \text{For } t_{ws} \leq 30 \text{ mm} \tag{6.39}$$

$$b = 0.362 - \left(3.77 \times 10^{-3}\right)\left(t_{ws}\right) + \left(6.122 \times 10^{-6}\right)\left(E_{ws}\right) \quad \text{For } t_{ws} \leq 30 \text{ mm} \tag{6.40}$$

For the case which t_b = 200 mm and σ_3 = 100 kPa, coefficients *a* and *b* can be written in the forms as

$$a = 0.252 - \left(13.48 \times 10^{-6}\right)\left(t_{ws}\right) - \left(1.907 \times 10^{-6}\right)\left(E_{ws}\right) - \left(50.890 \times 10^{-9}\right)\left(t_{ws}^2\right) + \left(0.266 \times 10^{-9}\right)\left(E_{ws}^2\right) + \left(8.645 \times 10^{-9}\right)\left(t_{ws}\right)\left(E_{ws}\right) \quad \text{For } t_{ws} \leq 30 \text{ mm} \tag{6.41}$$

$$b = 0.369 - \left(2.509 \times 10^{-3}\right)\left(t_{ws}\right) + \left(6.376 \times 10^{-6}\right)\left(E_{ws}\right) \quad \text{For } t_{ws} \leq 30 \text{ mm} \tag{6.42}$$

For the case which t_b = 100 mm and σ_3 = 200 kPa, coefficients *a* and *b* can be written in the forms as

$$a = 0.124 + \left(25.39 \times 10^{-6}\right)\left(t_{ws}\right) + \left(0.606 \times 10^{-6}\right)\left(E_{ws}\right) - \left(43.240 \times 10^{-9}\right)\left(t_{ws}^2\right) - \left(61.32 \times 10^{-12}\right)\left(E_{ws}^2\right) - \left(8.928 \times 10^{-9}\right)\left(t_{ws}\right)\left(E_{ws}\right) \quad (6.43)$$

For $t_{ws} \leq 30$ mm

$$b = 0.519 - \left(2.494 \times 10^{-3}\right)\left(t_{ws}\right) + \left(6.144 \times 10^{-6}\right)\left(E_{ws}\right) \quad (6.44)$$

For $t_{ws} \leq 30$ mm

For the case which t_b = 200 mm and σ_3 = 200 kPa, coefficients *a* and *b* can be written in the forms as

$$a = 0.125 - \left(26.21 \times 10^{-6}\right)\left(t_{ws}\right) + \left(0.370 \times 10^{-6}\right)\left(E_{ws}\right) - \left(66.940 \times 10^{-9}\right)\left(t_{ws}^2\right) - \left(0.106 \times 10^{-9}\right)\left(E_{ws}^2\right) + \left(8.957 \times 10^{-9}\right)\left(t_{ws}\right)\left(E_{ws}\right) \quad (6.45)$$

For $t_{ws} \leq 30$ mm

$$b = 0.543 - \left(2.496 \times 10^{-3}\right)\left(t_{ws}\right) + \left(6.407 \times 10^{-6}\right)\left(E_{ws}\right) \quad (6.46)$$

For $t_{ws} \leq 30$ mm

By considering Equations (6.35) - (6.46), we can see that coefficients *a* and *b* are written in polynomial form as

$$a = f_0^a + \left(f_1^a\right)\left(t_{ws}\right) + \left(f_2^a\right)\left(E_{ws}\right) + \left(f_3^a\right)\left(t_{ws}^2\right) + \left(f_4^a\right)\left(E_{ws}^2\right) + \left(f_5^a\right)\left(t_{ws}\right)\left(E_{ws}\right)$$

and

$$b = f_0^b + \left(f_1^b\right)\left(t_{ws}\right) + \left(f_2^b\right)\left(E_{ws}\right)$$

Consequently, the regression analysis is employed and it is found that coefficient f_i can be expressed as a polynomial function which comprises of t_b and σ_3 as

$$f_0^a = 0.868 + (53.000 \times 10^{-6})(t_b) - (8.697 \times 10^{-3})(\sigma_3) - (0.240 \times 10^{-6})(\sigma_3)(t_b) + (24.880 \times 10^{-6})(\sigma_3^2) \quad (6.47)$$

$$f_1^a = (0.256 \times 10^{-3}) - (2.521 \times 10^{-6})(t_b) - (1.721 \times 10^{-6})(\sigma_3) + (13.900 \times 10^{-9})(\sigma_3)(t_b) + (1.213 \times 10^{-9})(\sigma_3^2) \quad (6.48)$$

$$f_2^a = (2.561 \times 10^{-6}) - (25.000 \times 10^{-9})(t_b) - (26.86 \times 10^{-9})(\sigma_3) + (0.114 \times 10^{-9})(\sigma_3)(t_b) + (90.630 \times 10^{-12})(\sigma_3^2) \quad (6.49)$$

$$f_3^a = (4.948 \times 10^{-6}) - (4.236 \times 10^{-9})(t_b) - (29.43 \times 10^{-9})(\sigma_3) - (23.250 \times 10^{-12})(\sigma_3)(t_b) + (55.42 \times 10^{-12})(\sigma_3^2) \quad (6.50)$$

$$f_4^a = -(0.132 \times 10^{-6}) + (0.918 \times 10^{-9})(t_b) + (0.761 \times 10^{-9})(\sigma_3) - (4.475 \times 10^{-12})(\sigma_3)(t_b) - (0.581 \times 10^{-12})(\sigma_3^2) \quad (6.51)$$

$$f_5^a = -(11.68 \times 10^{-12}) + (1.352 \times 10^{-12})(t_b) + (2.259 \times 10^{-12})(\sigma_3) - (7.216 \times 10^{-15})(\sigma_3)(t_b) - (12.750 \times 10^{-15})(\sigma_3^2) \quad (6.52)$$

and

$$f_0^b = 0.034 + (0.505 \times 10^{-3})(t_b) + (3.271 \times 10^{-3})(\sigma_3) - (1.760 \times 10^{-6})(\sigma_3)(t_b) - (4.507 \times 10^{-6})(\sigma_3^2) \quad (6.53)$$

$$f_1^b = -(1.995 \times 10^{-3}) - (6.235 \times 10^{-6})(t_b) - (14.400 \times 10^{-6})(\sigma_3) + (53.560 \times 10^{-9})(\sigma_3)(t_b) + (42.700 \times 10^{-9})(\sigma_3^2) \quad (6.54)$$

$$f_2^b = (6.389 \times 10^{-6}) - (1.050 \times 10^{-9})(t_b) - (3.043 \times 10^{-9})(\sigma_3) + (21.2903 \times 10^{-12})(\sigma_3)(t_b) + (0.333 \times 10^{-12})(\sigma_3^2) \quad (6.55)$$

Equations above reveal that P_d of pavement structure can be predicted using a function which is composed of *N*, t_{ws}, t_b , E_{ws} and σ_3 as the variables.

6.6.2 Investigation of structural pavement column using HCTCRB as base course material

In this section, HCTCRB was adopted as a base course material used in the column-strip model for finite element analysis, Equations (6.30), (6.32) and (6.34) were then employed for computing the resilient modulus of base layer. After all cases of analysis were done, the permanent deformation obtained by each case of analysis was eventually formulated in a constitutive form. The constitutive formula given by this section can be used for predicting the maximum permanent deformation of pavement structure having thin wearing surface layer by engineers in design procedure.

The analysis result as shown in Figure 6.45 to Figure 6.56 revealed that the permanent deformation of the pavement structure can be expressed by nonlinear equation $P_d = aN^b$ as same as described in section 6.6.1. The results obtained in this section can be analysed further to find the effect of each factor on permanent deformation as described below.

Figure 6.45 - Figure 6.47 show analysis results for the case that HCTCRB was adopted as a base course material, confining stress (σ_3) applied around base layer was 50 kPa and thickness of base layer (t_b) was 100 mm. It can be obviously seen that P_d nonlinearly increased with *N* and it also gradually increased with t_{ws}.

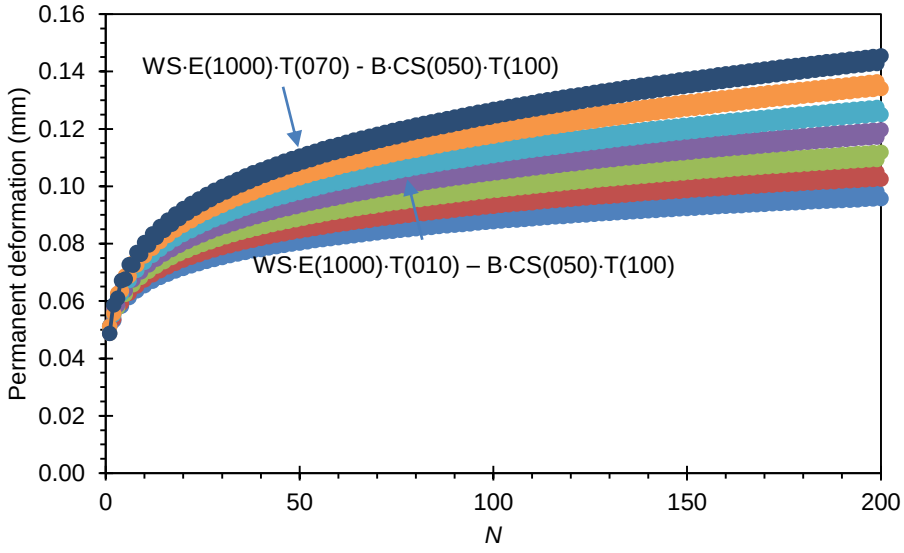

Figure 6.45 Permanent deformation on structural column of pavement in case of WS·E(1000)·T(*j*) – B·CS(050)·T(100) with HCTCRB

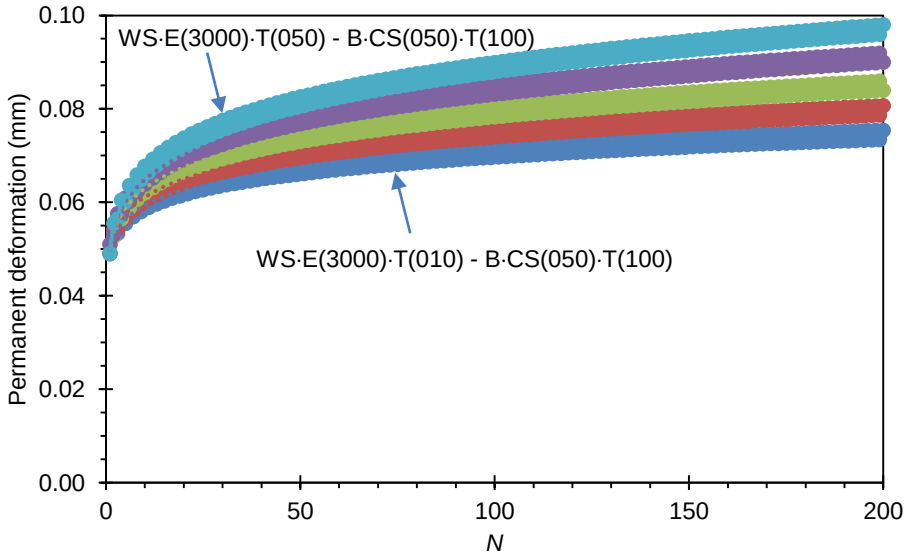

Figure 6.46 Permanent deformation on structural column of pavement in case of WS·E(3000)·T(*j*) – B·CS(050)·T(100) with HCTCRB

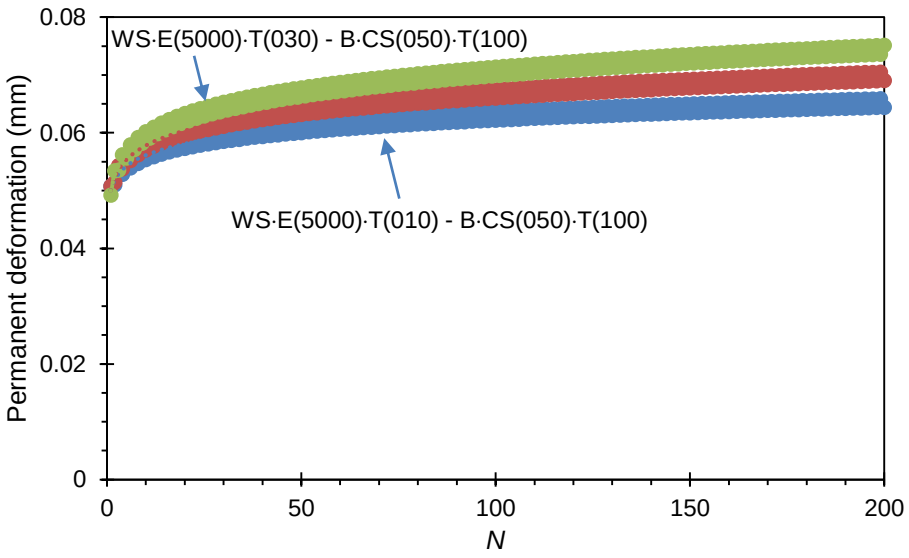

Figure 6.47 Permanent deformation on structural column of pavement in case of WS·E(5000)·T(*j*) – B·CS(050)·T(100) with HCTCRB

Figure 6.48 - Figure 6.50 show analysis results for the case that σ_3 = 50 kPa was applied around HCTCRB base layer and t_b = 200 mm. These figures also indicate that P_d nonlinearly increased with *N* and it gradually increased with t_{ws} too. However, the permanent deformation of each case is higher than that case of t_b = 100 mm.

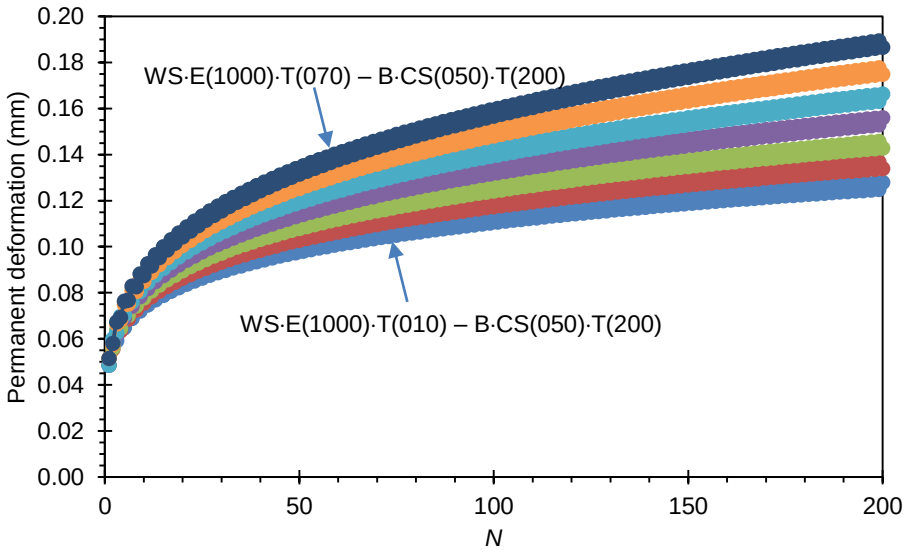

Figure 6.48 Permanent deformation on structural column of pavement in case of WS·E(1000)·T(*j*) – B·CS(050)·T(200) with HCTCRB

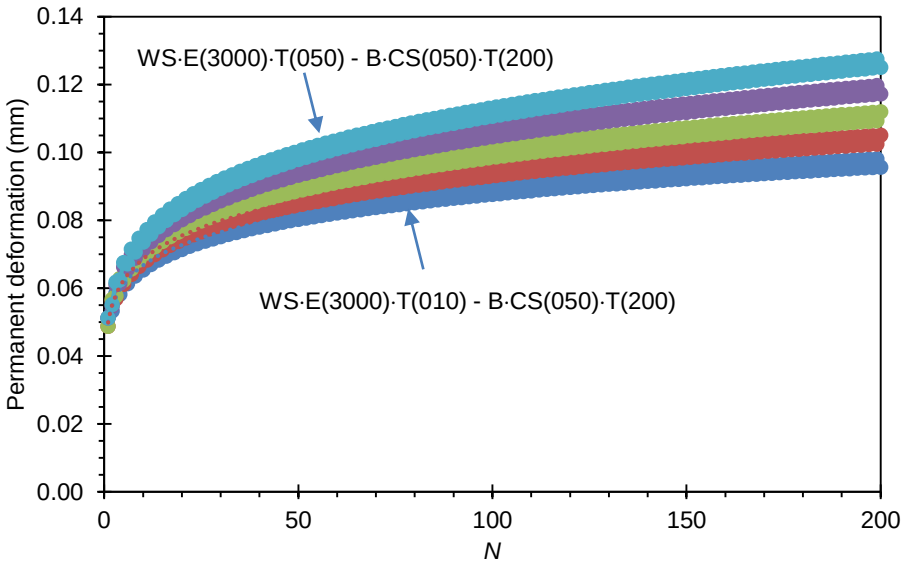

Figure 6.49 Permanent deformation on structural column of pavement in case of WS·E(3000)T(*j*) – B·CS(050)·T(200) with HCTCRB

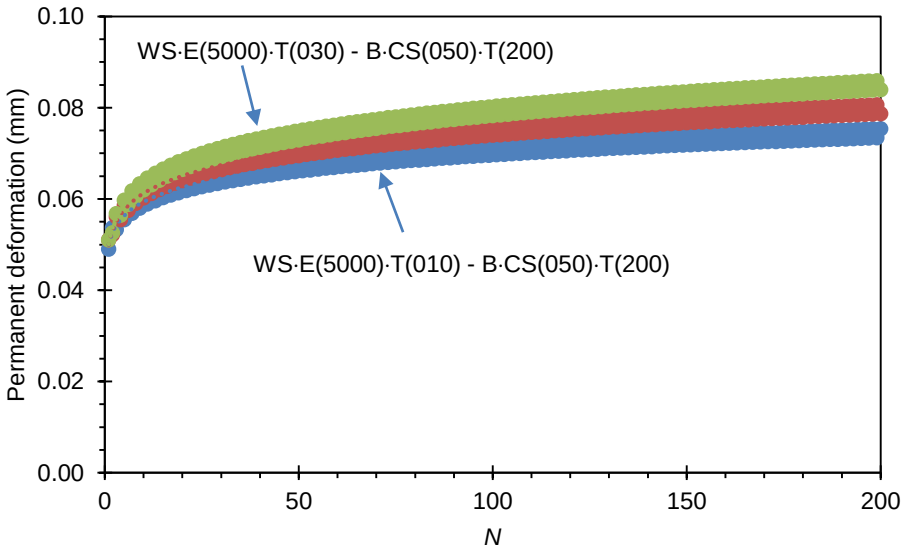

Figure 6.50 Permanent deformation on structural column of pavement in case of WS·E(5000)·T(*j*) – B·CS(050)·T(200) with HCTCRB

Figure 6.51 - Figure 6.53 show analysis results for the case that HCTCRB was adopted as a base course material, σ_3 = 100 kPa was applied around base layer and t_b = 100 mm. It can be seen obviously that P_d nonlinearly increased with *N* and it also gradually increased with t_{ws}.

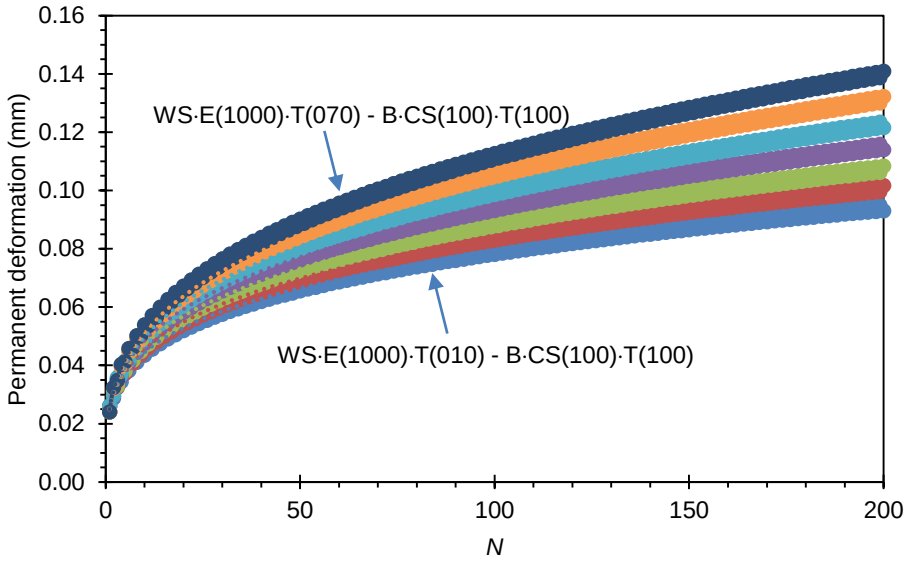

Figure 6.51 Permanent deformation on structural column of pavement in case of WS·E(1000)·T(*j*) – B·CS(100)·T(100) with HCTCRB

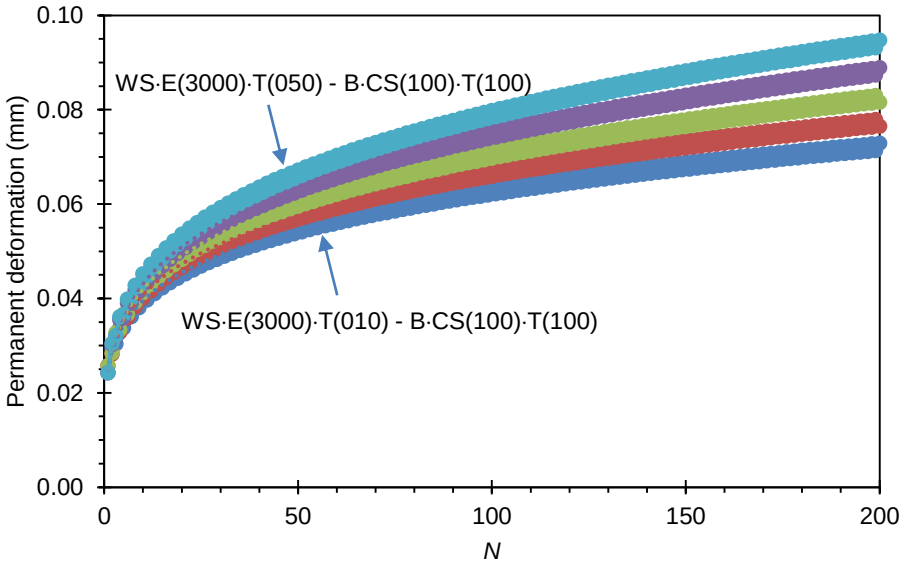

Figure 6.52 Permanent deformation on structural column of pavement in case of WS·E(3000)·T(*j*) – B·CS(100)·T(100) with HCTCRB

Figure 6.54 - Figure 6.56 show analysis results for the case that σ_3 = 100 kPa was applied around HCTCRB base layer and t_b = 200 mm. These figures also indicate that P_d nonlinearly increased with *N* and it gradually increased with t_{ws} too. However, the permanent deformation of each case is higher than that case of t_b = 100 mm.

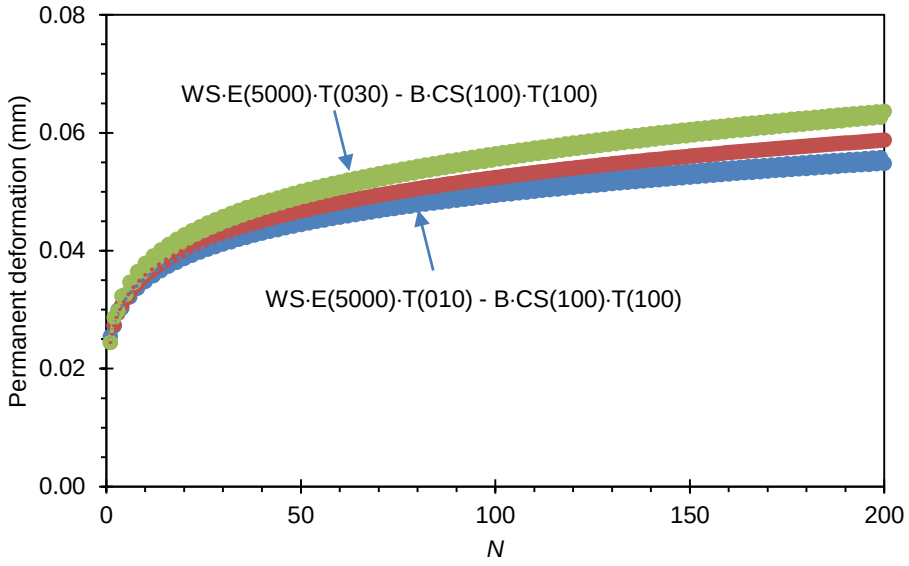

Figure 6.53 Permanent deformation on structural column of pavement in case of WS·E(5000)·T(*j*) – B·CS(100)·T(100) with HCTCRB

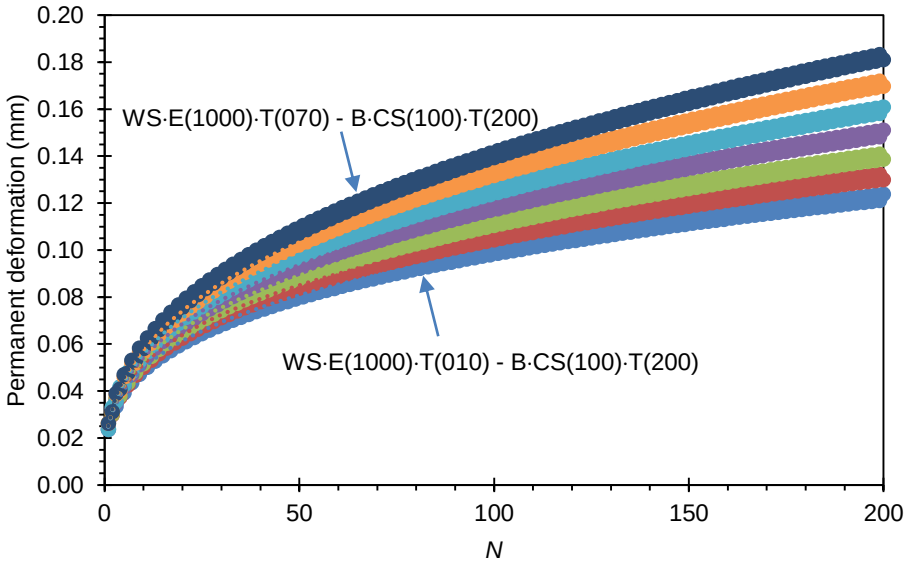

Figure 6.54 Permanent deformation on structural column of pavement in case of WS·E(1000)·T(*j*) – B·CS(100)·T(200) with HCTCRB

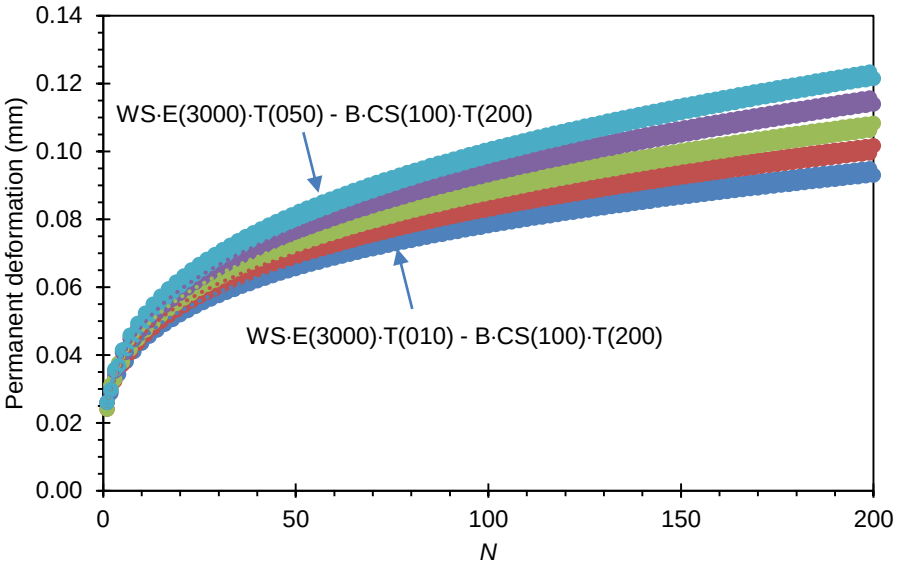

Figure 6.55 Permanent deformation on structural column of pavement in case of WS·E(3000)·T(*j*) – B·CS(100)·T(200) with HCTCRB

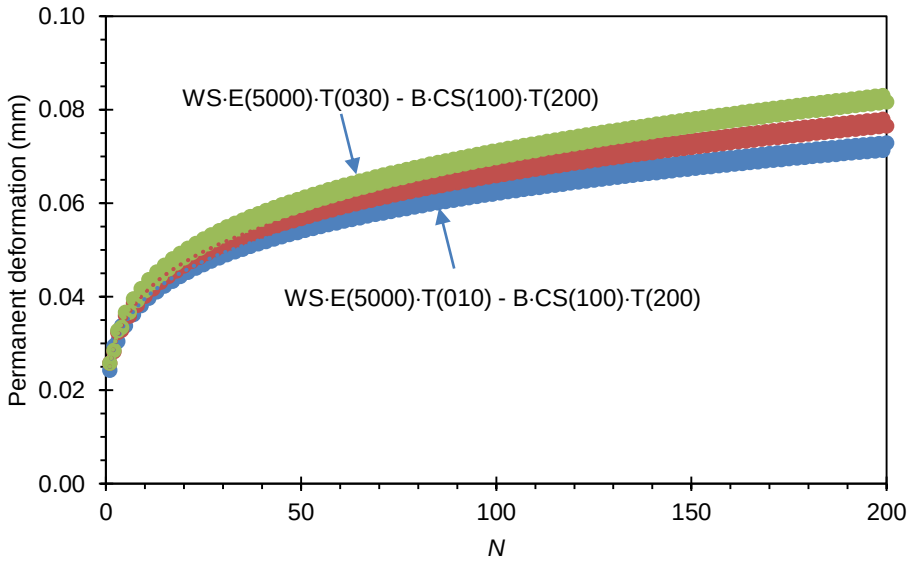

Figure 6.56 Permanent deformation on structural column of pavement in case of WS·E(5000)·T(*j*) – B·CS(100)·T(200) with HCTCRB

Figure 6.57 - Figure 6.59 show analysis results for the case that HCTCRB was adopted as a base course material, σ_3 = 200 kPa was applied around base layer and t_b = 100 mm. It can be obviously seen that P_d nonlinearly increased with *N* and it also gradually increased with t_{ws}.

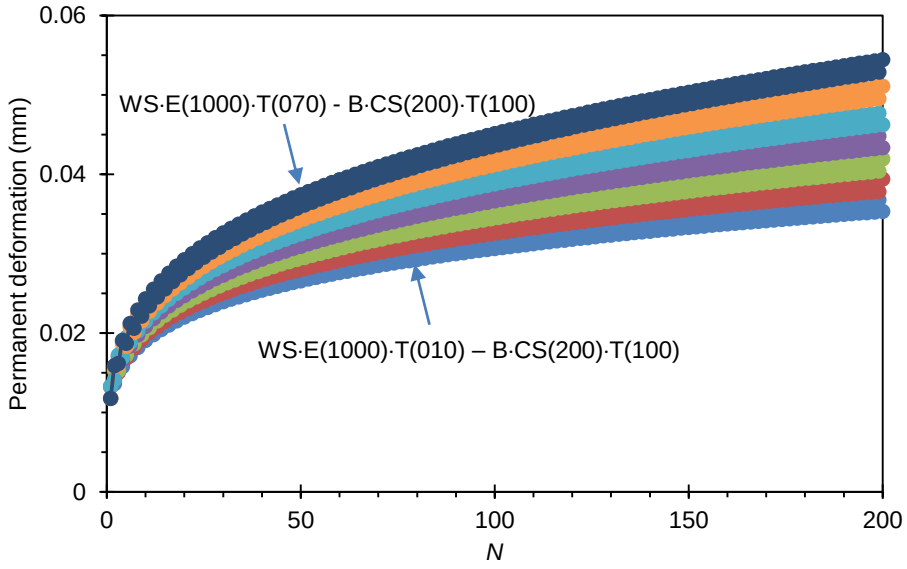

Figure 6.57 Permanent deformation on structural column of pavement in case of WS·E(1000)·T(*j*) – B·CS(200)·T(100) with HCTCRB

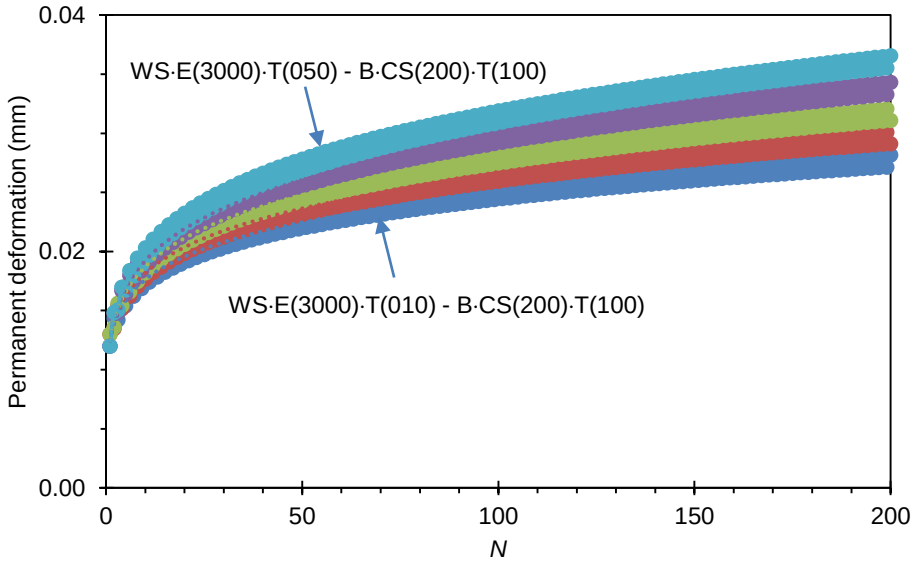

Figure 6.58 Permanent deformation on structural column of pavement in case of WS·E(3000)·T(*j*) – B·CS(200)·T(100) with HCTCRB

Figure 6.60 - Figure 6.62 show analysis results for the case that σ_3 = 200 kPa was applied around CRB base layer and t_b = 200 mm. These figures also indicate that P_d nonlinearly increased with *N* and it gradually increased with t_{ws} too. However, the permanent deformation of each case is higher than that case of t_b = 100 mm.

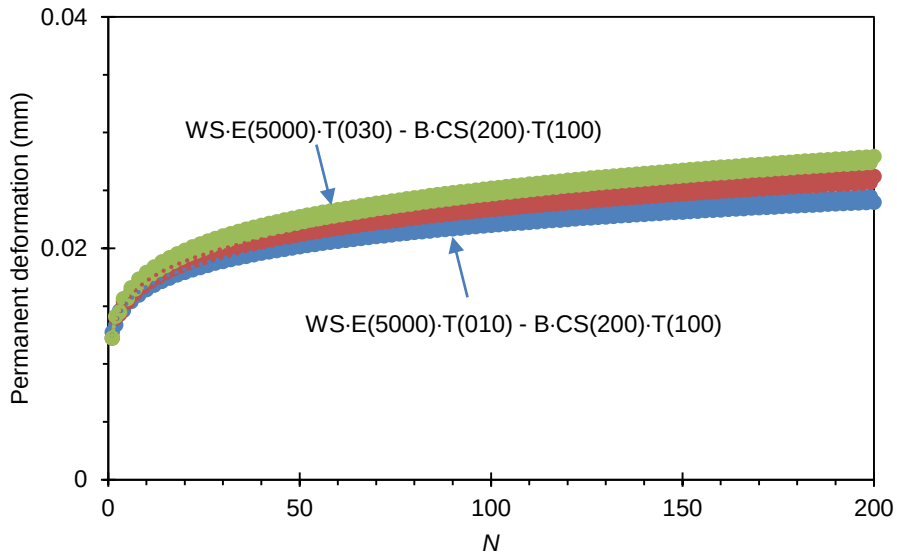

Figure 6.59 Permanent deformation on structural column of pavement in case of WS·E(5000)·T(*j*) – B·CS(200)·T(100) with HCTCRB

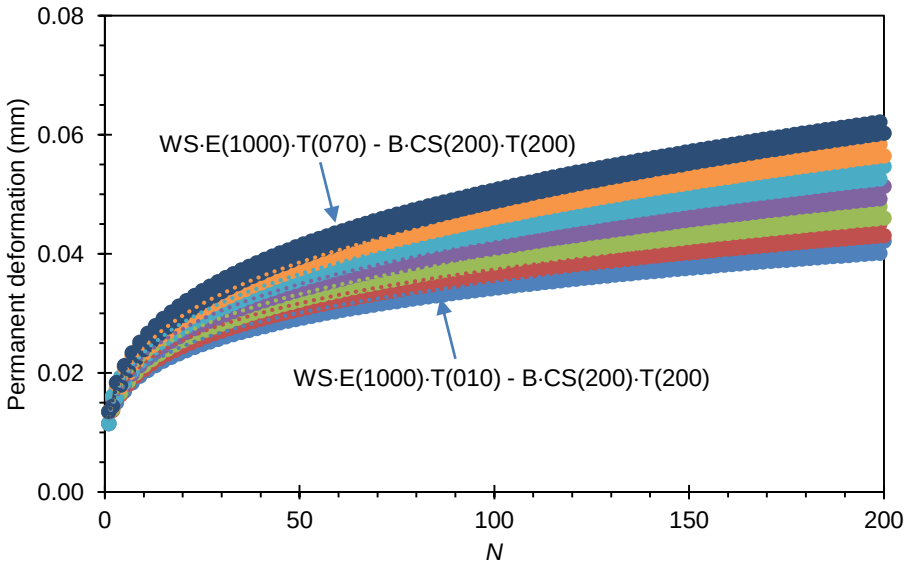

Figure 6.60 Permanent deformation on structural column of pavement in case of WS·E(1000)·T(*j*) – B·CS(200)·T(200) with HCTCRB

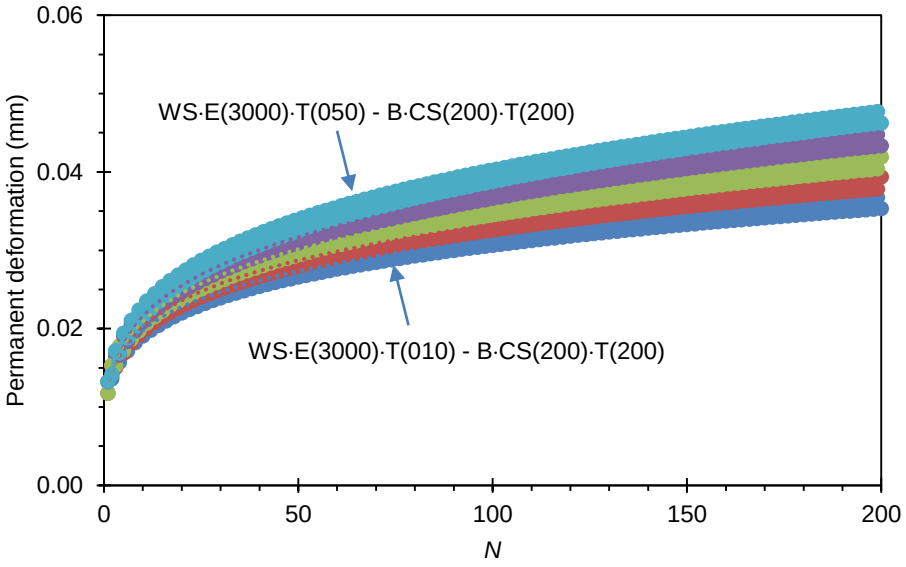

Figure 6.61 Permanent deformation on structural column of pavement in case of WS·E(3000)·T(*j*) – B·CS(200)·T(200) with HCTCRB

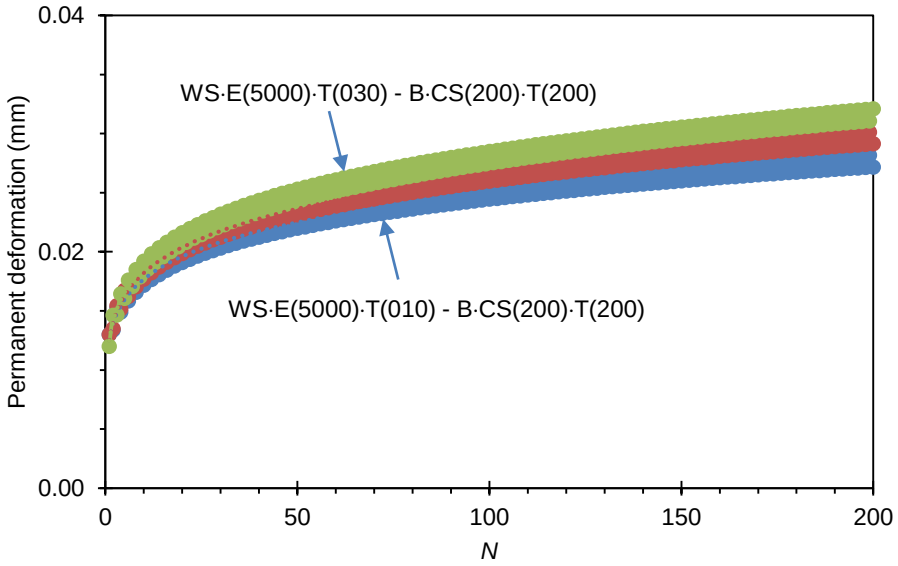

Figure 6.62 Permanent deformation on structural column of pavement in case of WS·E(5000)·T(*j*) – B·CS(200)·T(200) with HCTCRB

Finally, coefficients *a* and *b* for all cases that HCTCRB was adopted as a base course material can be summarised in a table form as seen in Table 6.9 and Table 6.10 for t_b = 100 mm and t_b = 200 mm, respectively.

Table 6.9 Coefficients *a*, *b* and R^2 of the nonlinear function for predicting the permanent deformations of the column strip under a wheel with HCTCRB and t_b = 100 mm

Wearing surface		σ_3 applied around base layer (thickness of base layer = 100 mm)								
E	Thickness	50 MPa			100 MPa			200 MPa		
(MPa)	(mm)	*a*	*b*	R^2	*a*	*b*	R^2	*a*	*b*	R^2
1000	10	0.050	0.125	0.985	0.025	0.250	0.996	0.012	0.199	0.981
	20	0.050	0.138	0.989	0.025	0.264	0.997	0.012	0.214	0.985
	30	0.050	0.150	0.991	0.025	0.276	0.997	0.012	0.226	0.988
	40	0.050	0.164	0.993	0.025	0.288	0.998	0.012	0.237	0.990
	50	0.050	0.175	0.995	0.025	0.314	0.998	0.012	0.249	0.992
	60	0.050	0.188	0.996	0.025	0.326	0.999	0.012	0.264	0.993
	70	0.050	0.200	0.997	0.025	0.300	0.998	0.012	0.276	0.994
3000	10	0.050	0.075	0.960	0.025	0.200	0.995	0.012	0.151	0.978
	20	0.050	0.088	0.974	0.025	0.213	0.996	0.012	0.162	0.983
	30	0.050	0.100	0.981	0.025	0.225	0.997	0.012	0.174	0.986
	40	0.050	0.113	0.987	0.025	0.239	0.997	0.012	0.189	0.990
	50	0.050	0.125	0.990	0.025	0.250	0.998	0.012	0.201	0.992
5000	10	0.050	0.050	0.939	0.025	0.150	0.994	0.012	0.125	0.990
	20	0.050	0.063	0.964	0.024	0.165	1.000	0.012	0.138	0.993
	30	0.050	0.075	0.977	0.025	0.175	0.997	0.012	0.150	0.994

Table 6.10 Coefficients *a*, *b* and R^2 of the nonlinear function for predicting the permanent deformations of the column strip under a wheel with HCTCRB and t_b = 200 mm

Wearing surface		σ_3 applied around base layer (thickness of base layer = 200 mm)								
E	Thickness	50 MPa			100 MPa			200 MPa		
(MPa)	(mm)	*a*	*b*	R^2	*a*	*b*	R^2	*a*	*b*	R^2
1000	10	0.050	0.176	0.992	0.025	0.301	0.997	0.012	0.227	0.978
	20	0.050	0.188	0.994	0.025	0.312	0.998	0.012	0.237	0.982
	30	0.050	0.200	0.995	0.025	0.324	0.998	0.012	0.249	0.985
	40	0.050	0.214	0.996	0.025	0.339	0.998	0.012	0.265	0.988
	50	0.050	0.226	0.997	0.025	0.351	0.998	0.012	0.276	0.990
	60	0.050	0.237	0.997	0.025	0.362	0.999	0.012	0.287	0.991
	70	0.050	0.250	0.998	0.025	0.374	0.999	0.013	0.299	0.993
3000	10	0.050	0.125	0.985	0.025	0.250	0.996	0.012	0.199	0.981
	20	0.050	0.138	0.989	0.025	0.264	0.997	0.012	0.214	0.985
	30	0.050	0.150	0.991	0.025	0.276	0.997	0.012	0.226	0.988
	40	0.050	0.163	0.993	0.025	0.288	0.998	0.012	0.237	0.990
	50	0.050	0.175	0.995	0.025	0.300	0.998	0.012	0.249	0.992
5000	10	0.050	0.075	0.960	0.025	0.200	0.995	0.012	0.150	0.978
	20	0.050	0.088	0.974	0.025	0.213	0.996	0.012	0.162	0.983
	30	0.050	0.100	0.981	0.025	0.225	0.997	0.012	0.176	0.987

Nevertheless, coefficients *a* and *b*, both in Table 6.9 and Table 6.10, can be expressed in a constitutive form by classifying the case of σ_3 and t_b as shown below;

For the case that t_b = 100 mm and σ_3 = 50 kPa, coefficients *a* and *b* can be written in the forms as

$$a = 0.050 - \left(20.590 \times 10^{-6}\right)\left(t_{ws}\right) - \left(57.72 \times 010^{-9}\right)\left(E_{ws}\right) \quad (6.56)$$
$$\left(0.448 \times 10^{-6}\right)\left(t_{ws}^2\right) + \left(5.056 \times 10^{-12}\right)\left(E_{ws}^2\right)$$
$$+\left(0.818 \times 10^{-9}\right)\left(t_{ws}\right)\left(E_{ws}\right)$$
For t_{ws} ≤ 30 mm

$$b = 0.152 - \left(3.749 \times 10^{-3}\right)\left(t_{ws}\right) + \left(6.301 \times 10^{-6}\right)\left(E_{ws}\right) \quad (6.57)$$
For t_{ws} ≤ 30 mm

For the case that t_b = 200 mm and σ_3 = 50 kPa, coefficients *a* and *b* can be written in the forms as

$$a = 0.050 - \left(20.020 \times 10^{-6}\right)\left(t_{ws}\right) + \left(9.071 \times 010^{-9}\right)\left(E_{ws}\right) \quad (6.58)$$
$$+\left(0.558 \times 10^{-6}\right)\left(t_{ws}^2\right) - \left(3.644 \times 10^{-12}\right)\left(E_{ws}^2\right)$$
$$-\left(0.838 \times 10^{-9}\right)\left(t_{ws}\right)\left(E_{ws}\right)$$
For t_{ws} ≤ 30 mm

$$b = 0.219 - \left(5.000 \times 10^{-3}\right)\left(t_{ws}\right) + \left(6.187 \times 10^{-6}\right)\left(E_{ws}\right) \quad (6.59)$$
For t_{ws} ≤ 30 mm

For the case that t_b = 100 mm and σ_3 = 100 kPa, coefficients *a* and *b* can be written in the forms as

$$a = 0.025 + \left(32.640 \times 10^{-6}\right)\left(t_{ws}\right) - \left(0.290 \times 010^{-6}\right)\left(E_{ws}\right) \quad (6.60)$$
$$-\left(1.028 \times 10^{-6}\right)\left(t_{ws}^2\right) + \left(44.060 \times 10^{-12}\right)\left(E_{ws}^2\right)$$
$$+\left(0.841 \times 10^{-9}\right)\left(t_{ws}\right)\left(E_{ws}\right)$$
For t_{ws} ≤ 30 mm

$$b = 0.294 - \left(4.982 \times 10^{-3}\right)\left(t_{ws}\right) + \left(6.325 \times 10^{-6}\right)\left(E_{ws}\right) \quad (6.61)$$
For t_{ws} ≤ 30 mm

For the case that t_b = 200 mm and σ_3 = 100 kPa, coefficients a and *b* can be written in the forms as

$$a = 0.025 - \left(15.590 \times 10^{-6}\right)\left(t_{ws}\right) + \left(30.820 \times 010^{-9}\right)\left(E_{ws}\right) + \left(0.450 \times 10^{-6}\right)\left(t_{ws}^2\right) - \left(0.319 \times 10^{-12}\right)\left(E_{ws}^2\right) - \left(0.871 \times 10^{-9}\right)\left(t_{ws}\right)\left(E_{ws}\right) \quad (6.62)$$

For $t_{ws} \leq 30$ mm

$$b = 0.344 - \left(4.998 \times 10^{-3}\right)\left(t_{ws}\right) + \left(6.148 \times 10^{-6}\right)\left(E_{ws}\right) \quad (6.63)$$

For $t_{ws} \leq 30$ mm

For the case that t_b = 100 mm and σ_3 = 200 kPa, coefficients *a* and *b* can be written in the forms as

$$a = 0.012 + \left(7.932 \times 10^{-6}\right)\left(t_{ws}\right) - \left(54.620 \times 010^{-9}\right)\left(E_{ws}\right) - \left(0.231 \times 10^{-6}\right)\left(t_{ws}^2\right) + \left(5.441 \times 10^{-12}\right)\left(E_{ws}^2\right) + \left(0.827 \times 10^{-9}\right)\left(t_{ws}\right)\left(E_{ws}\right) \quad (6.64)$$

For $t_{ws} \leq 30$ mm

$$b = 0.228 - \left(3.769 \times 10^{-3}\right)\left(t_{ws}\right) + \left(6.350 \times 10^{-6}\right)\left(E_{ws}\right) \quad (6.65)$$

For $t_{ws} \leq 30$ mm

For the case that t_b = 200 mm and σ_3 = 200 kPa, coefficients *a* and *b* can be written in the forms as

$$a = 0.012 - \left(5.097 \times 10^{-6}\right)\left(t_{ws}\right) + \left(57.310 \times 010^{-9}\right)\left(E_{ws}\right) + \left(0.323 \times 10^{-6}\right)\left(t_{ws}^2\right) - \left(1.535 \times 10^{-12}\right)\left(E_{ws}^2\right) - \left(2.528 \times 10^{-9}\right)\left(t_{ws}\right)\left(E_{ws}\right) \quad (6.66)$$

For $t_{ws} \leq 30$ mm

$$b = 0.261 - \left(3.752 \times 10^{-3}\right)\left(t_{ws}\right) + \left(6.299 \times 10^{-6}\right)\left(E_{ws}\right) \quad (6.67)$$

For $t_{ws} \leq 30$ mm

By considering Equations (6.56) - (6.67), we can see that coefficients *a* and *b* are written in polynomial form as

$$a = f_0^a + (f_1^a)(t_{ws}) + (f_2^a)(E_{ws}) + (f_3^a)(t_{ws}^2) + (f_4^a)(E_{ws}^2) + (f_5^a)(t_{ws})(E_{ws})$$

and

$$b = f_0^b + (f_1^b)(t_{ws}) + (f_2^b)(E_{ws})$$

Consequently, the regression analysis is employed and it is found that coefficient f_i can be expressed as a polynomial function which comprises of t_b and σ_3 as

$$f_0^a = 0.088 - (1.400 \times 10^{-6})(t_b) - (0.880 \times 10^{-3})(\sigma_3) + (2.509 \times 10^{-6})(\sigma_3^2) + (6.000 \times 10^{-9})(\sigma_3)(t_b) \quad (6.68)$$

$$f_1^a = -(45.180 \times 10^{-6}) + (1.264 \times 10^{-6})(\sigma_3) - (0.170 \times 10^{-6})(t_b) - (4.312 \times 10^{-6})(\sigma_3^2) - (0.276 \times 10^{-9})(\sigma_3)(t_b) \quad (6.69)$$

$$f_2^a = -(62.020 \times 10^{-9}) - (5.460 \times 10^{-9})(\sigma_3) + (1.712 \times 10^{-9})(t_b) + (22.770 \times 10^{-12})(\sigma_3^2) - (0.405 \times 10^{-12})(\sigma_3)(t_b) \quad (6.70)$$

$$f_3^a = (1.080 \times 10^{-6}) - (36.930 \times 10^{-9})(\sigma_3) + (5.720 \times 10^{-9})(t_b) + (0.128 \times 10^{-9})(\sigma_3^2) + (12.200 \times 10^{-12})(\sigma_3)(t_b) \quad (6.71)$$

$$f_4^a = (0.970 \times 10^{-9}) + (26.270 \times 10^{-12})(\sigma_3) - (8.335 \times 10^{-12})(t_b) - (55.100 \times 10^{-15})(\sigma_3^2) - (0.121 \times 10^{-12})(\sigma_3)(t_b) \quad (6.72)$$

$$f_5^a = -(1.322 \times 10^{-12}) + (0.868 \times 10^{-12})(\sigma_3) - (0.201 \times 10^{-12})(t_b) - (3.668 \times 10^{-15})(\sigma_3^2) + (0.217 \times 10^{-15})(\sigma_3)(t_b) \quad (6.73)$$

and

$$f_0^b = -0.175 + (6.409 \times 10^{-3})(\sigma_3) + (0.758 \times 10^{-3})(t_b) - (22.760 \times 10^{-6})(\sigma_3^2) - (2.187 \times 10^{-6})(\sigma_3)(t_b) \quad (6.74)$$

$$f_1^b = -(1.038 \times 10^{-3}) - (47.87 \times 10^{-6})(\sigma_3) - (12.670 \times 10^{-6})(t_b) + (0.164 \times 10^{-6})(\sigma_3^2) + (72.870 \times 10^{-9})(\sigma_3)(t_b) \quad (6.75)$$

$$f_2^b = (6.544 \times 10^{-6}) - (1.843 \times 10^{-9})(\sigma_3) - (1.750 \times 10^{-9})(t_b) + (6.333 \times 10^{-12})(\sigma_3^2) + (5.286 \times 10^{-12})(\sigma_3)(t_b) \quad (6.76)$$

Equations above reveal that P_d of pavement structure can be predicted using a function which is composed of *N*, t_{ws}, t_b , E_{ws} and σ_3 as the variables.

As explained above, the advanced analytical approach based on deformation concept using DSC was adopted in finite element analysis of the column-strip model to investigate the relationship between permanent deformation and engineering properties such as loading conditions, strength of materials and thickness of layer. The relations between all variables can be retrieved from Equations (6.35) - (6.76), which will be further investigated in the next section. The outcome relationships, i.e. relationships between t_{ws} and P_d, E_{ws} and P_d, t_b and P_d, σ_3 and P_d, can be used by engineers as the guidelines for design of flexible pavement having thin wearing surface layer.

6.7 Recommendation for design of flexible pavement having thin wearing surface layer

6.7.1 Relationship between thickness of wearing surface and permanent deformation

All analysis results, for both cases of pavements having CRB and HCTCRB as a base course material, indicate that P_d increased with higher t_{ws}. This was due to thin wearing surface only act as a covering of pavement structure.

Therefore both resilient and permanent deformations of structure were higher when the surcharge weight on the wearing surface increased.

6.7.2 Relationship between elastic modulus of wearing surface and permanent deformation

Although the thin wearing surface behaves as a covering of the pavement structure, its contribution to structural strength became more dominant when its strength such as elastic modulus increased. The FE analysis results reveal that all deformations (both R_d and P_d) reduced with an increase in elastic modulus of wearing surface. It can be explained that the wearing surface had more ability to carry the traffic load when its strength increased; and the load pressure distributed to underneath layers was consequently reduced. This led to lower deformations in the pavement structure.

6.7.3 Relationship between thickness of base layer and permanent deformation

The permanent deformation of pavement structure, either CRB or HCTCRB as a base course material, increased when the thickness of base layer was higher. The explanation of this phenomenon is that higher depth of base course layer led to more accumulated permanent deformation.

6.7.4 Relationship between confining stress in base layer and permanent deformation

Similar to the effect of the strength of wearing surface layer on permanent deformation, the permanent deformation of pavement structure decreased while the confining stress applied to the base layer increased.

6.7.5 Influence of material property on permanent deformation of pavement structure

6.7.5.1 Pavement structure using CRB as base course materials

By analysing all coefficients (f_0^a-f_5^a and f_0^b-f_2^b) in Equations (6.47) to (6.55), as illustrated in Figure 6.63 - Figure 6.64, it can be noticed that the magnitude

of permanent deformation (coefficient *a* in equation $P_d = aN^b$) greatly depends on the coefficients f_0^a and f_4^a which are mostly governed by the confining stress (σ_3) applied in the base layer, and the elastic modulus of asphalt concrete (E_{ws}), respectively. Coefficients f_0^a and f_4^a can be increased around 100% of the initial value as a result from the change of σ_3. Furthermore, the value of the term $(f_4^a)(E_{ws}^2)$ can be varied up to 5 times of f_0^a resulted from the change in E_{ws}.

The summation of the rest of the terms is relatively infinitesimal, its value is less than 10% of term f_0^a and $(f_4^a)(E_{ws}^2)$. Hence, the most influential factors on the value of "*a*" are σ_3 and E_{ws}.

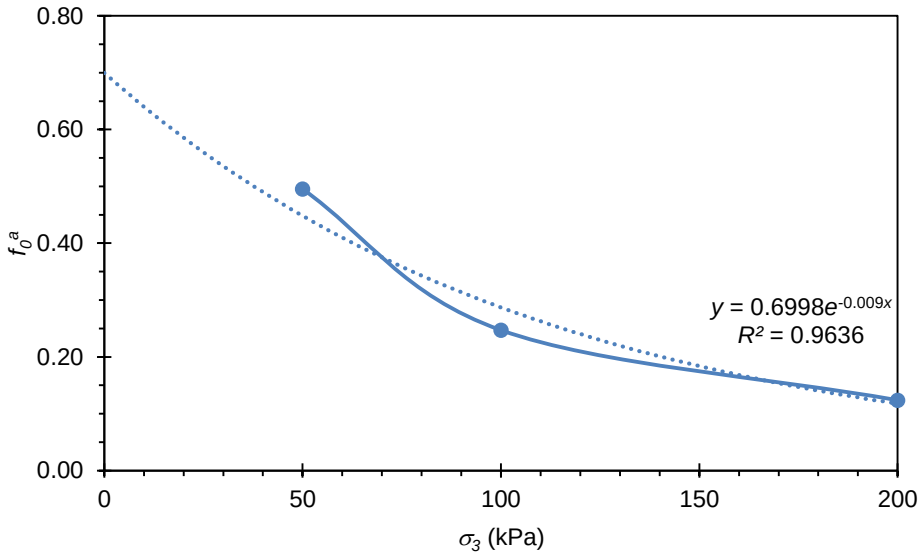

Figure 6.63 Value of coefficient f_0^a with CRB

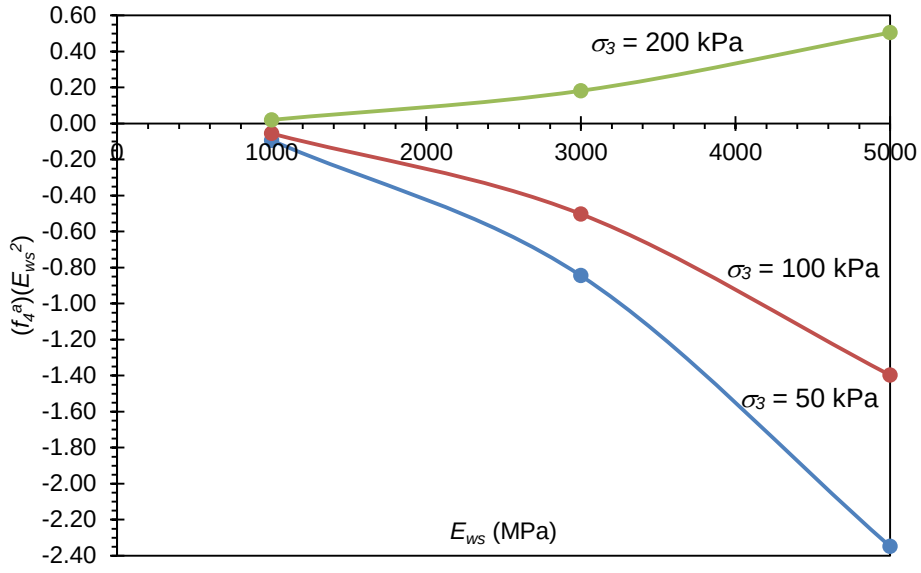

Figure 6.64 Value of the term $(f_4^a)(E_{ws}^2)$ with CRB

The shape of permanent deformation curve, which is governed by the coefficient "*b*" in equation $P_d = aN^b$, is mainly affected by coefficient f_0^b because the summation of the other terms, $(f_1^b)(t_{ws}) + (f_2^b)(E_{ws})$, is less than 30% of f_0^b. This means that σ_3 is the main factor affecting the value of *b* while t_b, t_{ws} and E_{ws} have a slight effect. It can be seen that coefficient f_0^b can be increased up to 14 time of its initial value resulted from the change in σ_3. Consequently, we can use σ_3 as the main variable for estimating the value of *b*, as seen in Figure 6.65.

According to the aforementioned explanation, the permanent deformation of a pavement structure can be computed using coefficients *a* and *b* which can be re-written as;

$$a = f_0^a + (f_4^a)(E_{ws}^2)$$

and

$$b = f_0^b$$

which

$$f_0^a = \left(699.823 \times 10^{-3}\right)(e)^{\left[\left(-8.911\times10^{-3}\right)\left(\sigma_3\right)\right]} \quad (6.77)$$

$$f_4^a = -\left(0.132 \times 10^{-6}\right) + \left(0.761 \times 10^{-9}\right)\left(\sigma_3\right) \quad (6.78)$$

$$f_0^b = \left(11.086 \times 10^{-3}\right)\left(\sigma_3\right)^{\left(723.555 \times 10^{-3}\right)} \quad (6.79)$$

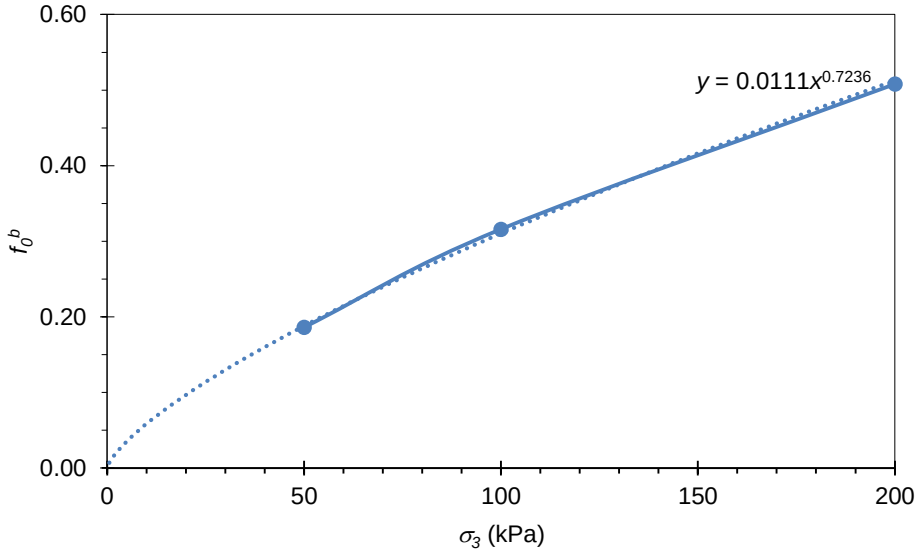

Figure 6.65 Value of coefficient f_0^b with CRB

6.7.5.2 Pavement structure using HCTCRB as base course materials

Based on Equations (6.68) to (6.76), the magnitude of the permanent deformation (coefficient "*a*" in equation $P_d = aN^b$) in HCTCRB pavements is mainly affected by the coefficients f_0^a, f_1^a and f_3^a. The values of both f_0^a and f_1^a are mostly occupied by the value of confining stress in base course layer (σ_3) while the value of f_3^a depended on the thickness of base layer (t_b), as shown in Figure 6.66 - Figure 6.68. Coefficient f_0^a can be increased around 100% of the initial value resulted from the change in σ_3. However, the coefficient f_1^a can be decreased around 3800 times of the initial value with an increase in σ_3. The most influential factor on value of f_3^a was the thickness of base layer (t_b) namely, f_3^a can be increased around 6800 times of its initial value resulted from the change in t_b. Furthermore, the value of term $(f_1^a)(t_{ws})$ and $(f_3^a)(t_{ws}^2)$ can be varied up to 970 times and 2930 times of f_0^a, respectively while the value of t_{ws} is changed. The contribution from the other terms is infinitesimal, i.e. less than 1% to that of the terms $(f_1^a)(t_{ws})$, $(f_3^a)(t_{ws}^2)$. Thus the most important factors affecting the value of "*a*" are σ_3, t_b and t_{ws}.

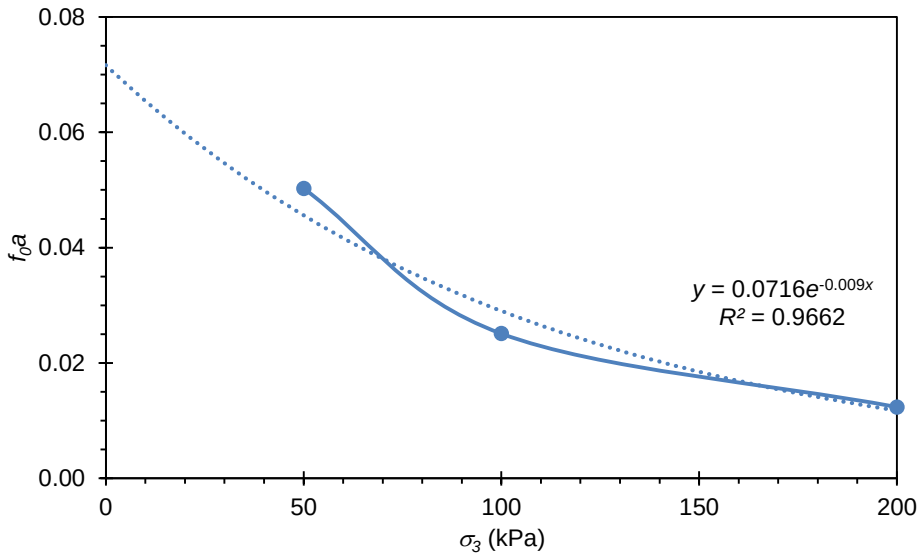

Figure 6.66 Value of coefficient f_0^a with HCTCRB

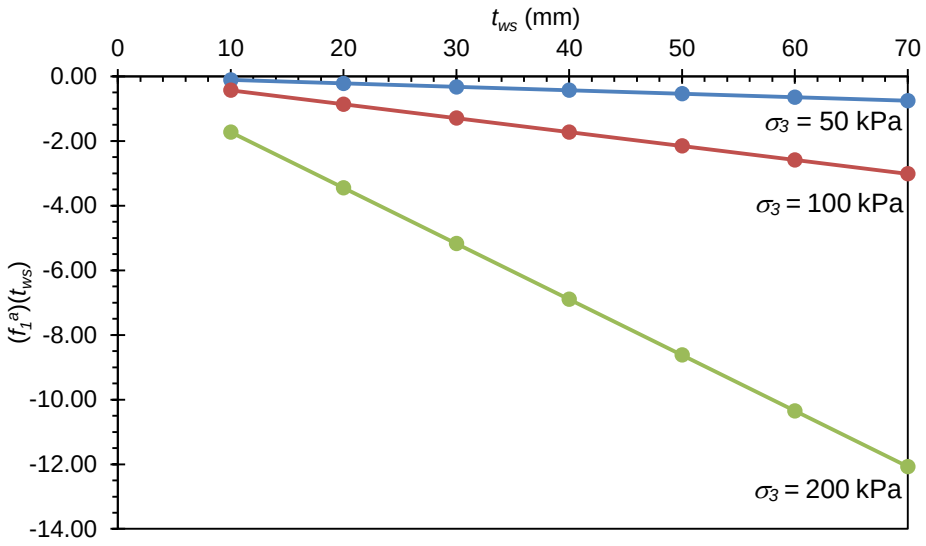

Figure 6.67 Value of the term $(f_1^a)(t_{ws})$ with HCTCRB

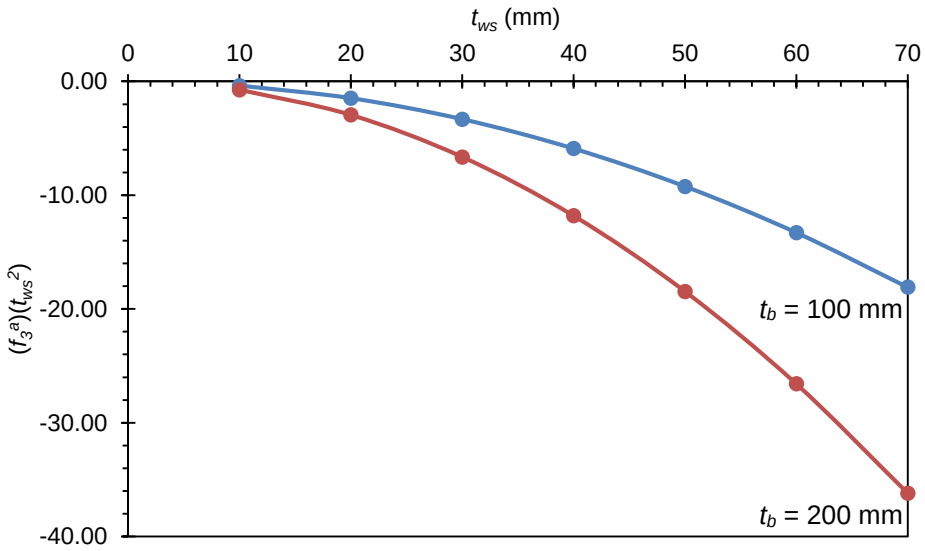

Figure 6.68 Value of the term $(f_3^a)(t_{ws}^2)$ with HCTCRB

The shape of the permanent deformation curve, i.e. coefficient *b* in equation $P_d = aN^b$, is governed by coefficient f_0^b and f_1^b. It was found that value of *b* was mostly occupied by σ_3, as seen in Figure 6.69 and Figure 6.70. Value of coefficient f_0^b can be decreased about half of its initial value with the change of σ_3. Nonetheless, the term $(f_1^b)(t_{ws})$ decreased in the overall value of the equation, i.e. around 1.5 times of f_0^b. Therefore it can imply that t_{ws} also significantly affected the value of "*b*". The term $(f_2^b)(E_{ws})$ can be neglected because its value was less than 20% of f_0^b. This indicated that E_{ws} had a slight effect on the value of *b*. Thus we can use σ_3 and t_{ws} as the main variables in estimating the value of "*b*".

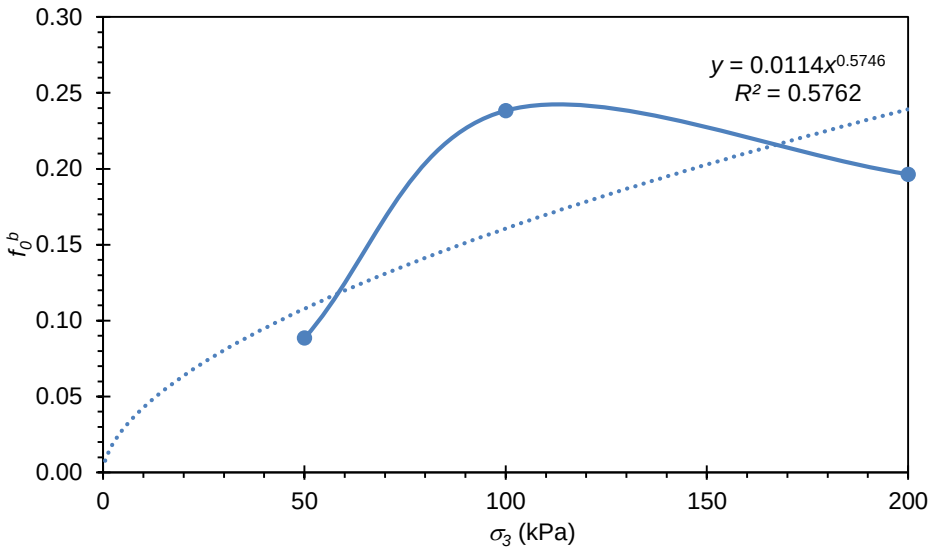

Figure 6.69 Value of coefficient f_0^b with HCTCRB

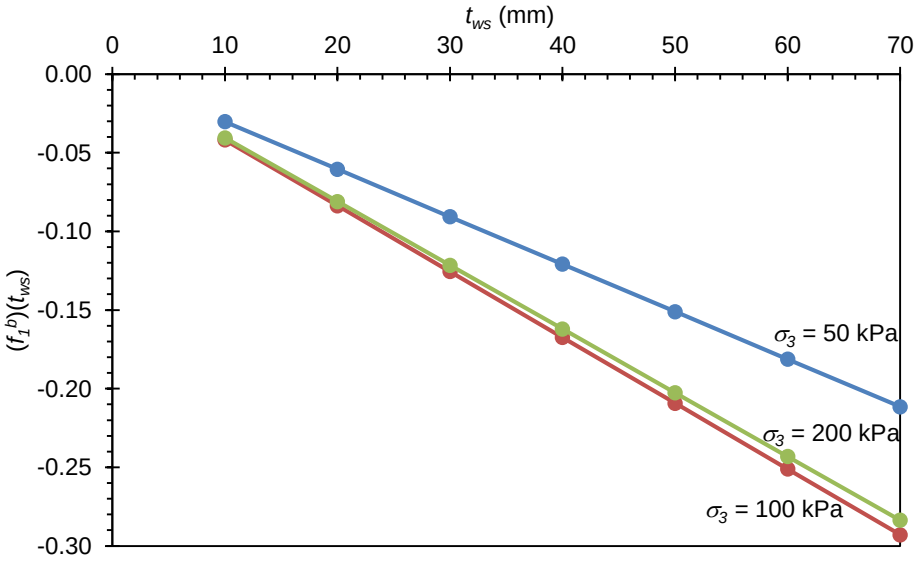

Figure 6.70 Value of the term $(f_1^b)(t_{ws})$ with HCTCRB

Eventually, the permanent deformation of the pavement structure, having HCTCRB as the base course, can be computed based on the coefficients "*a*" and "*b*" as re-written as;

$$a = f_0^a + (f_1^a)(t_{ws}) + (f_3^a)(t_{ws}^2)$$

and

$$b = f_0^b + (f_1^b)(t_{ws})$$

which

$$f_0^a = \left(71.626 \times 10^{-3}\right)(e)^{\left[\left(-9.028\times10^{-3}\right)\left(\sigma_3\right)\right]} \quad (6.80)$$

$$f_1^a = -\left(4.312 \times 10^{-6}\right)(\sigma_3^2) \quad (6.81)$$

$$f_3^a = \left(5.720 \times 10^{-9}\right)\left(t_b\right) \quad (6.82)$$

$$f_0^b = \left(11.392 \times 10^{-3}\right)\left(\sigma_3\right)^{\left(574.615\times10^{-3}\right)} \quad (6.83)$$

$$f_1^b = -\left(47.87 \times 10^{-6}\right)\left(\sigma_3\right) + \left(0.164 \times 10^{-6}\right)(\sigma_3^2) \quad (6.84)$$

The difference in the permanent deformation behavior between pavement having CRB and HCTCRB as a base course layer, can be distinguished by the strength of the base course materials. A normal base course material such as CRB (modulus less than 500 MPa), needs wearing surface layer to resist the wheel load thus the strength of wearing surface considerably affect the deformation. For pavement having a high standard material like HCTCRB as a base course material, HCTCRB was more capable to bear the wheel load. The contribution from the wearing surface became less dominant in comparison to that of CRB pavement.

6.8 Summary

This chapter presents a new approach for predicting the permanent deformation, which is a criterion for structural design of road pavement. The DSC is adopted to determine the deformation of base course materials.

Initially, the resilient and permanent deformation data of base course materials were evaluated through the Austroads standard test method. The deformations of 3D-finite element model of test specimen were also analysed. Then the disturbance function (*D*) was determined to eliminate the difference between experimental and finite element analysis results. Once obtained function *D*, the DSC formulae were used to compute deformation and resilient modulus of base course materials. Consequently, these deformation and modulus values were employed in finite element analysis of a newly proposed pavement model called “3D column-strip”.

The finite element analyses of 3D column-strip models under wheel pressure resulted in total deformation values over various configurations of pavement structures. The variation of pavement structures included thicknesses and elastic modulus values of asphalt wearing surface and base course materials as well as the confining pressure applied to pavements. Finally, constitutive model for predicting permanent deformation of pavement structures were formulated as expressed in Equations (6.77) - (6.84).

CHAPTER 7
CONCLUSIONS AND RECOMMENDATIONS

7.1 Conclusions

The work completed in this research covered mechanical property tests for CRB and HCTCRB, modelling of such materials' responses using the Disturbed State Concept (DSC), finite element analysis (FEA) of pavement models and RLT specimen, and a proposed 3D column strip for pavement analysis and design. The major findings resulting from this study are summarised below.

7.1.1 Materials characterisation

The first stage of this research emphasised on mechanical property tests of base course materials. The experimental results indicated that base course materials such as CRB and HCTCRB exhibited stress-dependent behaviour. The results from laboratory tests of base course materials can be summarised as follows:

- The angle of internal friction (ϕ) of CRB and HCTCRB were 44.4° and 41.9°, respectively, while the cohesion (c) of CRB and HCTCRB were 91.0 kPa and 145.7 kPa, respectively.

- The resilient moduli (M_r) varied around 100-300 MPa and 300-900 MPa for CRB and HCTCRB respectively.

- The maximum permanent deformations (P_d) were around 3.6 mm and 0.3 mm for CRB and HCTCRB respectively.

The second stage was an investigation on modelling of the behavioural responses to loadings of CRB and HCTCRB. The common used models for predicting M_r and P_d of base course materials, i.e. k-θ model and Sweere's model respectively, were consequently selected for this study. The results revealed that the effect of applied stress conditions cannot be taken into

account by the aforementioned models because they are based on a mechanistic-empirical approach, which can be explained as follows:

- The use of k-θ model in predicting the resilient moduli of both CRB and HCTCRB gave the results that were consistent with the experimental results but the realistic behaviour of the responses to loadings of materials cannot be exhibited. The reason is because k-θ model uses only bulk stress (θ = σ_1+σ_2+σ_3) as a variable, this means the effect of the applied stress condition such as the applied stress ratio $\left(\frac{\sigma_1}{\sigma_3}\right)$ is neglect. Thus there would be some considerable errors in terms of the resultant stresses and deformations when this model is employed.

- Sweere's model is widely used by pavement engineers in predicting the permanent deformations of base course specimens in RLT tests but an inaccuracy has been found obviously. Because this model uses only number of load repetition (N) as a variable thus a single curve is obtained. However, the realistic deformations of materials are influenced by the applied stresses, both σ_1 and σ_3, therefore Sweere's model would be considered as a rough prediction that represents only the trend of the permanent deformations of base course specimens.

In order to eliminate the limitations in using the models as stated above, DSC, which is based on the mechanistic approach, was selected to formulate the constitutive models of base course materials, i.e. the models for predicting stress-strain (σ-ε) relations, M_r and P_d. The advantage of DSC models has been explained in section 7.1.2.

7.1.2 Modelling of material responses using DSC

The third stage of this research is to identify the potential use of the disturbed state concept in the modelling of base course materials. DSC was considered as a unified and versatile concept and capable to capture the responses of base course materials to static and cyclic loading conditions. In this study, the DSC was used to formulate the model for predicting the elastic modulus (E),

resilient modulus, resilient deformation (R_d) and permanent deformation. The DSC models provided the promising results that mostly fitted with the experimental data because important factors, such as axial stress (σ_1), confining stress (σ_3), number of load repetition (N) etc., can be taken into account. The potential in using DSC models can be described as follows:

- The use of the DSC models in predicting the stress-strain relations of both CRB and HCTCRB gave the results that coincided with the experimental results. They can be used to construct the σ-ε curves of base course specimen resulted from both unconfined and confined triaxial tests because the ultimate stress (σ_{1u}) and σ_3 are the variables in the models. Moreover, these DSC models can be adopted by an advanced analytical approach for predicting E of base course materials in analysis procedure.

- The use of the DSC models for predicting the resilient moduli of both CRB and HCTCRB gave the results that were consistent with the experimental results. Moreover, the effect of the applied stress conditions $\left(\frac{\sigma_1}{\sigma_3}\right)$ on the behavioural responses of base course materials can be taken into account as a variable in these formulae. Because of this aspect of the models, the use of DSC models in predicting M_r of base course materials provided the results that was more realistic than the use of k-θ model, which is governed only bulk stress (θ). Similarly, these DSC models can be adopted by an advanced analytical approach for predicting M_r of base course materials in analysis procedure.

- The use of the DSC models for predicting the permanent deformation of base course specimens gave the results that were consistent with the experimental results. The DSC models provided the fitted curves which were better than that provided by Sweere's model because σ_1, σ_3 and N are the variables in formulae.

It was obviously found that the above outcome confirms the validities of the DSC models in providing the constitutive formulae for prediction of σ-ε

relations, M_r, and P_d which are the important engineering properties in analysis and design of road pavement. The advantage of DSC models is that the influential factors such as σ_1, σ_3, and N can be taken into account. Consequently, the use of DSC models in predicting the responses to loadings of base course materials can provide the results that are more realistic in the resultant stresses and deformations than the use of mechanistic-empirical models. In addition, these DSC models can be further employed to establish an advanced analytical approach for analysis of flexible pavement having thin wearing surface layer, as explained later in section 7.1.4.

7.1.3 Finite element analysis of 2D pavement structure and 3D RLT specimen

The fourth stage of the study aims to determine the stresses occur in the pavement structure and the specimen in RLT tests. ABAQUS program was used for finite element analysis of 2D pavement models and 3D RLT specimens. The analysis results revealed that overall behaviour of pavement structure was mostly governed by the properties of base course layer while the others layer contributed a small effect. The responses of base course materials resulted from these two types of models were also compared.

The results from finite element analysis of RLT specimens and pavement structure models, can be summarised as follows:

- The maximum principal stress occurred at bottom fibre of RLT specimen, these values were higher than the applied stresses (σ_1 and σ_3).

- Tensile stresses were generated in the RLT test specimen when the stress ratio $\left(\frac{\sigma_1}{\sigma_3}\right)$ was higher than 12.5.

- Due to a linear elastic assumption was adopted in analysis, the resultant stresses were therefore distributed linearly. Although the resultant stresses depended on structural configuration and material properties, it can be observed that the horizontal stress (σ_{xx}) and the vertical stress (σ_{yy}) in the base

course layer of pavement varied around 0-450 kPa and 250-600 kPa, respectively.

- The horizontal stress at the bottom fibre of the wearing surface layer was adopted as the criterion in classifying the behaviour of road pavement namely if the horizontal tensile stress is vanished, structural system of road pavement then behaves as a pavement structure having thin wearing surface layer. According to the results in this study, the thicknesses of asphalt wearing surface which the horizontal stresses at its bottom fibre did not undergo in tension (t_{wsn}) varied from 10-70 mm. The exact value of t_{wsn} can be calculated by using the proposed formula which depended on strength and thickness of materials in pavement structure especially in the base course material layer.

- Some stress stages, specified in the RLT test protocol (Voung and Brimble 2000; Austroads 2007), caused the induced stress in RLT test samples to be higher than the failure envelope of the material. Therefore, proper applied stresses and stress stages for conducting the RLT test were proposed for CRB and HCTCRB. Also, the applied stresses in the RLT test have been modified to correctly represent the stress conditions in pavement structure.

The results in this stage discovered that the stresses in base layer were varied along its depth and the deformations in structural system of road pavement having thin wearing surface layer mostly occupy by the deformation of base layer therefore M_r test of base course materials should be conducted using the suitable applied stresses that can represent the actual stresses in base layer of pavement structure. The use of the appropriate M_r in finite element analysis will eventually result in the realistic resultant stresses and deformations of pavement structure.

7.1.4 The advanced analytical approach for pavement structure

The last stage is to establish an advanced analytical approach for pavement structure having thin wearing surface layer. The Disturbed State Concept was adopted to form an analytical approach in which the resilient modulus and the permanent deformation can be taken into account in the calculation. In

General, the major purpose of structural analysis is to find the maximum stresses, the maximum deformations and their locations. According to the results from finite element analysis in the previous section, they revealed that the maximum stresses and the maximum deformations occurred underneath a wheel path therefore the column strip under a wheel was selected to analysis using 3D model. Consequently, the advantages of this approach are its simplicity and having less degree of freedom leads to less time of calculation. This is because that it is not necessary to perform FEA of whole structural section, only the 3D column-strip model is analysed.

As the proposed advanced analytical approach needed the value of resilient modulus (M_r) in the calculation, the deformation concept was therefore introduced for predicting the resilient and the permanent deformations (δ_r and δ_d) of base course materials. These deformations, both δ_r and δ_d, are required in finite element analysis for predicting M_r of base course materials in every loop of calculation. Initially, resilient deformation (δ_r^a) and permanent deformation (δ_d^a) of base course specimens were obtained from the Austroads standard test and finite element analyses of base course specimens were then performed. The assumption of this concept is that the maximum deformation of base course specimen which were obtained from FEA (δ_t) comprised of both the resilient and the permanent deformation parts ($\delta_t = \delta_r^e + \delta_d^a$) therefore $\delta_r^e = \delta_t - \delta_d^a$. Commonly, $\delta_r^e \neq \delta_r^a$ thus the disturbance function (D) was derived to eliminate the differences of deformation values resulted from the tests and finite element analyses. After the DSC models for predicting δ_r was formulated, it was employed further for predicting M_r ($M_r = \frac{\delta_d}{\varepsilon_r}$) used in FEA. Then, the given DSC model was adopted in finite element analysis of the proposed pavement structure, i.e. column strip under a wheel load. The 3D column-strip model was composed of 4 layers namely wearing surface, base, subbase and subgrade layers in which the properties of wearing surface and base layers were varied while the properties of the other layers were fixed. In analysis, thickness, modulus and confining stress of both wearing surface and base layer were varied and the confining stresses applied around each layer

were uniformly distributed. The maximum wheel loading of 20 kN (750 kPa of applied stress) was used in analysis and after all finite element analyses of 3D column-strip models were done, the constitutive models for predicting the maximum permanent deformation were then formulated. Finally, permanent deformation of pavement structure having thin asphalt surface can be predicted by the DSC equations which included the main factors such as t_{ws}, E_{ws}, t_b and σ_3.

After the aforementioned DSC equations were obtained, the influence of each factor on the deformation of pavement structure were then investigated and it was found that for normal standard base course material (modulus is lower than 500 MPa) such as CRB, the most influential factors on permanent deformation of pavement structure E_{ws} and σ_3. The contribution from the other factors to δ_d was less than 15%. However, for high standard base course such as HCRTRB, permanent deformation of pavement structure was mainly affected by t_{ws}, t_b and σ_3.

Consequently, it can be concluded that the resultant stresses and deformations provided by the proposed advanced analytical approach are more realistic than that provided by the mechanistic-empirical approach and it is also required lower computational effort. The great advantage of this approach is that the procedure for analysis and design of flexible pavement having thin wearing surface layer will consume less time because the permanent deformation, which is a major criterion in serviceability of road, can be predicted directly using the DSC equations.

7.2 Recommendations for future research

The use of the proposed advanced analytical model based on DSC can provide the results that are more realistic in the resultant stresses and deformations than the use of mechanistic-empirical model, however, some factors can be investigated further for improvement in the advantage of this approach, namely

1. The effect of cement content and moisture content on the strength of base course materials should be investigated.
2. The DSC modelling in this study was with the assumption that the relative intact (RI) phase was either fully plastic or linear elastic, therefore the use of nonlinear RI should be further investigated.
3. All structural analyses in this study were done based on linear elastic assumption namely elastic moduli were used for wearing surface, subbase and subgrade layers, and resilient modulus was used for base layer. Further research should carried out with nonlinear elastic, elasto-plastic, etc. for structural analysis of pavements.
4. The proposed deformation concept using DSC for analysis of pavement structure can provide reasonable results and can be applied for predicting the permanent deformation of pavement structure. However, other analytical models such as beam-columns, beam-columns on elastic foundation, discrete element model, can also be modelled for pavement structure and are recommended for base course materials which are normally a granular matter such as CRB and HCTCRB.

REFERENCES

AASHTO. 1993a. *Aashto Guide for Design of Pavement Structures (4th Edition)*. Washington, D.C.: American Association of State Highway and Transportation Officials (AASHTO).

———. 1993b. *Guide for Design of Pavement Structures*, *Guide for Design of Pavement Structures, 1993*. Washington, D.C.: Washington, D.C. : The Association.

———, ed. 2008. *Mechanistic-Emprical Pavement Design Guide:Manual of Practice*. Edited by Interim Edition: AASHTO: American Association of State Highway and Transportation Officials.

Abaza, Osama. 2007. "Simplified M-E Approach for the Design of Flexible Pavement Structures." *An-Najah University Journal for Research (N. Sc.)* 21: 22.

Abo-Hashema, Mostafa A., and Essam A. Sharaf. 2009. "Development of Maintenance Decision Model for Flexible Pavements." *International Journal of Pavement Engineering* 10 (3): 173 - 187. http://www.informaworld.com/10.1080/10298430802169457.

Adamson, Louise. 2011. "Structural Design of Pavements " GEOTECHNICAL AND GEOENVIRONMENTAL ENGINEERINGLecture. Department of Civil Engineering. University of Western Australia. Perth.

Akhaveissy, A.H., C.S. Desai, S.A. Sadrnejad, and H. Shakib. 2009. "Implementation and Comparison of a Generalized Plasticity and Disturbed State Concept for the Load-Deformation Behavior of Foundations." *International Journal of Science and Technology* 16 (3): 10. http://www.scientiairanica.com/issues/0088/2009/v16/n3.aspx.

Allou, Fatima, Cyrille Chazallon, and Pierre Hornych. 2007. "A Numerical Model for Flexible Pavements Rut Depth Evolution with Time." *International Journal for Numerical and Analytical Methods in Geomechanics* 31 (1): 1-22. http://dx.doi.org/10.1002/nag.521.

American Society for Testing and Materials. 2007. *Standard Test Method for Cbr (California Bearing Ratio) of Laboratory-Compacted Soils*. ASTM International www.astm.org/Standards/D1883.htm.

———. 2009. *Standard Test Method for Crb (California Bearing Ratio) of Soils in Place*. ASTM International www.astm.org/Standards/D4429.htm.

Australian Standard. 1997. Portland and Blended Cements. Accessed September, http://www.saiglobal.com.

Australian Standards. 1997. "Portland and Blended Cements." SAI Global.

Austroads. 2004. *Pavement Design-a Guide to the Structural Design of Road Pavements*. 3 vols. Vol. Second revision 2004: Austroad Inc.2004.

———. 2007. *Determination of Permanent Deformation and Resilient Modulus Characteristics of Unbound Granular Materials under Drained Conditions*.AUSTROADS

http://www.austroads.com.au/images/stories/T053_Repeated_Load_Triaxial.pdf.

———. 2008. *Guide to Pavement Technology*, *Part 2 : Pavement Structural Design*. Sydney, Australia: Austroads Incorporated.

———. 2010. *Guide to Pavement Technology*, *Part 2 : Pavement Structural Design*. Sydney, Australia: Austroads Incorporated.

Belay, Abraham, Eugene Obrien, and Dirk Kroese. 2008. "Truck Fleet Model for Design and Assessment of Flexible Pavements." *Journal of Sound and Vibration* 311 (3-5): 1161-1174. http://www.sciencedirect.com/science/article/B6WM3-4R70RCK-3/2/41b54aba8c3c41ada7ac8bce2c38661d.

Boresi, Arthur Peter, and Richard Joseph Schmidt. 2003. *Advanced Mechanics of Materials*. 6 ed. New York, USA: John Wiley & Sons, Inc.

Chandrupatla, Tirupathi R., and Ashok D. Belegundu. 2002. *Introduction to Finite Elements in Engineering*. 3rd ed. Upper Saddle River, New Jersey 07458: Prentice-Hall, Inc.

Cho, Yoon-Ho, B. McCullough, and José Weissmann. 1996. "Considerations on Finite-Element Method Application in Pavement Structural Analysis." *Transportation Research Record: Journal of the Transportation Research Board* 1539 (1996): 6. doi: 10.3141/1539-13.

Cockburn cement. 2006. General Specification (Cockburn General Purpose Portland Cement-Type Gp). Accessed November, http://www.cockburncement.com.au/.

———. 2007. General Specification (Cockburn General Purpose Portland Cement - Type Gp). 21st February 2008 Accessed 1st September http://www.cockburncement.com.au/.

Collins, I., and M. Boulbibane. 1998. "The Application of Shakedown Theory to Pavement Design." *Metals and Materials International* 4 (4): 832-837. http://dx.doi.org/10.1007/BF03026408.

Collins, I. F., A. P. Wang, and L. R. Saunders. 1993. "Shakedown Theory and the Design of Unbound Pavements." *Road & Transport Research* 2 (4): 12. http://worldcat.org/oclc/26087078

Dassault Systèmes Simulia Corporation. 2010. *Abaqus* Finite Element Analysis.

Desai, Chandra S., and Joseph Y. Chen. 2006. "Parameter Optimization and Sensitivity Analysis for Disturbed State Constitutive Model." *International Journal of Geomechanics* 6 (2): 75-88. http://link.aip.org/link/?QGM/6/75/1 http://dx.doi.org/10.1061/(ASCE)1532-3641(2006)6:2(75).

Desai, Chandra S., and Russell Whitenack. 2001. "Review of Models and the Disturbed State Concept for Thermomechanical Analysis in Electronic Packaging." *Journal of Electronic Packaging* 123 (1): 19-33. http://dx.doi.org/10.1115/1.1324675.

Desai, Chandrakant S. 2001. *Mechanics of Materials and Interfaces : The Disturbed State Concept*. 1st ed. Washington, D.C.: CSC Press.

———. 2007. "Unified Dsc Constitutive Model for Pavement Materials with Numerical Implementation." *International Journal of Geomechanics* 7 (2): 83-101. http://link.aip.org/link/?QGM/7/83/1 http://dx.doi.org/10.1061/(ASCE)1532-3641(2007)7:2(83).

FRÝBA, LADISLAV. 1995. "History of Winkler Foundation." *Vehicle System Dynamics: International Journal of Vehicle Mechanics and Mobility* 24 (sup 1): 6. http://www.informaworld.com/10.1080/00423119508969611.

Habiballah, Taha, and Cyrille Chazallon. 2005. "An Elastoplastic Model Based on the Shakedown Concept for Flexible Pavements Unbound Granular Materials." *International Journal for Numerical and Analytical Methods in Geomechanics* 29 (6): 577-596. http://dx.doi.org/10.1002/nag.426.

Hadi, Muhammad Najib S., and Beatrice Chandrani Bodhinayake. 2003. "Non-Linear Finite Element Analysis of Flexible Pavements." *Advances in Engineering Software* 34 (11-12): 6. http://www.sciencedirect.com/science/article/B6V1P-49JPPRM-9/2/49114942c170451f23de70003ec09ed6.

Hefer, Arno, and Tom Scullion. 2005. *Materials, Specifications, and Construction Techniques for Heavy-Duty Flexible Bases: Literature Review and Status Report on Experimental Sections* Texas, U.S.A.: Texas Department of Transportation Research and Technology Implementation Office. http://tti.tamu.edu/documents/0-4358-1.pdf.

Hetenyi, M. 1979. *Beams on Elastic Foundation*. Vol. XVI, *Theory with Applications in the Fields of Civil and Mechanical Engineering*. USA: The University of Michigan Press.

Huang, Y.H. 1993. *Pavement Analysis and Design*. N.J.,: Prentice-Hall, Englewood Cliffs,.

Hurrman, Rien M., L.T. Mo, M.F. Woldekidan, and T.O. Medani. 2007. Advanced Pavement Analysis Techniques *The 9th Conference on Asphalt Pavements for Southern Africa*, *Gaborone, Botswana,*2007. Gaborone, Botswana

Jitsangiam, Peerapong, and Hamid Nikraz. 2009. Characterization of Cement Treated Crushed Rock for Western Australia Roads *The 6th Regional Symposium on Infrastructure Development in Civil Engineering (RSID 6)*, *Bangkok, Thailand,*2009. Bangkok, Thailand

Kim, M., E. Tutumluer, and J. Kwon. 2009. "Nonlinear Pavement Foundation Modeling for Three-Dimensional Finite-Element Analysis of Flexible Pavements." *International Journal of Geomechanics* 9 (5): 14. doi: doi:10.1061/(ASCE)1532-3641(2009)9:5(195).

Kim, Y. Richard. 2009. *Modelling of Asphalt Concrete*. 1st ed. New York: McGraw-Hill.

Konrad, J. -M., and PH. D. Nguyen. 2006. "Implementation of the Tangent Modulus - Vertical Stress (E_t - Σ_v) Model for Flexible Pavements Analysis " *Canadian Geotechnical Journal* 43: 13. doi: 10.1139/T06-060.

Kuo, Chen-Ming, and Fang-Ju Chou. 2004. "Development of 3-D Finite Element Model for Flexible Pavements." *Journal of the Chinese Institute of Engineers* 27 (5): 11.

Lacey, Geraint, Guillermo Thenoux, and Fernando Rodríguez-Roa. 2008. "Three-Dimensional Finite Element Model for Flexible Pavement Analyses Based on Field Modulus Measurements." *The Arabian Journal for Science and Engineering* 33 (1B): 12.

Lamb, T W., and R W Whitman. 1979. *Soil Mechanics, Si Version*: John Wiley & Sons.

Lekarp, F., and A. Dawson. 1998. "Modelling Permanent Deformation Behaviour of Unbound Granular Materials." *Construction and Building Materials* 12 (1): 9-18. doi: Doi: 10.1016/s0950-0618(97)00078-0.

Luo, Zairen, Eddie Y. Chou, and Jianxiong Yu. 2006. Calibration of Fatigue Cracking Model of Flexible Pavements Using Mechanistic-Empirical Based Probabilistic Method *Atlanta, Georgia, USA*: ASCE. http://link.aip.org/link/?ASC/191/5/1.

Main Roads Western Australia. 1997. Dry Density/Moisture Content Relationship: Modified Compaction Fine and Medium Grained Soils. Accessed December, http://www.mainroads.wa.gov.au/.

———. 2003a. Crushed Rock Base Basecourse. Accessed December, http://www.mainroads.wa.gov.au/.

———. 2003b. *Specification for Hydrated Cement Treated Crushed Rock Base*. Main Roads Western Australia.

———. 2007. "Dry Density/Moisture Content Relationship: Modified Compaction Fine and Medium Grained Soils." In *Test Method WA133.1*.

———. 2010. "Pavements." Perth: Main Roads Western Australia.

———. 2012. Standards & Technical. Main Roads Western Australia. Accessed 3rd January, http://standards.mainroads.wa.gov.au/NR/mrwa/frames/standards.

Mincad Systems. 2012. *Circly 5 User Manual* [User Manual]. Melbourne: Mincad Systems Pty. Ltd.

Park, Dong-Yeob, Neeraj Buch, and Young-Chan Suh. 2001. "Development of Fatigue Cracking Prediction Model for Flexible Pavements." *KSCE Journal of Civil Engineering* 5 (4): 397-402. http://dx.doi.org/10.1007/BF02829113.

SAMARIS. 2004. *Selection and Evaluation of Models for Prediction of Permanent Deformations of Unbound Granular Materials in Road Pavement*.

Sane, S. M., C. S. Desai, J. W. Jenson, D. N. Contractor, A. E. Carlson, and P. U. Clark. 2008. "Disturbed State Constitutive Modeling of Two Pleistocene Tills." *Quaternary Science Reviews* 27 (3-4): 267-283. http://www.sciencedirect.com/science/article/B6VBC-4R8KTBK-1/2/1686382277b24259e698fa77572af55b.

Seed, H.B., C.K. Chan, and C.E. Lee. 1962. Resilience Characteristics of Subgrade Soils and Their Relation to Fatigue Failures in Asphalt Pavements *International Conference on the Structural Design of Asphalt Pavements*, *Ann Arbor, Michigan, USA,*

Siripun, Komsun. 2010. "Characterisations of Base Course Materials in Western Australia Pavements." Department of Civil Engineering , Faculty of Engineering and Computing, Curtin University of Technology, Perth. http://espace.library.curtin.edu.au/R?func=dbin_jump_full&object_id=147744&local_base=gen01-era02.

Siripun, Komsun, Peerapong Jitsangiam, and Hamid Reza Nikraz. 2009. "Characterization Analysis and Design of Hydrated Cement Treated Crushed Rock Base as a Road Base Material in Western Australia." *International Journal of Pavement Research and Technology* 2 (6): 7.

Theyse, H. L., M. De Beer, and F.C. Rust. 1996. "Overview of South African Mechanistic Pavement Design Method." *Transportation Research Record* (1539).

Timoshenko, Stephen P. 1940a. *Strength of Materials*. Second ed. 2 vols. Vol. 1, *Elementary Theory and Problems*. New York, United State of America: D. Van Nostrand Company, Inc.

———. 1940b. *Strength of Materials*. Second ed. 2 vols. Vol. 2, *Advanced Theory and Problems*. New York, United State of America: D. Van Nostrand Company, Inc.

Timoshenko, Stephen P., and S. Woinowsky-Krieger. 1959. *Theory of Plates and Shells*. Second ed. Singapore: McGraw-Hill, Inc.

Uzan, J. 1985. *Characterization of Granular Material*. Washington DC.

Velasquez, Raul, Mihai Marasteanu, Timothy R. Clyne, and Benjamin Worel. 2008. "Improved Model to Predict Flexible Pavment Temperature Profile." In *the Third International Conference on Accelerated Pavement Testing*, *Madrid, Spain*.

Ventsel, Eduard, and Theodor Krauthammer. 2001. *Thin Plates and Shells*, *Theory, Analysis and Applications*. New York, United State of America: Marcel Dekker, Inc.

Vermeer, P. A. 1982. "A Five-Constant Model Unifying Well-Established Concepts." In *International Workshop on Constitutive Relations for Soils*. Grenoble, France.

Voung, B.T, and R Brimble. 2000. "Austroads Repeated Load Triaxial Test Method-Determination of Permanent Deformation and Resilient Modulus Characteristics of Unbound Granular Materials under Drained Conditions." In *Aprg Document Aprg 00/33(Ma)*. Austroads.

Werkmeister, S., A. R. Dawson, and F. Wellner. 2004. "Pavement Design Model for Unbound Granular Materials." *Journal of Transportation Engineering* 130 (5): 665-674. http://link.aip.org/link/?QTE/130/665/1 http://dx.doi.org/10.1061/(ASCE)0733-947X(2004)130:5(665).

Werkmeister, Sabine, Andrew R. Dawson, and Frohmut Wellner. 2005. "Permanent Deformation Behaviour of Granular Materials." *Road Materials and Pavement Design* 6 (1): 31-51. doi: 10.1080/14680629.2005.9689998.

Wolff, H., and A. T. Visser. 1994. *Instn. Civil Engineers Transp. Journal* null (null): 259.

Wong, S. K., A. Kapoor, and J. A. Williams. 1997. "Shakedown Limits on Coated and Engineered Surfaces." *Wear* 203–204 (0): 162-170. doi: http://dx.doi.org/10.1016/S0043-1648(96)07388-7.

Xin, Xian Zuo, R. Park, H. Tanaka, University of Canterbury. Dept. of Civil Engineering., and Earthquake and War Damage Commission (New Zealand). 1992. "Behaviour of Reinforced Concrete Interior Beam-Column Joints Designed Using High Strength Concrete and Steel." Thesis (M S), University of Canterbury, Dept. of Civil Engineering, University of Canterbury, 1992., Christchurch, N.Z.

Youdale, G. 2009. Australian Pavement Research - the Last 20 Years. 6 August 2009 http://www.austStab.com.au/pdf/tp02.pdf.

Youdale, Geoff. 1996. Australian Pavement Research - the Last 20 Years. Accessed 3rd November, http://www.austStab.com.au/pdf/tp02.pdf.

Zarka, J., and J. Casier. 1979. "Elastic-Plastic Response of a Structure to Cyclic Loading: Practical Rules " *Mechanics today* 6: 106.

Every reasonable effort has been made to acknowledge the owners of copyright material. I would be pleased to hear from any copyright owner who has been omitted or incorrectly acknowledged.

APPENDIXES

Appendix A

Examples for parametric study of pavement structures

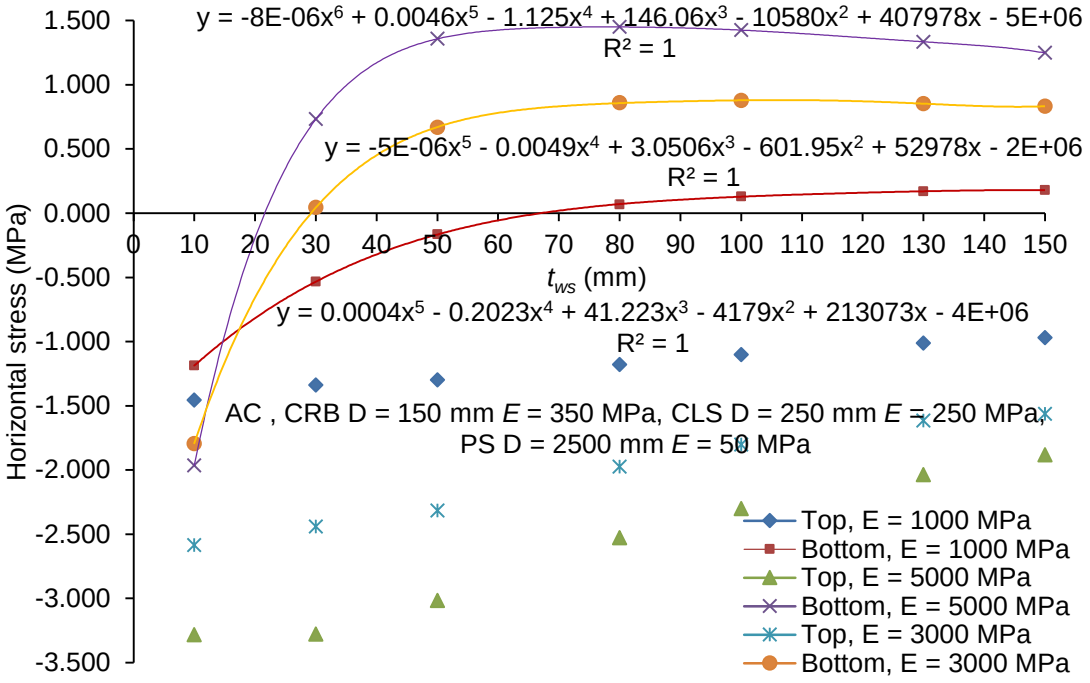

Figure A.1 The effect of strength and thickness of wearing surface layer on horizontal stress in wearing surface layer under a wheel path

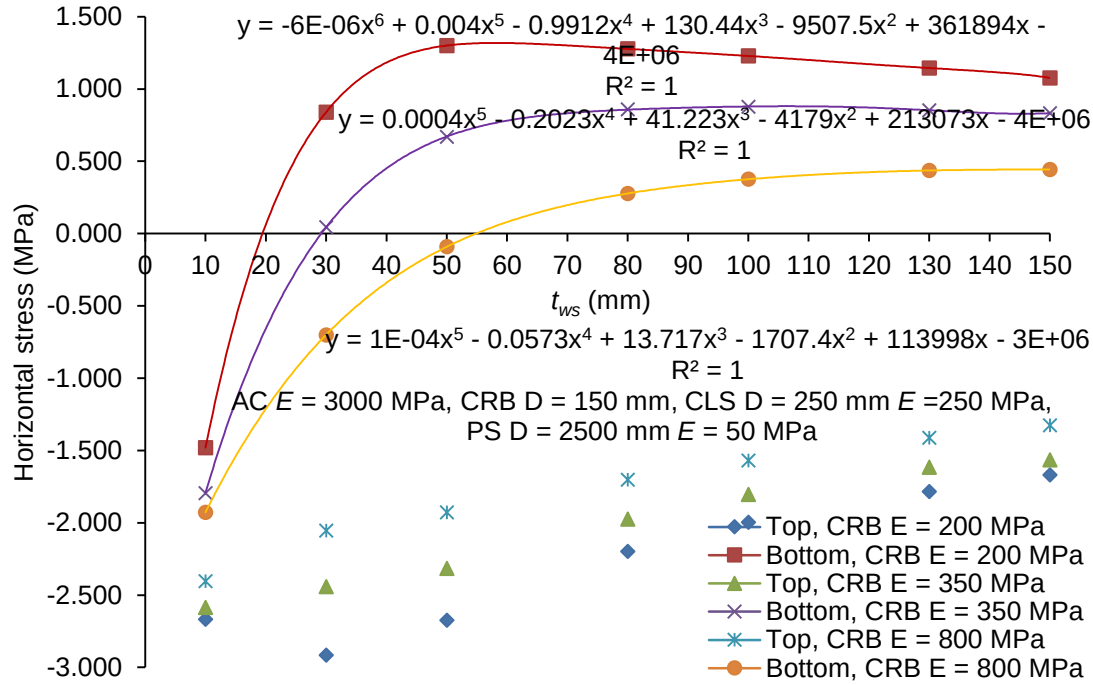

Figure A.2 The effect of strength of base layer and thickness of wearing surface layer on horizontal stress in wearing surface layer under a wheel path

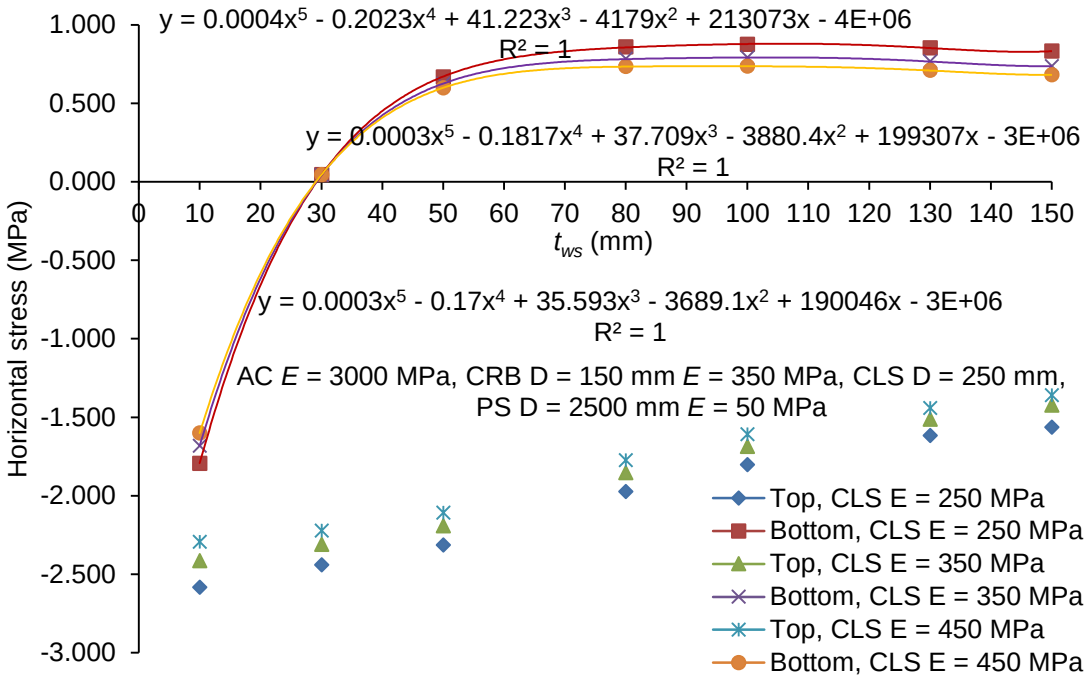

Figure A.3 The effect of strength of subbase layer and thickness of wearing surface layer on horizontal stress in wearing surface under a wheel path

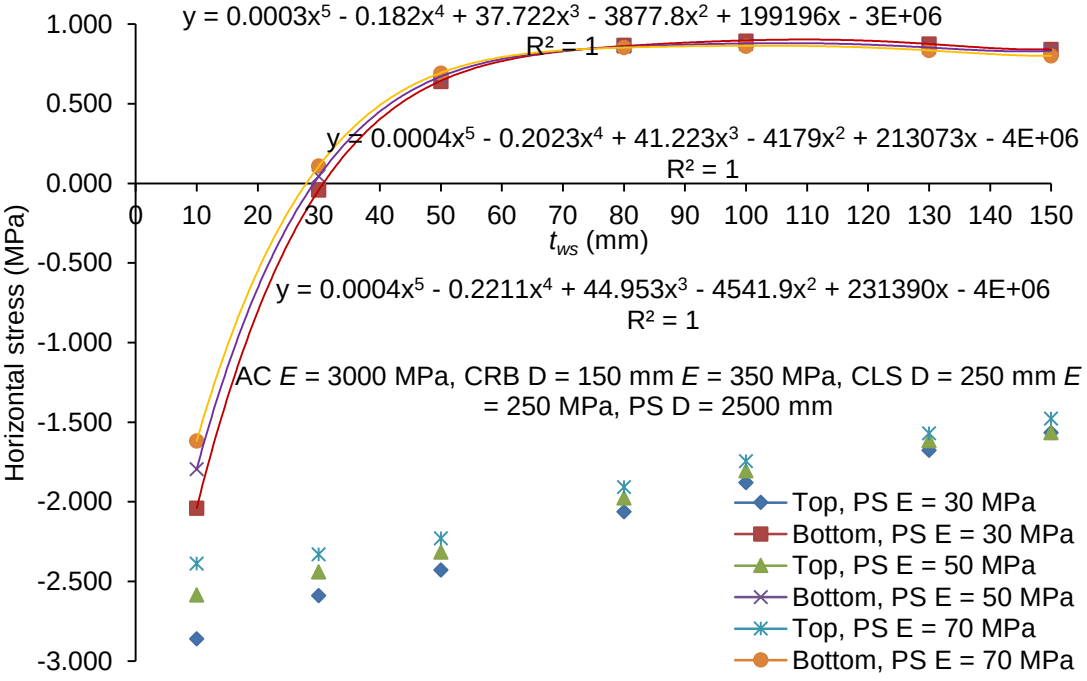

Figure A.4 The effect of strength of subgrade layer and thickness of wearing surface layer on horizontal stress in wearing surface layer under a wheel path

Appendix B

Examples for parametric study of the results from static triaxial tests

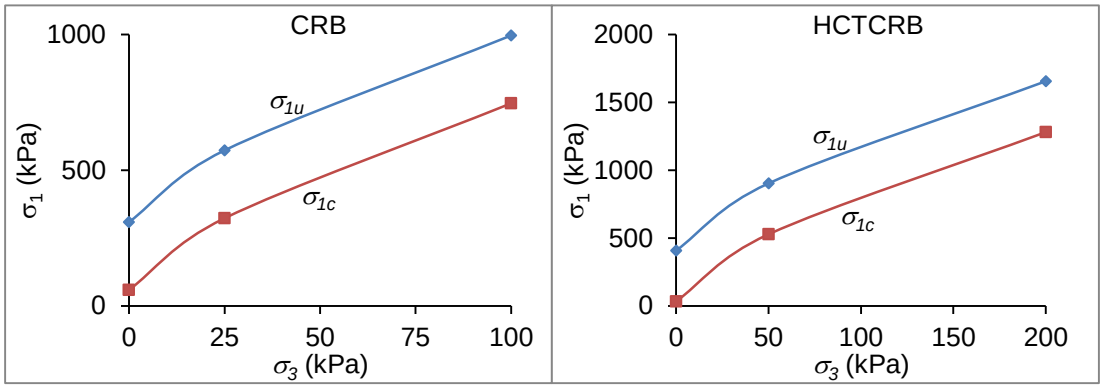

(a) (b)

Figure B.5 Trends of the ultimate stress and the fully adjusted state stress of (a) CRB and (b) HCTCRB

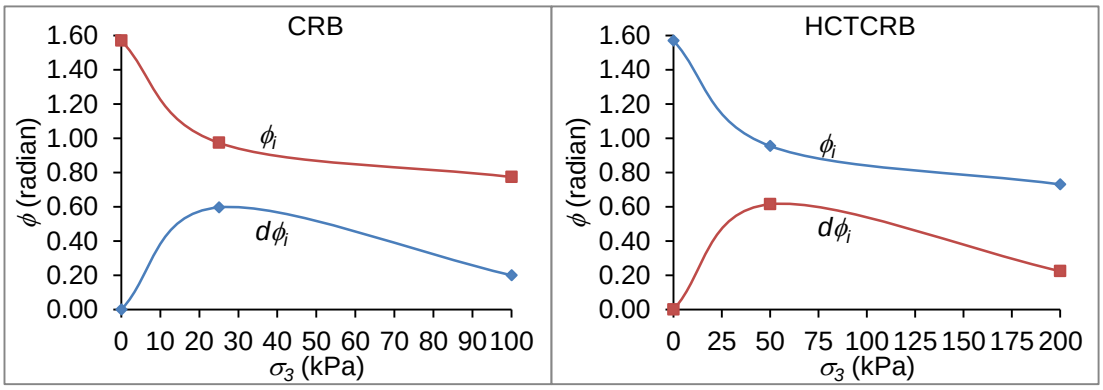

(a) (b)

Figure B.6 Trends of the friction angle and its differentiation corresponding to the confining stress of (a) CRB and (b) HCTCRB

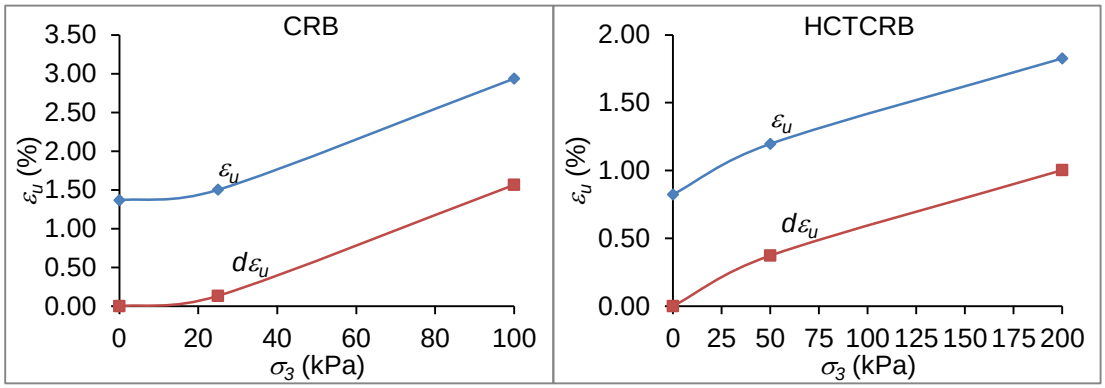

(a) (b)

Figure B.7 Trends of the strain at ultimate stress and the strain at rupture stress of (a) CRB and (b) HCTCRB

Appendix C

Examples of stress distribution in base layer

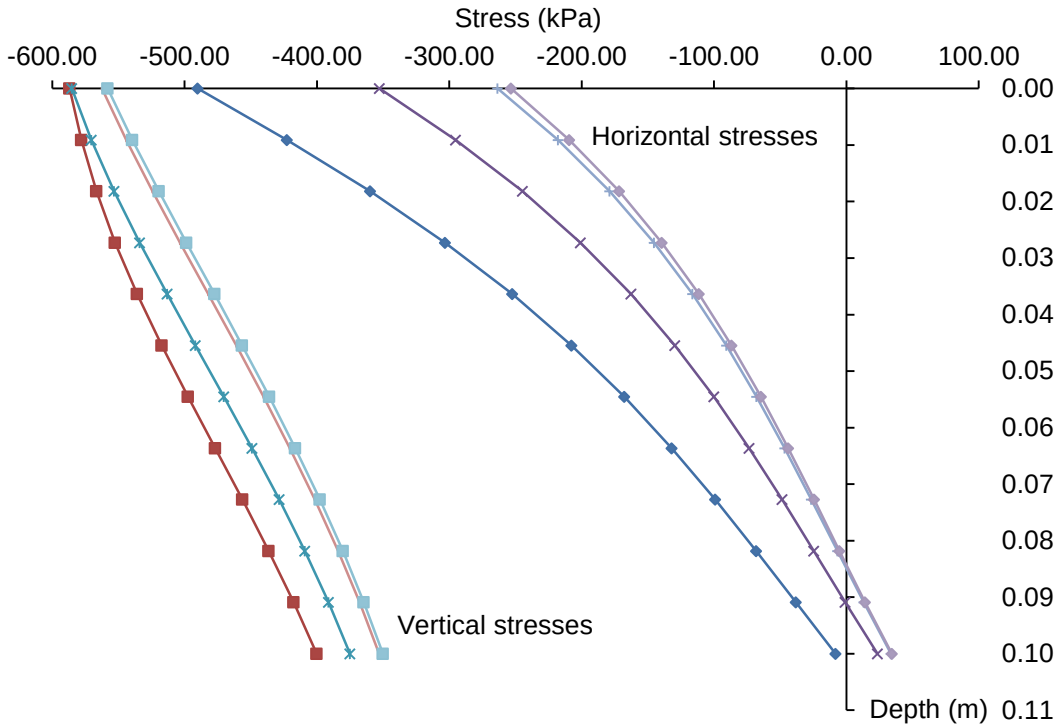

Figure C.8 Stress distribution in the base layer of WSTV-BE350 with t_b reduced to 100 mm and $t_{ws} \leq t_{wsn}$

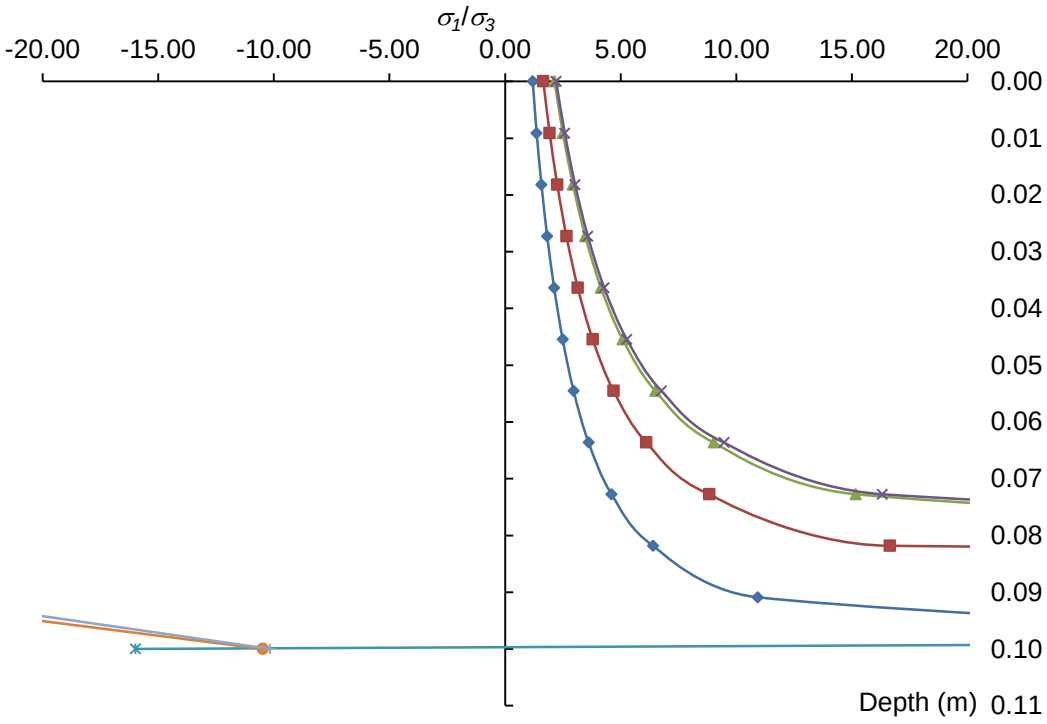

Figure C.9 Ratio of stress distribution in the base layer of WSTV-BE350 with t_b reduced to 100 mm and $t_{ws} \leq t_{wsn}$

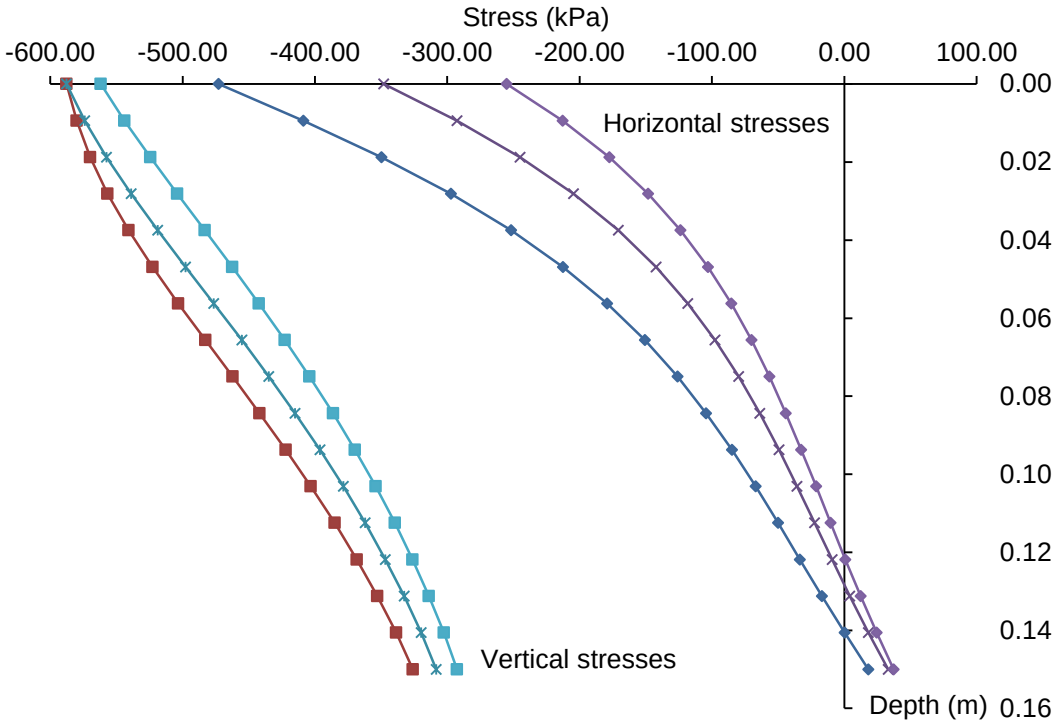

Figure C.10 Stress distribution in the base layer of WSTV-BE350 and $t_{ws} \leq t_{wsn}$

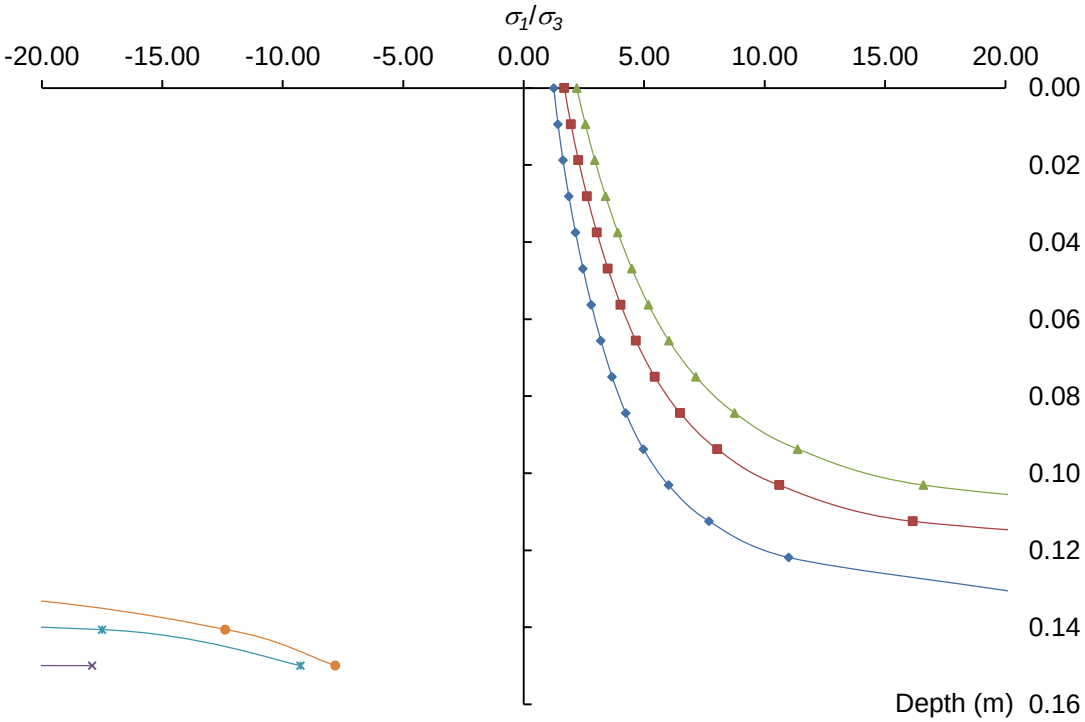

Figure C.11 Ratio of stress distribution in the base layer of WSTV-BE350 and $t_{ws} \leq t_{wsn}$

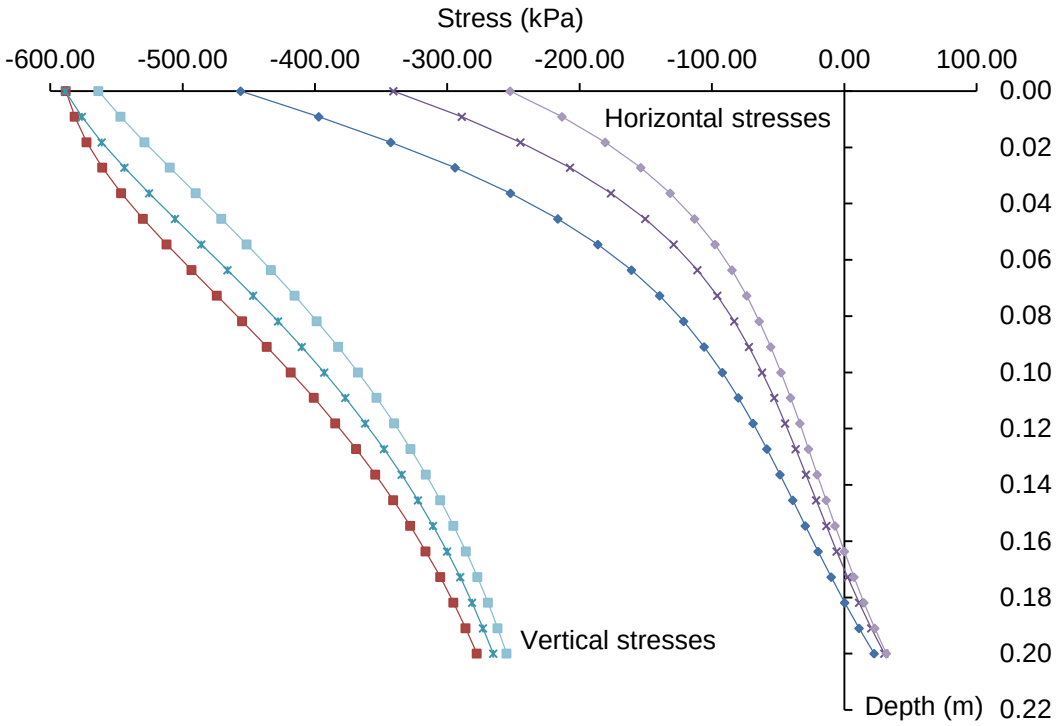

Figure C.12 Stress distribution in the base layer of WSTV-BE350 with t_b increased to 200 mm and $t_{ws} \leq t_{wsn}$

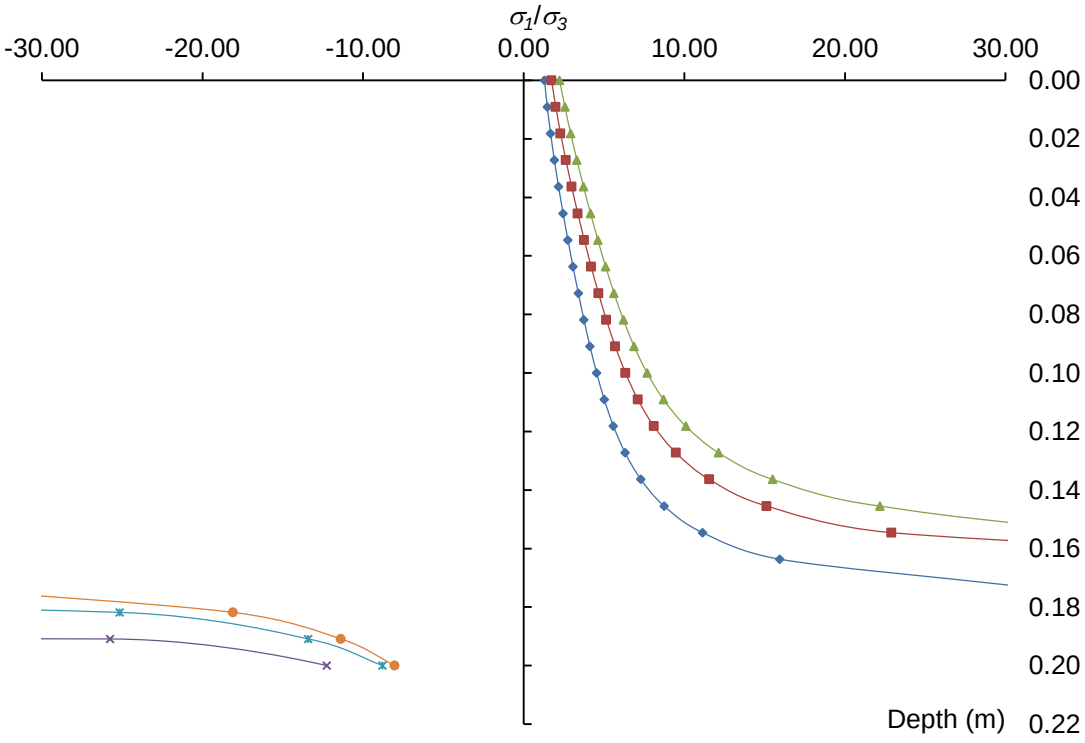

Figure C.13 Ratio of stress distribution in the base layer of WSTV-BE350 with t_b increased to 200 mm and $t_{ws} \leq t_{wsn}$

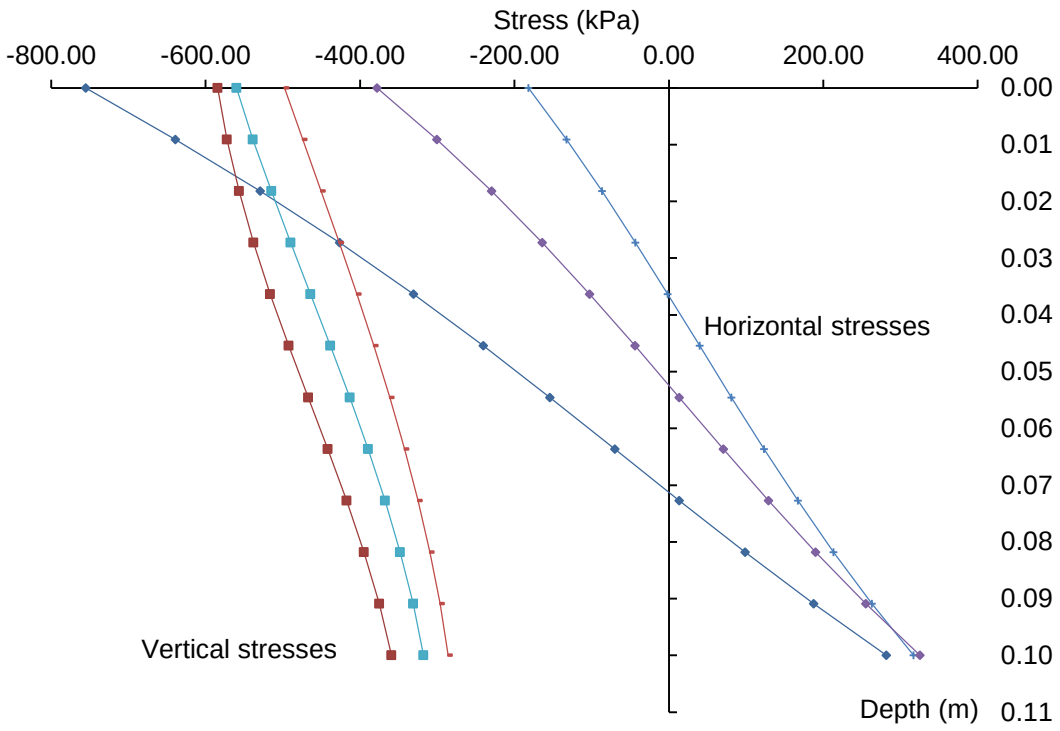

Figure C.14 Stress distribution in the base layer of WSTV-BE800 with t_b reduced to 100 mm and $t_{ws} \leq t_{wsn}$

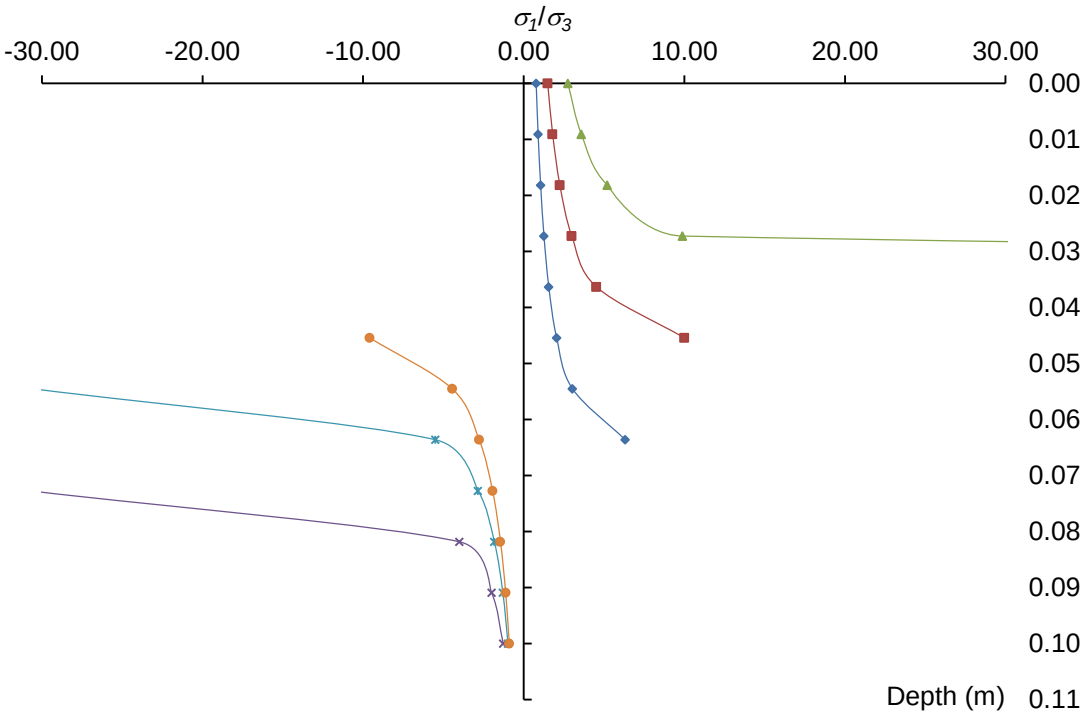

Figure C.15 Ratio of stress distribution in the base layer of WSTV-BE800 with t_b reduced to 100 mm and $t_{ws} \leq t_{wsn}$

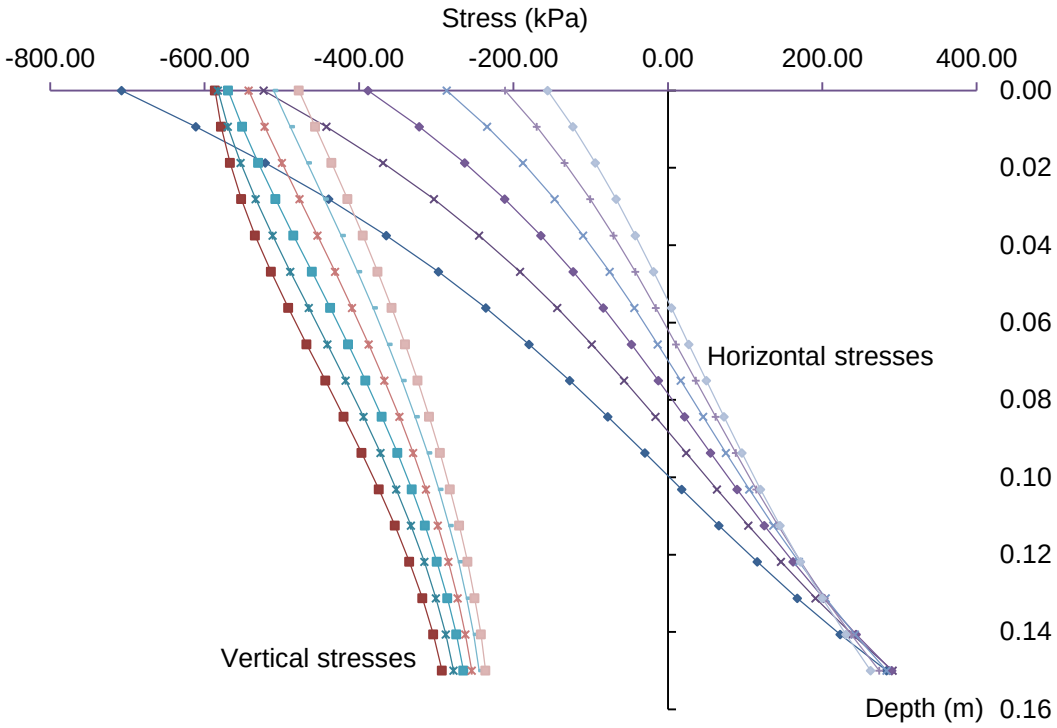

Figure C.16 Stress distribution in the base layer of WSTV-BE800 and $t_{ws} \leq t_{wsn}$

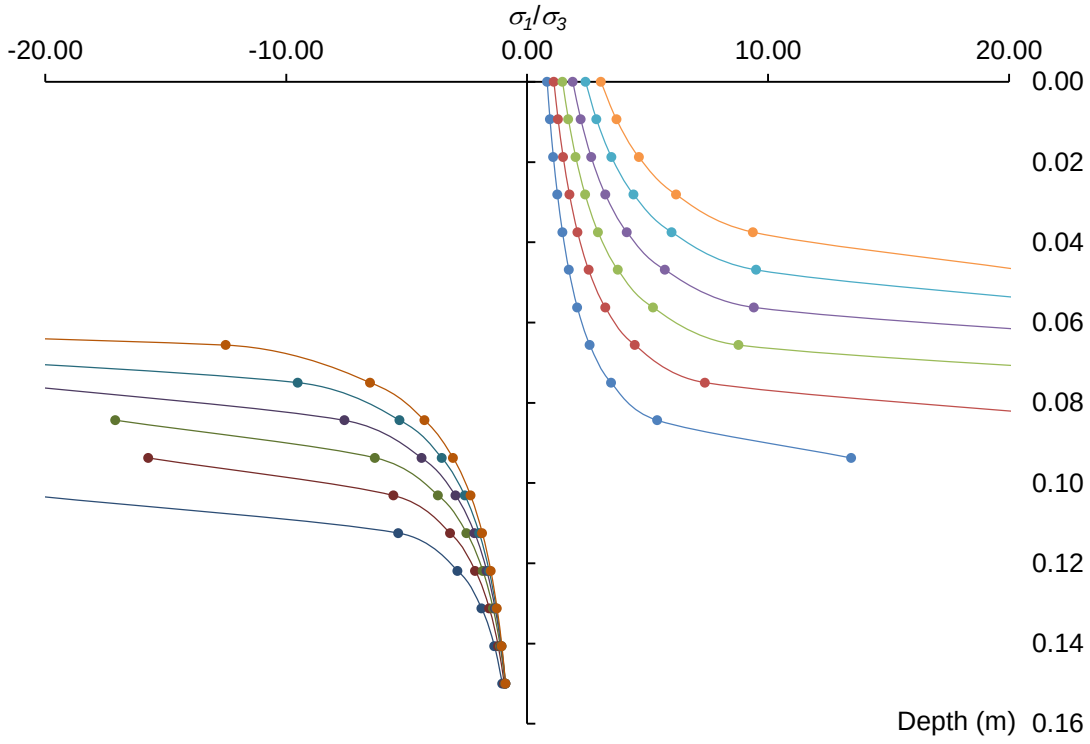

Figure C.17 Ratio of stress distribution in the base layer of WSTV-BE800 and $t_{ws} \leq t_{wsn}$

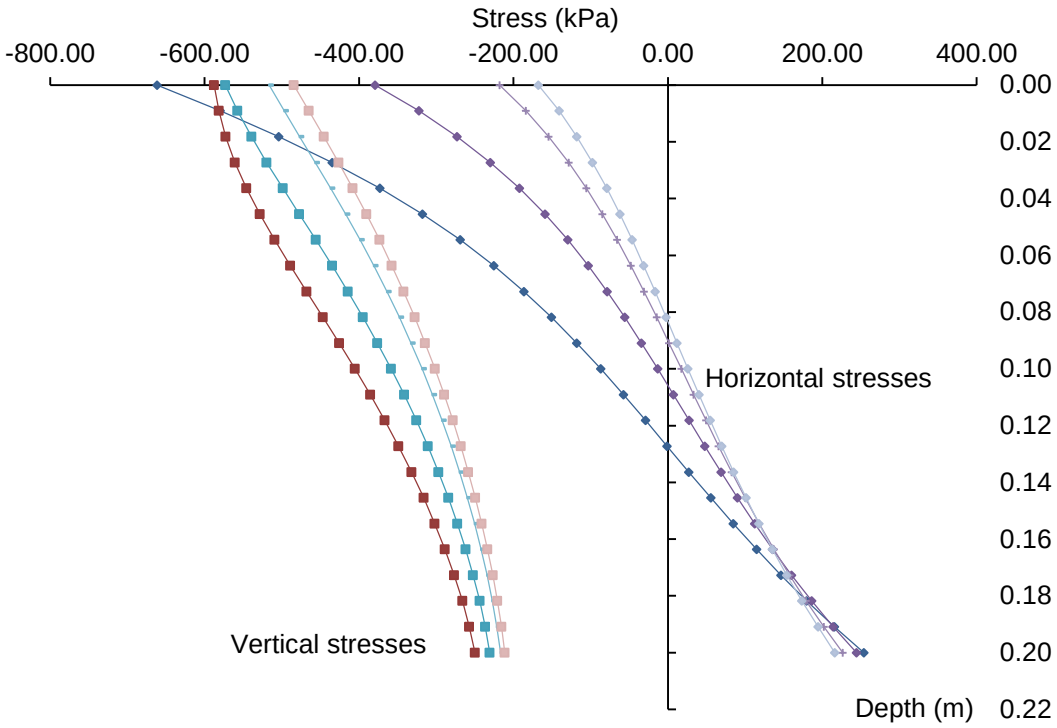

Figure C.18 Stress distribution in the base layer of WSTV-BE800 with t_b increased to 200 mm and $t_{ws} \leq t_{wsn}$

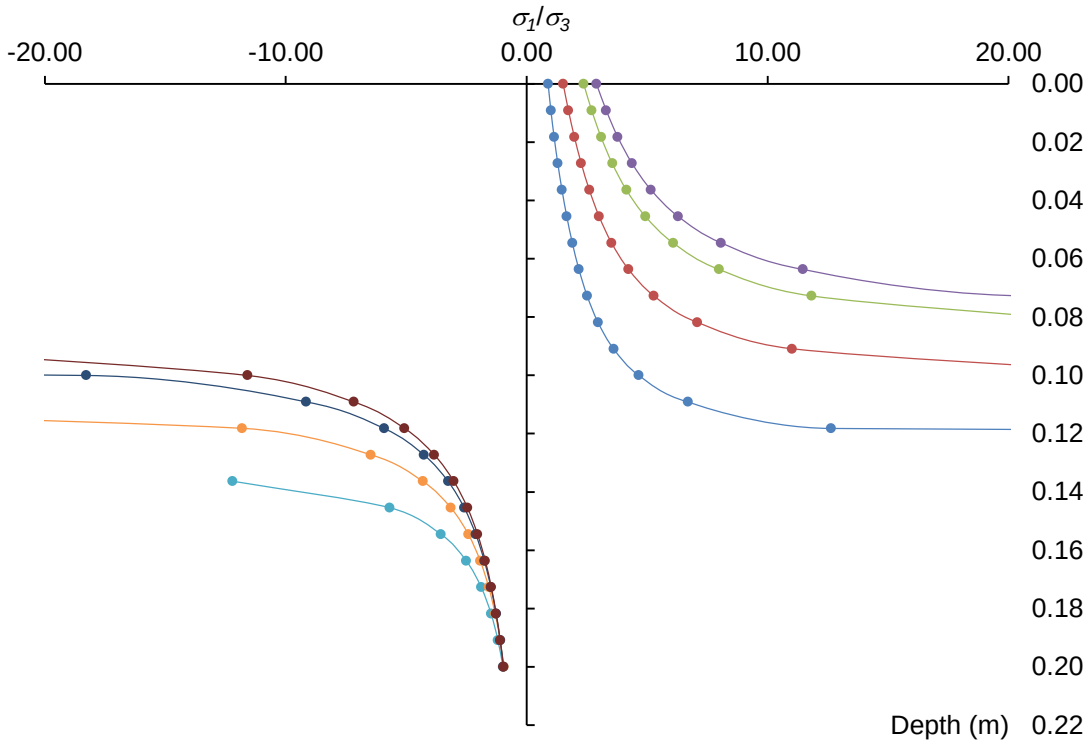

Figure C.19 Ratio of stress distribution in the base layer of WSTV-BE800 with t_b increased to 200 mm and $t_{ws} \leq t_{wsn}$

Appendix D
Example of ABAQUS script

The python language is an add-ins module in ABAQUS that normally use for writing the user-defined script in specific purpose. The example script below was written for finding the disturbed function (*D*) based on the deformation concept as explained in section 6.2 and the structure of algorithm was illustrated in Figure 6.1.

```
#----- Heading -----

from abaqus import *
from abaqusConstants import *
from math import *
from array import *
from odbAccess import *

import section
import regionToolset
import displayGroupMdbToolset as dgm
import part
import material
import assembly
import step
import interaction
import load
import mesh
import job
import sketch
import visualization
import xyPlot
import displayGroupOdbToolset as dgo
import connectorBehavior
import math

#++++++++++

#----- Function for finding minimum and maximum of output data -----

def MinMaxValue(x,y,z):
    Max=Min=0
    Max_Dummy=Min_Dummy=0
    PDCount=NDCount=0
    PCount=NCount=0
    for v in y:
        if v.data[x]>=Max:
            Max=v.data[x]
            if z=='Node':
                Max_Position=v.nodeLabel
            if z=='Element':
                Max_Position=v.elementLabel
            if PCount==0:
```

```
                Min_Dummy=v.data[x]
                if z=='Node':
                    Min_Dummy_Position=v.nodeLabel
                if z=='Element':
                    Min_Dummy_Position=v.elementLabel
                PCount=PCount+1
            elif v.data[x]<=Min_Dummy:
                Min_Dummy=v.data[x]
                if z=='Node':
                    Min_Dummy_Position=v.nodeLabel
                if z=='Element':
                    Min_Dummy_Position=v.elementLabel
            if v.data[x]<Min:
                Min = v.data[x]
                if z=='Node':
                    Min_Position=v.nodeLabel
                if z=='Element':
                    Min_Position=v.elementLabel
                if NCount==0:
                    Max_Dummy=v.data[x]
                    if z=='Node':
                        Max_Dummy_Position=v.nodeLabel
                    if z=='Element':
                        Max_Dummy_Position=v.elementLabel
                    NCount=NCount+1
            elif v.data[x]>=Max_Dummy:
                Max_Dummy=v.data[x]
                if z=='Node':
                    Max_Dummy_Position=v.nodeLabel
                if z=='Element':
                     Max_Dummy_Position=v.elementLabel
        if PCount==0:
            Max=Max_Dummy
            Max_Position=Max_Dummy_Position
        if NCount==0:
            Min=Min_Dummy
            Min_Position=Min_Dummy_Position
        #print 'Return =', Min, Min_Position, Max, Max_Position,
        return Min, Min_Position, Max, Max_Position

    def MinMaxSS(x,y,z):
        Max=Min=0
        Max_Dummy=Min_Dummy=0
        PDCount=NDCount=0
        PCount=NCount=0
        #if x=='mises': m1=v.mises
        for v in y:
            if x=='Mises': m1=v.mises
            elif x=='MaxPrincipal': m1=v.maxPrincipal
```

```
    elif x=='MidPrincipal': m1=v.midPrincipal
    elif x=='MinPrincipal': m1=v.minPrincipal
    if m1>=Max:
        Max=m1
        if z=='Node':
            Max_Position=v.nodeLabel
        if z=='Element':
            Max_Position=v.elementLabel
        if PCount==0:
            Min_Dummy=m1
            if z=='Node':
                Min_Dummy_Position=v.nodeLabel
            if z=='Element':
                Min_Dummy_Position=v.elementLabel
            PCount=PCount+1
    elif m1<=Min_Dummy:
        Min_Dummy=m1
        if z=='Node':
            Min_Dummy_Position=v.nodeLabel
        if z=='Element':
            Min_Dummy_Position=v.elementLabel
    if m1<Min:
        Min = m1
        if z=='Node':
            Min_Position=v.nodeLabel
        if z=='Element':
            Min_Position=v.elementLabel
        if NCount==0:
            Max_Dummy=m1
            if z=='Node':
                Max_Dummy_Position=v.nodeLabel
            if z=='Element':
                Max_Dummy_Position=v.elementLabel
            NCount=NCount+1
    elif m1>=Max_Dummy:
        Max_Dummy=m1
        if z=='Node':
            Max_Dummy_Position=v.nodeLabel
        if z=='Element':
                Max_Dummy_Position=v.elementLabel
if PCount==0:
    Max=Max_Dummy
    Max_Position=Max_Dummy_Position
if NCount==0:
    Min=Min_Dummy
    Min_Position=Min_Dummy_Position
#print 'Return =', Min, Min_Position, Max, Max_Position,
return Min, Min_Position, Max, Max_Position
```

```
#++++++++++

#----- Function for calculating permanent deformation -----

def FPd(w,x,y,z):
    if w=='CRB':
        if x==50:
            if y==175:
                FPd=0.686305701*(z)**0.049388479
            elif y==350:
                FPd=0.716783698*(z)**0.109543964
            elif y==450:
                FPd=0.881908626*(z)**0.092986651
            elif y==550:
                FPd=0.915923459*(z)**0.096576118
        elif x==100:
            if y==175:
                FPd=0.507311404*(z)**0.045066428
            elif y==350:
                FPd=0.516897313*(z)**0.132267948
            elif y==450:
                FPd=0.705464225*(z)**0.110591998
            elif y==550:
                FPd=0.837154221*(z)**0.101569418
        elif x==200:
            if y==175:
                FPd=1.201417354*(z)**0.026728441
            elif y==350:
                FPd=1.016758222*(z)**0.087666168
            elif y==450:
                FPd=1.064322982*(z)**0.086869288
            elif y==550:
                FPd=1.13942509*(z)**0.081853806
        else:
            a=(1.069)+(-0.0008533*y)+(-0.008533*x)+(2.89E-06*y**2)+(-6.42E-
06*x*y)+(5.21E-05*x**2)
            b=(-0.1001)+(0.0008897*y)+(0.0006048*x)+(-1.08E-06*y**2)+(1.87E-
07*x*y)+(-3.14E-06*x**2)
            FPd=a*(z)**b
    elif w=='HCTCRB':
        if x==50:
            if y==175:
                FPd=0.012710976*(z)**0.205329646
            elif y==350:
                FPd=0.026995483*(z)**0.178641293
            elif y==450:
                FPd=0.031848203*(z)**0.172013118
            elif y==550:
                FPd=0.033161036*(z)**0.186052823
```

```
        elif x==100:
            if y==175:
                FPd=0.021356268*(z)**0.180608387
            elif y==350:
                FPd=0.029982772*(z)**0.171241671
            elif y==450:
                FPd=0.03294784*(z)**0.170301502
            elif y==550:
                FPd=0.037977939*(z)**0.162604644
        elif x==200:
            if y==175:
                FPd=0.012890898*(z)**0.160753191
            elif y==350:
                FPd=0.015313652*(z)**0.152780357
            elif y==450:
                FPd=0.015233698*(z)**0.15847862
            elif y==550:
                FPd=0.015742759*(z)**0.163610082
        else:
            a=(-0.02103)+(0.000116*y)+(0.0004594*x)+(-5.83E-08*y**2)+(-
3.31E-07*x*y)+(-1.64E-06*x**2)
            b=(0.2669)+(-0.0002744*y)+(-0.0006286*x)+(2.61E-07*y**2)+(4.69E-
07*x*y)+(1.09E-06*x**2)
            FPd=a*(z)**b
    return FPd

#++++++++++

#----- Function for calculation resilient deformation -----

def FRd(w,x,y,z):
    if w=='CRB':
        if x==50:
            if y==175:
                FRd=0.106501953*exp(-0.000033262*z)
            elif y==350:
                FRd=0.201184925*exp(-0.000016518*z)
            elif y==450:
                FRd=0.215029579*exp(-0.000013671*z)
            elif y==550:
                FRd=0.225473732*exp(-0.000011465*z)
        elif x==100:
            if y==175:
                FRd=0.116420952*exp(-0.000017223*z)
            elif y==350:
                FRd=0.275811653*exp(-0.000012694*z)
            elif y==450:
                FRd=0.314606957*exp(-0.000017834*z)
            elif y==550:
```

```
            FRd=0.319657464*exp(-0.000014257*z)
        elif x==200:
            if y==175:
                FRd=0.127758796*exp(-0.000075766*z)
            elif y==350:
                FRd=0.190278629*exp(-0.000011636*z)
            elif y==450:
                FRd=0.2187254*exp(-0.00001661*z)
            elif y==550:
                FRd=0.229566533*exp(-0.000020713*z)
        else:
            a=(0.2859)+(0.04827*y)+(0.01675*x)+(-0.02315*y**2)+(-
0.005939*x*y)+(-0.05775*x**2)
            b=(-1.39E-05)+(-2.98E-06*y)+(1.29E-06*x)+(-6.42E-06*y**2)+(4.08E-
06*x*y)+(6.69E-06*y**3)+(-8.06E-06*x*y**2)
            FRd=a*exp(b*z)
    elif w=='HCTCRB':
        if x==50:
            if y==175:
                FRd=0.101528254*exp(-0.000019923*z)
            elif y==350:
                FRd=0.22790099*exp(-0.000019866*z)
            elif y==450:
                FRd=0.234255484*exp(-0.000011952*z)
            elif y==550:
                FRd=0.248954859*exp(-0.000010545*z)
        elif x==100:
            if y==175:
                FRd=0.078042466*exp(-0.000015682*z)
            elif y==350:
                FRd=0.196149382*exp(-0.00001883*z)
            elif y==450:
                FRd=0.207655141*exp(-0.000010352*z)
            elif y==550:
                FRd=0.22903512*exp(-0.000010699*z)
        elif x==200:
            if y==175:
                FRd=0.044323341*exp(-0.000010823*z)
            elif y==350:
                FRd=0.120773351*exp(-0.000006325*z)
            elif y==450:
                FRd=0.127959684*exp(-0.000006443*z)
            elif y==550:
                FRd=0.130953902*exp(-0.000006298*z)
        else:
            a=(0.1901)+(0.04139*y)+(-0.04068*x)+(-0.02444*y**2)+(-
0.0107*x*y)+(-0.005894*x**2)
            b=(-1.38E-05)+(2.98E-06*y)+(3.30E-06*x)+(7.22E-07*y**2)+(-9.12E-
07*x*y)+(8.65E-07*x**2)
```

```
            FRd=a*exp(b*z)
    return FRd

#++++++++++

#---------- Function for calculating relative intact ----------

def FRI(w,x,y,z):
    if w=='CRB':
        if x==50:
            if y==175:
                FRI=1199.858028233840*exp(-6.608171376548*z)
            elif y==350:
                FRI=0.429842375400*exp(0.032574744816*z)
            elif y==450:
                FRI=0.622364650046*exp(0.020872202448*z)
            elif y==550:
                FRI=0.942561871857*exp(0.013547415642*z)
        elif x==100:
            if y==175:
                FRI=0.171259548177*exp(0.161264792713*z)
            elif y==350:
                FRI=0.662910830009*exp(0.075968451716*z)
            elif y==450:
                FRI=0.805807206240*exp(0.055218169631*z)
            elif y==550:
                FRI=1.010108885065*exp(0.041706869661*z)
        elif x==200:
            if y==175:
                FRI=0.615593327556*exp(-6.609882320295*z)
            elif y==350:
                FRI=0.247037570277*exp(0.151252261409*z)
            elif y==450:
                FRI=0.510355914628*exp(0.115743826454*z)
            elif y==550:
                FRI=0.763340199083*exp(0.092295839341*z)
    elif w=='HCTCRB':
        if x==50:
            if y==175:
                FRI=0.292117504048*exp(0.086837467452*z)
            elif y==350:
                FRI=0.579752865395*exp(0.039205212700*z)
            elif y==450:
                FRI=0.748932213055*exp(0.028291515564*z)
            elif y==550:
                FRI=0.921380546273*exp(0.021267525276*z)
        elif x==100:
            if y==175:
                FRI=0.254822121056*exp(0.164527306806*z)
```

```
            elif y==350:
                FRI=0.518565274852*exp(0.080728954532*z)
            elif y==450:
                FRI=0.672068811575*exp(0.061101744502*z)
            elif y==550:
                FRI=0.823771257045*exp(0.048386654125*z)
        elif x==200:
            if y==175:
                FRI=0.246264765827*exp(0.304101014776*z)
            elif y==350:
                FRI=0.498843804041*exp(0.159129986094*z)
            elif y==450:
                FRI=0.644938507084*exp(0.123851199568*z)
            elif y==550:
                FRI=0.790599804747*exp(0.100728256764*z)
    return FRI

#++++++++++

#---------- Function for calculating the disturbance function ----------

def FD(w,x,y,z):
    if w=='CRB':
        a=(-0.3178)+(-978.5*1e-6)*x+(1611*1e-6)*y
        b=(-4.614)+(-2588.0*1e-6)*x+(6273*1e-6)*y
        d=(-4.954)+(-2721.0*1e-6)*x+(6185*1e-6)*y
    elif w=='HCTCRB':
        a=(-0.6834)+(-276.0*1e-6)*x+(2495*1e-6)*y
        b=(0.5362)+(-57.19*1e-6)*x+(2343*1e-6)*y
        d=(-1.165)+(-324.3*1e-6)*x+(180*1e-6)*y
    FD=(a*z+b)/(z+d)
    return FD

#++++++++++

#---------- Function for creating file name ----------

def FFN(w,x,y,z):
    a='C:/Temp/'
    if x<100:
        bs='_Mr_Cs00'
        bl='_Loc_Cs00'
    elif x<1000:
        bs='_Mr_Cs0'
        bl='_Loc_Cs0'
    else:
        bs='_Mr_Cs'
        bl='_Loc_Cs'
    if y<100:
```

```
        c='_Sd00'
    elif y<1000:
        c='_Sd0'
    else:
        c='_Sd'
    if z<10:
        d='_N000000'
    elif z<100:
        d='_N00000'
    elif z<1000:
        d='_N0000'
    elif z<10000:
        d='_N000'
    elif z<100000:
        d='_N00'
    elif z<1000000:
        d='_N0'
    else:
        d='_N'
    SFN=str(a)+str(w)+str(bs)+str(x)+str(c)+str(y)+str(d)+str(z)+'DC2.csv'
    LFN=str(a)+str(w)+str(bl)+str(x)+str(c)+str(y)+str(d)+str(z)+'DC2.csv'
    return SFN, LFN

#++++++++++

#----- Constant ------

h=0.200
N=200
MatType_Table=('CRB','HCTCRB')
SigmaDev_Table=(350,450,550)
Sigma3_Table=(50,100,200)

#++++++++++++++++++++++++++++

for k in range(2):

    MatType=str(MatType_Table[k])

    for l in range(3):

        for m in range(3):

            Sigma3=Sigma3_Table[l]
            SigmaDev=SigmaDev_Table[m]
            Sigma1=SigmaDev+Sigma3

            if MatType=='CRB':
                Density=2309
```

```
            E=((58.88*Sigma3)+493.30)/(Sigma3+14.55)
        if MatType=='HCTCRB':
            Density=2369
            E=((151.00*Sigma3)+3609.00)/(Sigma3+48.48)

#----- Array declaration -----

        Mr=N*['f']
        o=N*[""]

#++++++++++

        StressFileName, LocFileName = FFN(MatType,Sigma3,SigmaDev,N)

#----- Open own output file -----

        RMOutIntFile=open(StressFileName,'w')
        RMOutIntFile.write('N\t Sigma1\t\t Sigma3\t\t Sigma1/Sigma3\t Mr\t\t
Max. Uy\t Min.Uy\t\t Max. Mises\t Min. Mises\t Max. Sx\t Min. Sx\t Max. Sy\t
Min. Sy\t Max. Sz\t Min. Sz\t Max. Sxy\t Min. Sxy\t Max. Sxz\t Min. Sxz\t Max.
Syz\t Min. Syz\t Max-Max. Princ.\t Min-Max. Princ.\t Max-Mid. Princ.\t Min-
Mid. Princ.\t Max-Min. Princ.\t Min-Min. Princ.\t S1_Max_Mises\t
S2_Max_Mises\t S3_Max_Mises\t\t Pd\t\t Rd\t\t h\t\t dPd\t\t RdT\t\t Rdc\t\t
D\t\t RdD\n')
        RMOutIntFile.write('\t (Pa)\t\t (Pa)\t\t \t\t (Pa)\t\t (m)\t\t (m)\t\t (Pa)\t\t
(Pa)\t\t (Pa)\t\t (Pa)\t\t (Pa)\t\t (Pa)\t\t (Pa)\t\t (Pa)\t\t (Pa)\t\t (Pa)\t\t
(Pa)\t\t (Pa)\t\t (Pa)\t\t (Pa)\t\t\t (Pa)\t\t\t (Pa)\t\t\t (Pa)\t\t\t (Pa)\t\t\t
(Pa)\t\t (Pa)\t\t (Pa)\t\t\t (mm)\t\t (mm)\t\t (mm)\t\t (mm)\t\t (mm)\t\t (mm)\t\t\t\t
(mm)\n')

#++++++++++

#----- Open own location file -----

        RMOutLocFile=open(LocFileName,'w')
        RMOutLocFile.write('N\t Max. Uy\t Min. Uy\t Max. Mises\t Min. Mises\t
Max. Sx\t Min. Sx\t Max. Sy\t Min. Sy\t Max. Sz\t Min. Sz\t Max. Sxy\t Min.
Sxy\t Max. Sxz\t Min. Sxz\t Max. Syz\t Min. Syz\t Max-Max. Princ.\t Min-Max.
Princ.\t Max-Mid. Princ.\t Min-Mid. Princ.\t Max-Min. Princ.\t Min-Min. Princ\n')
        RMOutLocFile.write('\t (Node)\t\t (Node)\t\t (Node)\t\t (Node)\t\t
(Node)\t\t (Node)\t\t (Node)\t\t (Node)\t\t (Node)\t\t (Node)\t\t (Node)\t\t
(Node)\t\t (Node)\t\t (Node)\t\t (Node)\t\t (Node)\t\t (Node)\t\t\t (Node)\t\t\t
(Node)\t\t\t (Node)\t\t\t (Node)\t\t\t (Node)\n')

#++++++++++

        for i in range(N):
            Mdb()
            session.viewports['Viewport: 1'].setValues(displayedObject=None)
```

```
#----- Change model's name -----

        ModelName=str(MatType)+'_Specimen'
        mdb.models.changeKey(fromName='Model-1',
toName=str(ModelName))

#++++++++++

#----- Create model -----

        s =
mdb.models[str(ModelName)].ConstrainedSketch(name='__profile__',
                                             sheetSize=0.2)
        g, v, d, c = s.geometry, s.vertices, s.dimensions, s.constraints
        s.sketchOptions.setValues(decimalPlaces=6)
        s.setPrimaryObject(option=STANDALONE)
        s.ConstructionLine(point1=(0.0, -0.1), point2=(0.0, 0.1))
        s.FixedConstraint(entity=g[2])
        s.rectangle(point1=(0.0, 0.0), point2=(0.05, h))

        if i<10:
           PartName=str(MatType)+'_Sample_N=000000'+str(i+1)
        elif i<100:
           PartName=str(MatType)+'_Sample_N=00000'+str(i+1)
        elif i<1000:
           PartName=str(MatType)+'_Sample_N=0000'+str(i+1)
        elif i<10000:
           PartName=str(MatType)+'_Sample_N=000'+str(i+1)
        elif i<100000:
           PartName=str(MatType)+'_Sample_N=00'+str(i+1)
        elif i<1000000:
           PartName=str(MatType)+'_Sample_N=0'+str(i+1)
        else:
           PartName=str(MatType)+'_Sample_N='+str(i+1)

        p = mdb.models[str(ModelName)].Part(name=str(PartName),
dimensionality=THREE_D,
                                    type=DEFORMABLE_BODY)
        p = mdb.models[str(ModelName)].parts[str(PartName)]
        p.BaseSolidRevolve(sketch=s, angle=360.0,
flipRevolveDirection=OFF)
        s.unsetPrimaryObject()
        p = mdb.models[str(ModelName)].parts[str(PartName)]
        session.viewports['Viewport: 1'].setValues(displayedObject=p)
        del mdb.models[str(ModelName)].sketches['__profile__']

#++++++++++
```

```
#----- Create material properties -----

            mdb.models[str(ModelName)].Material(name=MatType)

mdb.models[str(ModelName)].materials[MatType].Density(table=((Density, ),
))

mdb.models[str(ModelName)].materials[MatType].Elastic(noTension=ON,
table=((
                E*1e6, 0.35), ))

#++++++++++

#----- Create model's section -----

mdb.models[str(ModelName)].HomogeneousSolidSection(name=MatType,
material=MatType,
                                                   thickness=None)
            p = mdb.models[str(ModelName)].parts[str(PartName)]
            c = p.cells
            cells = c.getSequenceFromMask(mask=('[#1 ]', ), )
            region = regionToolset.Region(cells=cells)

#++++++++++

#----- Assign model's section -----

            p = mdb.models[str(ModelName)].parts[str(PartName)]
            p.SectionAssignment(region=region, sectionName=MatType,
offset=0.0,
                        offsetType=MIDDLE_SURFACE, offsetField='')#,
#                           thicknessAssignment=FROM_SECTION)

#++++++++++

#----- Mesh generation -----

            p = mdb.models[str(ModelName)].parts[str(PartName)]
            p.seedPart(size=0.020, deviationFactor=0.1)
            elemType1 = mesh.ElemType(elemCode=C3D20R,
elemLibrary=STANDARD)
            elemType2 = mesh.ElemType(elemCode=C3D15,
elemLibrary=STANDARD)
            elemType3 = mesh.ElemType(elemCode=C3D10,
elemLibrary=STANDARD)
            p = mdb.models[str(ModelName)].parts[str(PartName)]
            c = p.cells
            cells = c.getSequenceFromMask(mask=('[#1 ]', ), )
            pickedRegions =(cells, )
```

```
            p.setElementType(regions=pickedRegions,
elemTypes=(elemType1, elemType2,
                                                elemType3))
            p = mdb.models[str(ModelName)].parts[str(PartName)]
            p.generateMesh()
            a = mdb.models[str(ModelName)].rootAssembly
            session.viewports['Viewport: 1'].setValues(displayedObject=a)

#++++++++++

#----- Model assembly -----

            a = mdb.models[str(ModelName)].rootAssembly
            a.DatumCsysByDefault(CARTESIAN)
            p = mdb.models[str(ModelName)].parts[str(PartName)]
            a.Instance(name=str(MatType)+' Sample-1', part=p,
dependent=ON)
            session.viewports['Viewport: 1'].assemblyDisplay.setValues(
               adaptiveMeshConstraints=ON)

#++++++++++

#----- Assign loading and boundary condition -----

            CurrentStepName='Stage 1'

mdb.models[str(ModelName)].StaticStep(name=str(CurrentStepName),
previous='Initial')

mdb.models[str(ModelName)].TabularAmplitude(name='Trapezoidal',
timeSpan=STEP,
                                            smooth=SOLVER_DEFAULT,
data=((0.0, 0.0), (0.3, 1.0), (1.0, 1.0), (1.3,

0.0), (1.5, 0.0), (2.0, 0.0), (2.5, 0.0), (3.0, 0.0)))

            a = mdb.models[str(ModelName)].rootAssembly
            s1 = a.instances[str(MatType)+' Sample-1'].faces
            side1Faces1 = s1.getSequenceFromMask(mask=('[#1 ]', ), )
            region = regionToolset.Region(side1Faces=side1Faces1)
            mdb.models[str(ModelName)].Pressure(name='Sigma 1',
createStepName=str(CurrentStepName),
                                        region=region, distributionType=UNIFORM,
field='', magnitude=1000*Sigma1,
                                        amplitude='Trapezoidal')

            a = mdb.models[str(ModelName)].rootAssembly
            s1 = a.instances[str(MatType)+' Sample-1'].faces
            side1Faces1 = s1.getSequenceFromMask(mask=('[#2 ]', ), )
```

```
            region = regionToolset.Region(side1Faces=side1Faces1)
            mdb.models[str(ModelName)].Pressure(name='Sigma 3',
createStepName=str(CurrentStepName),
                                        region=region, distributionType=UNIFORM,
field='', magnitude=1000*Sigma3,
                                        amplitude='Trapezoidal')

            a = mdb.models[str(ModelName)].rootAssembly
            mdb.models[str(ModelName)].Gravity(name='Selfweight',
createStepName=str(CurrentStepName), comp2=-9.807,
                                       distributionType=UNIFORM, field='')

            a = mdb.models[str(ModelName)].rootAssembly
            f1 = a.instances[str(MatType)+' Sample-1'].faces
            faces1 = f1.getSequenceFromMask(mask=('[#1 ]', ), )
            region = regionToolset.Region(faces=faces1)
            mdb.models[str(ModelName)].DisplacementBC(name='Top
support',

createStepName=str(CurrentStepName), region=region, u1=0.0, u2=UNSET,
u3=0.0,
                                        ur1=UNSET, ur2=UNSET, ur3=UNSET,
amplitude=UNSET, fixed=OFF,
                                        distributionType=UNIFORM,
fieldName='', localCsys=None)

            a = mdb.models[str(ModelName)].rootAssembly
            f1 = a.instances[str(MatType)+' Sample-1'].faces
            faces1 = f1.getSequenceFromMask(mask=('[#4 ]', ), )
            region = regionToolset.Region(faces=faces1)
            mdb.models[str(ModelName)].DisplacementBC(name='Bottom
support',

createStepName=str(CurrentStepName), region=region, u1=0.0, u2=0.0,
u3=0.0,
                                        ur1=UNSET, ur2=UNSET, ur3=UNSET,
amplitude=UNSET, fixed=OFF,
                                        distributionType=UNIFORM,
fieldName='', localCsys=None)

            session.viewports['Viewport:
1'].assemblyDisplay.setValues(loads=ON, bcs=ON,
                                                predefinedFields=ON,
connectors=ON, adaptiveMeshConstraints=ON)

#++++++++++
```

```
#----- Create Job -----

        if i<10:

JobName=str(MatType)+'Cs'+str(Sigma3)+'Sd'+str(SigmaDev)+'N_000000'+
str(i+1)
        elif i<100:

JobName=str(MatType)+'Cs'+str(Sigma3)+'Sd'+str(SigmaDev)+'N_00000'+st
r(i+1)
        elif i<1000:

JobName=str(MatType)+'Cs'+str(Sigma3)+'Sd'+str(SigmaDev)+'N_0000'+str(
i+1)
        elif i<10000:

JobName=str(MatType)+'Cs'+str(Sigma3)+'Sd'+str(SigmaDev)+'N_000'+str(i
+1)
        elif i<100000:

JobName=str(MatType)+'Cs'+str(Sigma3)+'Sd'+str(SigmaDev)+'N_00'+str(i+
1)
        elif i<1000000:

JobName=str(MatType)+'Cs'+str(Sigma3)+'Sd'+str(SigmaDev)+'N_0'+str(i+1)
        else:

JobName=str(MatType)+'Cs'+str(Sigma3)+'Sd'+str(SigmaDev)+'N_'+str(i+1)

        mdb.Job(name=str(JobName), model=str(ModelName),
description='',
            type=ANALYSIS, atTime=None, waitMinutes=0, waitHours=0,
queue=None,
            memory=90, memoryUnits=PERCENTAGE,
getMemoryFromAnalysis=True,
            explicitPrecision=SINGLE, nodalOutputPrecision=SINGLE,
echoPrint=OFF,
            modelPrint=OFF, contactPrint=OFF, historyPrint=OFF,
userSubroutine='',
            scratch='', multiprocessingMode=DEFAULT, numCpus=2,
numDomains=2)

#++++++++++

#----- Save model -----

        if i<10:
```

```
mdb.saveAs(pathName='C:/Temp/'+str(MatType)+'Cs'+str(Sigma3)+'Sd'+str(
SigmaDev)+'_RMT_N_000000'+str(i+1))
            elif i<100:

mdb.saveAs(pathName='C:/Temp/'+str(MatType)+'Cs'+str(Sigma3)+'Sd'+str(
SigmaDev)+'_RMT_N_00000'+str(i+1))
            elif i<1000:

mdb.saveAs(pathName='C:/Temp/'+str(MatType)+'Cs'+str(Sigma3)+'Sd'+str(
SigmaDev)+'_RMT_N_0000'+str(i+1))
            elif i<10000:

mdb.saveAs(pathName='C:/Temp/'+str(MatType)+'Cs'+str(Sigma3)+'Sd'+str(
SigmaDev)+'_RMT_N_000'+str(i+1))
            elif i<100000:

mdb.saveAs(pathName='C:/Temp/'+str(MatType)+'Cs'+str(Sigma3)+'Sd'+str(
SigmaDev)+'_RMT_N_00'+str(i+1))
            elif i<1000000:

mdb.saveAs(pathName='C:/Temp/'+str(MatType)+'Cs'+str(Sigma3)+'Sd'+str(
SigmaDev)+'_RMT_N_0'+str(i+1))
            else:

mdb.saveAs(pathName='C:/Temp/'+str(MatType)+'Cs'+str(Sigma3)+'Sd'+str(
SigmaDev)+'_RMT_N_'+str(i+1))

#++++++++++

#----- Submission for analysis -----
            mdb.jobs[str(JobName)].submit(consistencyChecking=OFF)
            mdb.jobs[str(JobName)].waitForCompletion()

#++++++++++

#----- Show results -----

            ResultFile=str(JobName)+'.odb'
            o = session.openOdb(name=str(ResultFile))
            session.viewports['Viewport: 1'].setValues(displayedObject=o)
            session.viewports['Viewport:
1'].viewportAnnotationOptions.setValues(legendFont='-*-verdana-medium-r-
normal-*-*-140-*-*-p-*-*-*')
            session.viewports['Viewport:
1'].viewportAnnotationOptions.setValues(legendMinMax=ON,
legendPosition=(2, 98))

            InterpretOdb = openOdb(path=str(ResultFile))
```

```
            InterpretStep = InterpretOdb.steps[str(CurrentStepName)]
            InterpretFrame = InterpretStep.frames[-1]
            Displacement = InterpretFrame.fieldOutputs['U'].values
            AllElements = InterpretOdb.rootAssembly.elementSets[" ALL
ELEMENTS"]

Stress=InterpretFrame.fieldOutputs['S'].getSubset(region=AllElements,positio
n=ELEMENT_NODAL).values

            Min_Mises, Min_Mises_Location, Max_Mises,
Max_Mises_Location=MinMaxSS('Mises',Stress,'Node')
            Min_Max_Principal, Min_Max_Principal_Location,
Max_Max_Principal,
Max_Max_Principal_Location=MinMaxSS('MaxPrincipal',Stress,'Node')
            Min_Mid_Principal, Min_Mid_Principal_Location,
Max_Mid_Principal,
Max_Mid_Principal_Location=MinMaxSS('MidPrincipal',Stress,'Node')
            Min_Min_Principal, Min_Min_Principal_Location,
Max_Min_Principal,
Max_Min_Principal_Location=MinMaxSS('MinPrincipal',Stress,'Node')
            Min_U1, Min_U1_Location, Max_U1,
Max_U1_Location=MinMaxValue(0,Displacement,'Node')
            Min_U2, Min_U2_Location, Max_U2,
Max_U2_Location=MinMaxValue(1,Displacement,'Node')
            Min_S11, Min_S11_Location, Max_S11,
Max_S11_Location=MinMaxValue(0,Stress,'Node')
            Min_S22, Min_S22_Location, Max_S22,
Max_S22_Location=MinMaxValue(1,Stress,'Node')
            Min_S33, Min_S33_Location, Max_S33,
Max_S33_Location=MinMaxValue(2,Stress,'Node')
            Min_S12, Min_S12_Location, Max_S12,
Max_S12_Location=MinMaxValue(3,Stress,'Node')
            Min_S13, Min_S13_Location, Max_S13,
Max_S13_Location=MinMaxValue(4,Stress,'Node')
            Min_S23, Min_S23_Location, Max_S23,
Max_S23_Location=MinMaxValue(5,Stress,'Node')

            for v in Stress:
                if v.nodeLabel==Max_Mises_Location:
                    Max_Mises_Max_Principal=v.maxPrincipal
                    Max_Mises_Mid_Principal=v.midPrincipal
                    Max_Mises_Min_Principal=v.minPrincipal

            Pd=FPd(MatType,Sigma3,SigmaDev,i+1)
            dPd=FPd(MatType,Sigma3,SigmaDev,i+1)-
FPd(MatType,Sigma3,SigmaDev,i)
            RdT=FRd(MatType,Sigma3,SigmaDev,i+1)

            Rd=Min_U2*1e3+dPd
```

```
            Rdc=FRd(MatType,Sigma3,SigmaDev,10000)
            D=FD(MatType,Sigma3,SigmaDev,i+1)
            RdD=((1-D)*(-1*Rd))+(D*Rdc)

#++++++++++

#----- Checking variables and writing selected output to the file -----

            if Rd<0:
               if RdD<0 or RdD>1.50*RdT:
                  Rd=Rd
                  RdD=1.50*RdT
                  RMOutIntFile.write('%d\t %.3e\t %.3e\t %.3f\t\t %.6e\t %.3e\t
%.3e\t %.3e\t %.3e\t %.3e\t %.3e\t %.3e\t %.3e\t %.3e\t %.3e\t %.3e\t
%.3e\t %.3e\t %.3e\t %.3e\t %.3e\t\t %.3e\t\t %.3e\t\t %.3e\t\t %.3e\t\t
%.3e\t %.3e\t %.3e\t\t %.3e\t %.3e\t %.3e\t %.3e\t %.3e\t %.3e\t %.3e\t
%.3e\t' % (i+1, 1000*Sigma1, 1000*Sigma3, Sigma1/Sigma3, E*1e6,
Max_U2, Min_U2, Max_Mises, Min_Mises, Max_S11, Min_S11, Max_S22,
Min_S22, Max_S33, Min_S33, Max_S12, Min_S12, Max_S13, Min_S13,
Max_S23, Min_S23, Max_Max_Principal, Min_Max_Principal,
Max_Mid_Principal, Min_Mid_Principal, Max_Min_Principal,
Min_Min_Principal, Max_Mises_Max_Principal, Max_Mises_Mid_Principal,
Max_Mises_Min_Principal, Pd, Rd, h*1e3, dPd, RdT, Rdc, D, RdD))
                  RMOutIntFile.write('***\n')
               else:
                  Rd=Rd
                  RMOutIntFile.write('%d\t %.3e\t %.3e\t %.3f\t\t %.6e\t %.3e\t
%.3e\t %.3e\t %.3e\t %.3e\t %.3e\t %.3e\t %.3e\t %.3e\t %.3e\t %.3e\t
%.3e\t %.3e\t %.3e\t %.3e\t %.3e\t\t %.3e\t\t %.3e\t\t %.3e\t\t %.3e\t\t
%.3e\t %.3e\t %.3e\t\t %.3e\t %.3e\t %.3e\t %.3e\t %.3e\t %.3e\t %.3e\t
%.3e\n' % (i+1, 1000*Sigma1, 1000*Sigma3, Sigma1/Sigma3, E*1e6,
Max_U2, Min_U2, Max_Mises, Min_Mises, Max_S11, Min_S11, Max_S22,
Min_S22, Max_S33, Min_S33, Max_S12, Min_S12, Max_S13, Min_S13,
Max_S23, Min_S23, Max_Max_Principal, Min_Max_Principal,
Max_Mid_Principal, Min_Mid_Principal, Max_Min_Principal,
Min_Min_Principal, Max_Mises_Max_Principal, Max_Mises_Mid_Principal,
Max_Mises_Min_Principal, Pd, Rd, h*1e3, dPd, RdT, Rdc, D, RdD))
            else:
               if RdD<0 or RdD>1.50*RdT:
                  Rd=Min_U2
                  RdD=1.50*RdT
                  RMOutIntFile.write('%d\t %.3e\t %.3e\t %.3f\t\t %.6e\t %.3e\t
%.3e\t %.3e\t %.3e\t %.3e\t %.3e\t %.3e\t %.3e\t %.3e\t %.3e\t %.3e\t
%.3e\t %.3e\t %.3e\t %.3e\t %.3e\t\t %.3e\t\t %.3e\t\t %.3e\t\t %.3e\t\t
%.3e\t %.3e\t %.3e\t\t %.3e\t %.3e\t %.3e\t %.3e\t %.3e\t %.3e\t %.3e\t
%.3e\t' % (i+1, 1000*Sigma1, 1000*Sigma3, Sigma1/Sigma3, E*1e6,
Max_U2, Min_U2, Max_Mises, Min_Mises, Max_S11, Min_S11, Max_S22,
Min_S22, Max_S33, Min_S33, Max_S12, Min_S12, Max_S13, Min_S13,
```

```
Max_S23, Min_S23, Max_Max_Principal, Min_Max_Principal,
Max_Mid_Principal, Min_Mid_Principal, Max_Min_Principal,
Min_Min_Principal, Max_Mises_Max_Principal, Max_Mises_Mid_Principal,
Max_Mises_Min_Principal, Pd, Rd, h*1e3, dPd, RdT, Rdc, D, RdD))
                    RMOutIntFile.write('***\n')
                else:
                    Rd=Min_U2
                    RMOutIntFile.write('%d\t %.3e\t %.3e\t %.3f\t\t %.6e\t %.3e\t
%.3e\t %.3e\t %.3e\t %.3e\t %.3e\t %.3e\t %.3e\t %.3e\t %.3e\t %.3e\t %.3e\t
%.3e\t %.3e\t %.3e\t %.3e\t %.3e\t\t %.3e\t\t %.3e\t\t %.3e\t\t %.3e\t\t %.3e\t\t
%.3e\t %.3e\t %.3e\t\t %.3e\t %.3e\t %.3e\t %.3e\t %.3e\t %.3e\t %.3e\t
%.3e\t' % (i+1, 1000*Sigma1, 1000*Sigma3, Sigma1/Sigma3, E*1e6,
Max_U2, Min_U2, Max_Mises, Min_Mises, Max_S11, Min_S11, Max_S22,
Min_S22, Max_S33, Min_S33, Max_S12, Min_S12, Max_S13, Min_S13,
Max_S23, Min_S23, Max_Max_Principal, Min_Max_Principal,
Max_Mid_Principal, Min_Mid_Principal, Max_Min_Principal,
Min_Min_Principal, Max_Mises_Max_Principal, Max_Mises_Mid_Principal,
Max_Mises_Min_Principal, Pd, Rd, h*1e3, dPd, RdT, Rdc, D, RdD))
                    RMOutIntFile.write('***\n')

            RMOutLocFile.write('%d\t %d\t\t %d\t\t %d\t\t %d\t\t %d\t\t %d\t\t
%d\t\t %d\t\t %d\t\t %d\t\t %d\t\t %d\t\t %d\t\t %d\t\t %d\t\t %d\t\t %d\t\t\t
%d\t\t\t %d\t\t\t %d\t\t\t %d\t\t\t %d\n' % (i+1, Max_U2_Location,
Min_U2_Location, Max_Mises_Location, Min_Mises_Location,
Max_S11_Location, Min_S11_Location, Max_S22_Location,
Min_S22_Location, Max_S33_Location, Min_S33_Location,
Max_S12_Location, Min_S12_Location, Max_S13_Location,
Min_S13_Location, Max_S23_Location, Min_S23_Location,
Max_Max_Principal_Location, Min_Max_Principal_Location,
Max_Mid_Principal_Location, Min_Mid_Principal_Location,
Max_Min_Principal_Location, Min_Min_Principal_Location))

#++++++++++

#----- Change variables for using in the next loop -----

            E=SigmaDev*1e3/(RdD*1e-3/0.200)/1e6

            h=0.200-(Pd*1e-3)

#++++++++++

#----- Close the output file -----

        RMOutIntFile.close()
        RMOutLocFile.close()

#++++++++++
```